Novel BODIPY Photosensitizers and corresponding nano-conjugates in an *in vitro* antimicrobial and anticancer study

by

Maxwell Thatyana

For

The degree of a Doctor of Philosophy in Materials Sciences

A thesis submitted to the Faculty of Health Sciences, University of the Witwatersrand, Johannesburg

In fulfillment of the requirements for the degree of Doctor of Philosophy in Materials Sciences, 2020

DECLARATION

I Mr M. Thatyana (1170953) declare that this thesis is my own work. It is being submitted for the degree of Doctor of Philosophy to the University of The Witwatersrand, Johannesburg. It has not been submitted before for any degree or examination at this or any other University.

Signature of candidate

…11…. day of…December……...2020

DEDICATION

This study is dedicated to the mighty God who has always been my strength throughout the pain and tribulations. To my family, I would like to thank them for their support. I would also like to dedicate this thesis to mama N. Ngqose and tata G. Ngqose, my grandmother K.N. Thatyana who lost their lives during my studies, and to my mother N. F. Thatyana for always giving me love, support, and strength to keep going. This thesis is also dedicated to my wife and kids who are my strongest pillar of strength whenever I needed them.

PUBLICATIONS AND CONFERENCES

Publications and Peer-Reviewed Manuscript(s)

Thatyana M., Siwe Noundou X., Krause R.W.S., Patel M., and Moeno S., *Synthesis of Novel BODIPY photosensitizers towards bioimaging or photodynamic therapy applications,* Submitted to Journal of Organic & Biomolecular Chemistry.

Co-authored book chapter(s)

Velaphi C. Thipe, Maxwell Thatyana, Fanelwa R. Ajayi, Patrick B. Njobeh, and Kattesh V. Katti (**2020**). *Hybrid nanomaterials utilized for detection, detoxification, and management of mycotoxins*. In Kamel A. Abd-Elsalam, *Multifunctional Hybrid Nanomaterials for Sustainable Agri-food and Ecosystems*, page 271 – 282, ISBN: 978-0-12-821354-4.

Conferences

Thatyana M., Patel M., and Moeno S., *Synthesis and characterization of Metallic Pt nanorods BODIPY conjugates for photodynamic therapy application,* **SACI/RSCSA young chemists' symposium**, University of the Witwatersrand, 01/12/2016 (Awarded third-best Ph.D. Oral Presentation)

Thatyana M., Patel M., and Moeno S., *Photodynamic antimicrobial and antifungal activity of selectively functionalized BODIPY PSs*. **SACI Inorg. 2017**, Cape Town; *Oral Flash talk and Poster*.

Thatyana M., Patel M., and Moeno S., *Novel BODIPY-Pt NR Nanoconjugates in vitro Antimicrobial Photodynamic Inactivation of selected Bacterial and Fungal species*: **9th Cross-faculty postgraduate symposium**, *Oral Presentation*, Wits: 10/2018

Thatyana M., Patel M., and Moeno S., *Novel BODIPY-Pt NR Nanoconjugates in vitro Antimicrobial Photodynamic Inactivation of selected Bacterial and Fungal species*: European food and nutrition congress and world colloid conference, *Video*, Viena Austria, 25-26-10-2018. DOI: 10.4172/2324-9323-C5-020.

Thatyana M., Patel M., and Moeno S., *Novel BODIPY-Pt NR Nanoconjugates in vitro Antimicrobial Photodynamic Inactivation of selected Bacterial and Fungal species*, **Cross Faculty Symposium**, University of the Witwatersrand, 2019, Oral presentation

ABSTRACT

Introduction

The photon-based initiated therapeutic modalities particularly photodynamic therapy (PDT), have shown significant clinical potential in surface-based and deep-seated tumor treatment as well as antimicrobial and antiviral treatment. Photodynamic therapy involves the use of photosensitizers, a directed light of specific wavelength, and molecular oxygen to generate phototoxic oxygen species of which cell death is realized. Boron dipyrromethene (BODIPY) photosensitizers (PSs) have in recent years gained much attention due to their interesting photophysical and photochemical properties and their potential application as anti-microbial and anti-cancer agents. Despite the progress made in this field, the design, synthesis, and modification of BODIPY PSs as anti-cancer and anti-microbial agents has been slow.

Methods

This study focuses on the design, synthesis, functionalization of BODIPY PSs, and Platinum-based nanoconjugates and their characterization. An acid condensation of an aldehyde and a pyrrole method was used for the synthesis of novel BODIPY PSs. The functionalization of some BODIPY PSs was carried out using the amide bond linker to afford sequential extended conjugation of iodine functional groups. The influence of functional groups on the photoactivity of the novel PSs was investigated with the attention on BODIPY PSs containing carboxylic acid (-COOH), amine (NH_2), sulfamoyl- (SO_2NH_2), Sulfonic acid (SO_3H), and iodine (I) groups. Synthesized PSs were screened for their anti-microbial activity using the disc diffusion technique.

Stock solutions of *Staphylococcus aureus*, *Streptococcus pyogenes*, *Escherichia coli*, *Pseudomonas aeruginosa*, *Candida albicans*, *Candida tropicalis*, *Candida glabrata*, and *Candida parapsilosis* were obtained from the Department of Oral Biological Science microbiology laboratory, University of the Witwatersrand. The minimum inhibitory concentration assays were carried out in 96 well plates, bacterial cultures were cultured in Mueller Hinton broth (MHB) and *Candida* was cultured in sabouraud dextrose broth (SAB). For preliminary cytotoxicity studies, the normal HaCat cells and human UCT Mel-1 cancer cells were obtained from the University of Cape Town, gifted by Dr. E.L. Wilson, Department of Haematology, at the Groote Schuur Hospital, Cape Town. All cell lines were cultured in Dulbecco's Modified Eagle's Medium (DMEM) supplemented with 10% (v/v) heat-

inactivated fetal bovine serum, 100 U/mL penicillin, and 100 mg/mL streptomycin incubated at 37 ºC, 5% CO_2 until 90% confluence was reached. Phototoxicity of microorganisms with BODIPY PSs was carried out using the 32 (65 mW/cm^2) LED lights mounted on a stand, placed at a height of 5 cm from cells, and irradiated for 45 minutes. Comparative phototoxicity study of HaCat and UCT Mel-1 cell lines with BODIPY PSs and hypericin was carried out with a ~1.5 J/cm^2 lightbox with two F15T8 15W/UVA PUVA lamps (wavelength 320-410 nm/peak 351 nm).

Results

BODIPY PSs were successfully synthesized their photochemical properties were studied with UV-Vis and fluorescence. The results showed that upon oxidation the fluorescence is quenched by 40% for BODIPY 1 and 50% for BODIPY 3. Moreover, following functionalization with bulk units the fluorescence intensity was quenched by 45 % for BODIPY 8 to 10. Furthermore, functionalization with iodine groups resulted in negligible to no fluorescence of BODIPY PSs. Their structural elucidation was confirmed with mass spectrometry, FTIR, XRD, and NMR and the results confirmed the synthesis of the desired BODIPY PSs. BODIPY 1 to 5, 7 to 9, and 6.1 to 6.5 showed negligible phototoxicity in anti-microbial studies with MIC >10-30 mg/mL. However, BODIPY 10 showed activity with a MIC 2.08 mg/mL for *S. pyogenes* and 4.17 mg/mL for *C. Albicans*. Furthermore, BODIPY 6 showed anti-microbial activity at MIC of 0.26 mg/mL against bacteria and >0.25 pM against fungal species. After further purification with silica, biobeads and Sephadex BODIPY 6 PSs showed a MIC of 65-130 µg/mL for *Candida*. BODIPY 6.6 with extended iodine moieties showed MIC of 130 µg/mL upon irradiation for 45 minutes. The Pt-nanoconjugates showed an improvement of 10% for bacterial and 18% for fungal induced cell killing capacity of the BODIPY PSs. For cytotoxicity studies, both BODIPY 6 and BODIPY 6.6 showed phototoxicity efficacy at a concentration <3 µM. BODIPY 6 showed a cell viability of 56% compared to its counterpart hypericin with 46% while the cell viability for BODIPY 6.6 was 60%. Pt-nanoconjugates also demonstrated an improved cell killing efficacy of BODIPY PSs which is desired for targeted and enhanced PDT activity.

Conclusion

BODIPY PSs have demonstrated potential for use as agents for photodynamic inactivation of microbial species as well as anti-cancer PDT agents for melanoma cell lines. BODIPY PSs showed that the activity for antimicrobial application follows the order

H<COOH<NH_2<SO_3H<SO_2NH_2 respectively. Furthermore, iodine substituted BODIPY induced both anti-microbial (65 µM concentration) and anticancer (<3 µM concentration) properties even at lower concentrations. No statistically significant differences between hypericin and BODIPY 6 p-value 0.40 were observed, but in comparison with BODIPY 6.6, there was a significant statistical difference p-value 0.0074 after irradiation with 1 J/cm^2 light. These results demonstrated that BODIPY 6 showed more activity for both microorganisms compared to its counterpart BODIPY 6.6. Pt-nanoconjugates improved the solubility and photoactivity of the novel BODIPY PSs. Phototoxicity analysis studies demonstrate that BODIPY 6 and BODIPY 6.6 exhibit potential for their application in photodynamic inactivation (PDI) and PDT of microorganisms and melanoma skin cancer cells respectively. Therefore, these BODIPY PSs have the potential to serve as anti-cancer and antimicrobial agents.

ACKNOWLEDGEMENTS

I would like to first thank my supervisor Dr. S. Moeno for accepting me in her research group and her assistance throughout my studies. I appreciate everything that you have done for me. I would also like to show my unbounded appreciation to my co-supervisor Prof. M. Patel, with her unwavering guidance, her acceptance of me in her research group meant a lot to me. Thank you, Prof, for the opportunity you have given to me to learn and support that molded me to be a better man in my intellectual capacity. The times we have to share in the lab learning from your techniques and your willingness to guide and share knowledge is greatly appreciated.

I would also like to show my appreciation to my colleagues' Dr. M. Ngoepe and K. Mnqiwu for their assistance with the analysis of the NMR results; your help is very much appreciated. I know we would go very far as a team. I extend my appreciation to Miss M. Sebelemetja for her assistance in performing some tests with the microbiology work. To Malefaso and Matladi who were interns in our microbiology lab, thank you so very much for your input in my studies. I would like to extend my appreciation to Dr. M. Makatini and Mr. T. Mbele for allowing me to use their facilities in their lab in the Chemistry Department University of the Witwatersrand. Your input in my study is very much appreciated by the characterization and analysis of the results. Much appreciation goes to Dr. N. Dlamini (from the University of Johannesburg, Department of Chemical Sciences, Doornfontein) for his financial support and analysis of my samples in his group.

My appreciation goes to Q.E. Chere for her support ever since I started my research journey, thank you so much for believing in me and continued support. Thanks, my little and only sister L.L. Thatyana for her support every time I needed her, you are the best sister anyone could ever ask for.

My greatest appreciation goes to the National Research Foundation for funding my studies from the beginning to the end; I am honored to have their support.

TABLE OF CONTENTS

LIST OF SCHEMES

LIST OF TABLES

LIST OF FIGURES

APPENDICES

LIST OF ABBREVIATIONS

$^1O_2$	- Singlet oxygen
API	- Antimicrobial photodynamic inactivation
$BF_3.OEt_2$	- boron trifluoro ethyl etherate
BODIPY	- Boron dipyrromethene
Conc.	- Concentration
DABA	- Diaminobenzoic acid
DABSA	- Diamonobenzenesulfonic acid
DCM	- Dichloromethane
DiPEA	- N,N-diisopropylethylamine
DLS	- Dynamic light spectroscopy
DMEM	- Dulbecco's Modified Eagle's Medim
DMF	- Dimethylformamide
DMSO	- Dimethyl sulfoxide
EtOH	- Ethanol
FTIR	- Fourier Transform Infra-red Spectroscopy
HRLC-MS	- High resolution liquid chromatography-mass spectrometer
Hyp	- Hypericin
ISC	- Intersystem crossing
LED	- Light emitting diodes
MBC/MFC	- Minimum bactericidal concentration and minimum fungicidal concentration
MeOH	- Methanol

MIC - Minimum inhibitory concentration

MS - Mass Spectroscopy

NAC - Non-albican *Candida*

NMR - Nuclear magnetic Resonance spectroscopy

NRs - Nanorods

PACT - Photodynamic anti-microbial chemotherapy

PDI - Photodynamic inactivation

PDT - Photodynamic therapy

Ppm - parts per million

PSs - Photosensitizers

ROS - Reactive oxygen species

SAB - Sabouraud dextrose broth

SEM - Scanning electron microscopy

TEM - Transmission electron microscopy

TFA - Trifluoroacetic acid

TLC - Thin layer chromatography

CHAPTER 1

Introduction

1.1 Synopsis

Photodynamic therapy is a well-established and a noninvasive clinically approved modality for targeted disruption of pathologic cells and tissue (Li *et al*., 2018, 2019; Yu *et al*., 2018; Agostinis *et al*., 2011). The PDT modality has drawn considerable attention for global research (Yang *et al*., 2019; Li *et al*., 2019). Photodynamic therapy provides a potential treatment approach for drug-resistant microorganisms (Hamblin *et al*., 2004) and malignant cancers (Agostinis *et al*., 2011). For PDT to take effect, the interaction of a light activable molecule (a photosensitizer), light, and molecular oxygen are needed (Lincoln *et al*., 2017). Following the light activation of a photosensitizer (PS), the intersystem crossing of the PS molecules and the subsequent production of highly reactive singlet oxygen ($^1O_2$) species and radicals takes place (Lincoln *et al*., 2017). The $^1O_2$ species may then induce oxidative damage to nearby nucleic acids, lipids as well as proteins leading to cell death (Lincoln *et al*., 2017).

Photodynamic agents (PSs) are generally nontoxic (when not irradiated) to surrounding cells, but upon targeted irradiation, they become highly toxic in tumor cells through the generation of toxic $^1O_2$ and reactive radicals (Li *et al*., 2019). The search, creation, and analysis of optimal PDT agents from a photochemical-photophysical perspective, a photostable compound (in relation with $^1O_2$ mediated oxidation), with absorption of high extinction coefficient in the NIR region, and high yields of reactive ROS species generation (Laine *et al*., 2017; Lincoln *et al*., 2017). From a synthetic view, important properties have to be considered, these include (i) ease of preparation and functionalization of the core structure, (ii) incorporation of heavy atoms (Br and I) to enhance the rate of ISC (a radiation less process involving a transition between the two electronic states with different states spin multiplicity), and (iii) incorporation of the electron-withdrawing group (typically at the (8)-meso-position) to enhance the stability of the PSs by preventing the addition of $^1O_2$ to the PSs core (Lincoln *et al*., 2017). Also, structural modifications may explore the extension of conjugation to facilitate large extinction coefficients suitable for long-wavelength absorptions (Komatsu *et al*., 2011; Zhang *et al*., 2014; Shank *et al*., 2013).

The ideal PSs may find applications in medical diagnosis (Kobayashi *et al*., 2010), biomarkers (Yang *et al*., 2014), sensors (including environmental for different ions) (Sunahara *et al*., 2007)

and may be used in anticancer therapies (Ozlem *et al*., 2009). Most of the promising PSs are the 4,4-difluoro-4-bora-3a,4a-diaza-s-indacene (BODIPY) PSs. This interest in these types of PSs is with the ability to modify their spectral properties (quantum yields of fluorescence, emission, and the position of absorption wavelength in a wide range) and characterized by their multifunctioning capabilities (Ozlem *et al*., 2009). This study seeks to synthesize, modify, and characterize BODIPY PS analogs with multifunctional groups and to study their potential application as antimicrobial and anticancer agents for PDT. The different functional groups on the chromophore structure were studied and tested for their possible application as antimicrobial agents (see chapter 5) and a preliminary study conducted to determine their potential as anticancer agents (see chapter 6).

1.2 Research conceptualization

1.2.1 Problem statement

Photosensitizers and PDT photosensitization have attracted attention due to their interesting properties. In the past decades, research conducted by various research groups globally had the aim to improve and/or find new PSs. However, most of the studied PSs have been reported to show some drawbacks leaving a huge gap for more research to be conducted on PDT photosensitization. These drawbacks include but are not limited to: (i) limited solubility (which leads to their hydrophobicity hence rendering them useless in the application for PDT); (ii) insufficient production of reactive oxygen species (ROS) (this leads to the PSs being unused because of the lack of cell killing efficacy); and (iii) absorption in the blue region of the electronic spectrum (this limits the use of PSs in the deep-seated malignant cells and tissues). This study seeks to address these limitations.

1.2.2 Justification for the study

Previous studies on BODIPY PSs have been centered on the development of soluble BODIPY analogs and their application for bioimaging. However, a growing interest has merged for BODIPY application as antimicrobial as well as anticancer agents. BODIPY PSs are known for their absorption in the visible range, high fluorescence quantum yields, lack of triplet state photosensitization, and lack of solubility. This study was designed to overcome the above-mentioned limitations encountered with BODIPY PSs. As such, the synthesized BODIPY PSs were functionalized with moieties that enhanced their solubility, quenching the fluorescence quantum yields, enhancing their triplet state photosensitization by incorporation of heavy

atoms which enhanced their intersystem crossing known to facilitate reactive oxygen species production. Furthermore, this study will show the functionalization of BODIPY PSs to increase their potency for induced cell killing. It will show that heavy-atom incorporation onto the BODIPY PS structure renders the desired properties and that the use of Pt-NRs as carrier vehicles enhances the drug solubility, increases the bioavailability of BODIPY PSs, and increases their antimicrobial and anticancer capacity. Additionally, this study will demonstrate that BODIPY PSs can be applied for the photosensitization of malignant tumors and photoinactivation of microbial species.

1.2.3 Research purpose statement

The purpose of this study was to synthesize novel boron dipyrromethene (BODIPY) PSs containing different functional groups on their structural periphery and to study their potential application as antimicrobial drugs and anticancer agents.

1.3 Aims and Objectives of this study

1.3.1 Aim

This study aimed to synthesize, functionalize and characterize BODIPY PSs with varied functional groups and to prepare their resulting platinum nanoconjugates, then study for their potential application in PDT of selective microbial organisms and malignant skin cancer.

1.3.2 Objectives

- To synthesize BODIPY photosensitizers with different terminal moieties such as carboxyl, sulfhydryl, iodine, and amine groups.
- To synthesize platinum nanorods (Pt NRs) gold nanorods (Au NRs) and nanoparticles of other shapes (spherical and cuboidal).
- To characterize the prepared BODIPY photosensitizers using the following techniques NMR, FTIR, Mass Spec, UV-Vis, and Fluorescence spectroscopy.
- To characterize the prepared nanoparticles using the following techniques XRD, UV-Vis, DLS (zeta sizer), TEM, and SEM.
- To screen the antimicrobial potential of the prepared BODIPY photosensitizers.
- To determine the minimum inhibitory concentrations for selected bacterial and fungal species.

- To determine the photodynamic inactivation (referred to as PDI in this study) effectiveness and efficiency of the synthesized BODIPYs and their corresponding nanoconjugates on selected bacterial (*staphylococcus aureus, streptococcus pyrogenes, Escherichia coli, pseudomonas aeruginosa)* and fungal (*Candida albicans. Candida tropicalis, Candida parapsilosis and Candida glabrata*) species.
- To attach the BODIPY photosensitizers that show activity to the prepared nanoparticles and characterize them using the techniques: UV-Vis, TEM, SEM, and XRD.
- To determine the photodynamic inactivation efficiency of the synthesized BODIPYs and their resulting nanoconjugates on selected bacterial and fungal species.
- To screen the anticancer potential of the photosensitizers and nanoconjugates against one cancer cell line Melanoma (Mel-1) and a normal (HaCat keratinocyte) cell line.
- To carry out phototoxicity studies using the active photosensitizers and their corresponding nanoconjugates on cancer (Mel-1) and non-cancer (HaCat) cell line under optimal irradiation.
- To compare the cell (selected UCT Mel-1 and HaCat cell line) killing efficiency of the prepared BODIPY photosensitizers and corresponding conjugates against that of a commercial photosensitizer in use (e.g. hypericin).

1.4 Outline of the thesis

Chapter one gives an introductory synopsis of PDT background and photosensitizers highlighting their interest in research in recent years. This chapter also outlines the research conceptualization which takes into consideration the: (i) problem statement, (ii) justification of the study, and (iii) lastly to highlight the aims and objectives of the study.

Chapter two gives a detailed literature review on the history of BODIPY PSs, their synthesis and structural modifications, and electronic properties. This chapter also highlights their significant synthetic approaches and applications in various scientific studies from imaging to sensors. Moreover, this chapter outlines the overview of work conducted by other research groups using functionalized BODIPY PSs and their applications in a variety of scientific research fields. Also, this chapter touches on different nanomaterials, their morphological aspects, and their advantages as drug delivery systems. The advantages of using one dimensional (e.g. nanorods) nanoparticles over other shapes are considered and highlighted. Furthermore, the literature on bacterial and fungal species is explored and the background on melanoma cell lines is explained.

In **Chapter Three**, a brief principle on the instrumentation and techniques used in the characterization of the synthesized BODIPY PSs is given. This chapter also provides a detailed synthesis method that was used to prepare these PSs. Furthermore, this chapter gives synthetic methods for nanoparticles that were screened. Detailed experimental procedures for anti-microbial PDI study and the cytotoxicity study are also provided.

Chapter four of this thesis shows the acquired spectroscopic results and data. It presents optical properties including photochemical properties of the BODIPY PSs studied in this work. It further elucidates the structures using MS analysis, computed elemental composition, ^{1}H and ^{13}C NMR. This chapter also shows detailed results on XRD for BODIPY PSs as well as nanoparticles and resultant nanoconjugates. Furthermore, this chapter shows obtained results on SEM and TEM analysis including the size distribution of nanoparticles using DLS (zeta sizer).

Chapter five demonstrates the antimicrobial activity of BODIPY PSs. It shows acquired data from disc diffusion study and minimum inhibitory concentration study of BODIPY PSs and nanoconjugates.

Chapter six contains the results from a preliminary study carried out to demonstrate the efficacy of some photo-active BODIPY PSs (BODIPY 6 and 6.6). This chapter discusses the dark toxicity study as well as phototoxicity study on UCT Mel-1 cancer cell lines. Furthermore, the results are presented as a mean ± standard deviation and student t-test for the BODIPY PSs to compare their phototoxicity with that of a well know Hypericin PSs.

Chapter seven gives the conclusions, future directions, and suggestions for potential studies to overcome the challenges encountered during the study.

1.5 References

Agostinis P., Berg B., Cengel K.A., Foster T.H., Girotti A.W., Gollnick S.O., Hahn S.M., Hamblin M.R., Juzeniene A., Kessel D., Korbelik M., Moan J., Mroz P., Nowis ., Piette J., Wilson B.C. and Golab J., 2011; Photodynamic therapy of cancer: An update, *CA-Cancer J. Clin*., 61(1): 250-281.

Hamblin M.R., and Hasan T., 2004; Photodynamic therapy: A new antimicrobial approach to infectious disease? *Photochem. Photobiol. Sci*., 3(1): 436-450.

Kobayashi H., Ogawa M., Alford R., Choyke P.L., and Urano Y., 2010; New strategies for fluorescent probe design in medical diagnostic imaging, *Chem. Rev*., 110(1): 2620-2640.

Komatsu T., Oushiki D., Takeda A., Miyamura M., Ueno T., Terai T., Hanaoka K., Urano Y., Mineno T., and Nagano T., 2011; Rational design of boron dipyrromethene (BODIPY)-based photobleaching-resistant fluorophores applicable to a protein dynamics study, *Chem. Commun*., 47(1): 10055-10057.

Laine M., Barbosa N.A., Kochel A., Osiecka B., Szewczyk G., Sarna T., Ziółkowski P., Wieczorek R., and Filarowski A., 2017; Synthesis, structural, spectroscopic, computational and cytotoxic studies of BODIPY dyes, *Sensors, and Actuators B*, 238(1): 548-555.

Li M., Long S., Kang Y., Guo L., Wang J., Fan J., Du J., and Peng X., 2018; De Novo design of phototheranostic sensitizers based on structure-inherent targeting for enhanced cancer ablation, *J. Am. Chem. Soc*., 140(46): 15820-15826.

Li M., Xia J., Tian R., Wang J., Fan J., Du J., Long S., Song X., Foley J.W., and Peng X., 2018; Near-Infrared light-initiated molecular superoxide radical generator: Rejuvenating photodynamic therapy against hypoxic tumors, *J. Am. Chem. Soc*., 140(44): 14851-14859.

Li M., Xiong T., Du J., Tian R., Xiao M., Guo L., Long S., Fan J., Sun W., Shao K., Song X., Foley J.W., and Peng X., Superoxide radical photogenerator with amplification effect: surmounting the Achilles' Heels of Photodynamic Oncotherapy 2019; *J. Am. Chem. Soc*., 141(6): 2695-2702.

Lincoln R., Durantini A.M., Greene L.E., Martínez S.R., Knox R., Becerra M.C., and Cosa G., 2017; meso-Acetoxymethyl BODIPY dyes for photodynamic therapy: improved photostability of singlet oxygen photosensitizers, *Photochem. Photobiol. Sci*., 16(1): 178-184.

Ozlem S., and Akkaya A.U, 2009; Thinking outside the silicon box: molecular AND logic as an additional layer of selectivity in singlet oxygen generation for photodynamic therapy, *J. Am. Chem. Soc.,* 131(1): 48-49.

Shank N.I., Pham H.H., Waggoner A.S., and Armitage A.B., 2013; Twisted cyanines: A non-planar fluorogenic dye with superior photostability and its use in a protein-based fluoromodule, *J. Am. Chem. Soc*., 135(1): 242-251.

Sunahara H., Urano Y., Kojima H., and Nagano T, 2007; Design and synthesis of a library of BODIPY-based environmental polarity sensors utilizing photoinduced electron-transfer-controlled fluorescence ON/OFF switching, *J. Am. Chem.Soc*., 129(1): 5597-5604.

Yang G., Tian J., Chen C., Jiang D., Xue Y., Wang C., Gao Y. and Zhang W., 2019; An oxygen self-sufficient NIR-responsive nanosystem for enhanced PDT and chemotherapy against hypoxic tumors, *Chem. Sci*., 10(1): 5766-5772.

Yang Z., Cao J., He Y., Yang J.H., Kim T., Peng X., and Kim J.S., 2014; Macro-/microenvironment-sensitive chemosensing and biological imaging, *Chem. Soc. Rev*., 43(1): 4563-4602.

Yu Z., Ge Y., Sun Q., Pan W., Wan X., Li N., and Tang B., 2018; A pre-protective strategy for precise tumor targeting and efficient photodynamic therapy with a switchable DNA/upconversion nanocomposite, *Chem. Sci*., 9(14): 3563-3569.

Zhang S., Fan J.L., Li Z.Y., Hao N.J., Cao J.F., Wu T., Wang J.Y., and Peng X.J., 2014; A bright red fluorescent cyanine dye for live-cell nucleic acid imaging, with high photostability and a large stokes shift, *J. Mater. Chem. B*, 2(1): 2688-2693.

CHAPTER 2

Literature Review

2.1 Introduction

Cancer and microbial infections are among the leading causes of death globally. Although there have been advances made in the availability of various therapeutic modalities, current chemotherapy efficiency remains questionable and the prognosis for the majority of cancer diagnosed patients remains very poor (Lin *et al*., 2015; Yen *et al*., 2018). On the other hand, pathogens have shown versatility in the development of anti-microbial-resistant (AMR) mechanisms, which remains the recognized global health problem. Despite efforts for the discovery of new drugs for the treatment of life-threatening diseases, microorganisms remain resistant to anti-microbial agents/drugs. Meanwhile, cancer remains unresponsive to no effect to many therapeutic agents (WHO, 2018). For those diseases responding to therapeutic agents, the treatment effect is normally short-lived as resistance develops to the initial therapeutic regiments (Lin *et al*., 2015; WHO, 2018; Yen *et al*., 2018). With that said, there is a need for new and effective compounds to overcome challenges encountered with the former therapeutic agents. Photodynamic therapy (PDT) is a non-invasive emerging therapeutic modality and is gaining popularity (Ozlem and Akkaya, 2009). PDT makes use of a photosensitizer and light of a specific wavelength in the presence of molecular oxygen to generate reactive oxygen species which results in cell killing (Ozlem and Akkaya, 2009).

Different photosensitizers (PSs) have been synthesized from hematoporphyrin (Hp) (Thudichum, 1867; Hoppe-Seyler, 1871) to xanthene (Amatguerri *et al*., 1990). Some challenges encountered by these drugs include but are not limited to bioavailability at the diseased site, selectivity, photosensitivity even after therapy, purity, dark toxicity, etc. (Dougheti *et al*., 1975). However, Boron-dipyrromethenes (BODIPY) PSs came to the rescue by addressing these challenges and they have gained popularity in recent years. Since the inception of BODIPY discovery, attention has been focused on their synthesis and modification towards application in PDT and photodynamic inactivation (PDI) respectively.

Boron-dipyrromethenes is also known as BODIPY dyes (having the core; 4,4-difluoro-4-bora-3a,4a-diaza-s-indacene) are a group of fluorescent photosensitizers. This class of fluorophore dyes displays interesting properties including high chemical stability, photostability, high quantum yields, tunable emission, and sharp fluorescence peaks. In the past two decades, many

structurally diverse BODIPY dyes have been synthesized and applied in varied studies (Boens *et al*., 2012). BODIPY dyes are the least explored photosensitizers for photodynamic therapy of tumors. The main reason for this is that they show greater fluorescing propensity than intersystem crossing (a transition where an excited molecule is promoted to a higher energy excited state to the ground triplet state) then a transfer of energy to the molecular oxygen and production of reactive oxygen species is realized. However, BODIPY dyes to be used for PDT as anti-tumor agents can be modified to facilitate intersystem crossing (ISC) and to improve the photophysical properties of these photosensitizers. This can be achieved by the incorporation of heavy atoms (halogens) in their structure to introduce the heavy atom effect which in turn enhances triplet state photosensitization (Yogo *et al*., 2005). The spin-coupling effect of these heavy atoms facilitates a greater population of the triplet state which in turn leads to the production of singlet oxygen in larger quantities. This then leads to an enhanced PDT effect on cells leading to cell mortality respectively.

2.2 Photodynamic therapy

Photodynamic therapy (PDT) is a surface-based modality used for the treatment of age-related macular degeneration, as well as surface-based and non-deep-seated malignant tumors (Dougherty *et al*., 1998). A combination of photosensitizers and a red to near infra-red (IR) light is required for this treatment. Photodynamic therapy is a minimally invasive form of treatment that involves light irradiation of photosensitizers to produce reactively strong singlet oxygen species (Dougherty *et al*., 1998). The reactively strong singlet oxygen species is a cytotoxic species with the capacity to kill cancer cells. These singlet oxygen species cause direct damage to cancer cells, by targeting cell immune response activation, and vascular shut down (Dougherty *et al*., 1998). This therapy has the disadvantage of damaging neighboring healthy cells but it is still considered better than conventional therapies because of its non-invasive nature.

As much as singlet oxygen is one of the species by which PDT activity unfolds, other species in the form of radical species are encountered. The two different oxygen species are as a result of the two different mechanisms by which PDT can unfold. The mechanisms of PDT suggest that: a photosensitizer (PS) once promoted to the excited singlet state can undergo intersystem crossing to the lowest triplet state, where it can generate reactive oxygen species (ROS) in the form of singlet oxygen or radicals (Dougherty *et al*., 1998) as shown in **Figure 2.1** below. Tumor cells may then be killed via apoptosis or necrosis (Pervaiz and Olivo, 2006).

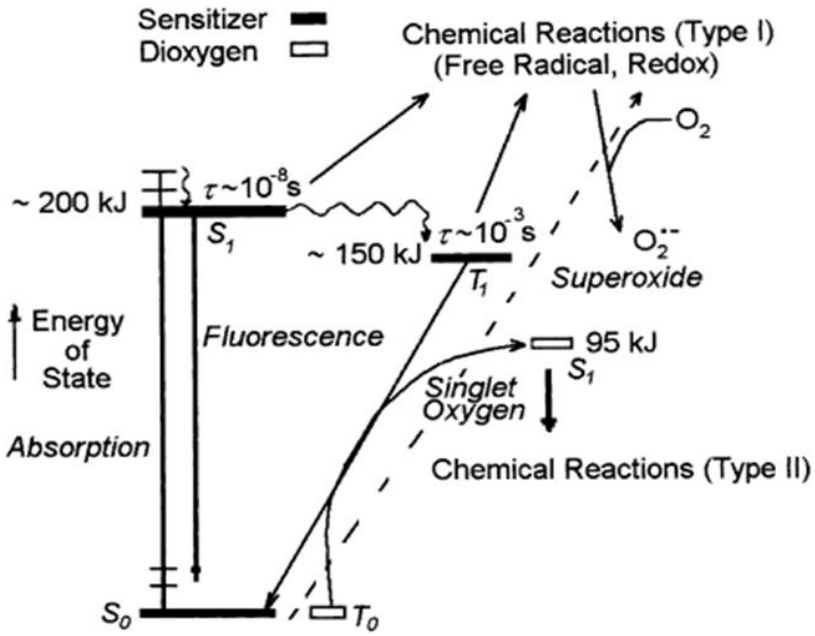

Figure 2.1: Jablonski diagram showing reactive oxygen species production (adapted from DeRosa and Crutchley, 2002)

The nature of the cell death mechanism depends greatly on the localization of the PS within the cell and the amount of active singlet oxygen produced (Pervaiz and Olivo, 2006). Plasma membrane or lysosome localized photosensitizer is prone to promote necrosis and apoptosis. The internalization of photosensitizers will favor apoptotic cell death through the activation of nucleases and proteases, which are hydrolytic enzymes responsible for DNA fragmentation and intracellular structure degradation (Reed, 2000).

PDT can unfold either through the Type I or Type II mechanism. In the Type I mechanism, the energy from a PS is transferred to a substrate molecule that forms radicals, these further interact with oxygen, giving rise to free oxygen radicals' production (Dolmans et al., 2003; Josefsen and Boyle, 2008). On the other hand, in the Type II mechanism, molecular oxygen interacts directly with the photosensitizer in the excited triplet state, resulting in the production of highly reactive singlet oxygen as shown in **Fig. 2.1** (Dougherty *et al*., 1998). The Type II PDT mechanism is the most predominant mechanism in which the destruction of the target tumor tissue is brought about by the photosensitizer generated singlet oxygen species (Dolmans *et al*., 2003).

During excitation of a photosensitizer with light, three major reactions of excited species may occur: electron transfer which is a type I reaction resulting in the production of radical species; energy transfer which is the type II reaction in which the production of a singlet oxygen species

is observed and lastly photobleaching. Between these three major reaction pathways, the type II reaction which involves energy transfer is the most important pathway in the production of singlet oxygen and where cell damage can be realized (Bonnett, 1995). **Figure 2.2** below shows the photosensitization of a photosensitizer and its changes in energy transitions phases to biomolecules interaction. The singlet oxygen production mechanism can be summarized as follows:

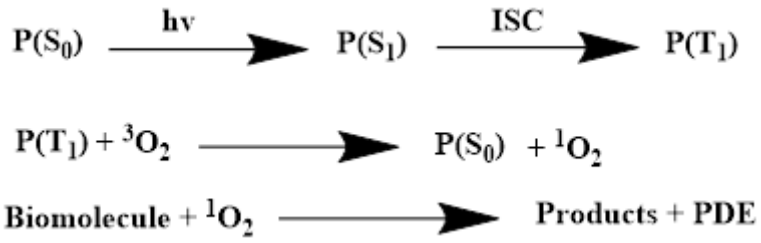

Figure 2.2 mechanism for singlet oxygen production (adapted from Bonnett, 1995)

The known mechanisms of cell killing in PDT include; direct killing (also known as necrosis), and tumor vasculature shut down and finally immune system targeting (by opening ways to facilitate cell killing, also known as apoptosis) (Dolmans *et al*., 2003).

The work carried out by Korbelik and co-workers reported on the accumulation of photosensitizers in tumor tissues (Kobelik *et al*., 1996) and they observed a reduction of tumor cell growth. However, Kobelik and coworkers (1996); noted that cell killing was not achieved completely. This group reported that photosensitizers injected intravenously do not always go to the desired tumor cells which are a long distance from the vasculature (Kobelik *et al*., 1996). Furthermore, they observed that the PDT activity is limited by the amount of oxygen availability during therapy. The group speculated that this was due to the complete consumption of oxygen and secondly due to the lack of microvasculature fresh oxygen to reach the tumor region (Tromberg *et al*., 1990, Pogue *et al*., 2001). To curb this challenge, it was suggested that the therapy should be carried at different times with different doses, this allows for enough availability of oxygen to the desired site (Dolmans *et al*., 2003). **Figure 2.3** below shows different PDT cell death mechanisms.

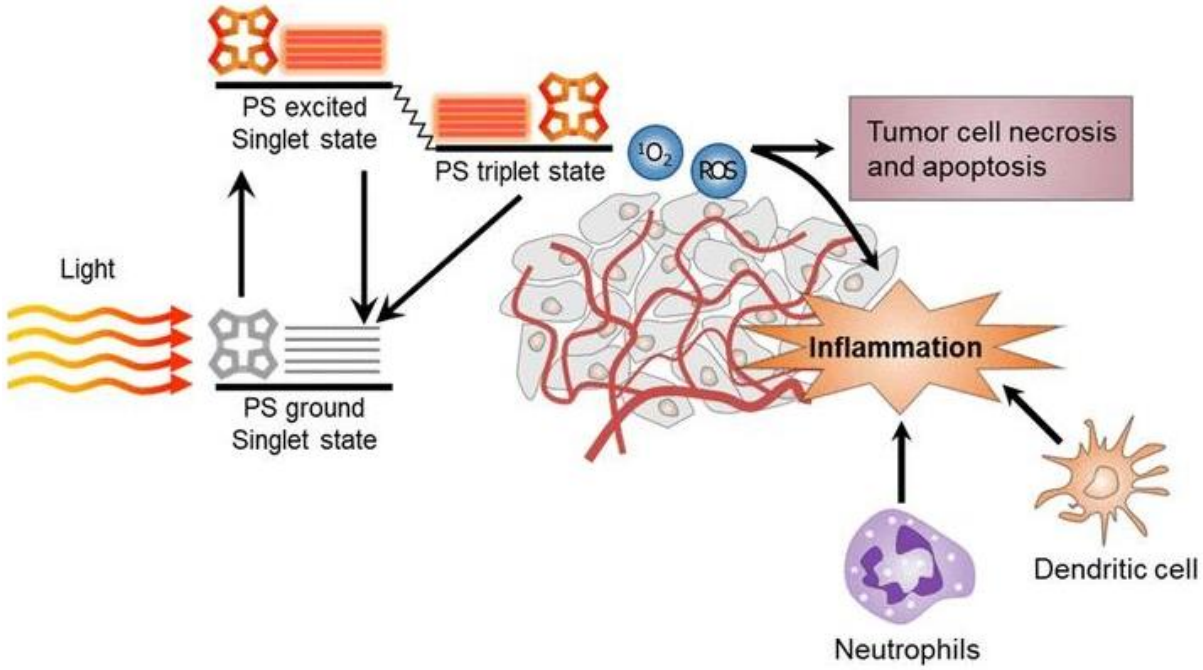

Figure 2.3 Biological response of photodynamic therapy (Adapted from Hwang *et al*., 2019)

Many studies have verified that some biomolecules can react with singlet oxygen. Since these are cell biomolecules that are responsible for cell activities, they may result in a vascular shutdown (Bonnett, 1995).

2.3 Different light sources used in PDT

PDT relies on the application of focused light delivery (Morton, 2004). This light can be applied either directly or through an optical fiber to tumors (for those that are internal and not readily accessible). However, PDT is limited by the amount of light penetration into the tissues which in turn can hamper deep-seated cancer treatment (Clark *et al*., 2003). Two fundamental aspects of PDT include the delivery of adequate light and the corresponding light source (Wan and Lin, 2014). Various light sources currently in use for surface PDT include; lasers, metal halide lamps, light-emitting diodes (LEDs), fluorescent lamps, and xenon filtered lamps (Clark *et al*., 2003).

Light-emitting diodes (LEDs) have emerged as the more widely used light source. LEDs are complex semiconductors that convert electrical current into incoherent narrow-spectrum light (Barolet, 2008). Diodes offer extensive advantages for use in both the clinical and laboratory environments, with the choice of emission ranging between 350 to 1100 nm (UV to NIR) respectively (Barolet, 2008). The advantage of diodes is that they are cost-effective and versatile (Barolet, 2008). LEDs and laser light sources are very different in the form of light

they deliver and ultimately this accounts for the optical power output differences observed between the two (Neupane *et al*., 2010). The light from LEDs is non-coherent and can also have a bandwidth that is either narrow or broad, this makes LED a good source for PDT application (Barolet, 2008). Light-emitting diodes are a gentler source of light in comparison to lasers, with significantly lower energy outputs (Zelickson, 2005). Therefore, LEDs are a choice of the light source because they do not deliver enough power to damage tissues (heating effects) and do not have the same risk of accidental eye damage that lasers carry (Barolet, 2008). In contrast, this study will focus on the use of LED light for the sensitization of the synthesized BODIPY PSs outlined in this study.

2.4 Photosensitizers

2.4.1 Photosensitizers in PDT

Photosensitizers in PDT may be classified into two categories, the porphyrins, and nonporphyrins. The porphyrin-derivative PSs may be further categorized as first (hematoporphyrin (HpD) (Lipson *et al*., 1967), second (5-aminolevulinic acid) (Ethirajan *et al*., 2011), and third-generation photosensitizers (monoclonal antibodies PSs (mAB-PSs)) (Moser, 1998). First-order PSs included the derivatives of hematoporphyrin (HpD) and photofrin. The second-order generation of PSs was developed to overcome challenges associated with the first order PSs including prolonged skin photosensitization and suboptimal tissue penetration during PDT (Nayak, 2005). These second-generation PSs were chemically pure compared to the first generation and absorbed light at longer wavelengths with less skin photosensitization. Further to this, the third generation of PSs was developed and it refers to the second generation of PSs bound to carriers such as antibodies and liposomes for selective targeting of tumor tissues, and this is the most active research area in the field of PDT (Juzeniene *et al*., 2007). Although the preclinical stage PSs are mostly porphyrin derivatives. Other nonporphyrin derivatives PSs (BODIPY) are entering pre-clinical and clinical stages. Much research work is employed in the synthesis of pure chemical PS derivatives with enhanced activity and minimized side effects. **Figure 2.4** shows different chemical structures of porphyrin-based and nonporphyrin-based photosensitizers.

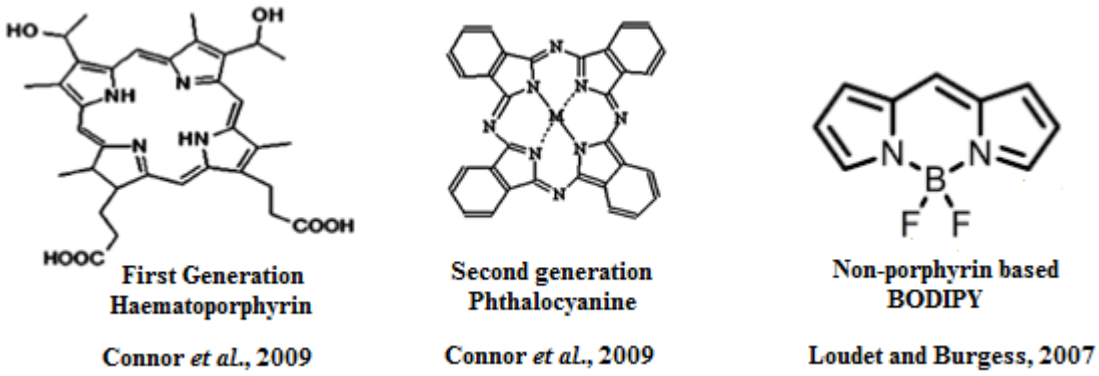

Figure 2.4 Porphyrin and non-porphyrin photosensitizers

To date, many efforts have been made to develop a variety of substituted PSs including cationic PSs such as chalcogenopyrylium dyes, phenothiazinium, and benzo[a]phenothiazinium derivatives, which also include methylene blue and toluidine blue (Leonard *et al*., 1999). The majority of cationic dyes selectively accumulate in transformed cells with the mitochondria as their main cellular target (Leonard *et al*., 1999). Nevertheless, novel PSs classes are being developed (e.g. being the 4,4-difluoro-4-bora-3a,4a-diaza-s-indacene, also known as boron dipyrromethenes difluoride: BODIPY dyes). They are promising an exciting new approach in the field of PDT. Moreover, challenges such as photosensitivity, low absorbance wavelength, and dark toxicity associated with the use of porphyrin and nonporphyrin-based PSs have limited their applications in PDT. Therefore, there is a need for a new exploration of new classes of compounds (Gorman *et al*., 2004).

2.5 BODIPY Photosensitizers

BODIPY PSs (4,4-Difluoro-4-bora-3a,4a-diaza-s-indacenes) in the past decades have found many applications due to their characteristics. Some of their renowned characteristics are that they are strong UV light absorbing molecules with narrow emission profiles, high quantum yields, and sharp fluorescence peaks, and they are easy to functionalize (Zhang *et al*., 2009, Boens *et al*., 2012). Furthermore, these photosensitizers are relatively stable in their physicochemical environment (they are insensitive to the pH and polarity of their environment) meaning their emission and absorption characteristics do not change much by the change of solvents. Moreover, their fluorescence characteristics are easily tuned by modification with other small functional moieties. These properties have rendered them available for the labeling of DNA (Shah *et al*., 1990) and proteins (Karolin *et al*., 1994). However, there are some undesirable properties of these molecules for applications in many biotechnology studies; these

include their lack of solubility in water and emission wavelengths mostly less than 600 nm. Thus, in recent years their framework modification has led to their use for live-cell imaging.

The BODIPY photosensitizers belong to a family of fluorescent compounds with a central heterocyclic core. They were first discovered by Triebs and Kreuzer in 1968 (Triebs and Kreuzer, 1968). The significance of their discovery was brought to light when their possible application as potential fluorescence probes was realized by Boyle and his co-workers (Boyle *et al*., 2011) in the 1990s.

Figure 2.5 shows the boron dipyrromethane structure and its transformation stages to dipyrrin (BODIPY) and different numbering positions (Adapted from Loudet and Burgess, 2007). **Figure 2.5(1A)** shows a dipyrromethane formed after acid treatment of pyrrole and an aldehyde. After the oxidation reaction of **Figure 2.5 (1A)** it produces an unstable dipyrrin complex shown in **Figure 2.5 (1B)** which then after complexation with trifluoro boron ethyl etherate forms a stable and highly fluorescent dipyrromethene (boron dipyrrin **Figure 2.5 (1C**)). In the BODIPY core structure **Figure 2.5 (1C)**, position 8 is normally known as the meso-position, whereas positions 1, 2, 6, and 7 are beta positions and 3 and 5 are the alpha positions (Wood and Thompson, 2007). **Figure 2.5** shows the numbering system of the BODIPY PSs.

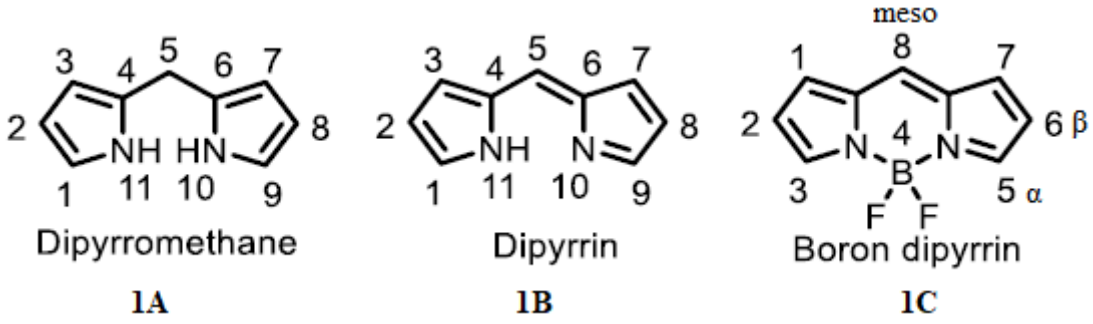

Figure 2.5 The BODIPY dyes numbering system (Adapted from Wood and Thompson, 2007)

In the past two decades, BODIPY dyes have seen many reviews (Ziesssel *et al*., 2008). For instance, one review by Loudet and Burgess (2007), elaborated on different synthetic routes and reported on the spectroscopic properties of different BODIPY PS derivatives. Moreover, a review by Ziessel and co-workers (2008) elaborated on the photophysical properties and the chemistry behind BODIPY dyes including but not limited to: synthetic condensations, electrophilic substitutions, the nucleophilic substitution of leaving groups, metal-catalyzed

cross-coupling, extending the degree of π electron conjugation, and so forth. Furthermore, a review by Boyle and co-workers (2011), reported on the use of BODIPY dyes in fluorescent electroscopic light active materials used for imaging of cells (Boyle *et al*., 2011). In 2012, an overview of BODIPY dyes as photodynamic therapy photosensitizers of cancers was reported by Awuah and You (Awuah and You, 2012). Boens and co-workers (Boens *et al*., 2012) described the various synthesis of different BODIPY dyes as fluorescent indicators. In another study, Shen and co-workers (2014) reported on BODIPY structure modification methods for long-wavelength absorbing BODIPY dye synthesis (Shen *et al*., 2014). Ravikanth (2015) reported on the synthesis, properties, and application of halogenated BODIPY dyes at the pyrrole carbons of the BODIPY core structures (Ravikanth *et al*., 2015).

2.6 Triplet state PSs

An increase in reports on the synthesis of triplet state PSs have been observed, but most of these reports are centered on fluorescent molecules. Therefore, heavy atom induced or red-shifted PSs referred to as triplet state PSs are known to enhance intersystem crossing due to spin coupling of the heavy atoms on BODIPY periphery (Zhao *et al*., 2015). The broader scope of studied PSs can be divided into two: those that contain heavy atoms and those without heavy atoms. The heavy atom PSs can be divided into two: (i) the Bromo- and Iodo- substituted organic photosensitizers and (ii) the transition metal complex containing PSs respectively. Halogenated molecules are preferred candidates more than transition metal complexes due to the complications or limitations associated with transition metal complexes associated with toxicity and prolonged sensitization after therapy (Amatguerri *et al*., 1990). The current research focus on the most popular PSs of the nonporphyrin groups in this context includes the BODIPYs and xanthene. Recent studies were conducted on naphthalene diimides, as well as; Rose Bengal, Erythrosin B, Eosin blue, and Eosin Yellow which are xanthene-based PSs as shown in **Fig. 2.6** (Amatguerri *et al*., 1990).

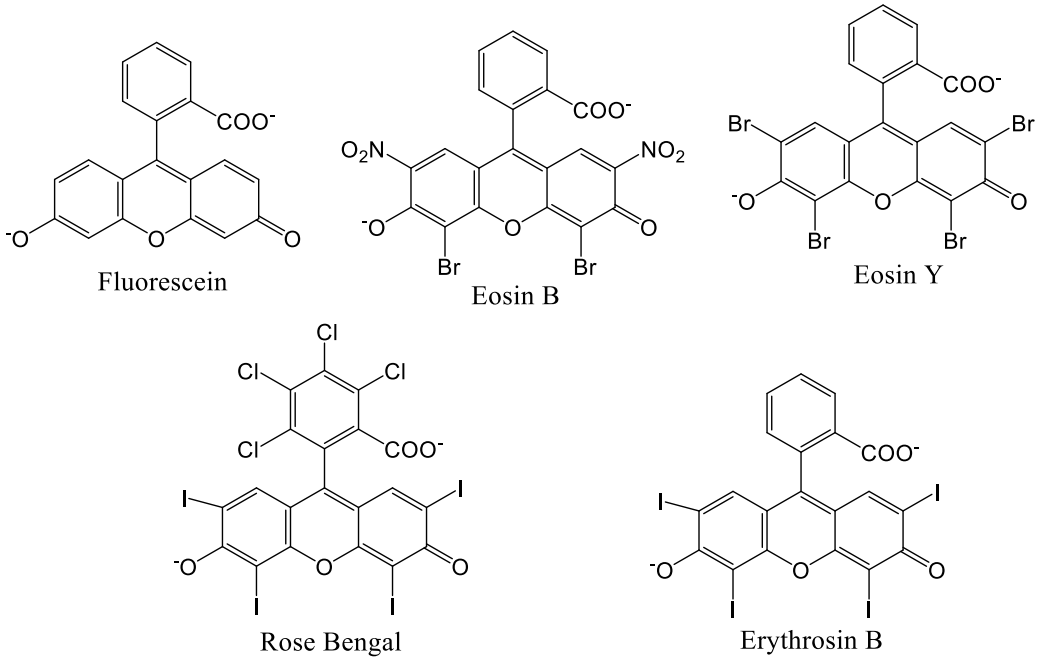

Figure 2.6 Fluorescein and its halogenated derivatives as triplet PSs (Adapted from Amatguerri *et al*., 1990).

The compounds shown in **Fig 2.6** are known for their application for staining in microscopy. However, their major drawback is associated with their limited structural functionalization which restricts their absorption wavelength in the visible region (Amatguerri *et al*., 1990). Due to this problem, more attention to BODIPY PSs studies has gained momentum in this topic to overcome the observed challenges associated with other PSs. The most successful candidates in the triplet state photosensitization topic include the BODIPYs and perylene which were noted for their synthesis simplicity (Amatguerri *et al*., 1990). BODIPY derivatives have the advantage of the ease of functionalization as shown in **Fig. 2.7** below. However, many of the synthesized BODIPY PSs have been shown to have the absorption wavelength in the range of 500 nm to 800 nm (Ortiz *et al*., 2012).

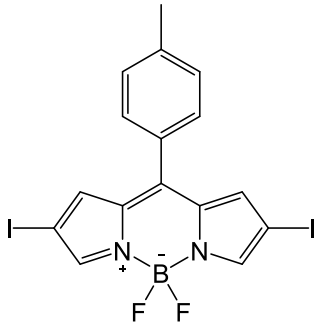

Figure 2.7 Diiodo functionalized Bodipy (Adapted from Ortiz *et al*., 2012).

2.7 Application of BODIPY dyes

2.7.1 BODIPY dyes in cell imaging

Extensive research in biology using BODIPY PSs has been conducted and it showed these compounds to have application in biological tagging or on cell imaging (Courtis *et al*., 2014; Kosaka *et al*., 2009). Fluorescence imaging plays a pivotal role in cell imaging as it provides useful information both *in vitro* and *in vivo* for both clinical and preclinical applications. Also, cell imaging provides high sensitivity, ability to multiplex colors, low costs, and portability (portable fluorescing light devices) (Kosaka *et al*., 2009). However, the most challenging step in the development of these molecular probes is the identification of suitable organic fluorophores of interest for biological labeling (or imaging) without the compounds perturbing biomolecular activity (Courtis *et al*., 2014; Johnson *et al*., 2009). The BODIPY dyes in live cells or *in vivo* imaging are associated with an appropriate balance of PSs lipophilicity and aqueous solubility which enhances membrane permeability while minimizing lipid membrane staining (Johnson *et al*., 2009). The ideal candidate group for biological imaging should be chemically stable, maintain photostability in oxidative aqueous media, and can readily traffic through cellular compartments (Johnson *et al*., 2009). BODIPY PSs fulfill some of the requirements for routine imaging as well as for conjugation to small molecules and protein targets of interest (Courtis *et al*., 2014).

The study by Courtis and co-workers (2014), demonstrated the use of small monoalkoxy BODIPY PSs as probes for bioimaging (CMA-BODIPYs, also termed MayaFluors). The group developed BODIPYs for hybrid optical and/or positron emission topographic imaging. Courtis and his team observed that the BODIPY biological profiling in living cells demonstrated excellent membrane permeability, showed a lack of cytotoxicity, and had low nonspecific binding. Furthermore, they did not observe a differential propensity of Mayafluors to bleaching compared to their counterpart difluoro BODIPY derivatives (Courtis *et al*., 2014). In addition to these observations, the MayaFluors were demonstrated not to impact with the living cell viability even after prolonged incubation at concentrations much higher for imaging purposes. Therefore, the Mayafluors are good candidates for use in bioimaging of the cells. **Figure 2.8** shows the synthesized BODIPY (Mayafluors) which were used in cell imaging in the Courtis group.

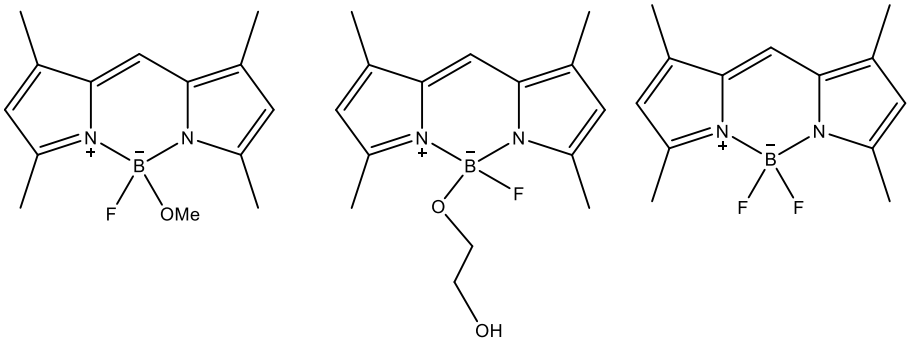

Figure 2.8 MayaFluors BODIPYdyes for imaging (Adapted from Courtis *et al*., 2014)

2.7.2 BODIPY dyes in Photodynamic Therapy (PDT) - Antitumor agents

As mentioned earlier, there are various clinically approved PDT agents based on tetrapyrroles (including chlorins, bacteriochlorins, and porphyrins) (Kue *et al*., 2016; Doherty *et al*., 2016). However, their major drawback is their difficulty to synthesize and modify. Therefore, BODIPY PSs in PDT has emerged as a new strategy for PDT applications with great interest over the past years. BODIPY for PDT applications has to be modified to enhance singlet to triplet intersystem crossing (Kamakew *et al*., 2013). Photomortality in PDT is known to occur through triplet state photosensitization. Consequently, BODIPY PSs are modified with heavy atoms to facilitate triplet state photosensitization through heavy atom spin-coupling. However, heavy atoms are not added at positions that disrupt planarity which would decrease conjugation (Nagano *et al*., 2005). Nagano and co-workers first reported a 2,6-diiodo-BODIPY analog for $^1O_2$ generation in PDT. **Figure 2.9 A** shows the BODIPY analog that Nagano's group investigated and their results obtained. In another study, Akkaya and co-workers synthesized 2,6-dibrominated analog containing oligo ethylene glycol fragments to promote water-solubilities (Akkaya *et al*., 2006). The compound had an EC50 at 200 nM concentration against K256 cells as shown in **2.9 B**. **Figure 2.9** shows some BODIPY PSs in PDT.

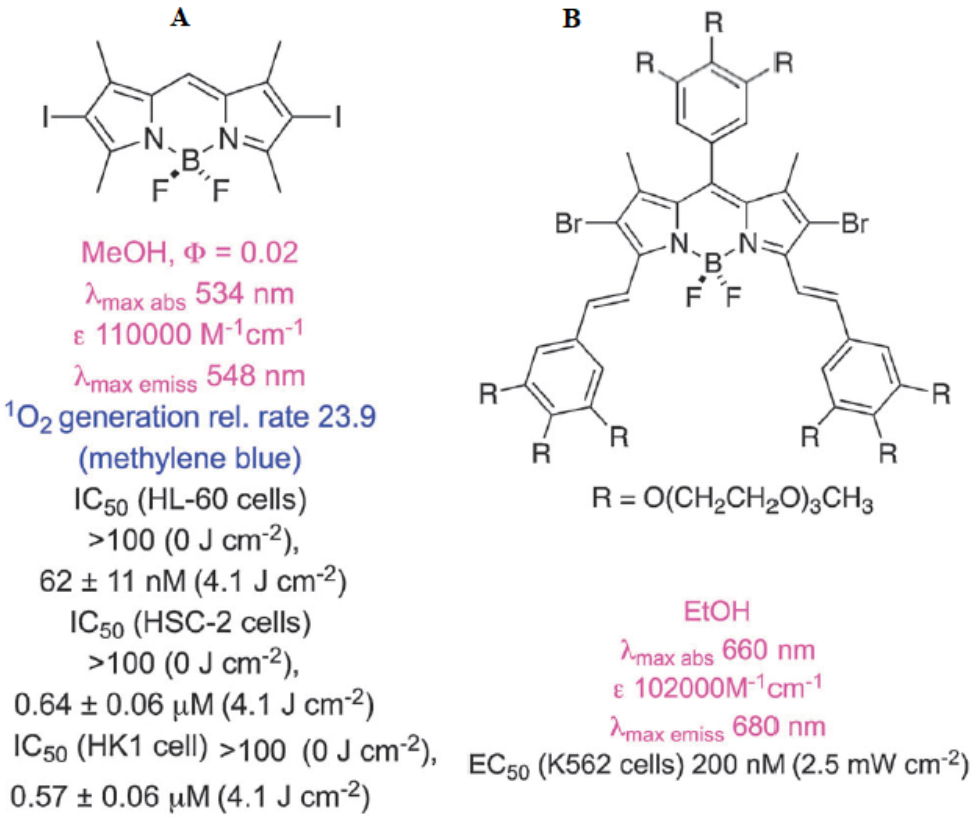

Figure 2.9 Some BODIPY PSs used in PDT (Adapted from Nagano *et al*., 2005; Akkaya *et al*., 2006)

Consequently, Photodynamic therapy has emerged as a favorable clinically approved modality for the treatment of neoplastic and nonmalignant lesions (Agostinis *et al*., 2011; Dolmans *et al*., 2003). For PDT to be realized, a photosensitizer, light of specific wavelength (depending on the absorption profile of the PSs), and oxygen are required. The PS is administered to the diseased site and then subjected to an irradiation light source to produce the reactive oxygen species (typically singlet oxygen and radical species from ground oxygen) to introduce cell damage and ultimately cell death (Mroz *et al*., 2011; Triesscheijn *et al*., 2006). The radiation of the PSs enhances the conversion of the PSs to the triplet state via intersystem crossing from the excited singlet state (Hamblin and Hasan, 2004; Moan and Berg, 1991). In the treatment of cancer, the PDT agent destroys the vasculature surrounding the tumor cells and then activates immunological responses against the cells (Juarranz *et al*., 2008). The main advantage of PDT is its dual selectivity potential in that it involves focusing light onto the targeted tissue (tumor region) and preferential accumulation of the PS at the diseased tissue over normal tissue (Castano *et al*., 2004).

Some photosensitizers are clinically approved but they have demonstrated some disadvantages associated with photobleaching or phototoxicity even after the PDT treatment (Bonnett and Martinez, 2001). The work done by Laine and co-workers (2017), undertook a cytotoxicity study on three synthesized BODIPY PSs containing the methyl, methyl benzoate, and chloro functional groups (see **2.10**). Laine and co-workers (2017) reported on the lowered cytotoxic effect of the meso carbonyl effect of compound 1 (as shown in **2.10**) which was reduced due to the steric effect of the methyl groups on positions 1 and 7 respectively. Meanwhile, for other PSs such as compound 2 (in **2.10**), the cytotoxic effect was enhanced due to the heavy atom effect (cell viability <30% at 10 µM concentration) of the moieties at positions 3 and 5 pyrrolic positions. Consequently, compound 3 showed little photoactivity with cell viability of >80% (Laine *et al*. 2017). Their study indicated that the presence of the methyl benzoate enhanced the cell penetration of the compounds 1 and 2 respectively (Laine *et al*., 2017).

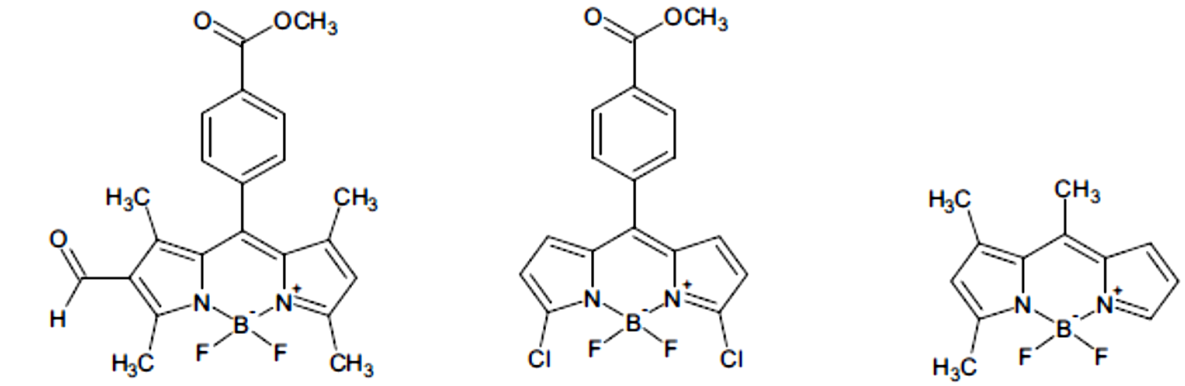

Figure 2.10 Cytotoxic effect of functionalized BODIPY PSs on colon cancer SW480 cells (Adapted from Laine *et al*., 2017)

2.7.3 BODIPY dyes as antimicrobial agents

There is an increasing demand for novel antibiotics to overcome the speedy development of drug resistance mechanisms observed in clinical isolates of both gram-negative bacteria and gram-positive bacteria. Antimicrobial resistance (AMR) has placed a crucial emphasis on the search for new methods and approaches to overcome this challenge (Kim and Lee, 2003; Hurdle *et al*., 2005). A study by Lincoln and co-workers (Lincoln *et al*., 2017), reported on the photodynamic inactivation (PDI) of *E. coli* ATCC 25922 bacterial strain with photoinactivation minimum inhibitory concentrations of less than 50 µM for the 2,6-diiodo-8-acetoxymethyl BODIPY and 2,6-dibromo-8-acetoxymethyl BODIPY PSs. Zou and co-workers (2017),

investigated the influence of BODIPY incorporation of more heavy atoms (mostly multi-substituted) to the BODIPY structure. They conclude that heavy-atom incorporation into BODIPY PSs demonstrated low phototoxicity (irradiation with light) on HeLa cells while increased dark toxicity (without irradiation) was observed (Zou *et al*., 2017). This was attributed to the competition of the heavy-atom effect. The group also noted that di-substituted BODIPY PSs with heavy atoms exhibited more phototoxicity compared to their counterparts multi-substituted heavy atom PSs. This observation suggested that increasing heavy atom incorporation onto BODIPY PSs enhances dark toxicity as opposed to phototoxicity (Zou *et al*., 2017). **Figure 2.11** below shows an AcO-BODIPY PSs with different heavy atoms used for the rationalization of heavy atom effect on cell killing ability.

	R^{I}	R^{II}	Q.Y
H_2BOAc	CH_2OAc	H	n.a
Br_2BOAc	CH_2OAc	Br	0.84
I_2BOAc	CH_2OAc	I	0.98
2I-BDP	H	I	0.98

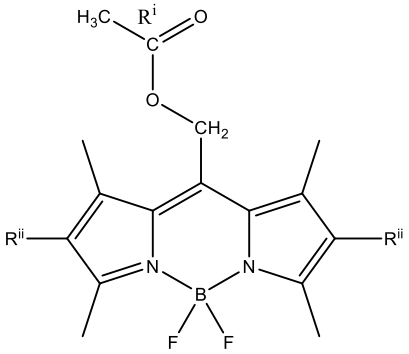

Figure 2.11 structure of AcO-BODIPY (Adapted from Lincoln *et al*., 2017).

Furthermore, in another study carried out by Carpenter and co-workers (Carpenter *et al*., 2015) against bacteria, fungi, and viruses, photoinactivation of both gram-negative and gram-positive at low concentrations, the 2,6-diiodo-1,3,5,7-tetramethyl-8-(N-methyl-4-pyridyl)-4,4-difluoro-boraindacene (DIMPy-BODIPY) PSs also demonstrated antimicrobial photodynamic inactivation (API) activity against three fungal species with moderate to low MIC concentrations (1 µM against *C. Albicans* ATCC-90028, 0.5 µM against *C. neoformans* ATCC-64538, and a MIC of 1 µM against *C.glabrata* ATCC-15545 respectively). Moreover, the viability of viruses was affected by BODIPY PS shown in **Fig. 2.12** as observed by Carpenter and colleagues (2015), for Dengue 1 virus cells where viability was reduced by 6log fold units (at 0.1 µM and 0.5 µM) in vesicular stomatitis virus and by (5 µM) in human adenovirus-5 respectively (Carpenter *et al*., 2015). The studies show that iodine or heavy atom induced

BODIPY PSs exhibit both antibacterial, antifungal, and antiviral PDI even at lower (nM magnitude) concentrations.

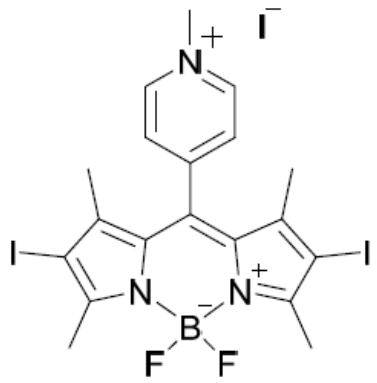

Figure 2.12 Iodo-cationic BODIPY (Adapted from Carpenter *et al*., 2015).

2.7.4 BODIPY dyes for environmental monitoring

An example of a novel environment-sensitive BODIPY probe was reported on by Nagano and co-workers (Nagono *et al*., 2007). Their study involved the synthesis of BODIPY based probes in which well-controlled fluorescence (resulting from the use of different meso-aryl groups) was studied (Nagono *et al*., 2007). Limitations associated with these probes are due to their shorter absorption wavelengths (<550 nm). Environment-sensitive fluorescence probes absorbing and emitting in the far-red to the NIR region are of great importance and desirable.

Studies such as the one conducted by Yu and co-workers (Yu *et al*., 2017) demonstrated the synthesis of pyrrolyl-BODIPY PSs (**Figure 2.13**) showing intense longer absorption wavelength (570-624 nm) and fluorescence emissions (582-654 nm) in polar solvents. Furthermore, a decrease in fluorescence emission was observed with a decrease in solvent dipole moment. These longer absorption wavelength PSs are thus potential agents for environmental-sensitive fluorescence probes (Yu *et al*., 2017).

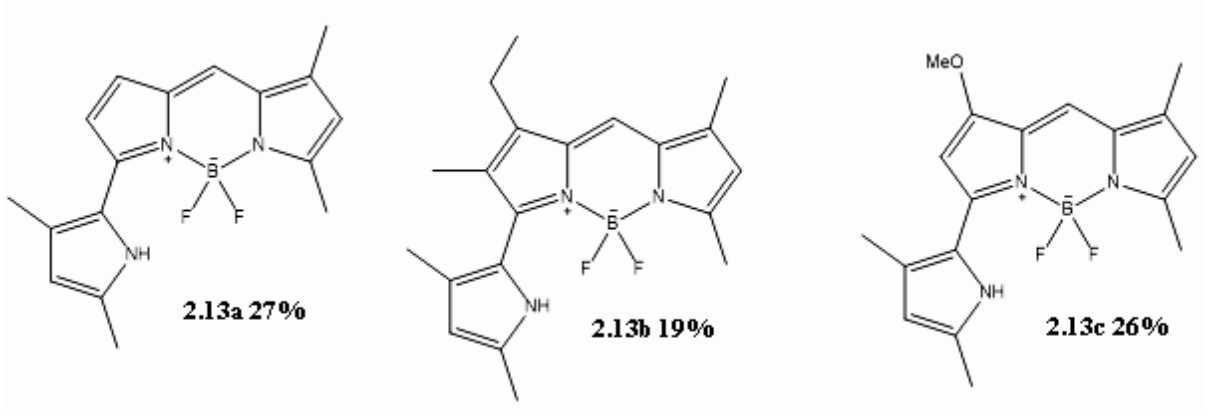

Figure 2.13 pyrrolylBODIPY PSs environmental-sensitive fluorescence probes (Adapted from Yu *et al*., 2017).

2.7.5 BODIPY dyes as biosensors

Biosensors are analytical devices with a biological receptor used to convert a biological response into an electrical signal (Mehrotra, 2016). Distinctively, a biosensor must be independent of physical parameters (such as pH and temperature), should be highly selective and reusable (Cammann, 1977; Thevenot *et al*., 2001). There are three groups of biosensors based on their mechanisms for materials to be used in biosensors: these include, microbe based (containing microorganisms), biocatalysts (comprising enzymes), and bio-affinity (including antibodies and nucleic acids) (Wang *et al*., 2018).

Updike and Hicks (1967) reported on the first enzyme-based biosensor. Enzyme biosensors were based on immobilization methods such as adsorption of enzymes by covalent bonding, van der Waals forces and ionic bonding (Mehrotra, 2016). The commonly used enzymes for this application include; oxidoreductases, amino oxidases, peroxidase, and polyphenol oxidase (Wang, 2008; Akyilmaz *et al*., 2010; Venugopal, 2002). Since the inception of biosensors, applications in many scientific fields including medical fields, and food industry, were found to provide enhanced stability (in terms of reusability) and sensitivity compared to their traditional antibody-targeted-based biosensor counterparts (Mehrotra, 2016; Jean and Shah, 2008).

A study carried out used BODIPY PSs to stain lipids in *Magnaporthe oryzae* (*M. oryzae*) cells. This comes as a possible substitute for the Nile red PS in the study of lipids dynamics in plant pathogenic fungi. They observed that BODIPY PSs were able to distinctly label lipids in the

cells of mycelia and conidia (Wang *et al*., 2018). Furthermore, BODIPY PSs labeled lipid cells were essentially similar to those labeled by Nile red (with poor solubility and susceptibility to quenching). However, BODIPYs shown in **Figure 2.14** displayed enhanced fluorescence labeling capacity, higher specificity, and lowered background compared to the Nile red for lipid dynamics in *Magnaporthe oryzae* (Wang *et al*., 2018). Moreover, Wang and co-workers (2018) realized that BODIPY PSs used to stain the germinating *M. oryzae* conidia allowed the lipid dynamics to be tracked. **Figure 2.14** shows the BODIPY PSs used for biosensors in the study by the Wang group.

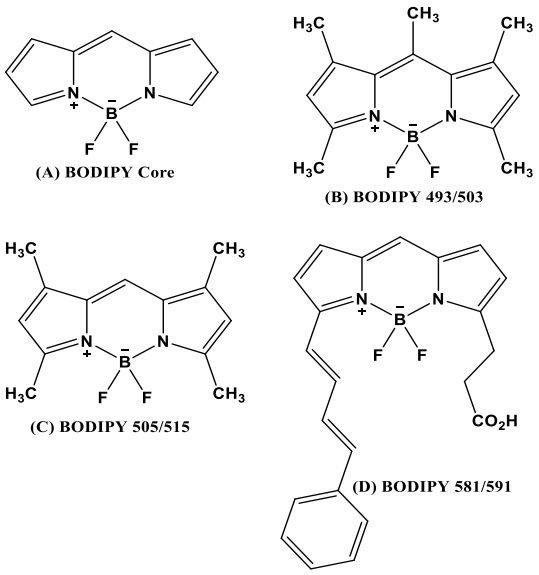

Figure 2.14 BODIPY PSs for lipid dynamics studies (Adapted from Wang *et al*., 2018)

2.8 Synthetic methods for BODIPY dyes

The BODIPYs are primarily formed by the reaction between 2,4-dimethylpyrrole and acetic anhydride in the presence of a complexing agent (boron trifluoride diethyl etherate, $BF_3.OEt_2$), as shown in the **scheme. 2.1** respectively.

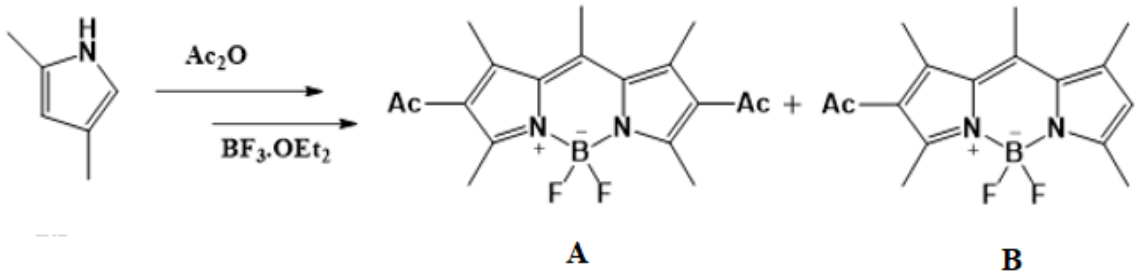

Scheme 2.1 First synthesis of BODIPY 2.15A and 2.15B by Triebs and Kreuzer (Adapted from Triebs and Kreuzer, 1968)

Varied synthetic methods of BODIPY dye derivatives have been identified and used by different research groups in the past few years. Synthesis of BODIPY dyes starts from the condensation of pyrrole with an electrophilic carbonyl compound such as an aldehyde, an acyl chloride, or an acid aldehyde (Loudet and Burgess, 2007). However, the intermediate (unsaturated dipyrromethene) is observed to be unstable and can result in polymerization or may undergo porphyrin formation (Yogo *et al*., 2005). This has led to the use of a pyrrole substituted at position 2 in most synthetic routes because this position has the least electrophilicity and positive charge (Yogo *et al*., 2005). Burgess and the co-worker (Loudet and Burgess, 2007) illustrated three major BODIPY synthetic routes (from pyrrole and aldehyde, pyrrole and an acid chloride, and lastly a pyrrole and a ketopyrrole).

2.8.1 Synthesis of BODIPY dyes from pyrroles and aldehydes

The most simple and straightforward method to achieve symmetrical BODIPY compounds is the acid-catalyzed condensation of an aldehyde with two molecules of pyrrole to afford a dipyrromethane **Scheme 2.2 (2.2A)** (Boens *et al*., 2012). In this reaction, the pyrrole is used as a solvent (Gryko *et al*., 2012) to avoid polymerization of BODIPY PSs. The reaction with substituted pyrrole does not require an excess of pyrrole and it is carried out in normal organic solvents such as dichloromethane, chloroform, and acetonitrile among others. The formed dipyrromethane is then oxidized immediately after preparation resulting in a dipyrromethene as shown in **scheme 2.2 (2.2B)** which is less stable. Addition of a base (triethylamine (Et_3N) or diisopropylethylamine (i-Pr_2Net), followed by boron trifluoride diethyl etherate ($BF_3.Et_2O$), results in symmetric BODIPY dyes as shown in **scheme 2.2 for** BODIPY **2.2**.

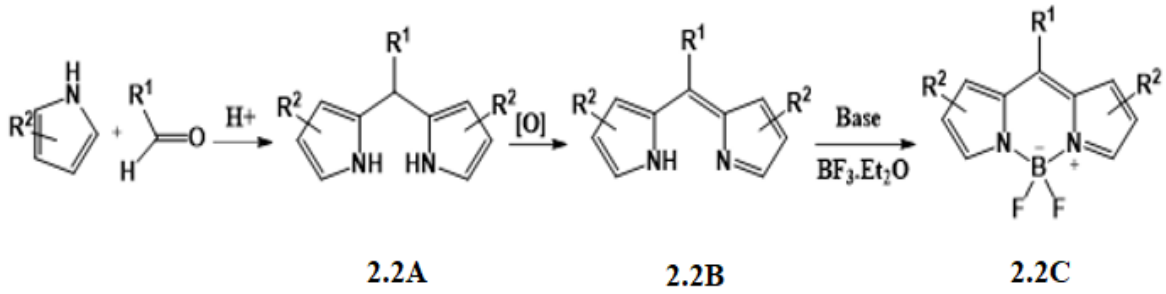

Scheme 2.2 Synthesis of BODIPY dyes through aldehyde condensation in the presence of a pyrrole (Adapted from Wagner *et al*., 1996).

Using the acid-catalyzed condensation of an aldehyde, a large number of BODIPY dyes can be synthesized from readily (commercially) available pyrroles, affording varied substituents on the pyrrole (R_1) and the meso (R_2) position of the BODIPY dye. Other studies have demonstrated that substituents at positions-1 and 7 of the BODIPY dye limits the aromatic group rotation at the meso-position (Boens *et al*., 2012). This results in an orthogonal geometry with reduced electronic coupling between the meso-substituent and the dye (Boens *et al*., 2012). This method involves a one-pot synthesis without having to isolate the intermediates. Vicente and co-workers (Vicente *et al*., 2013) for example, synthesized BODIPY **2.3a** from the reaction between a substituted pyrrole and a phenyl ether aldehyde as illustrated in **scheme 2.3.**

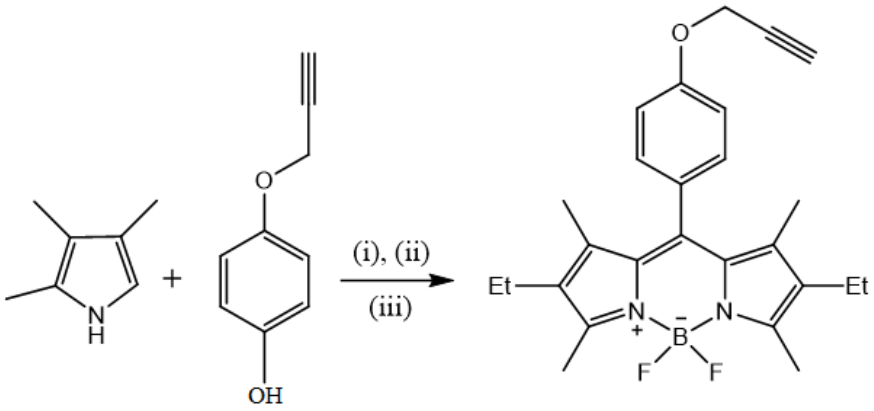

Scheme 2.3 synthesis of substituted BODIPY dye; Reagent and conditions; (i) TFA and CH_2Cl_2; (ii) DDQ; (iii) NEt_3, $BF_3.OEt_2$, 84% (Adapted from Vicente *et al*., 2013).

2.8.2 Synthesis of BODIPY dyes from ketopyrroles by condensation of pyrroles with acid chlorides or benzaldehyde derivatives

Another method of synthesis is that involving the use of ketopyrroles (Tahtaoui *et al*., 2007). This method can be carried out in a one-pot synthesis as well. Unsymmetrical BODIPY dyes, substituted or unsubstituted at meso-position cannot be prepared using the carboxylic acid and aldehyde methods (Li *et al*., 2006). They can be synthesized using ketopyrrole condensation with a second pyrrole in the presence of a Lewis acid and complexed with boron trifluoro ethyl etherate ($BF_3.Et_2O$) followed with the addition of a base to give unsaturated BODIPY dyes as shown in **scheme 2.4**.

Scheme 2.4 Synthesis of unsymmetrical BODIPY 2.18a from ketopyrrole (adapted from Tahtaoui *et al*., 2007)

The advantage of condensation of pyrroles with acid chlorides or benzaldehyde derivatives method is that it does not make use of an oxidation agent which can result in the formation of many by-products (Tahtaoui *et al*., 2007). Furthermore, symmetrical or unsymmetrical BODIPYs can be formed in a one-pot synthesis method without the need for isolation of the unstable dipyrromethene dihydrochloride salt intermediate which is difficult to remove (Adapted from Boens *et al*., 2012). However, there is a need in this method, for the isolation of the ketopyrrole intermediate to synthesize an unsymmetrical BODIPY dye derivative. For example, Duportail and co-workers (Tahtaoui *et al*., 2007) used this method to synthesize BODIPY **2.5C** as shown in **scheme 2.5**. A ketopyrrole (as shown in **scheme**) is first synthesized from the reaction of 4-iodobenzoyl chloride with a magnesium salt of 2,4-dimethylpyrrole (which is formed by deprotonation with methyl magnesium bromide (MeMgBr). Then, condensation of a ketopyrrole with the second 2,4-dimethylpyrrole in the presence of phosphoryl chloride ($POCl_3$) results in the formation of dipyrromethene (**2.5b)** as shown in **scheme 2.5**. The resulting product is finally complexed with boron trifluoro ethyl etherate ($BF_3.Et_2O$) in the presence of triethylamine producing the symmetrical BODIPY (**in scheme 2.5)**.

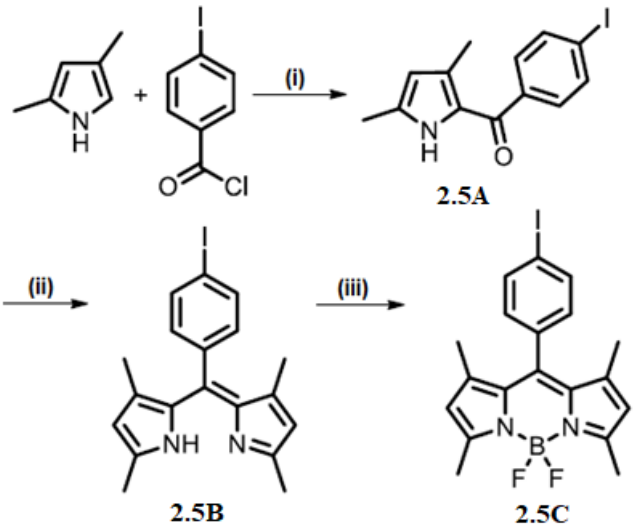

Scheme 2.5 Synthesis of symmetrical BODIPY, Conditions and reagents; (i) methyl magnesium bromide, ethyl etherate, 35 °C, 30 min, 81%; (ii) 2,4-dimethylpyrrole, phosphoryl chloride, CH_2Cl_2/pentane, 0 °C, r.t., 24 h, 46 %; (iii) $BF_3.OEt_2$, triethylamine (Et_3N), toluene, 80 °C, 30 min, 80 % (Adapted from Boens *et al*., 2012).

2.8.3 Synthesis of BODIPY dyes from carboxylic acids

Another method for the synthesis of symmetric BODIPY dyes is the acid-catalyzed condensation of pyrroles with an acylium equivalent, such as acid chlorides, an aldehyde, or an orthoester (Ziessel *et al*., 2006). In this synthetic route, often the acylpyrrole intermediate is not isolated. It is reacted with an excess of pyrrole under acidic conditions to form a dipyrromethene. Dipyrromethene is then treated with a base and complexed with boron trifluoride ethyl etherate ($BF_3.OEt_2$) to afford a symmetrical BODIPY dye as shown in **scheme 2.6** to afford **BODIPY 2.6A**.

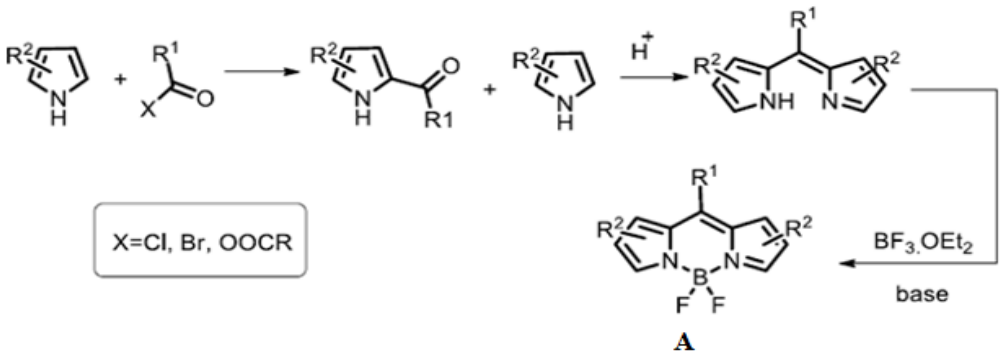

Scheme 2.6 General synthetic diagram for symmetrical BODIPYs from acylation of pyrrole followed by condensation and complexation (Adapted from Boens *et al*., 2012).

2.9 Functionalization methods of BODIPY dyes

The functionalization of BODIPY dyes is an imperative feature in the study and application of the organic dyes. BODIPY dyes are easy to functionalize using different methods. Refer to BODIPY core numbering system (**Figure 2.5/6**)

Substitution at the meso-position is the most preferred mode of functionalization of BODIPY dyes. Some studies have revealed that substitution at the meso-position with aryl groups has an unnoticeable effect on the BODIPY absorption and emission bands (Loudet and Burgess, 2007). However, substitution at positions 1 and 7 as shown in **Figure 2.15** with methyl groups shows higher fluorescence quantum yields than for their un-substituted BODIPY counterparts. Notably, this is because substitution at this position prevents free rotation of the phenyl rings substituted at the meso-position as illustrated in the figure below (Loudet and Burgess, 2007).

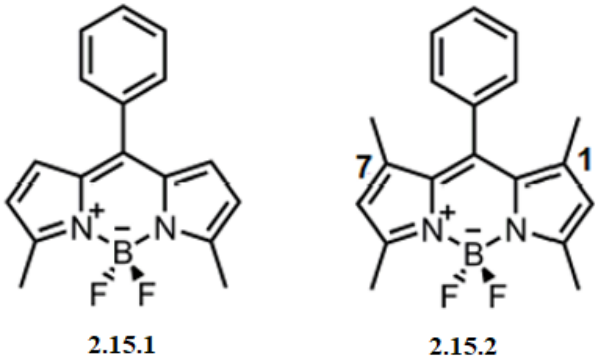

2.15.1 2.15.2

Figure 2.15 BDP1 phenyl substituted BODIPY, 2 aryl-substituted at positions 1 & 7 (Adapted from Lakshmi *et al*., 2016). The fluorescence quantum yields in literature for BODIPY 1 & 2 were found to be 0.19 and 0.65 in methanol.

Functionalization at position 2 and position 6 is of interest to most researchers. These positions can afford the attachment of a variety of substituents to the BODIPY core structure such as sodium sulfate (Burgess *et al*., 2008) and halogenation (Loudet and Burgess, 2007) to mention a few. Studies carried out by Triebs *et al*., (1968) demonstrated electrophilic sulfonation of BODIPY core structures at positions 2 and 6 **figure 2.16** resulting in the stability and solubility (in aqueous solutions) of BODIPY PSs compared to the BODIPY core that was not functionalized.

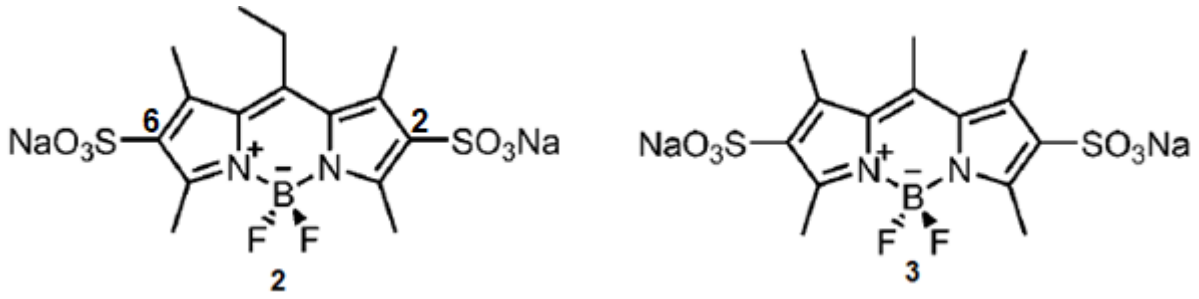

Figure 2.16 BODIPY core functionalized at positions 2 and 6 (Burgess *et al*., 2008)

In another study reported on by Loudet and Burgess, (2007), they demonstrated that functionalization of BODIPY at positions 2 and 6 could be achieved by using bromine (Br) and iodine (I) (resulting in dibrominated and diiodinated BODIPY derivatives respectively) which are heavy atoms. These also showed enhanced red shifting of absorption and emission maxima. **Figure 2.17** shows the substitution at positions 2 and 6 of the pyrrolic BODIPY positions.

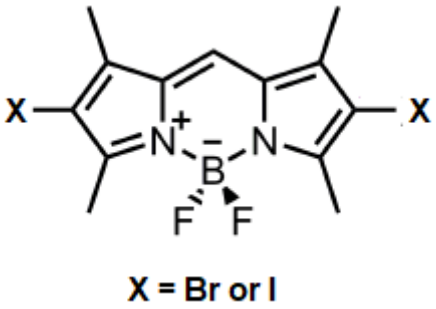

Figure 2.17 Heavy atom functionalized BODIPY core (Loudet and Burgess, 2007).

Substitution at position 3 and 5 of the BODIPY core as seen in **Figure 2.18** has also been attempted by many (Ulrich *et al*., 2008; Loudet and Burgess, 2007; Rohand *et al*., 2006; Rurack *et al*., 2001). Functionalization at positions 3 and 5 has a significant effect on absorption and emission spectral shifting and fluorescence quantum yields (Ulrich *et al*., 2008). However, substituents at this position will dictate this differently. Loudet and Burgess, (2007), observed that substitution with an amine and thioalkaloides at positions 3 and 5 resulted in bathochromic shifting on both absorption and emission spectra (Loudet and Burgess, 2007).

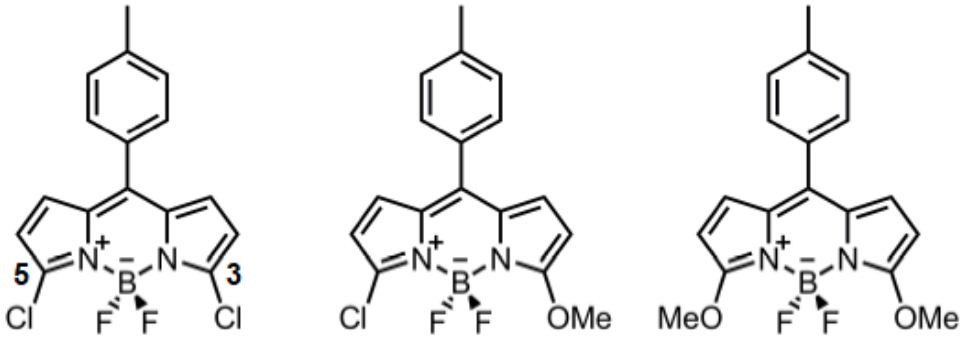

Figure 2.18 BODIPY functionalized at positions 3 and 5 (Ulrich *et al*., 2008).

Functionalization at positions 3 and 5 with methyl groups affords high yields with the Knoevenagel reactions due to the methyl group's acidic character (Shah *et al*., 1990, Rurack *et al*., 2001). Also, possible functionalization methods at positions 3 and 5 would include the: transition metal-catalyzed reactions such as the Stille reaction, Suziki reactions, Heck coupling, and Sonogashira reactions (Shah *et al*., 1990; Yogo *et al*., 2005). These reactions afford BODIPY dyes with extended conjugation and broad emission maxima (Boyer *et al*., 1993). **Figure 2.19** shows some of the synthesized BODIPY dyes functionalized at positions 3 and 5 by different research groups.

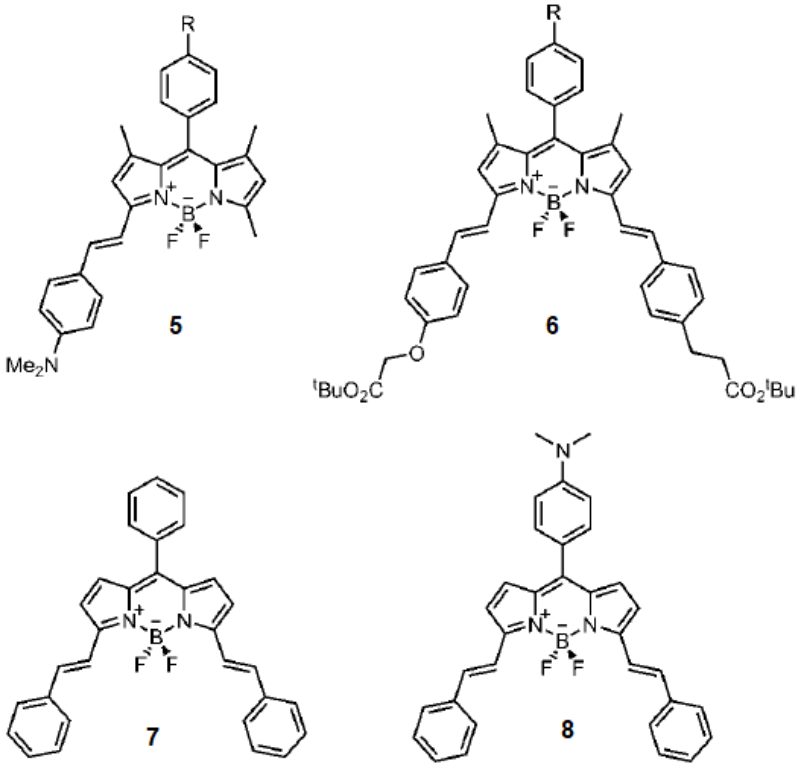

Figure 2.19 BODIPY dyes with extended conjugation from literature (Adapted from Shah *et al*., 1990; Yogo *et al*., 2005; Rohand *et al*., 2006; Rurack *et al*., 2001)

Furthermore, substitution can be carried out on the B-(4-position) of the pyrrolic boron center. Ulrich and co-workers (2005) realized that it was possible to substitute the fluorides of the BF_2 moiety of the BODIPY core under different conditions. This was achieved by substitution of fluorine (F) atoms with ethylene by treating the BODIPY dyes with lithiated ethynylaryls (**Figure 2.20**) in tetrahydrofuran (THF) under mild reaction conditions (Ulrich *et al*., 2005). This approach introduces a wide range of ethynylaryl moieties at the boron center of the BODIPY dyes by replacing the fluoride atoms. Moreover, this leads to the introduction of functional groups such as ethynylanthracene, ethynylpyrene, ethynylterpyridine, ethynylperylene as well as other protected ethynyl groups **Figure 2.20** (Goze *et al*., 2007). **Figure 2.20** demonstrates a summary of different synthetic methods for the functionalization and synthesis of varied BODIPY PSs.

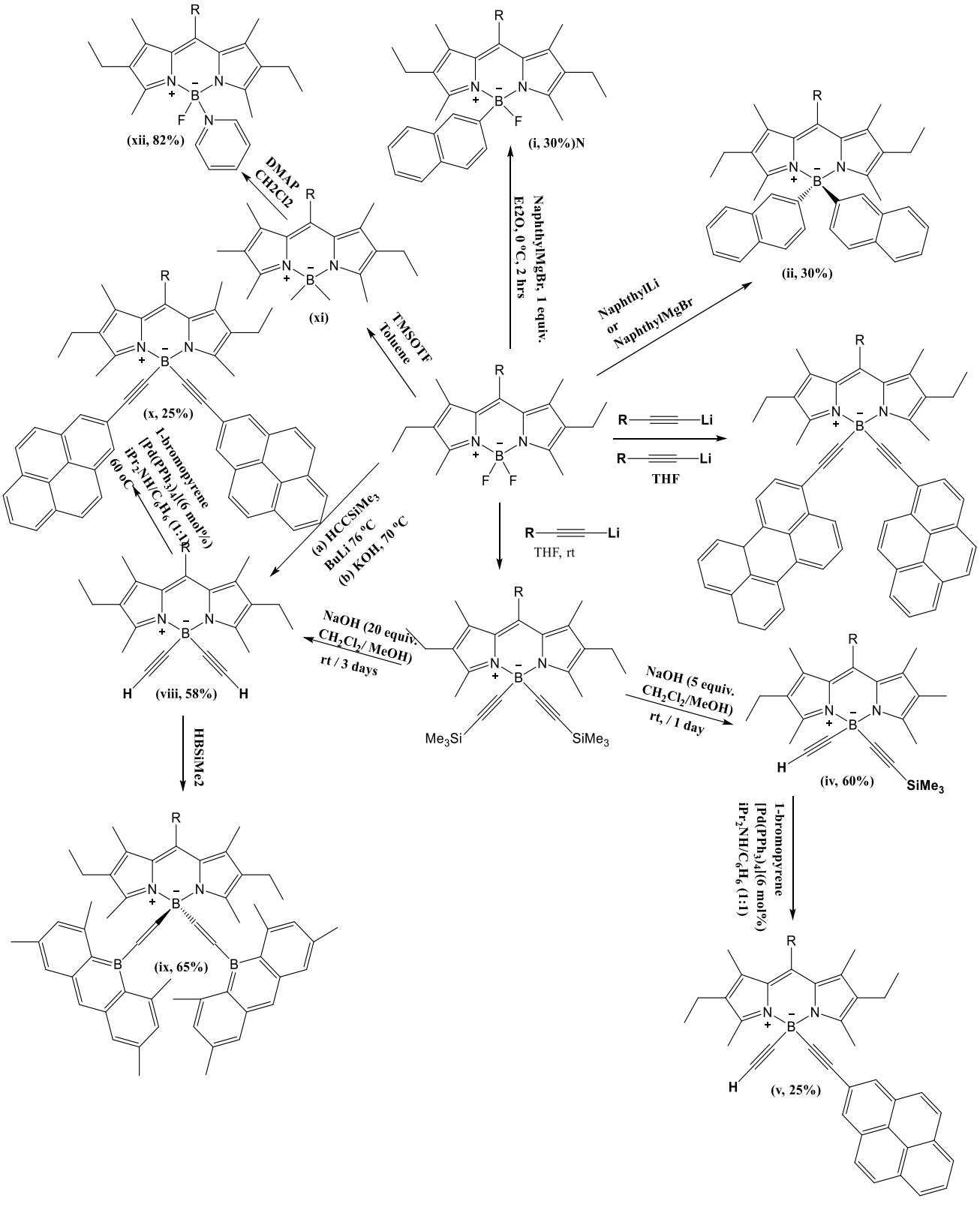

Figure 2.20 Other synthetic methods for BODIPY Derivatives (Adapted from Lakshmi *et al*., 2016; Awuah *et al*., 2012).

2.10 Photochemical and Photophysical properties of BODIPY dyes

Many desirable photochemical and photophysical properties of BODIPY dyes arise from the fully conjugated dipyrrin system that contains the boron bridged nitrogen core (Loudet and Burgess, 2007; Ziessel *et al*., 2007; Boens *et al*., 2012). The BODIPY dye framework commonly demonstrates fluorescent quantum yields greater than 0.50 depending on the structural framework and their extinction coefficients are frequently beyond 50000 $M^{-1}cm^{-1}$. BODIPY dyes also demonstrate narrow absorption and emission bands around 500 nm with minimum stokes shift(s) commonly below 15 nm (Loudet and Burgess, 2007, Ziessel *et al*., 2007; Umezawa *et al*., 2009; Ni and Wu, 2014). The BODIPY framework holds the potential for structural modifications that allow for fine-tuning of their chemical and photochemical properties. **Figure 2.21** highlights the role of structural modifications to the BODIPY core with small molecules and their influence on optical properties. **Figure 2.21** demonstrates eight BODIPY derivatives. Seven of these differ from the core BODIPY molecule by the substituents attached at the β, α-pyrrolic, and meso positions. The BODIPY dyes differ from BODIPY 1 and 5 in that they possess di (BODIPY 2 and 6), tetra (BODIPY 3 and 7), and hexamethyl groups (BODIPY 4 and 8) at the pyrrolic positions of the BODIPY structure (Tram *et al*., 2009; Bandichhor *et al*., 2006; de Wael *et al*., 1977). Additionally, **Figure 2.21** also demonstrates the meso-phenyl adducts of these BODIPY derivatives BODIPY 5 to 8 (Bröring *et al*., 2008; Kee *et al*., 2005) which shows different photophysical properties.

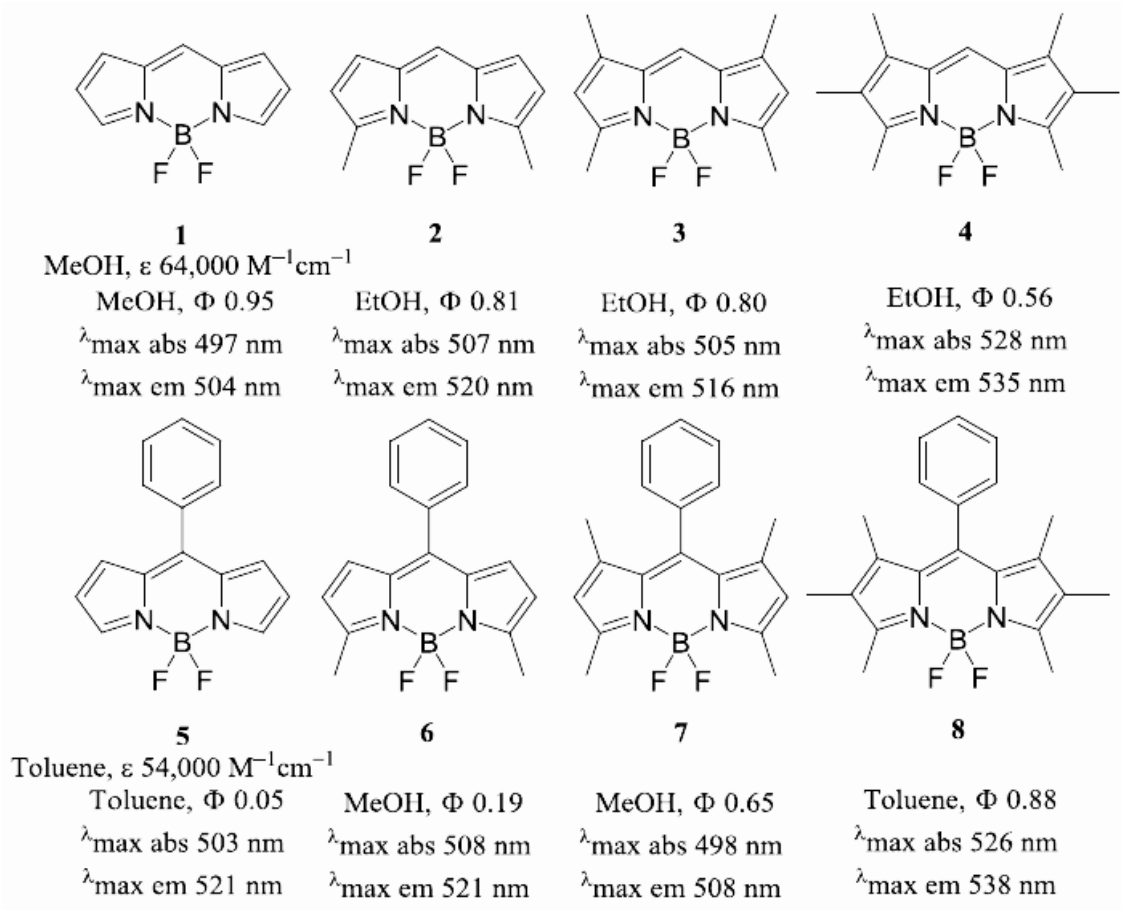

Figure 2.21 Properties of BODIPY dyes (Adopted from de Wael *et al*., 1977; Bandichhor *et al*., 2006)

Various factors affect the fluorescence strength of BODIPY dyes (Boens *et al*., 2012). However, two primary modifications result in the most significant bolstering of fluorescence and quenching effects of fluorescence quantum yields. The first modification that enhances or quenches fluorescence quantum yields would be the presence or the absence of a functional group at the meso-position depending on its electronic nature and steric freedom (Loudet and Burgess, 2007). The second modification results from the type and level of substitution on the BODIPY periphery along with positions 1-3 and 5-7 as a collective. The most relevant fluorescence quantum yield modification was witnessed through functionalization at the meso-position of the BODIPY core (Loudet and Burgess, 2007). As demonstrated in **Figure 2.21**, the comparisons of BODIPY 1 and BODIPY 5 substituted at meso-position with a phenyl ring, their fluorescence quantum yields, and extinction coefficients were recorded to be 0.05 for BODIPY5 as opposed to 0.95 for BODIPY1. The study indicated that the extended conjugation position 8 or meso-substitution with a benzene ring quenches the fluorescence capacity of the BODIPY PS. Quenching is explained by the freedom of electrons delocalization and rotation

on the phenyl ring at the meso-position of the BODIPY core structure (Loudet and Burgess, 2007).

Last but not least on BODIPY dyes is their characterization. The main method by which BODIPY PSs can be characterized includes but is not limited to FTIR spectroscopy which establishes the presence of functional groups on the skeleton structure. NMR spectroscopy was are used to study the proton and carbon chemical shifts to elucidate the BODIPY structures while mass spectrometry is used to study the elemental and molecular charge to mass ratio and their fragmentation patterns. UV-Vis and Fluorescence spectroscopy are used to study the optical properties (as shown in chapter 4). As highlighted earlier, there are many other instruments used to study these molecules respectively.

2.11 Drug delivery systems

Drug delivery systems are defined as the formulation of drugs suitable for oral administration (tablets) or intravenous administration (in solution) (Suhasini and Babu, 2016). The development of new drugs is time-consuming and comes at a high cost. The improvement of the efficacy of old drugs has been attempted using different methods such as dosage titration, therapeutic drug monitoring, and individualizing drug therapy. Also, drug delivery at a controlled rate, targeted delivery, and slow delivery is globally being pursued (Suhasini and Babu, 2016).

Classifications of drug delivery systems include; transdermal delivery systems, implantable drug delivery systems, carrier-based delivery systems, nasal delivery systems, and variable release delivery systems (Suhasini and Babu, 2016). Moreover, these new approaches can improve the effectiveness of drugs by reducing problems associated with solvency and protect drugs from harsh environments (such as a change in pH and photodegradation) (Nirmala and Nagarajan, 2016; Koushik *et al*., 2016). Additionally, these can control drug concentration at the site of activity, lessen the time of introduction at a non-focus tissue and enhance therapeutic consistency (Koushik *et al*., 2016; Gopi *et al*., 2016; Nirmala and Nagarajan, 2016; Mandal, 2016; Dudhipala *et al*., 2016). Advantages associated with drug delivery include; the ease of drug administering, quick onset of action and absorption, favorable environment and simple formulations, bioavailability, and accurate dosing consistency (Koushik *et al*., 2016). However, disadvantages would be the insufficient availability of data for penetration enhancers and unfavorable immunogenic reactions that may occur (Koushik *et al*., 2016; Gopi *et al*., 2016; Nirmala and Nagarajan, 2016; Mandal, 2016; Dudhipala *et al*., 2016).

There have been great advancements in drug delivery systems in recent years which have enabled simpler routes of drug administration (Zhu, 2013; Suhasini and Babu, 2016). Wide research on drug delivery systems on their ability to deliver drugs to a designated target tissue has been carried out. The use of drug carriers (materials that play a crucial role in the delivery and effectiveness of drugs) are at the forefront of targeted delivery of drugs (Kondrashina *et al*., 2013; Gallud A and Silva, 2013; Suedee, 2013; Mostafavi and Babu, 2013; Zhu, 2013). However, there are varieties of drug carriers with varied limitations including; nanoparticles, implants, liposomes, nerve fiber polymers, micelles, vesicles, microspheres liquid crystals, and others. (Suhasini and Babu, 2016). This study is centered on the metallic rod-shaped nanoparticles because of their properties such as small size to volume ratio, solubility, cell permeability, etc. to mention but a few. Furthermore, nanorods have gained more interest in therapeutic applications, because they possess large surface area for drug carriers, electronic properties (aspect ratio), solubility, and cell penetration (Suhasini and Babu, 2016).

2.12 Nanoparticles

The prefix" nano," means "dwarf" in Greek and a nanometer is a metric unit of length denoting one billionth of a meter or 10^{-9} m (Mansoori and Soelaiman, 2005). Nanoparticles are particles with one of their three dimensions smaller than 1000 nm (Busbee *et al*., 2003). They can have a crystalline or amorphous form. Many nanoscale materials are characterized by their shape and size-dependent, catalytic, optical, and electronic properties (Busbee *et al*., 2003). Nanomaterials have gained increasing attention in research due to their potential applications in diverse fields (Eustis and El-Sayed, 2006; Hu *et al*., 2006; Yin and Alivisatos, 2005). Since the inception of nanotechnology over the past decades, many researchers and research groups were able to synthesize nanomaterials with controllable and varied shapes. These include zero-dimensional nanomaterials (nanospheres and nanoshells) (Liang *et al*., 2004; Pedireddy *et al*., 2014; Gao *et al*., 2012), One-dimensional nanomaterials (nanorods and nanowires) (Ye *et al*., 2012; Wang *et al*., 2004; Tang *et al*., 2002), two-dimensional nanomaterials (nanoplates, nanoprisms, nanosheets, and nanodisks) (Zhang *et al*.,2011; Chen *et al*., 2014) and finally three-dimensional nanomaterials (nanoflowers) for various applications (Chen *et al*., 2009). However, the practical applicability of these nanomaterials has been limited by their high production cost and low volume production. Hence, the development of high-quality nanomaterials production in large scale synthetic protocols is highly desirable.

The physical and chemical properties of nanoparticles change completely from the properties of their bulk materials (Buzea *et al*., 2007). This is because there is a change in physical properties since there is a transition from micrometer to nanometer sizes (Buzea *et al*., 2007; Nagarajan and Hatton, 2008). The particle size and the surface area to volume ratio are the major factors predominating the quantum effect of nanoparticles (Munoz-Florez et al., 2011). As particles become smaller and smaller in size, they exhibit the quantum mechanical behavior of the particles (Munoz-Florez *et al*., 2011). Also, nanoparticles are classified based on morphology, composition, dimensionality, and agglomeration (Buzea *et al*., 2007). Below in **Figure 2.22** shows the classification of nanoparticle dimensionality, morphology, agglomeration, and composition.

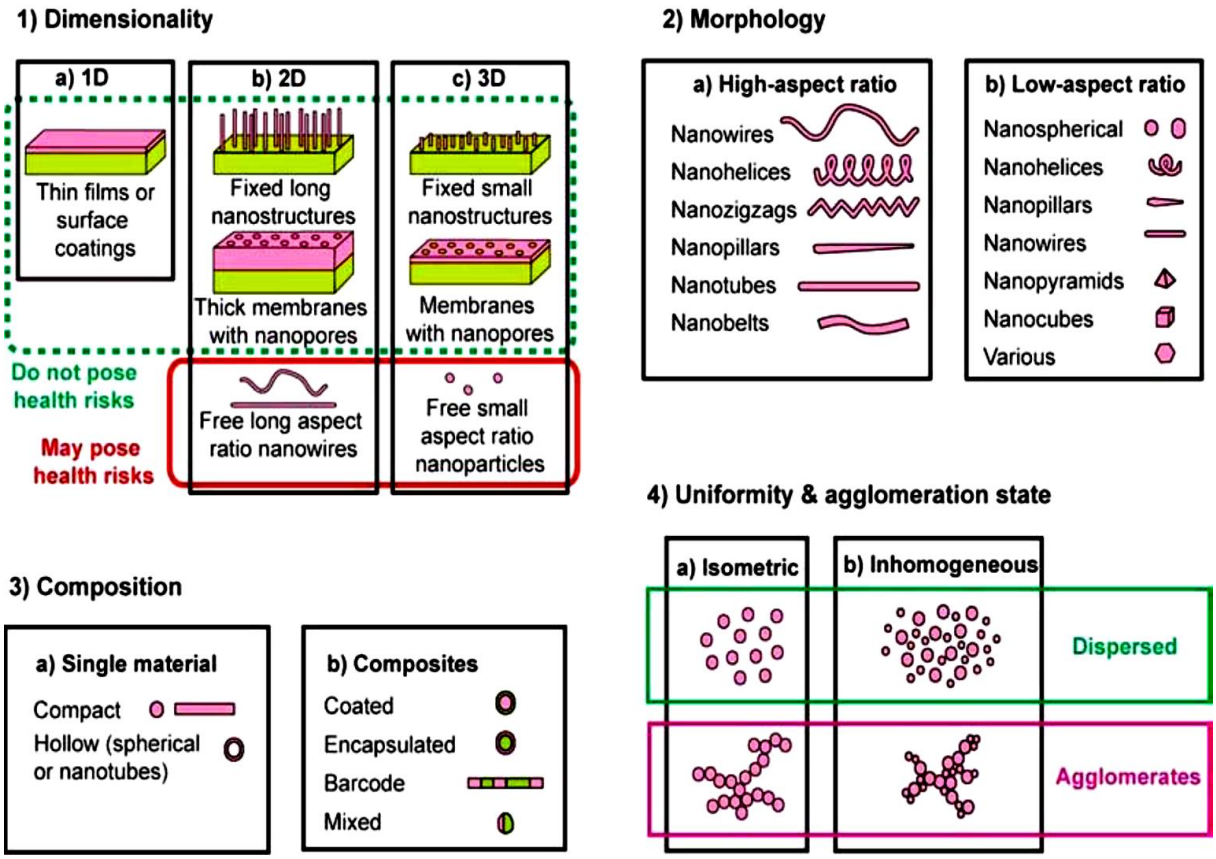

Figure 2.22 Classification of nanostructured material (Adapted from Buzea *et al*., 2007)

Two-dimensional metal nanostructures have been studied extensively in recent years due to their potential application in a wide range of fields from medicine to sensors. These interests arise from their attractive properties including solubility, great surface area to volume ratio,

electronic and optical properties, mechanical and catalytic properties (Xia *et al*., 2003). Their potential applications as active components of nanophotonic devices, fabrication of sensing devices, nanoscale electronic and magnetic nanoparticles (Gu *et al*., 2006).

This study demonstrates the use of two-dimensional nanoparticles (Pt NRs) as potential drug carriers to overcome the challenges associated with drug solubilization and drug concentration for enhancing the therapeutic agents' efficiency. The choice for Pt NRs in this study emanates from their use as delivery vehicles and also due to their photothermal properties (they have been shown to result in less heat effect upon irradiation with light), enhance adsorption efficiency (loading capacity) which facilitates drug loading and their large production in their synthesis procedure (Buzea *et al*., 2007, Shanmugam *et al*., 2005).

Moreover, the size distribution, surface charge, and surface area, degree of aggregation, and surface chemistry are important parameters that require measurement. Nanoparticles may be characterized by TEM (size distribution), SEM (morphology), XRD (crystallinity and patterns), DLS (surface charge and size distribution). Nanoparticle size and shape are the most studied parameters in the characterization of these materials.

2.12.1 Metallic Nanoparticles

Metallic nanoparticles have unique properties compared to their large bulk materials particularly with properties such as high surface plasmon resonance (SPR), luminescence, and combined light scattering (Kelly *et al*., 2003). It has been shown in recent research that SPR position on the spectral scale is very sensitive to size (Kelly *et al*., 2003), shape (Sosa *et al*., 2003), and the environment (Meskinies *et al*., 2016; Bulevinets *et al*., 2017). These properties are very important in determining the optical and physicochemical properties of these nanoparticles. Nanotechnology has made it easy to tune the characteristics of metallic materials. These metallic materials properties can be completely changed by altering their confinement of electromagnetic components and their large surface to volume ratio (Sao, 2009). As a result, metal particles at a nano size scale exhibit outstanding optical, chemical, electrical, physical, and catalytic properties compared to their bulk counterparts (Burda, 2005; Wilcoxon, 2006; Daniel, 2004).

The interesting and overwhelming interest of metallic nanoparticles is influenced by their size, shape, morphology, composition, and crystallinity (Shanmugam *et al*., 2005, Dickson and Lyon 2000). In essence, the synthesis of metallic nanoparticles can be adopted by controlling

the above-mentioned parameters. Various synthesis methods have been explored and reported using and include electrochemical synthesis and solution phase synthesis (Tian, 2007), template-based growth synthesis (Jana, 2001), and photochemical synthesis (Jin, 2001).

Among these synthetic approaches, the solution-phase reduction method is a widely utilized method due to its remarkable advantages. These specifically include flexibility in controlling the reaction parameters, cost-effectiveness and simplicity, the possibility of large quantity production, and easy surface modification. The solution-phase synthesis involves the reduction of metal ions in the presence of a surfactant (capping or stabilizing agent) with a reducing agent in the reaction mixture. The formation of nanoparticles (PNs) involves growth mechanisms and nucleation (LaMer, 1950). Therefore, it was with these remarkable properties that this study was centered on the use of metallic nanoparticles to serve as drug delivery vehicles.

2.12.2 Other nanoparticles used in drug delivery systems

2.12.2.1 Liposomes

Liposomes are spherical mixtures of perishable vesicles whose size varies from low micrometers to tens of micrometers in diameter (Gundogdu *et al*.,2013; Vashist and Venkatesh, 2012). They are comprised of a bilayer sometimes derived from phospholipids with mixed lipoids chains or outlined chemical chains and heads of artificial lipids (Liu, 2012; Gundogdu *et al*., 2013). The drug may be entrapped either at the phospholipid bilayer interphase or in binary compound volume (Swain, 2012). This drug carrier vehicle is advantageous in increasing drug concentration levels in cancerous cells and decreases the exposure to normal cells. The selectivity of the nanoparticles is enhanced by functionalization with targeting agents (Swain, 2012; Swaminathan and Jablonski, 2012; Liu, 2012). Furthermore, liposomes (**Figure 2.23**) which enhance the therapeutic results of anti-cancer agents because of their hydrophilic tail and hydrophobic internal structure that can deliver to the targeted area. Moreover, liposomes play a crucial role in bioavailability, solubility, targeting, prolonged drug release, and sweetening (Swain, 2012; Swaminathan and Jablonski, 2012; Liu, 2012). This can be achieved by the synthetic design of the liposomal nanoparticle and their targeted release can be achieved by the use of biodegradable materials/polymers (Gundogdu et al.,2013).

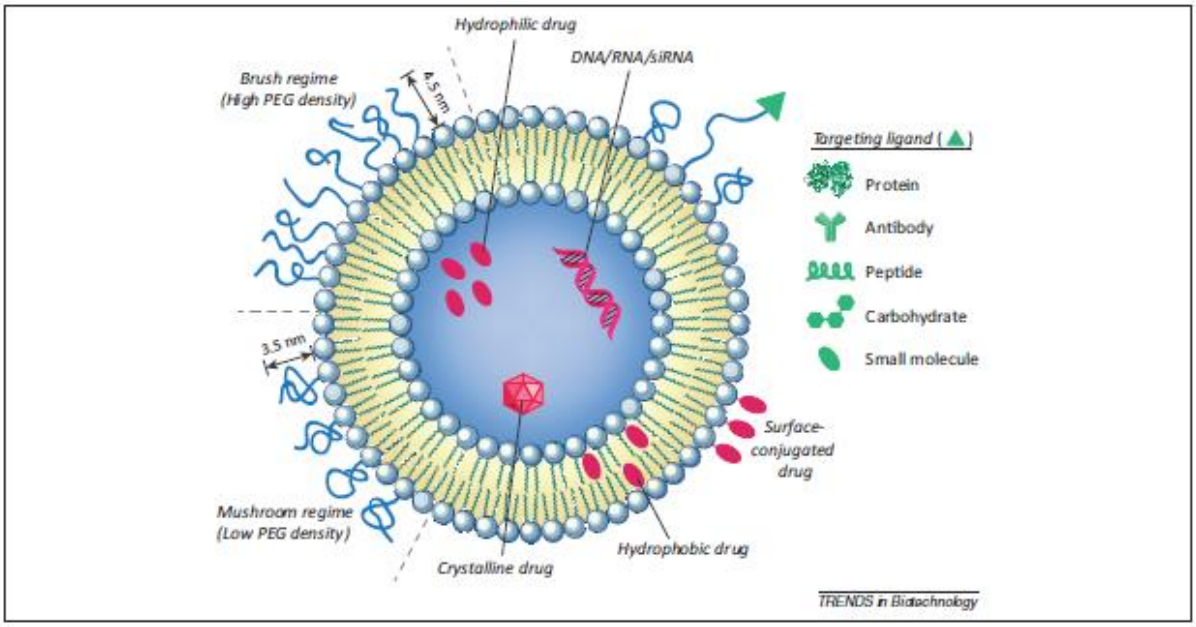

Figure 2.23 Structural and design considerations for liposomal drug delivery (Adapted from Noble *et al*., 2014)

Micelles are nano-analogs developed from amphiphilic polymers (Noble *et al*., 2014). Micelles form aggregates of nanosized diameters (Kabanov et al., 1995); when individual polymer chains (the monomers) are dissolved directly in the aqueous solution above a threshold concentration (known as the critical micelle concentration CMC) and solution temperature (critical micelle temperature). In a dialysis method, amphiphilic polymers with very low water solubility are dissolved in a volatile solvent then dialyzed against an aqueous buffer solution to form micelles (Allen *et al*., 1999). Their preferred use is because of their synthesis from biodegradable polymers which makes them easy to clear from the body after drug delivery (Noble *et al*., 2014). Below in **Figure 2.24** is a polymer micelle nanoparticle that shows the preparatory route and the structure of a micelle nanoparticle.

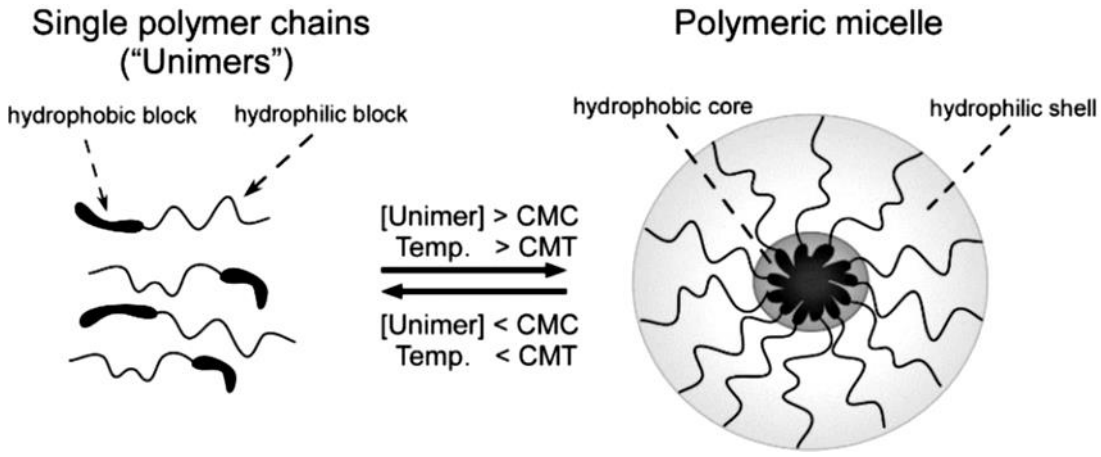

Figure 2.24 Schematic diagram of a polymer micelle (Adapted from Buzea *et al*., 2007)

2.13 Microbial species and their virulence factors

2.13.1 Background

The problem of antibiotic resistance in pathogenic microbial species is a global challenge that has gained heightened attention in recent years. This has resulted in increased research efforts to come up with alternative effective ways for treating bacterial and fungal infections, and cancers. Many approaches have been widely studied and resistance is persistent, hence the introduction of alternative methods including photodynamic antimicrobial chemotherapy (PACT) or antimicrobial photodynamic inactivation (API) (Dlugaszewska *et al*., 2017). Photodynamic antimicrobial chemotherapy or API is similar to photodynamic therapy (PDT) against neoplastic cells (Dlugaszewska *et al*., 2017).

Generally, these therapies are based on the monitoring of an anticancer or an antimicrobial agent (photosensitizer) which accumulates in the microbial or the tumor cells. These photosensitizers (PSs) then generate toxic species known as reactive oxygen species (ROS) that causes cell damage or cell death upon irradiation with light. Photosensitizers when under irradiation with a light of a specific wavelength get excited from the ground state to the excited state. High energy PSs undergo intersystem crossing (ISC) to triplet excited state. Once in the triplet state, PSs transfer energy to the molecular oxygen to generate ROS in the form of single oxygen species ($^1O_2$), hydroxyl radical species ($HO^{\cdot}$**),** and super oxygen (O_2^-) (Zhou *et al*., 2016).

Many studies have been carried out by different research teams around the globe, with PACT showing great effectiveness *in vitro* and *in vivo* studies against; fungi (Tavares *et al*., 2010),

bacteria (Allison *et al*., 2010), viruses (Shirasu *et al*., 2013) and protozoa (Vatansever *et al*., 2013). Photodynamic antimicrobial chemotherapy was found to be an option for the control of antimicrobial biofilms formation (Dlugaszewska *et al*., 2017).

2.13.2 Photosensitizer Antimicrobial compounds

Antibacterial and antifungal photodynamic inactivation (API) studies have proven to be a promising method to curb problems associated with resistance of microorganisms to anti-microbial agents. Novel photosensitizers with properties to kill bacteria and fungi are worthy of pursuing in the current research (Taraszkiewicz *et al*., 2013; Collins *et al*., 2010; Junqueira *et al*., 2012). Most of the extensively studied dyes include but are not limited to: porphyrins, phenothiazine, cyanines, phthalocyanines (Pcs), and boron dipyrromethene (BODIPY) dyes. Phthalocyanines are porphyrin related heterocyclics that draw a lot of attention due to their physicochemical and potential application in medicine and technology (Ranyuk *et al*., 2013; Yano *et al*., 2011). The physicochemical properties of these exciting compounds can be enhanced through the addition of a metal cation in the centre of the phthalocyanine core (Mack and Kobayashi, 2011). However, their applications are limited due to their side effects that include: photosensitization even after therapy. Major challenges on the application of porphyrin-based PSs involve a lipophilic-hydrophilic balance for the desired effect of PSs (Yano *et al*., 2011).

Another class of interesting compounds or PSs that has gained very much interest in recent decades is the boron dipyrromethenes also known as (BODIPY dyes). BODIPY complexes are less toxic and they are stable at physiological pH environments, making them ideal candidates for biological applications (Chang *et al*., 2017). The variety of BODIPYs synthetic methods allows manipulating different strategies to achieve an adequate relationship between the BODIPY structure and the desired photophysical and spectroscopic characteristics (Loudet and Burgess, 2007; Wood and Thompson, 2007). Thus, BODIPY structures are modified to increase their singlet-to-triplet intersystem crossing for applications in PDT and PDI/aPDT (Dichiara *et al*., 2017). Therefore, attachment of heavy atoms directly to the BODIPY on the s-indacene ring produces a long-lived electronic excited triplet state enabling efficient production of reactive oxygen species (Yogo *et al*., 2005). This study is centered on the synthesis of BODIPY PSs due to the above-mentioned properties and physical characteristics.

2.13.3 General background on pathogens

Pathogens are known to be microscopic organisms that have the potential to cause infections. There are different types of pathogens including bacteria, fungi, protozoa (including ameaba, plasmodium), and viruses (Eigenbrode *et al*., 2018). Furthermore, these pathogens may cause minor or life-threatening illnesses; it is worth mentioning that not all microbes are pathogenic. The human body consists of thousands of bacterial, protozoa, and fungal species that are part of human flora also called commensals. These are beneficial microorganisms and important for the proper functioning of biological activities including immune system functions and digestion. They become pathogenic when they colonize locations in the body that are germ-free or when the immune system is compromised. In contrast, pathogenic organisms have common goals of survival and multiplying in the host. Pathogens survival conforms by infecting their host, bypass the hosts' immune response, reproduce and transmit to other hosts (Bailey, 2018).

Transmission of pathogens can occur in two different ways including (i) direct transmission (through the direct body to body contact). This type of transmission can occur through mother-to-child as exemplified with Zika, HIV, and syphilis. Furthermore, direct transmission can also occur through kissing (herpes simplex virus), touching (MRSA), and sexual contact (human papillomavirus HPV). Another way of transmission is (ii) indirect transmission which may occur with contact between a contaminated substance with a pathogen. Examples of indirect transmission include airborne pathogens (through sneezing and coughing), droplets (contained in blood or saliva), foodborne (eating contaminated food), waterborne (consumption of contaminated water), vector-borne (through insect bites), and zootonic that are spread from animals to humans (Bailey, 2018; Abebe *et al*., 2020).

There are diverse known pathogens and they consist of both prokaryotic and eukaryotic organisms with the most commonly known being bacteria and viruses. Bacteria are prokaryotic cells that produce toxins and enzymes that cause diseases. Whereas, viruses are particles of nucleic acids (RNA or DNA) engulfed within a capsid which is a protein shell. They take over their host cell machinery and make copies of themselves thereby causing diseases, this results in the cell destruction activity (Bailey, 2018). Examples of eukaryotes include fungi, parasitic worms, and protozoan protists.

2.13.4 Bacterial pathogens

Major threats to human health continue to be a problem due to infectious diseases across the globe. Factors that contribute greatly to these challenges include but are not limited to lifestyle changes (including increased migration), antibiotic drug resistance by pathogens, immunosuppressed patients, and threats due to bioterrorism (Silva, 2012). Hence, the classification of these infectious agents regarding their infective lifestyles in their host and their corresponding pathogenic implications must be defined (Silva, 2012). In symbiotic associations, the cause of disease by microbes is characterized by parasitism. Thus, pathogenic microorganisms when associated with their hosts and living from pathogenicity resulting to host damage, become infectious, even when they may live differently in terms of replication or survival in the environments (Yildiz, 2007).

Bacterial pathogen resistance and multiplication in environments originates solely through the transmission from water, vectors, and air to humans and animal hosts, and promotes interaction with free-living protozoa (Yildiz, 2007). Therefore, these are contributing factors for microbial survival that increase a pathogen's change from being a disease producer; but these are not functional factors *in vivo* infections. Furthermore, the ability for extracellular replication *in vitro*, metabolic pathways, and corresponding genes different from those used in extracellular growth in the host are requirements (Fuchs *et al*., 2012). Classically, infectious agents are known to be intracellular, extracellular, and obligate intracellularly (Brubaker, 1985).

2.13.5 Intracellular Pathogens

Intracellular classical microorganisms' examples include: *Mycobacterium tuberculosis*, *Listeria monocytogenes*, *Brucella abortus*, *Coxiella burnetii*, *Chlamydia trachomatis*, *Salmonella enterica* to mention but a few, and the typical infectious diseases caused by these include: tuberculosis, listeriosis, brucellosis, and salmonellosis (Pamer, 2008). Intracellular pathogenic bacteria establish a relationship in the susceptible host which includes the intracellular multiplication stage (Moulder, 1962; 1985). For intracellular pathogens to establish infection, they have to make contact with the appropriate cell of the host that will afford suitable intracellular conditions for growth. These pathogens have been classified as facultative or obligate (Moulder, 1985). This classification was based on the absence (in-obligate intracellular bacteria) or presence (in-facultative intracellular bacteria) of the capacity

to reproduce in a cell-free environment (Suter, 1956; Moulder, 1985). Intracellular bacterial pathogens use large amounts of host cells professionally (macrophages) and non-professional (phagocytes like epithelial and endothelial cells) and hepatocytes (Moulder, 1985; Pamer, 2008). After target host cell entry, the pathogens may follow diverse cytosolic or vacuole pathways (Knodler and Celli, 2010).

2.13.6 Extracellular pathogens

Some typical examples of extracellular pathogens include *Staphylococcus aureus*, *Escherichia coli*, *Streptococcus pyogenes*, *Pseudomonas aeruginosa* (Weiser and Nahm, 2008). They cause some infections such as osteomyelitis, scarlet fever, some forms of pneumonia, wound, and urinary tract infections (Nahm *et al*., 1999; Weiser and Nahm, 2008). For extracellular pathogens to produce diseases, they use any portal of entry provided the satisfactory fluid medium is established on the site of injury (Stuart and Ezekowitz, 2005). Moreover, these pathogens multiply extracellularly on the hosts' sites such as vascular, body cavity fluids, mucosal surfaces, lymphatic, and interstitial spaces (Stuart and Ezekowitz, 2005). Furthermore, virulence mechanisms are used by extracellular pathogens to evade antimicrobial capacity of the humoral immunity and phagocytosis thus enhancing extracellular multiplication (Weiser and Nahm, 2008). Moreover, they use these mechanisms in contrast with the intracellular pathogens that promote host cell entry including macrophages and phagocytes as epithelial cells (Sansonetti, 2001).

In the present context of bacterial pathogens, important information that highlights examples in the classification of these organisms as extracellular is well documented (Weiser and Nahm, 2008). This defines their entry into the host cells *in vivo* resulting in an intracellular residence phase relevant for initiation of extracellular infections, where diverse virulence factors specific to each pathogen produce the disease (Weiser and Nahm, 2008). Some examples of extracellular pathogens that use intracellular phase initiation include *S. pyogenes* (Cole *et al*., 2010), *E. coli* (Croxenan and Finlay, 2010), *S. aureus* (Garzoni and Kelley, 2009), *Helicobacter pylori* (Allen, 1999) to mention a few.

The bacteria domain is divided into two groups based on the cell wall and reaction to a Gram stain method. Hence, the term gram-negative and gram-positive was introduced. The major difference between the gram-negative to the gram-positive bacteria is related to their chemical composition and cell wall structure. The gram-positive bacteria are characterized by their uniform thick dense layered cell walls (**Fig. 2.25**). Whereas, the gram-negative bacteria cell

walls are much complex because of the additional lipoprotein layer they have and another outer membrane layer (Hancock, 1997). These structural differences are further characterized by the bacteria biochemical composition. The gram-positive bacterial cell wall is constituted mostly by peptidoglycan (made up of chains of amino sugar backbone glycan (N-acetylglucosamine and N-acetyl muramic acid linkers)) held together by peptide bridges. Additionally, the gram-positive bacteria cell wall constitutes of polylphosphate polymers such as polyglycerol phosphate and polyribitol phosphate (teichoic and teichuroic acids) (Hancock, 1997).

In gram-negative bacteria, peptidoglycan makes up a small portion of the cell wall composition. Gram-negative bacteria cells' outer membrane has a predominance of proteins and lipids, and polysaccharides extend to the aqueous environment. As in the cell membrane, the outer membrane consists of two leaflets each with lipid molecules with their hydrophilic groups directed away from the membrane towards the aqueous environment and the hydrophobic group facing inwards holding the leaflets together. The lipid membrane attachments are covalently bonded to the polysaccharide forming a lipid-polysaccharide called lipopolysaccharide (which is a strongly negatively charged molecule) (Hancock, 1997).

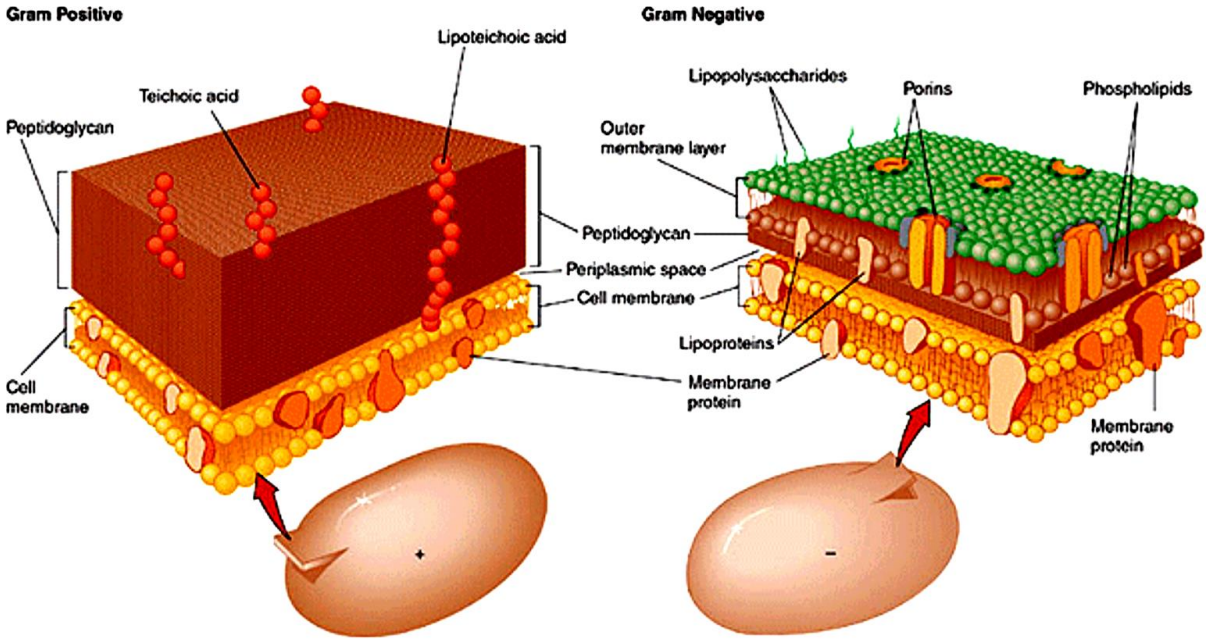

Figure 2.25 schematic difference between gram-positive (left) and gram-negative bacteria cell wall and cytoplasmic membrane (Adapted from Hancock, 1997)

2.13.6.1 Virulence factors of *Staphylococcus aureus*

Staphylococcus aureus (**Figure 2.26**) is an example of extracellular pathogens, it is known to be a major human and animal opportunistic pathogens responsible for nosocomial and community-associated infections with high morbidity and mortality rates (Felden *et al*., 2011). *S. aureus* is a potent Gram-positive bacterium that can bypass all host defense system barriers. This bacterium possesses a wide range of virulence factors such as hemolysin, coagulase, cytolysin, enterotoxin, and DNase (Kurlenda *et al*., 2012) (**Table 2.1)**. A third of healthy persons is said to be asymptotically colonized intranasally with *S. aureus* without any significant association to diseases (Bien *et al*., 2011). However, diseases caused by this bacterium range from life-threatening invasive diseases including but not limited to, pneumonia, endocarditis, septicemia, and osteomyelitis, also minor skin and soft tissue infections (Leng *et al*., 2011). *S. aureus* is also a prominent pathogen in biofilm-related infections found in most medical devices (Ma *et al*., 2012). The treatment and avoidance of *Staphylococcal* infections are still a challenge in most cases due to the spread and emergence of drug-resistant bacterium strains (Kurlenda *et al*., 2012). *S. aureus* broad range of infections are related to a wide range of virulence factors that allows it to invade, adhere to the surfaces and avoid the immune system, resulting in it causing harmful toxic effects to its host (Bien *et al*., 2011). *S. aureus* infections can be divided into three different types such as toxinoses (e.g. food poisoning), superficial lesions (e.g. wound infections), toxic shock syndrome toxin (TSST), and scalded skin syndrome (de Sousa and Lencastre, 2004).

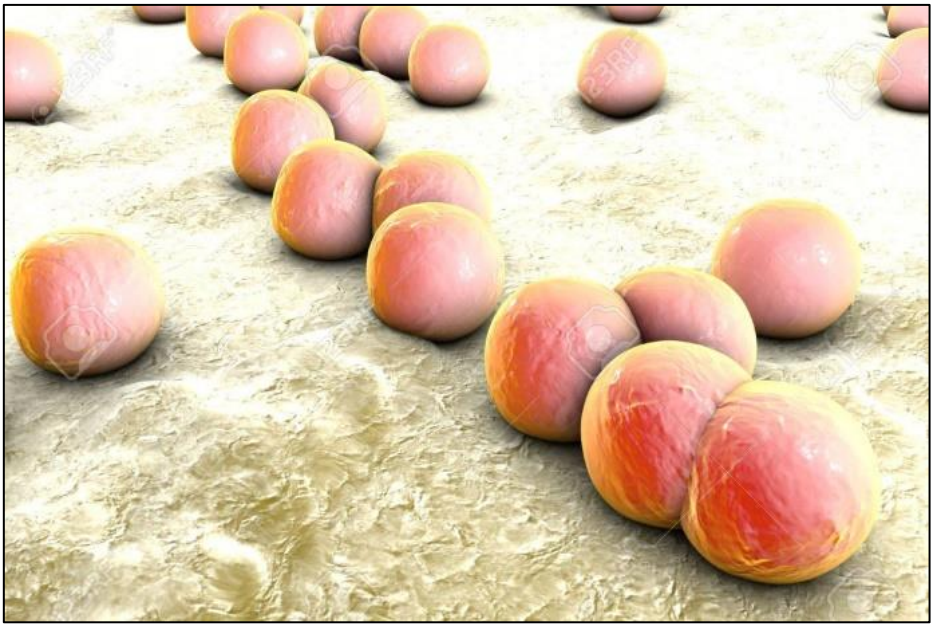

Figure 2.26 *Staphylococcus aureus* cells (Adapted from Kon, 2018)

Table 2.1 selected virulence factors involved in the pathogenesis of *S. aureus* (Adapted from Kurlenda *et al*., 2012)

Type of virulence factors	Selected factors	Genes	Associated clinical syndromes
Involved in attachment	MSCRAMMs (e.g clumping factors, fibronectin binding proteins, collagen and bone sialoprotein-binding proteins	*ctfA, ctfB, fnbA, fnbB, sdr, ddp*	Endocarditis, osteomyelitis, septic arthritis and prosthetic device, catheter infections
Involved in persistence	Biofilm accumulation (e.g. polysaccharide intercellular adhesion), small colony variants, and intracellular persistence.	*Ica locus, hemB mutation*	Relapsing infections, cystic fibrosis, and syndromes as described above for attachment
Involve in evading/destroying host defenses	Leukocydins (e.g. PVL and γ-toxin), capsular polysaccharides (e.g. 5 and 8), protein A, CHIPS, Eap, and phenol-soluble modulins.	*lukS-PV, lukF-PV, hlg, cap5 and 8* gene clusters, *spa, chp, eap, psm-α* gene cluster	Invasive skin infections and necrotizing pneumonia (CA-MRSA strains that cause these are associated PVL) abscesses (associated with capsular polysaccharides).
Involved in tissue invasion/penetration	Proteases, lipases, nucleases, hyaluronate lyase, phospholipase C, and metalloproteases (elastase).	*V8, hysA, hla, plc, sepA*	Tissue destruction and metastatic infections
Involved in toxin-mediated diseases and / or sepsis	Enterotoxins, toxic shock syndrome toxin 1, exfoliative toxin A and B, α-toxin, peptidoglycan, and lipoteichoic acid	*sea-q (no sef), tstH, eta, etb, hla*	Food poisoning, toxic shock syndrome, scalded skin syndrome, bullous impetigo, and sepsis syndrome.
With a poorly defined role in virulence	Coagulate, ACME and bacteriocin	*arc cluster, opp-3 cluster, bsa*	

2.13.6.2 Virulence factors of *Streptococcus pyogenes*

Streptococcus pyogenes (which is a group A *streptococcus*) is a Gram-positive extracellular bacterium pathogen (**Fig. 2.27**). These bacteria colonize the skin and throat and they are responsible for a range of suppurative infections and nonsuppurative sequelae (Cunningham, 2000). As a pathogen, *S. pyogenes* developed complex virulence factor mechanisms to avoid host defenses (**Table 2.2**). Due to these virulence factors, they cause pharyngitis, impetigo, and scarlet fever. Many decades of epidemiological studies have reported distinct throat and skin strains of *S. pyogenes*. Thus, it became evident that there were serotypes of group A streptococci which possessed strong tendencies to cause throat infections, similarly with serotypes that were associated with impetigo (Bisno, 1995, Wannamaker, 1970). It was reported in the past decades that they were also a common cause of childbed fever or puerperal sepsis (Cunningham, 200).

In recent years, the group A *streptococci* have been identified to be responsible for streptococcal toxic shock syndrome and have gained the most attention as a “flesh-eating” bacterium (Working Group on Severe *Streptococcal* infections, 1993). *S. pyogenes* invades the skin and soft tissues and destroys severely the infected tissues or limbs. Investigations of the group A streptococcus has demonstrated its significant role in the development of post-streptococcal infection sequelae including reactive arthritis, acute rheumatic fever, and glomerulonephritis (Cunningham, 2000). In recent years it has been reported that group A *streptococcal* infections are associated with movement and attention deficit disorder and Tourette's syndrome (Cunningham, 2000).

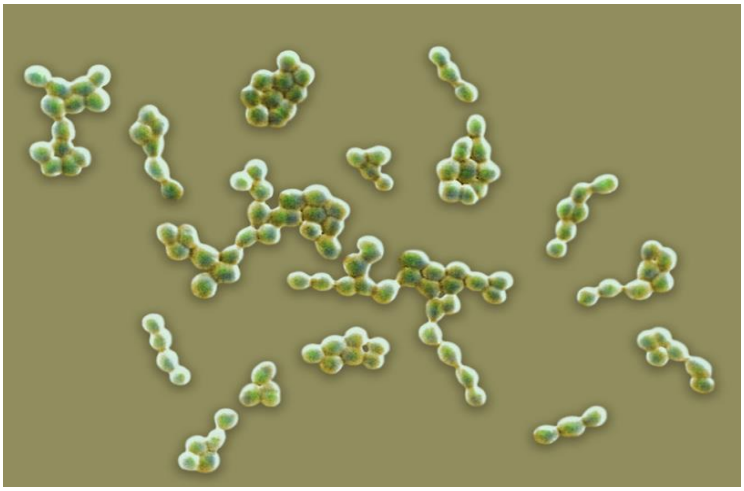

Figure 2.27 *Streptococcus pyogenes* cells (Adapted from Fred Hossler, visited 10 August 2018)

Table 2.2 Virulence factors of group A streptococcal adhesins and their host cell receptors (Adapted from Cunningham, 2000)

Adhesin	Host cell receptor	comment
LTA	Epithelial cells/fibronectin receptors	-
M protein	Hep-2 cells Keratinocytes/CD46 receptor, factor H	1L-6 production
Protein F/Sfbf	Epithelial cell/fibronectin/CD46 receptor on keratinocytes	1L-1 and prostaglandin E2 production
Fibronectin-binding protein (FBP54)	Fibronectin/fibrinogen	-
Serum opacity factor	Fibronectin	-
Hyaluronic acid capsule	Keratinocyte/CD44 (hyaluronate receptor)	-
Glyceraldehyde-3-phosphate dehydrogenase	Pharyngeal epithelium/fibronectin/cytoskeletal protein/plasminogen plasmin	-
Fibronnectin-binding protein (29 kDa)	Fibronectin	-

Vitronectin-binding protein (70 kDa)	Vitronectin	-
Galactose-binding protein	Galactose	-
Collagen-binding protein	Collagen	-

2.13.6.3 Virulence factors of *Escherichia coli*

Escherichia coli since its recognition in 1885, it has become the most comprehensively studied bacterial species (**Figure 2.28**). *E. coli* are easily manipulated and grown in the laboratory, are readily enabled to genetic manipulation, and they naturally acquire genetic elements. While *E. coli* isolates from beneficial flora of the intestine, some of its strains have evolved pathogenic mechanisms that cause infectious disease to both humans and animals (Donnenberg and Whittam, 2001). The *E. coli* bacterial strains can cause extraintestinal or diarrheagenic infections to humans. Traditionally, the enteric *E. coli* infections are divided into six pathotypes whose pathogenicity profile allows for their identification through virulence factors, phylogenetic profile, and clinical diseases (**Table 2.3**). These are *Enterohamerrhagic E. coli* (EHEC), *Enterotoxigenic E. coli* (ETEC), *Enteropathogenic E. coli* (EPEC), *Diffusily Adherent E. coli* (DAEC), *Enteroinvasive E. coli* (EIEC), and *Enteroaggregative E. coli* (EAEC) (Nataro and Kaper, 1998, Kaper *et al*., 2004).

Two more strains emerged recently, these are the Adherent Invasive *E. coli* (AIEC) associated with Crohn disease and do not cause diarrheagenic infections (Croxen and Finlay, 2010) and the other one is known as Shiga Toxin (Stx) producing *Enteroaggregate E. coli* (STEAEC). *E. coli* strains are categorized also by their serogroups, for example, *E. coli* O175, O referring to the LPS O-antigen or serotype e.g. *E. coli* O157 : H7 where H refers to the flagellar antigen (Wolf, 1997). However, many serotypes are contained by each pathotype (e.g. 117 ETEC serotype was distinguished), some serotypes may belong to various pathotypes e.g. O26:11 which can be an EPEC or EHEC (Wolf, 1997). **Table 2.3** describes the virulence factors of *E. coli* was (Adapted from Clements *et al*., 2012).

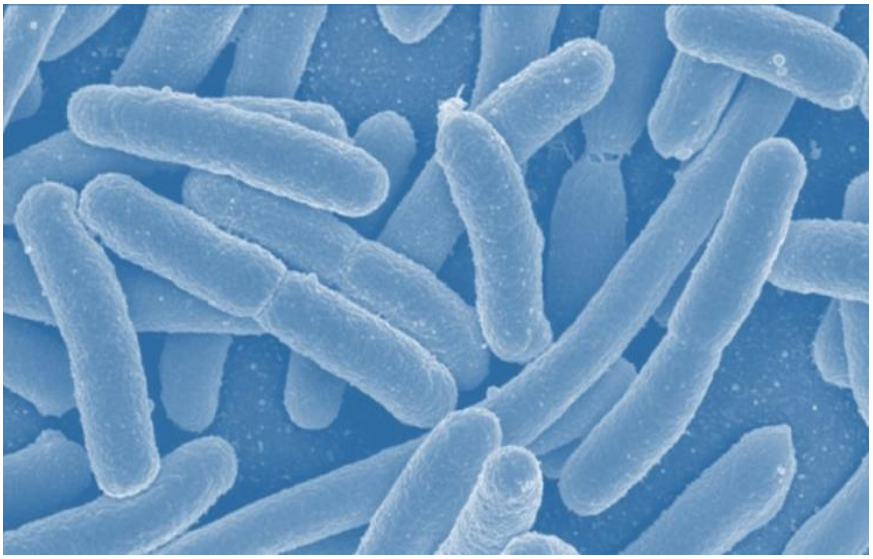

Figure 2.28 *Escherichia coli* bacteria strains (Adapted from Clements et al., 2012)

Table 2.3 List of enteric *E. coli* pathotypes and their virulence factors (Adapted from Clements *et al*., 2012)

Pathotype	Adhesin	Toxin	T3SS	SPATE	Disease
ETEC	Colonization factors (CF) Porcine A/E associated adhesion (Paa)	Heat-labile enterotoxin (LT), Heat-stable enterotoxin (ST), cytolysin A (ClyA)	-	ETEC autotransporter A (EatA)	Acute watery diarrhea (<5yo) Travelers diarrhea

EAEC	Aggregative adherence fimbriae (AAF) (I, II, Had), Toxigenic invasion loci A (Tia)	EAEC heat-stable enterotoxin 1 (EAST1), Shigella enterotoxin (ShET)1, Hemolysin E (HlyE)	+/-	Plasmid-encoded toxin (Pet) Protein involved in intestinal colonization (Pic), Secreted autotransporter toxin (Sat), Shigella igA-like protease homology (SigA),	Traveler,s diarrhea, infant diarrhea
STEAEC	AAF IrgA homolog adhesion (iha)	Shiga toxin (Stx)	-	Pic, Pet	Food poisoning
DAEC	Afimbrial (Afa) or fimbrial (Dr) adhesion	-	-	Sat	Acute diarrhea (<50yo)
AIEC	Type 1 pili, Long polar fimbriae (LPF)	-	-	-	Crohn disease
EPEC	Intimin, Bundle forming pili (BFP), Paa, LPF,lha, EhaA	-	LEE encoded	EspC	Infant diarrhea
EIEC (Shigella)	-	SHET1/2	pINV encoded	Shigella extracellular protein (Sep) A Sig	Shigellosis

2.13.6.4 Virulence factors of *Pseudomonas aeruginosa*

One of the most increasing dominant opportunistic pathogens with the common cause of hospital-acquired infections (HAI) is the *Pseudomonas aeruginosa* (**Figure 2.29**). *P. aeruginosa* is a major cause of infections particularly to patients who are immunocompromised including bone marrow transplant patients, neutropenic cancer, and acquired immunodeficiency syndrome (AIDS) patients, or patients with metabolic disorders or burn victims (Pinheiro *et al*., 2008). These bacteria produce adhesive, invasive, and toxigenic virulence compounds that facilitate the development of infections (**Table 2.4**). It is also

believed that *P. aeruginosa* is a major cause of lung infection in patients diagnosed with cystic fibrosis (CF), which may result in the formation of a biofilm and may attach to human mucin in the lower respiratory tract (Whiteley *et al*., 2001; Finnan *et al*., 2004).

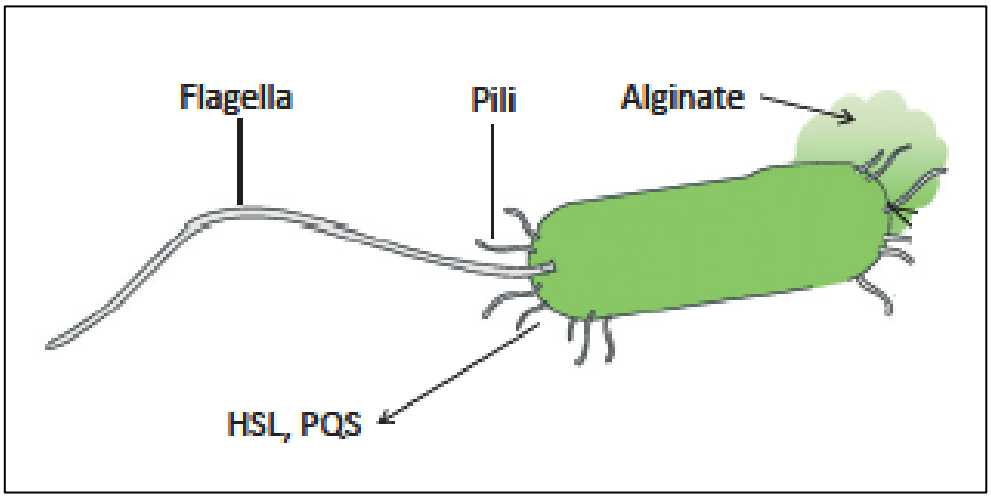

Figure 2.29 *Pseudomonas aeruginosa* strain (Adapted from Shaan *et al*., 2013)

Table 2.4 Virulence factors of *Pseudomonas aeruginosa* (Adapted from Trateva and Mitov, 2011)

Pathogenic function	**Cell-associated factors**	**Extracellular factors**
Adhesion	Type IV pili, carbohydrate-binding proteins (lectines), Glycocalix, Alginate slime (biofilm)	-
Adhesion facilitators	-	Neuraminidase (sialidase)

Mptality/chemotaxis	Flagella (swimming motility), retractile pili (twitching motility)	-
Invasion	-	Elastase (LasA and LasB), Alkaline protease, Haemolysin (phospholipases and rhamnolipid), Cytotoxin (leukocidin), Pyocyanin pigment, Siderophores and siderophores uptake systems
Toxinogenesis	Lypopolisaccharide (endotoxin), LecA and LecB lectins	Exotoxin A
Dissermination	-	Type III cytotoxin effectors (ExoS, ExoU, ExoT, ExoY), Enterotoxin
Antiphagocytic surface properties	Slime layers, Glycocalix, Lipoposaccharides	-
Defence against serum	Slime layers	Protease enzymes
Bactericidal reaction	Glycocalix, Lipoposaccharides	-
Defence against immune response	Slime layers, Glycocalix	Protease enzymes

2.13.7 Fungal pathogens

Fungal species are eukaryotic organisms (diversely from yeast, rusts, mushrooms, molds, and lichens to microsporidia) that constitute five of the kingdoms (i.e. Fungi, Prokaryotae, Animalia, Plantae, and Protista) as classified in the current system of living organisms (Liu, 2014). Like other eukaryotic kingdoms (including Protista, Animalia, and Plantae), fungi hold a membrane-bound nucleus with chromosomal DNA consisting of non-coding regions (introns) and coding regions called exons (Liu, 2014). Furthermore, fungi possess membrane-bound cytoplasm organelles (e.g. mitochondria), sterol-containing membranes, 80S ribosomes

and they produce a variety of soluble carbohydrates and storage compounds including disaccharides, sugar alcohols, and polysaccharides (Liu, 2014). Because fungi lack chloroplasts, they resemble the Protista and Animalia; thus, requiring preformed organic compounds as energy sources (Liu, 2014). Furthermore, although fungi and Plantae possess a cell wall and vacuoles, they may reproduce sexually or asexually, have haploid nuclei, and generate spores (Liu, 2014).

Moreover, Fungi differ from Plantae by the presence of chitin (which exists also in the exoskeleton of arthropods) instead of cellulose in the cell walls and the absence of chloroplasts (Liu, 2014). Fungi also differ from Prokaryotae by having a nuclear membrane, cell wall and plasma membrane respectively. However, fewer (<500) of the known fungal species (including 200 yeast species) are known to cause human infections (Liu, 2014). Fungi are divided into two major categories based on their morphological criteria: Filamentous fungi (true fungi) and unicellular fungi called yeasts. Accounting for the bulk of fungal species, filamentous fungi produce tubular, elongated, and thread-like (filamentous) cellular structures (known as hyphae), which contain multiple nuclei and extend at their tips (Liu, 2014).

Since the 1980s, there has been an increase in reports on the prevalence and incidences of invasive fungal infections, especially in the population of immunocompromised patients including those hospitalized with serious underlying diseases (Arendrup *et al*., 2005; Espinel-Ingroff *et al*., 2009). *Candida* species are normal microbiota belonging to an individual's gastrointestinal tract, mucosal oral cavity, and vagina (Shao *et al*., 2007), and they are responsible for some clinical infection manifestations from the bloodstream to mucocutaneous overgrowth infections (Eggimann *et al*., 2003). The *Candida* species in healthy humans are commensal but may cause systemic infections in immunocompromised individuals due to their great adaptability to different hosts. The genus of *Candida* is composed of a heterogeneous group of organisms, with more than 17 of known different *Candida* species being aetiological agents of human infections. However, more than 90% of the causes of invasive infections are due to *Candida albicans, Candida tropicalis, Candida glabrata, Candida krusei* and *Candida parapsilosis* (Pfaller *et al*., 2007).

2.13.7.1 Virulence factors of *Candida albicans* (*C. albicans*)

Candida albicans is an opportunistic fungus species found in various parts of humans and animals and is the most common species that causes candidiasis (**Figure 2.30**). The genus of *C. albicans* is associated with many superficial to deep-seated infections (Nasution *et al*.,

2013). The major organism associated with infections is *Candida albicans*, but some organisms such as *Candida parapsilosis* and *Candida krusei* also exist as organisms that can be pathogenic to humans (Mayer *et al*., 2013). *Candida albicans* in humans are frequently isolated from the mucosal surface of the mouth, gastrointestinal tract, and esophagus tract. Therefore, *C. Albicans* is found to an isolate from the oral cavity as normal flora and causes candidiasis with various manifestations and clinical symptoms (Mathews, 1994; Fonzi, 2001). The oral candidiasis pathogenicity is a complex process that no factor has been reported to be the cause of (Gillmore, 1998). Infections of *C. Albicans* are associated closely with their virulence factors (Batchtiar, 1997).

Candida albicans appears as gram-positive, oval-shaped (**Figure 2.30**) with size between 2-3 x 4-6 µm and has budded cells that resemble elongated hyphae or pseudohyphae (Brooks *et al*., 1995). These fungal yeast ferment glucose and maltose producing acid and gas, ferment acid from sucrose but do not react with lactose. The fermentation of carbohydrates and morphology and properties distinguish colonies of other *Candida* species (Diamond, 1993). The manifestation of candidiasis is due to opportunities allowing *C. Albicans* to selectively express virulence factors required for *C. albicans* to exist as pathogens (Chaffin *et al*.,1998). *Candida albicans* virulence factors include adherence and coaggregation, immune system interference, interference of complement, interference of phagocytosis, and phenotype switching (Nasution, 2013). Also, Candida produces biofilm and tissue-damaging hydrolytic enzymes called proteinase and phospholipase (Nasution, 2013).

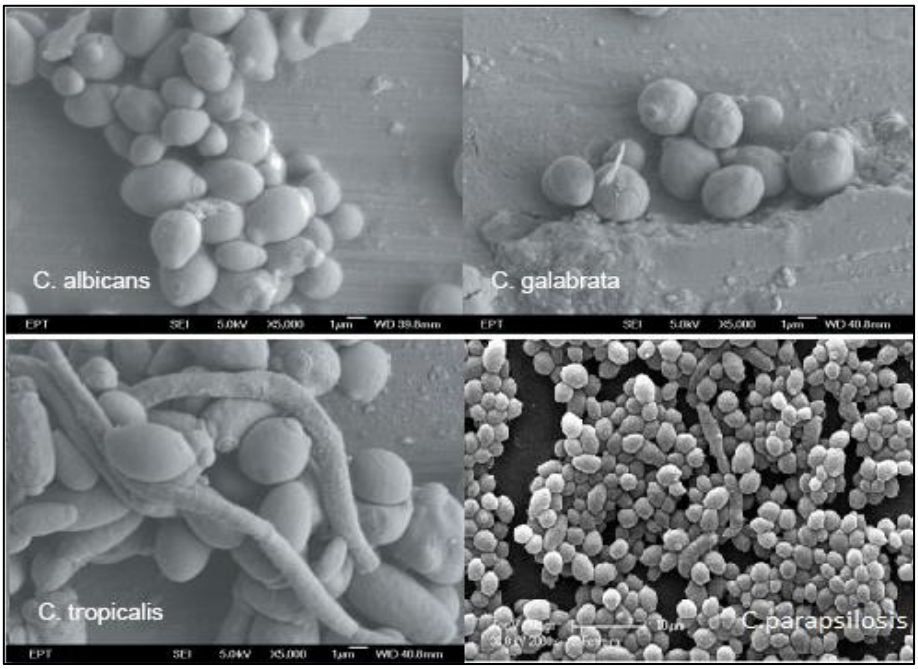

Figure 2.30 Scanning electron microscopy micrographs of *Candida species* (Adapted from Ferreira *et al*., 2009; Meurman *et al*., 2007)

2.13.7.2 Non-albicans *Candida* (NAC) species

Candida infections have been reported to have increased in the past few decades (Ying and Chunyang, 2011). Although among *Candida* species, *Candida albicans* remains the predominant aetiological agent found in various candidiasis clinical forms, recent studies documented a shift towards non-albicans *Candida* (NAC) species (Dan *et al*., 2002). The appearances of NAC and causes of various pathogenic *Candida* spp. are not distinguishable but the problems become acute because different NAC species exhibit different degrees of resistance either acquired, intrinsic, or both to the commonly used antifungal drugs (Johnson *et al*., 1995). The NAC spp. increased isolation rates and their gradual antifungal susceptibility profile shift underlines the need for their early and accurate diagnosis along with antifungal susceptibility testing for selecting appropriate antifungal agents for therapy. The most common *Candida* virulence factors include germination, hyphal switching, production of extracellular hydrolytic enzymes, and surface recognition (Ying and Chunyang, 2011). Of these virulence factors, extracellular hydrolytic enzymes play a pivotal role in adherence and tissue damage in the infection caused by *Candida* (Schaller *et al*., 2005).

Globally, Non-albicans *Candida* spp. accounts for more than half of the non-superfacial *Candida* infections cases (Ann Chai *et al*., 2010). The most common of the *Candida* NAC species with more than two-thirds of nosocomial candidemia were due to *C. tropicalis* and the second most prevalent *Candida* species after *C. albicans* in many spectral infections including: cutaneous, systemic candidiasis, superficial and subcutaneous (Kothavade *et al*., 2010). Moreover, *Candida tropicalis* was found to be significantly involved in various human pathologies such as urinary tract infections, osteomyelitis, fungemia, endocarditis to name some (Negri *et al*., 2012). Virulence factors found to have been expressed by the strains of *C. tropicalis* include adhesins, biofilm formation, hemolysin, phenotypic switching, and production of enzymes like phospholipase, esterase, proteinase, etc. which contribute to the pathogenicity of candidiasis (Adler-Shohet *et al*., 2001).

Candida parapsilosis is one of the NAC species with dramatically increased incidences over the past few decades. This *Candida* species has been reported as the second most commonly isolated Candida species from blood cultures (Colombo *et al*., 2006, Colombo *et al*., 2007; Costa-de-Oliveira *et al*., 2008; Messer *et al*., 2006). *Candida parapsilosis* initially was

considered non-pathogenic, but later it was identified as the causative agent of a fatal case of endocarditis in intravenous drug users in 1940 (Joachim and Polayes, 1940). Exogenous infections due to contaminated medical instruments are also common (Trofa *et al*., 2008).

While on the other hand, *Candida glabrata* like most of *Candida* species is an opportunistic pathogen and is a part of the normal microbiota of the mouth, gastrointestinal and vaginal tracts in humans (Bialkova and Šubík, 2006; Rodrigues *et al*., 2014), and it does not cause disease in some individuals. However, in immunosuppressed hosts, *C. glabrata* can become a cause of disease due to some disturbances in the normal environment (Rodrigues *et al*., 2014, Riera *et al*., 2012). Due to rising concerns of antimicrobial resistance and the limited efficient antifungal drug treatments currently available, the study carried out by Rodrigues *et al.* (Rodrigues *et al*., 2014) noted that *C. glabrata* pathogenicity could be attributed to its ability to form biofilms and its relatively high resistance to traditional antifungal therapies. The virulence factors associated with *C. glabrata* compared to other pathogenic yeast species like *C. albicans* are still poorly understood even to date. *Candida glabrata* can still be considered to be less virulent when compared to *C. Albicans* (Fidel *et al*., 1999; Bialkova and Šubík, 2006; Li *et al*., 2007; Riera *et al*., 2000). Furthermore, for *C. glabrata* to be able to secrete proteases, it led to being originally called *Torulopsis glabrata* (Rodrigues *et al*., 2014). The species was later reclassified to *Candida* because of its human pathogenicity (Fidel *et al*., 1999). The major differences between *C. albicans* and *C. glabrata* are the inability of *C. glabrata* to secrete certain proteases and form true hyphae (Desai *et al*., 2011).

2.14 Metastatic melanoma

2.14.1 Background

Cancers are caused by induced gene mutation environments which in turn trigger the proliferation of cells at an abnormal rate (Wilcken, 2016). These abnormal cell proliferation produces either malignant or benign tumors (Martin *et al*., 2013). The classification of cancers is determined by the following factors: (i) the tumor origin, (ii) the type of cells which the tumor resembles, (ii) the location of the tumor, and (iv) the stage of the tumor (DeSantis *et al*., 2014). However, malignant tumors often tend to spread to the surrounding tissues and find their way to other organs and parts of the body by lymphatic or circulatory systems thereby causing metastasis (Alderton, 2015). Due to the ability of cancer cells to metastasize, this makes treatment redundant and difficult in the annihilation of cancer cells (Swavey and Tran, 2013).

Because of the increasing number of new reported diagnostic cases annually, cancer is regarded as one of the most predominant health threats to everyone globally (Siegel *et al*., 2016). Therefore, there are many clinically approved conventional cancers treatments available such as; surgical interventions, radiotherapy, chemotherapy, and/or the combination; but these are more reliant on the location, the type, and stage of cancer (Guimaraes *et al*., 2013). However, these treatments are often invasive and sometimes induce severe side effects after treatment to patients (DeSantis *et al*., 2014). The development of new alternative therapeutic forms of treatments that mitigate these unwanted side effects are of paramount importance (DeSantis *et al*., 2014).

2.14.2 Different types of skin cancer cells

Skin cancers are named and identified according to the cell from which they originated and their clinical behavior (Esserman *et al*., 2014). There are three known general types of skin cancer: the cutaneous malignant melanomas (CMM), basal cell carcinoma (BCC), and squamous cell carcinomas (SCC) (Jayaraman *et al*., 2014). The BCC and SCC are referred to as noninvasive or non-melanocytic skin cancers since they do not originate from skin melanocytes and they do not spread to the surrounding healthy tissues (Allen, 2013). However, the cutaneous malignant melanoma cells tend to spread to the surrounding tissues and are considered to be metastatically invasives (Eggermont *et al*., 2014). Moreover, melanoma is the most lethal and aggressive form of cancer due to its capacity to metastasize and acquire resistance to chemotherapy (Soengas and Lowe, 2003). Melanoma is rather a rare tumor that accounts for less than 4% of the skin cancer cases, but it is the most responsible for the high mortality rate responsible for 80% of skin cancer deaths (Kuphal and Bosserhoff, 2009). Furthermore, melanoma occurs as a result of malignant transformation of melanocytes (Shain and Bastian, 2016; Jhappan *et al*., 2003) that give rise to a different set of histopathological appearances, neoplasms with biochemical cascade mutations and clinical features (Bastian, 2014, Ossio *et al*., 2017).

Metastatic malignant melanoma remains the world's devastating and deadliest skin cancer (Davids and Kleeman, 2011) and is a highly malignant tumor that develops from transformed melanocytes (Garbe and Blum, 2001; Oppermann *et al*., 2005). It’s potential to metastasize rapidly leads to poor prognosis (Helmbatch *et al*., 2001). These tumors demonstrate a wide range of factors that contribute to their resistance to traditional treatment modalities. Also, despite significant scientific interventions and advances made in the past decades with

chemotherapeutics and melanocytic targets, the prognosis and metastatic melanoma remain a challenge (Kleemann *et al*., 2014). Therefore, the development of improved therapeutic modalities is crucial to address the identified challenges.

Furthermore, early detection of localized melanoma can be cured through surgical interventions; however, there is no data regarding therapy for metastatic melanoma or melanoma with metastatic potential. The first line of therapy is surgical resection followed by extensive radiation and/or chemotherapy (Amendoeira *et al*., 2020; Soengas and Lowe, 2003; Zbytek *et al*., 2008). However, due to melanoma inherent resistance to traditional therapeutic modalities, various methods such as radiotherapy (Moncrieff *et al*., 2008), immunotherapy (Carlson *et al*., 2005), gene therapy (Carlson *et al*., 2005, Thompson *et al*., 2005), and bio-chemotherapy (Yamamura *et al*., 2008; Chudnovsky *et al*., 2005; Slominski *et al*., 2004) have been developed and undergone various clinical trials, but their outcomes remained negligible. Despite all these interventions, there is still a need for the development of novel and effective therapeutic modalities to treat melanoma cells. Also, BODIPY PSs is an immerging class of PSs that may be used in PDT. Photodynamic therapy stands as a possible modality that is noninvasive which can be used in conjunction with the current traditional treatments. This chapter demonstrates the preliminary photodynamic therapy potential of novel synthesized BODIPY PSs and their nanoconjugates for the treatment of cancerous melanoma cells (UCT Mel-1) and non-cancer HaCat keratinocyte cell lines. The interest to investigate the cell lines outlined in this study is due to the mortality rate of melanoma cancers and their malignancies.

BODIPY PSs in metastatic melanoma skin cancer photodynamic therapy is still a study that is not heavily explored; therefore, a lot of work has been done on non-melanoma skin cancers (Kamkaew *et al*., 2013). However, a study by Gibbs and coworkers (2013) studied BODIPY PSs with meso-phenyl and meso-thienyl groups on human carcinoma HEp2 cells (Gibbs *et al*., 2013). They observed that the 2,6-diiodo substituted BODIPY PSs showed great phototoxicity (IC50 3.5-28 μM at 1.5 J/cm^2) compared with the non-iodinated BODIPYs (Gibbs *et al*., 2013). Furthermore, a study by Lazzarato and co-workers (2019), demonstrated 2,6-diiodo-BODIPY PSs with meso-substituted phenyldiazene and methoxymethyl anticancer efficacy on A357 and SKMEL28 cancer cell lines. The synthesized BODIPY PSs demonstrated the photogeneration of $^1O_2$ and nitric oxide (NO) which were found to induce phototoxicity on the cells studied (Lazzarato et al., 2019). Lazzarato's group also observed that these BODIPY PSs induced photoactivity at 2.5-5 μM concentration respectively.

2.15 References

~~Eigenbrode S.D., Bosque-Perez N.A., and Davis T.S., 2018; Insect-borne plant pathogens and their vectors: ecology, evolution, and complex interactions. Annu. Rev. Entomol., 63(1): 169-91.~~

Abebe E., Gugsa G., and Ahmed M., 2020; Review on Major Food-Borne Zoonotic Bacterial Pathogens. Review on major food-borne zoonotic bacterial pathogens. J. Tropic. Med., 1(1): 1-19.

Adler-Shohet F., Waskin H. and Lieberman J.M., 2001. Amphotericin B lipid complex for neonatal invasive candidiasis. *Arch. Dis. Child Fetal Neonatal ed*. 84(1):131-133.

Agostinis P., Berg K., Cengel A.K., Foster H.T., Girotti A.W., Gollnick S.O., Hahn M.S., Hamblin R.M., Juzeniene A., Kessel D., Korbelik M., Moan J., Mroz P., Nowis D., Piette J., Wilson C.B. and Golab J., 2011; Photodynamic therapy of cancer: An update, *CA Cancer J. Clin*., 61(4): 250-281.

Agostinis P., Berg K., Cengel A.K., Foster H.T., Girotti A.W., Gollnick S.O., Hahn M.S., Hamblin R.M., Juzeniene A., Kessel D., Korbelik M., Moan J., Mroz P., Nowis D., Piette J., Wilson C.B. and Golab J., 2011; Photodynamic therapy of cancer: An update. *CA Cancer J. Clin.*, 61(1): 250-281.

Akyilmaz E, Yorganci E, Asav E., 2010; Do copper ions activate tyrosinase enzyme? A biosensor model for the solution. *Bioelectrochemistry*., 78(2):155-160.

Alderton G.K, 2015; Metastasis: Spreading the Seed. *Nat. Rev. Cancer*, 15(5): 255.

Allen C., Maysinger D. and Eisenberg A., 1999; Nano-engineering block copolymer aggregates for drug delivery, *Coll. Surfaces, B: Biointerfaces*. 16(1): 3-27.

Allen D.C., 2013; Non-melanocytic skin carcinoma. In: Cameron IR, Morton M, Bolesworth J, Schad B, eds. Histopathology Reporting. London, England: Springer; 2013:197-206.

Allison, W.T., Barthel, L.K., Skebo, K.M., Takechi, M., Kawamura, S., and Raymond, P.A., 2010; Ontogeny of cone photoreceptor mosaics in zebrafish. *J. Comp. Neurol.*, 518(20): 4182-4195.

Amatguerri F., Lopezgonzalez M.M.C., Martinezutrilla R. and Sastre R., 1990; Singlet oxygen photogeneration by ionized and un-ionized derivatives of Rose Bengal and Eosin Y in diluted solutions, *J. Photochem. Photobiol. a-Chem.*, 53(2): 199-210.

Amendoeira A., García L.R., Fernandes A.R, and Baptista P,V., 2019; Light Irradiation of Gold Nanoparticles Toward Advanced Cancer Therapeutics, *Adv. Therap*., 3(1): 1900153, 1-11.

Anabela Tavares, Carla M. B. Carvalho, Maria A. Faustino, Maria G. P. M. S. Neves, João P. C. Tomé, Augusto C. Tomé, José A. S. Cavaleiro, Ângela Cunha, Newton C. M. Gomes, Eliana Alves and Adelaide Almeida, 2010; Antimicrobial Photodynamic Therapy: Study of Bacterial Recovery Viability and Potential Development of Resistance after Treatment. *Mar. Drugs*, 8(1): 91-105.

Andres P.R., Bielefeld J.D., Henderson J.I., Janes D.B., Kolagunta V.R., Kubiak P.C., Mahoney J.W. and Osifchin G.R., 1996; Self-Assembly of a Two-Dimensional superlattice of molecularly linked metal clusters, *Science*, 273(5282): 1690-1693.

Ann Chai L.Y., Denning D.W. and Warn P., 2010; Candida tropicalis in human disease. *Crit. Rev. Microbiol.*, 36(4): 282-298.

Arbogast J. W., Darmanyan A. P., Foote C. S., Rubin Y., Diederich F. N., Alvarez M. M., Anz S. J., Whetten R. L., 1991; Photophysical properties of C60, *J. Phys. Chem-Us*., 95(1): 11-12.

Arendrup M. C., Fuursted K., Gahrn-Hansen B., Jensen I. M., Knudsen J. D., Lundgren B., Schønheyder H. C. and Tvede M., 2005; Seminational surveillance of fungemia in Denmark: notably high rates of fungemia and numbers of isolates with reduced azole susceptibility. *J. Clin. Microbiol.*, 43(1): 4434-4440.

Atilgan S., Ekmekci Z., Dogan A.L., Guc D., and Akkaya U., 2006; Water soluble distyryl-boradiazaindacenes as efficient photosensitizers for photodynamic therapy, *Engin. Chem. Commun*. (1): 4398-4400.

Awuah S.G. and You Y., 2012; Boron dipyrromethene (BODIPY)-based photosensitizers for photodynamic therapy, *RSC Adv*., 2(1), 11169-11183.

Awuah S.G., Nicholas K., You Y., Glatzhofer D., Richter-Addo D., Harrison R., 2012; Design and synthesis of NIR BODIPY dyes: Application for in vivo fluorescence imaging and photodynamic therapy, Thesis study, University of Oklahoma.

Bailey R., 2018; A guide to different types of pathogens, http://www.thoughtco.com/types-of-pathogens-4135656 (Accessed, 18 05 2018).

Bandichhor R., Thivierge C., Bhuvanesh N.S.P. and Burgess K., 2006; 4,4-Difluoro-1,3,5,7-tetramethyl-4-bora3a,4a-diaza-s-indacene, *Acta Crystallogr. Sect. E*, 62(10): 4310-4311.

Banfi S., Caruso E., Zaza S., Mancini M., Gariboldi M.B. and Monti E., 2012; Synthesis and photodynamic activity of a panel of BODIPY dyes. *J. Photochem. Photobiol. B: Biology*, 114(1): 52-60.

Barolet M.D., 2008; Light-emitting diodes (LEDs) in dermatology, *Semin Cutan. Med. Surg*., 27(4): 227-238.

Bastian B.C., 2014; The Molecular Pathology of Melanoma: An Integrated Taxonomy of Melanocytic Neoplasia. *Annu. Rev. Pathol. Mech. Dis*., 9(1): 239-271.

Batchtiar B.M., 1997; some factors affecting virulence pathogenicity of Candida albicans candidiasis in mouth. *J. Dent. Univ. Indonesia*, 4(1): 704-706.

Batrakova E.V., Bronich T.K., Vetro J.A. and Kabanov V.A., 2014; Nanoparticulates as drug carriers. *Int J Nanomedicine., 9:2833-2848.*,

Benstead M., Mehl G.H. and Boyle R.W., 2011; BODIPYs as components of novel light active materials. *Tetrahedron*, 67(1), 3573-3601.

Bialkova A. and Šubík J., 2006; Biology of the pathogenic yeast Candida glabrata. Folia Microbiol., 51(1): 3-20.

Bien J., Sokolova O., Bozko P., 2011; Characterization of Virulence Factors of Staphylococcus aureus: Novel Function of Known Virulence Factors That Are Implicated in Activation of Airway Epithelial Proinflammatory Response. *J. Pathog*., 601905(1): 1-13.

Boens N., Leen V. and Dehaen W., 2012; Fluorescent indicators based on BODIPY, *Chem. Soc. Rev*., 41(3): 1130-1172.

Bonnett R and Martinez G., 2001; Photobleaching of sensitizers used in photodynamic therapy, *tetrahedron*, 51(1): 9513-9547.

Bonnett, R., 1995; Photosensitizers of the porphyrin and phthalocyanine series for photodynamic therapy, *Chem. Soc. Rev*., 24(1), 19-33.

Boyer J.H., Haag A.M., Sathyamoorthi G., Soong M.L. and Thangaraj K., 1993; Pyrromethene-BF_2 complexes as laser dyes: 2, *Heteroat. Chem.*, 4(1): 39-49.

Bröring M., Krüger R., Link S., Kleeberg C., Köhler S., Xie X., Ventura B. and Flamigni L., 2008; Bis(BF2)-2,2'-bidipyrrins (BisBODIPYs): Highly fluorescent BODIPY dimers with large stokes shifts, *Chem. Eur. J*., 14(10): 2976-2983.

Brubaker R.R., 1985; Mechanisms of bacterial virulence. *Annu. Rev. Microbiol*., 39(1): 21-50.

Burda, C., Chen, X., Narayanan and R., El-Sayed, M. A. (2005), "Chemistry and properties of nanocrystals of different shapes", *Chem. Rev*., 105(4), 1025-1102.

Busbee B.D., Obare S.O. and Murphy C.J., 2003; An improved synthesis of high-aspect-ratio gold nanorods, *Adv. Mater*., 15(5): 414-416.

Buzea C., Blandino I.I.P. and Robbie K., 2007; Nanomaterials and nanoparticles: sources and toxicity, *Biointerphases*, 2(4): 17-172.

Buzea C., Pacheco L.I., and Robbie K., 2007; "Nanomaterials and Nanoparticles: Sources and Toxicity," *Biointerphases*, 2(4): 17-71.

Cammann K. and Fresen Z. 1977; Bio-sensors based on ion-selective electrodes, *Anal. Chem*., 287(1):1-9.

Carlson J.A., Ross J.S., Slominski A., Linette G., Mysliborski J., Hill J., Mihm Jr. M., 2005; Molecular Diagnostics in Melanoma, *J. Am. Acad. Dermatol*., 52(1): 743-75.

Carpenter B.L., Situ X., Scholle F., Bartelmess J., Weare W.W. and Ghiladi R.A., 2015; Anti-viral, anti-fungal and anti-bacterial activities of a BODIPY-based photosensitizer, *Molecules*, 20(6): 10604-10621.

Castano A.P., Demidova T.N. and Hamblin M.R., 2004; Mechanisms in photodynamic therapy: Part two-cellular signaling, cell metabolism and modes of cell death, *Photodiagn. Photodyn. Ther*., 1(1): 279-293.

Chaffin W.L., Lopez-Ribot J.L., Casanova M.,Gozalbo D. and Martínez JP., 1998; Cell wall and secreted proteins of Candida albicans: identification, function, and expression. *Microbiol. Mol. Bio. Rev*., 62(1): 130-180.

Chan J., Dodani S.C., and Chang C.J., 2012; Reaction-based small-molecule fluorescent probes for chemoselective bioimaging. *Nat. Chem*., 4(1): 973-984.

Chen B., Pogue B.W., Hoopes P.J., Hasan T., 2006; Vascular and cellular targeting for photodynamic therapy. *Crit Rev Eukaryot Gene Expr* 16(4): 279-305.

Chen L., Ji F., Xu Y., He L., Mi Y., Bao F., Sun B., Zhang X. and Zhang Q., 2014; High-yield seedless synthesis of triangular gold nanoplates through oxidative etching, *Nano Lett*., 14(12): 7201-7206.

Chen X., Zhang J.J, Xuan J. and Zhu J.J., 2009; Myoglobin/gold nanoparticles/carbon spheres 3-D architecture for the fabrication of a novel biosensor, *Nano Res*., 2(1): 210-219.

Chudnovsky Y., Khavari P.A., Adams A.E., 2005; Melanoma Genetics and the Development of Rational Therapeutics. *J. Clin. Invest*., 115(1): 813-24.

Clark C, Bryden A, Dawe R., Moseley H., Ferguson J. and Ibbotson S.H., 2003; Topical 5-aminolaevulinic acid photodynamic therapy for cutaneous lesions: Outcome and comparison of Light Sources, *Photodermatol. Photoimmunol. Photomed*., 19(3): 134-41.

Clements A., Young J.C., Constantinou N. and Frankel G., 2012; Infection strategies of enteric pathogenic Escherichia coli. *Gut Microbes*, 3(2): 71-87.

Cole J.N., Pence M.A., von Köckritz-Blickwede M., Hollands A., Gallo R.L., Walker M.J., Nizet V., 2010; M Protein and Hyaluronic Acid Capsule Are Essential for In Vivo Selection of covRS Mutations Characteristic of Invasive Serotype M1T1 Group A Streptococcus1. *mBio*., (4): e00191-10.

Collins TL, Markus EA, Hassett DJ, Robinson JB. 2010. The effect of a cationic porphyrin on Pseudomonas aeruginosa biofilms. *Curr. Microbiol*. 61:411–416.

Colombo A.L., Guimaraes T., Silva L.R., de Almeida Monfardini L.P., Cunha A.K., Rady P., Alves T. and Rosas R.C., 2007; Prospective observational study of candidemia in São Paulo, Brazil: incidence rate, epidemiology, and predictors of mortality. *Infect. Control Hosp. Epidemiol.*, 28(5): 570-576.

Colombo A.L., Nucci M., Park B.J, Nouer A.S., Arthington-Skaggs B., da Matta D.A., Warnock D. and Morgan J., 2006; Epidemiology of candidemia in Brazil: a nationwide sentinel surveillance of candidemia in eleven medical centres. *J. Clin. Microbiol*. 44(1):2816-2823.

Costa-de-Oliveira S., Pina-Vaz C., Mendonca D. and Goncalves Rodrigues A., 2008; A first Portuguese epidemiological survey of fungaemia in a university hospital. *Eur. J. Clin. Microbiol. Infect. Dis.*, 27(5): 365-374.

Courtis A.M., Santos S.A., Guan Y., Hendricks J.A., Ghosh B., Szantai-Kis D.M., Reis S.A., Shah J.V., and Mazitschek R., 2014; Monoalkoxy BODIPYs a fluorophore class for bioimaging, *Bioconjugate Chem*., 25(6): 1043-1051.

Courtis A.M., Santos S.A., Guan Y., Hendricks J.A., Ghosh B., Szantai-Kis D.M., Reis S.A, Shah J.V., and Mazitschek R., 2014; Monoalkoxy BODIPYs, a fluorophore class for bioimaging. *Bioconjug Chem*., 25(6): 1043-105.

Croxenan M.A., and Finlay B.B., 2010; Molecular mechanisms of Escherichia coli pathogenicity. *Nat. Rev. Microbiol*., 8(1): 26-38.

Cunningham M.W., 2000; Pathogenesis of group A streptococcal infections. *Clin. Microbiol.Rev*., 13(3): 470-511.

da Silva G.D., Fialho S.L., Siqueira R.C., Jorge R., Cunha Júnior A. da S., 2010; Implants as drug delivery devices for the treatment of eye diseases, Brazil. *J. Pharmac. Sci*., 46(3): 585-595.

Dan M., Poch F. and Levin D., 2002; High rate of vaginal infections caused by non-C. albicans Candida species among asymptomatic women Med. *Mycol*., 40(1): 383-386.

Daniel M.-C., and Astruc D., 2004, Gold Nanoparticles: assembly, supramolecular chemistry, quantum-size-related properties, and applications toward biology, catalysis, and nanotechnology, *Chem. Rev*., 104(1), 293-346.

Davids L.M. and Kleemann B., 2011; Combating Melanoma: The Use of Photodynamic Therapy as a Novel, Adjuvant Therapeutic Tool. *Cancer Treat. Rev*., 37(1): 465-475.

Davids L.M., Kleemann B., Cooper S. and Kidson S.H., 2009; Melanomas Display Increased Cytoprotection to Hypericin-Mediated Cytotoxicity Through the Induction of Autophagy. *Cell Biol. Int*., 33(10): 1065-1072.

de Sousa M.A., and Lencastre de H., 2004; Bridges from hospitals to the laboratory: genetic portraits of methicillin-resistant Staphylococcus aureus clones. *FEMS Immunology and Medical Microbiology*, 40(2): 101-111.

de Wael E.V., Pardoen J.A., van Koeveringe J.A. and Lugtenburg J., 1977; Pyrromethene–BF2 complexes (4,4′-difluoro-4-bora-3a,4a-diaza-s-indacenes). Synthesis and luminescence properties. *Recl. Trav. Chim. Pays-Bas*, 96(12): 306-309.

DeRosa M.C. And Crutchley R.J., 2002; Photosensitized singlet oxygen and its applications, *Coord. Chem. Rev*., 234(1): 351-371.

Desai C., Mavrianos J. and Chauhan N., 2011; Candida glabrata Pwp7p and Aed1p are required for adherence to human endothelial cells. *FEMS Yeast Res*., 11(1): 595-601.

DeSantis C.E, Lin C.C, Mariotto A.B, et al., 2014; Cancer Treatment and Survivorship Statistics. *CA Cancer J Clin*., 64(4): 252-271.

Descalzo, A. B.; Xu, H. J.; Shen, Z.; Rurack, K., 2008; Spectroscopy, Imaging, and Probes, Wolfbeis, *O. S., Ed*., 1130(1): 164-171.

Diamond R.D., 1993; Interactions of phagocytic cells with Candida and other opportunistic fungi. *Arch. Med. Res*., 24(1): 361-369.

Dichiara M., Prezzavento O., Marrazzo A., Pittala V., Salerno L., Rescifina A. and Amata E., 2017; Recent advances in drug discovery of phototherapeutic non-porphyrinic anticancer agents. *Eur. J. Med. Chem*., 142(1): 459-485.

Dickson M R and Lyon A L., 2000; Unidirectional plasmon propagation in metallic nanowires, *J. Phys. Chem. B*, 104(26): 6095-6098.

Dlugaszewska J., Szczolko W., Koczorowski T., Skupin-Mrugalska P., Teubert A., Konopka K., Kucinska M., Murias M., Düzgüneş N., Mielcarek J., Goslinski T., 2017; Antimicrobial and anticancer photodynamic activity of a phthalocyanine photosensitizer with N -methyl morpholiniumethoxy substituents in non-peripheral positions. *J. Inorg. Biochem*., 172(1): 67-79.

Doherty R.E., Sazanovich I.V., McKenzie L.K., Stasheuski A.S., Coyle R., Baggaley E., Bottomley S., Weinstein J.A., Bryant H.E., 2016; Photodynamic killing of cancer cells by a Platinum(II) complex with cyclometallating ligand. *Scientific Reports*, 6 (1): 22668

Dolmans D. E. J. G. J., Fukumura D., and Jain R.K., 2003; Photodynamic therapy for cancer, *Nat. Rev. Cancer*, 3(1): 380-387.

Donnenberg M., and Whittam T.S., 2001; Pathogenesis and evolution of virulence in enteropathogenic and enterohemorrhagic Escherichia coli. *J. Clin. Invest*., 107(5):539-48.

Dougherty T., Gomer C., Henderson B., Jori G., Kessel D., Korbelik M., Moan J., Peng Q. J. 1998; Photodynamic Therapy, *J. Natl. Cancer Inst*., 90 (12): 889- 905.

Dougherty T.J., Grindey G.B., Fiel R., Weishaupt K.R., and Boyle D.G., 1975; Photoradiation Therapy. II. cure of animal tumors with hematoporphyrin and light, *J. National Can. Inst.*, 55(1), 115-121.

Dudhipala N, Narala A., Janga K.Y., and Bomma R., 2016; Amoxycillin trihydrate floating-bioadhesive drug delivery system for eradication of helicobacter pylori: Preparation, In Vitro and Ex Vivo Evaluation, *J Bioequiv Availab*., 8(3): 118-124.

Eigenbrode S.D., Bosque-Perez N.A., and Davis T.S., 2018; Insect-borne plant pathogens and their vectors: ecology, evolution, and complex interactions. Annu. Rev. Entomol., 63(1): 169-91.

Eggermont A.M.M, Chiarion-Sileni V., Grob J.J., Dummer R., Wolchok J.D., Schmidt H., Hamid O., Robert C., Ascierto P.A., Richards J.M., Lebbé C., Ferraresi V., Smylie M., Weber J.S., Maio M., Konto C., Hoos A., de Pril V., Gurunath R.K., de Schaetzen G., Suciu S., Testori A., 2014; Adjuvant Ipilimumab Versus Placebo After Complete Resection of High-Risk Stage III Melanoma (EORTC 18071): A Randomised, Double-Blind, Phase 3 Trial, 16(5):522-530.

Espinel-Ingroff A., Canton E., Peman J., Rinaldi M. G. and Fothergill A. W., 2009; Comparison of 24-Hour and 48-Hour Voriconazole MICs as Determined by the Clinical and Laboratory Standards Institute Broth Microdilution Method (M27-A3 Document) in Three Laboratories: Results Obtained with 2,162 Clinical Isolates of Candida spp. and Other Yeasts *J. Clin. Microbiol*., 47(1): 2766-2771.

Esserman L.J., Thompson I.M., Reid B., Nelson P., Ransohoff D.F., Welch H.G., Hwang S., Berry D.A., Kinzler K.W., Black W.C., Bissell M., Parnes H., Srivastava S., 2014; Addressing Overdiagnosis and Overtreatment in Cancer: A Prescription for Change. *Lancet Oncol*., 15(6): 234-242.

Eustis S. and El-Sayed M.A., 2006; Why gold nanoparticles are more precious than pretty gold: Noble metal surface plasmon resonance and its enhancement of the radiative and nonradiative properties of nanocrystals of different shapes, *Chem. Soc. Rev*., 35(1): 209-217.

Felden B., Vandenesch F., Bouloc P. and Romby P., 2011; The Staphylococcus aureus RNome and Its Commitment to Virulence. *PLoS Pathog*., 7(1): e1002006.

Ferreira A.J.G., Carr J.H., Starling C.E.F., de Resende A.E. and Donlan R.M., 2009; Biofilm formation and effect of caspofungin on biofilm structure of Candida species bloodstream isolates. *antimicrob. Agents chemother*., 53(10): 4377-4384.

Fidel P.L., Vazquez J.A., Sobel J.D., 1999; Candida glabrata: review of epidemiology, pathogenesis, and clinical disease with comparison to C. albicans. *Clin. Microbiol. Rev*., 12(1): 80-96.

Finnan S., Morrissey J.P., O'Gara F., Boyd E.F., 2004; Genome diversity of Pseudomonas aeruginosa isolates from cystic fibrosis patients and the hospital environment. *J. Clin. Microbiol.*, 42(1): 5783-5792.

Fonzi W.A. and Calderon R.A., 2001; Virulence factors of Candida albicans. *Trends Microbiol*., 327(1): 333-339.

Fuchs T.M., Eisenreich W., Heesemann, J., and Goebel,W., 2012; Metabolic adaptation of human pathogenic and related nonpathogenic bacteria to extra- and intracellular habitats. *FEMS Microbiol. Rev*., 36(1): 435-462.

Gallud A, Silva AD, Maynadier M, Basile I, Fontanel S, Lemaire C., Maillard P., Blanchard-Desce M., Mongin O., Morère A., Durand J-O., Raehm L., Garcia M. and Gary-Bobo M., 2013; Functionalized nanoparticles for drug delivery, one- and two-photon photodynamic therapy as a promising treatment of retinoblastoma., *J Clin Exp Ophthalmol* 4: 288.

Gao C.B., Vuong J., Zhang Q., Liu Y.D. and Yin Y.D., 2012; One-step seeded growth of Au nanoparticles with widely tunable sizes, *Nanoscale*, 4(1): 2875-2878.

Garbe C. and Blum A., 2001; Epidemiology of cutaneous melanoma in Germany and worldwide, Skin Pharmacol. *Appl. Skin. Physiol*., 14(5): 280-290.

Garzoni C., and Kelley W. L., 2009; Staphylococcus aureus: new evidence for intracellular persistence. *Trends Microbiol*., 17(1): 59-65.

Gibbs J.H., Robins L/T., Zhou Z., Bobadova-Parvanova P., Cottam M., McCandless G.T., Fronczek F.R., and Vicente M.G.H., 2013; Spectroscopic, computational modeling and

cytotoxicity of a series of meso-phenyl and meso-thienyl-BODIPYs. *Bioorg. Med. Chem*., 21(18): 5770-5781.

Gillmore B.T., Retsinas E.M., Lorenz J.S., 1998; An C3b receptor of candida albicans structure, function and correlates for pathogenicity. *J. Infect. Dic*., 157(1): 34-38.

Gopi S, Amalraj A. and Thomas S., 2016; Effective drug delivery system of biopolymers based on nanomaterials and hydrogels - A Review. *Drug Des*., 5(2): 129.

Gorman, A., J. Killoran, O'Shea C., Kenna T., Gallagher W.M., and O'Shea D.F., 2004; In vitro demonstration of the heavy-atom effect for photodynamic therapy, *J. Am. Chem. Soc.* 126(34), 10619–10631.

Goze C, Ulrich G, Ziessel R., 2007; Tetrahedral boron chemistry for the preparation of highly efficient "Cascatelle" devices, *J. Org. Chem*., 72(2): 313-322.

Gryko D.T, Gryko D. and Lee H.C., 2012; , C.-H. 5-Substituted dipyrranes: Synthesis and reactivity, *Chem. Soc. Rev*., 41(1): 3780-3789.

Gu X., Nie C., Lai K., and Lin C., 2006; Synthesis of silver nanorods and nanowires by titrate-reduced route in aqueous solution, *Mater. Chem. Phys*., 96(1): 217-222.

Guimarães I.S., Daltoé R.D., Herlinger A.L., Madeira K.P., Ladislau T., Valadão I.C., Junior P.C.L.M., Teixeira S.F., Amorim G.M., dos Santos D.Z., Demuth K.R., and Rangel L.B.A., 2013; Conventional cancer treatment. In: Cancer Treatment-Conventional and Innovative Approaches: In Tech. London, England: InTechOpen Limited; 2013.

Gundogdu E., Baspinar Y., Koksal C., Ince I., and Karasulu E., 2013; A Microemulsion for the oral drug delivery of pitavastatin. *Pharmaceut. Anal. Acta*., 4(1): 209.

Hamblin M.R. and Hasan T., 2004; Hasan TPhotodynamic therapy: a new anti-microbial approach to infectious disease, *Photochem. Photobiol. Sci*., 3(5): 436-450.

Hancock R.E.W., 1997; The bacterial outer membrane as a drug barrier. *Trends Microbiol*., 5(1): 37-42.

Helmbach H., Rossmann E., Kern M.A., Schadendorf D., 2001; Drug-resistance in Human Melanoma. *Int. J. Cancer*., 93(5): 617-622.

Hoppe-Seyler, F. 1871; About the chemical composition of pus, *Medicinal-chemical studies*, 4(1): 486-501.

Hossler F., https://visualsunlimited.photoshelter.com/image/I0000fEbrbYy0LKU.

Hu M., Chen J., Li Z.-Y., Au L., Hartland G.V., Li X., Marquez M. and Xia Y., 2006; Gold nanostructures: engineering their plasmonic properties for biomedical applications, *Chem. Soc. Rev.*, 35(1): 1084-1094.

Hurdle J.G, O'Neill A.J. and Chopra I. 2005; Prospects for aminoacyl-tRNA synthetase inhibitors as new anti-microbial agents. *Antimicrob. Agents Chemother*, 49(12): 4821-4833.

Hwang H.S., Shin H., Han J., and Na K., 2018; Combination of photodynamic therapy (PDT) and anti-tumor immunity in cancer therapy. *J. Pharma. Invest*., 48(1): 143-151.

Hwang H.S.., Shin H., Han J., and Na K., 2018; Correction to: Combination of photodynamic therapy (PDT) and anti-tumor immunity in cancer therapy, *J. Pharma. Invest*., 48:143–151.

Jana, N. R., Gearheart, L., and Murphy, C. J., 2001; Seed-Mediated growth approach for Shape-Controlled synthesis of spheroidal and rod-like gold nanoparticles using a surfactant template, *Adv. Mater*., 13(18): 1389-1393.

Jayaraman S.S, Rayhan D.J, Hazany S., Kolodney M.S, 2014; Mutational Landscape of Basal Cell Carcinomas by Whole-Exome Sequencing. *J. Invest. Dermatol*., 134(1): 213-220.

Jean G.W., and Shah S.R., 2008; Epidermal growth factor receptor monoclonal antibodies for the treatment of metastatic colorectal cancer. *Pharmacotherapy*, 28: 742-754.

Jhappan C., Noonan F.P., and Merlino G., 2003; Ultraviolet Radiation and Cutaneous Malignant Melanoma, *Oncogene*, 22(20): 3099-3112.

Jin, R., Cao, Y., Mirkin, C. A., Kelly, K. L., Schatz, G. C. and Zheng, J. G., 2001; "Photoinduced conversion of silver nanospheres to nanoprisms", *Science*, 294(5548), 1901-1903.

Joachim H. and Polayes S., 1940; Subacute endocarditis and systemic mycosis (monilia). *JAMA*, 115(3): 205-208.

Johnson E.M., Warnock D.W., Luker J., Porter S.R. and Scully C., 1995; Emergence of azole drug resistance in Candida species from HIV-infected patients receiving prolonged fluconazole therapy for oral candidosis. *J. Antimicrob. Chemother*., 35(1): 103-114.

Johnson T.W., Dress K.R. and Edwards M., 2009; Using the golden triangle to optimize clearance and oral absorption, *Bioorg. Med.Chem. Lett*., 19(19): 5560-5564.

Josefsen L. B., Boyle R. W., 2008; Photodynamic therapy and the development of metal-based photosensitizers, *Met. Based Drugs*, 276109.

Juarranz A., Jaen P., Sanz-Rodriguez F., Cuevas J., and Gonzalez S., 2008; Photodynamic therapy of cancer. Basic principles and applications, *Clin. Transl. Oncol.*, 10(1): 148-154.

Junqueira J.C., Jorge A.O.C., Barbosa O.J., Rossoni R.D., Vilela S.F.G., Costa A.C.B.P., Primo F.L., Gonçalves J.M., Tedesco AC. and Suleiman J.M.A.H., 2012; Photodynamic inactivation of biofilms formed by Candida spp., Trichosporon mucoides, and Kodamaea ohmeri by cationic nanoemulsion of zinc 2,9,16,23-tetrakis(phenylthio)-29H, 31H-phthalocyanine (ZnPc). *Lasers Med. Sci*., 27(1): 1205-1212.

Juzeniene, A., Peng Q., and Moan J., 2007; Milestones in the development of photodynamic therapy and fluorescence diagnosis, *Photochem. Photobiol. Sci*. 6(1): 1234-1245.

Kabanov A.V., Nazarova I.R., Astafieva I.V., Batrakova E.V., Alakhov V.Y., Yaroslavov A.A. and Kabanov V.A., 1995; micelle formation and solubilization of fluorescent probes in poly(oxyethylene-b-oxypropylene-b-oxyethylene) solutions, *Macromolecules*., 28(1): 2303-2314.

Kamkaew A. and Burgess K., 2013; Double-Targeting Using a TrkC Ligand Conjugated to Dipyrrometheneboron Difluoride (BODIPY) Based Photodynamic Therapy (PDT) Agent. *J. Med. Chem*., 56(19): 7608-7614.

Kamkaew A., Lim S.H., Lee H.B., Kiew L.V., Chung L.Y., and Burgess K., 2013; BODIPY dyes in photodynamic therapy. *Chem. Soc. Rev*., 42(1): 77-88.

Kaper J.B., Nataro J.P., Mobley H.L., 2004; Pathogenic Escherichia coli. *Nat. Rev. Microbiol*., 2(1): 123-40.

Karolin J., Johansson L. B. A., Strandberg L., Ny T., 1994; Fluorescence and absorption spectroscopic properties of dipyrromethene boron difluoride (bodipy) derivatives in liquids, lipid-membranes, and proteins. *J. Am. Chem. Soc*., 116(1): 7801.

Kee H.L., Kirmaier C., Yu L., Thamyongkit P., Youngblood W.J., Calder M.E., Ramos L., Noll B.C., Bocian D.F., Scheidt W.R., Birge R.R., Lindsey J.S. and Holten D., 2005; Structural control of the photodynamics of Boron-Dipyrrin complexes, *J. Phys. Chem. B*, 109(43): 20433-20443.

Kelly, K. L., Coronado, E., Zhao, L. L. and Schatz, G. C., 2003; The optical properties of metal nanoparticles: The influence of size, shape, and dielectric environment, *J. Phys. Chem. B*, 107(3), 668-677.

Kim S.Y, Lee J., 2003; 3-D-QSAR study and molecular docking of methionyl-tRNA synthetase inhibitors, *Bioorg Med Chem*., 11(1): 5325-5331.

Kleemann B., Loos B., Scriba T.J, Lang D. and Davids L.M., 2014; PloS ONE, 9(7): e103762.

Knodler L.A.,and Celli J., 2011; Eating the strangers within: host control of intracellular bacteria via xenophagy. *Cell. Microbiol*., 13(9): 1319-1327.

Kondrashina O.V., 2013; A Targeted Drug Delivery System of Gd3+ for Neutron Capture Therapy against Cancer is Metalorganic Magnetic Nanoparticles. *J. Nanomed. Biotherapeutic. Discov*., 3(1): 116.

Korbelik M., Krosl G., Krosl J., and Dougherty G.J., 1996; The role of host lymphoid populations in the response of mouse EMT6 tumor to photodynamic therapy. *Cancer Res*., 56(1): 5647-5652.

Korbelik, M. and Krosl, G., 1994; Cellular levels of photosensitizers in tumors: the role of proximity to the blood supply, *Br. J. Cancer*, 70(4): 604-610.

Kosaka N., Ogawa M., Choyke PL. and Kobayashi H., 2009; Clinical implications of near-infrared fluorescence imaging in cancer, *Future Oncol*., 5(9):1501-1511.

Kothavade R.J., Kura M.M., Valand A.G. and Panthaki M.H., 2010; Candida tropicalis: its prevalence, pathogenicity and increasing resistance to fluconazole. *J. Med. Microbiol*., 59(8): 873-880.

Koushik O.S., Rao Y.V., Kumar P., and Karthikeyan R.., 2016; Nano Drug Delivery Systems to Overcome Cancer Drug Resistance – A, Review. *J. Nanomed. Nanotechnol*., 7(3): 378.

Kue C.S., Kamkaew A., Burgess K., Kiew L.V., Chung L.Y., Lee H.B., 2016; Small molecules for active targeting in cancer. *Med. Res. Rev*., 36(3): 494-575.

Kue C.S., NG S.Y., Voon S.H., Kamkaew A., Chung L.Y., Kiew L.V., and Lee H.B., 2018; Recent strategies to improve boron dipyrromethene (BODIPY) for photodynamic cancer therapy: an updated review, *Photochem. Photobiolo. Sci*., 11(1): 1-48.

Kuphal S. and Bosserhoff A., 2009; Recent Progress in Understanding the Pathology of Malignant Melanoma. *J. Pathol*., 219(4): 400-409.

Kurlenda J., Grinholc M., 2012; Alternative therapies in Staphylococcus aureus diseases. *Acta. Biochim. Pol.*, 59(2):171-184.

Lakshmi, V., Sharma, R., and Ravikanth, M., 2016; Functionalized borondipyrromethenes and their applications. *Rep. Org. Chem*. 6(1): 1–24.

LaMer, V. K. and Dinegar, R. H. (1950), "Theory, production, and mechanism of formation of monodispersed hydrosols", *J. Am. Chem. Soc*., 72(11), 4847-4854.

Lazzarato L., Gazzano E., Blangetti M., Fraix A., Sodano F., Picone G.M., Fruttero R., Gasco A., Riganti C., and Sortino S., 2019; Combination of PDT and NOPDT with a Tailored BODIPY Derivative, *Antioxidants*, 8(1): 531-545.

Leng B-F., Qiu J-Z., Dai X-H., Dong J., Wang J-F., Luo M-J., et al., 2011; Allicin reduces the production of α-toxin by Staphylococcus aureus. *Molecules*, 16(1): 7958-7968.

Leonard, K. A., M. I. Nelen, T. P. Simard, S. R. Davies, S. O. Gollnick, A. R. Oseroff, S. L. Gibson, R. Hilf, L. B. Chen and M. R. Detty 1999; Synthesis and Evaluation of Chalcogenopyrylium Dyes as Potential Sensitizers for the Photodynamic Therapy of Cancer. *J. Med. Chem*. 42(19), 3953–3964.

Li L., Han J., Nguyen B., and Burgess K., 2008; Syntheses and Spectral Properties of Functionalized, Water-Soluble BODIPY Derivatives. *J. Org. Chem*., 73(1): 1963-1970.

Li L., Redding S. and Dongari-Bagtzoglou A., 2007; Candida glabrata: an emerging oral opportunistic pathogen. *J. Dent. Res*., 86(1): 204-215.

Li Z.G., Mintzer E. and Bittman R., 2006; First synthesis of free cholesterol-BODIPY conjugates. *J. Org. Chem*., 71(4): 1718-1721.

Liang H.P., Zhang H.M., Hu J.S., Guo Y.G., Wan L.J. and Bai C.L., 2004; Pt Hollow Nanospheres: Facile Synthesis and Enhanced Electrocatalysts, *Angew. Chem., Int. Ed*., 43(1): 1540-1543.

Lin J., Nishino K., Roberts M.C., Tolmasky M., Aminov R.I., and Zhang, L., 2015; Mechanisms of antimicrobial resistance, *Microbiol*., 6(1): 1-3.

Lincoln R., Durantini A.M. Greene E.L., Martínez S.R., Knox R., Becerra M.C., and Cosa G., 2017; meso-Acetoxymethyl BODIPY dyes for photodynamic therapy: improved photostability of singlet oxygen photosensitizers, *Photochem. Photobiol. Sci*., 16(1): 178-184.

Lipson R.L., Baldes E.J., and Gray M.J., 1967; Hematoporphyrin derivative for detection and management of cancer. *Cancer*, 20(12): 2255-2257.

Liu Dongyou, 2014; Molecular detection of human fungal pathogens. Taylor and Francis CRC Press, Boca Raton, Florida, USA. ISBN: 9781439812402.

Liu R., 2012; Nanostructured lipid carriers as the most promising approach in ocular drug delivery system, *J. Nanomed. Biotherapeut. Discov*., 2(4): 116.

Loudet A. and Burgess K., 2007; BODIPY Dyes and Their Derivatives: Syntheses and Spectroscopic Properties, *Chem. Rev*., 107(11): 4891-4932.

Loudet A. and Burgess K., 2007; BODIPY dyes and their derivatives: syntheses and spectroscopic properties. *Chem. Rev*., 107(1): 4891-4932.

Lu H., Mack J., Yanga Y., and Shen Z., 2014; Structural modification strategies for the rational design of red/NIR region BODIPYs. *Chem. Soc. Rev*., 43(1): 4778-4823.

Mack J. and Kobayashi N., 2011; Low Symmetry Phthalocyanines and Their Analogues. *Chem. Rev*., 111(2): 281-321.

Mandal B., 2016; Personalized Nanotheranotics for Cancer. *J. Biotechnol Biomater*., 6(1): 127.

Mansoori A.G. and Soelaiman T.A.F., 2005; Nanotechnology-An Introduction for the Standards Community, *J. ASTM Int*., 2(6): 1-21.

Martin T.A, Ye L., Sanders A.J, Lane J., and Jiang W.G. Cancer invasion and metastasis: molecular and cellular perspective. In: Jandial R, ed. Madame Curie Bioscience Database. Austin, TX: Landes Bioscience; 2013. https://www.ncbi.nlm.nih.gov/books/ NBK164700/.

Mathews R.C., 1994; Pathogenicity determinants of Candida albicans: potential targets for immunotherapy? *Microbiol.*, 140(1): 1505-1511.

Mayer F.L., Wilson D. and Hube B., 2013; Candida albicans pathogenicity mechanisms. *Virulence*, 4(2): 119-128.

Mehrotra P., 2016; Biosensors and their applications – A review, *J. Biol. Craniofacial Res*., 6(2):153-159.

Messer S.A., Jones R.N. and Fritsche T.R., 2006; International Surveillance of Candida spp. and Aspergillus spp.: Report from the SENTRY Antimicrobial Surveillance Program (2003). *J. Clin. Microbiol*., 44(1):1782-1787.

Meurman J.H., Siikala E., Richardson M. and Rautemaa R., 2007; A. Méndez-Vilas (Ed.): 719-731.

Moan J. and Berg K., 1991; The Photodegradation of Porphyrins in Cells Can Be Used to Estimate the Lifetime of Singlet Oxygen, *Photochem. Photobiol*., 53(4): 549-553.

Moncrieff M.D., Martin R., O'Brien C.J., Shannon K.F., Clark J.R., Gao K., McCarthy W.M., and Thompson J.F.., 2008; *Ann. Surg. Oncol*., 15(1): 3022-3027.

Morton CA., 2004; Photodynamic therapy for nonmelanoma skin cancer and more? *Arch. Dermatol*.,140:116-120.

Moser, J. G. 1998; Definitions and general properties of 2nd and 3rd generation photosensitizers. In Photodynamic Tumor Therapy: 2nd and 3rd Generation Photosensitizers (Edited by J. G. Moser), p. 256. Harwood Academic Publishers, Amsterdam.

Mostafavi S.H. and Babu J.R., 2013; Nano-sized drug delivery, *J. Mol. Pharm. Org. Process. Res*., 1(1): 108.

Moulder J.W., 1962; The Biochemistry of Intracellular Parasitism. Chicago: The University of Chicago Press.

Moulder J.W.; 1985; Comparative biology of intracellular parasitism. *Microbiol. Rev*., 49(1): 298-337.

Mroz P., Hashmi J.T, Huang Y-Y., Lange N., and Hamblin M.R., 2011; Stimulation of anti-tumor immunity by photodynamic therapy. *Expert. Rev. Clin. Immunol*., 7(1):75-91.

Munoz-Flores B.M., Kharisov B.I., Jimenez-Perez V.M., Martínez P.E., and Lopez S.T., 2011; Recent Advances in the Synthesis and Main Applications of Metallic Nanoalloys, *Ind. Eng. Chem. Res*., 50(1): 7705-7721.

Nagarajan R., and Hatton T.A., 2008; Nanoparticles: Synthesis, Stabilization, Passivation, and Functionalization, xi–xiv. ISBN: 9780841269699 0841269696

Nahm M.H., Apicella M.A., and Briles D.E., 1999; "Immunity to extracellular bacteria," in Fundamental Immunology, ed.W.E. Paul (Philadelphia, PA, Lippincott Raven),1373-1386.

Naidoo C., Kruger C.A, and Abrahamse H., 2018; Photodynamic Therapy for Metastatic Melanoma Treatment: A Review, Technol. *Cancer Research and Treatment*, 17(1): 1-15.

Nasution A.I., 2013; Varulence factor and pathogenicity of Candida albicans in Oral Candidiasis. *World J. dent*., 4(4): 267-271.

Nataro J.P. and Kaper J.B., 1998; Diarrheagenic Escherichia coli. *Clin. Microbiol. Rev*., 11(1):142-201.

Nayak, C. S. 2005; Photodynamic therapy in dermatology, *Indian J. Dermatol. Venereol. Leprol*., 71(3): 155-160.

Neupane J., Ghimire S., Shakya S., Chaudhary L., and Shrivastava V.P., 2010; "Effect of light emitting diodes in the photody-namic therapy of rheumatoid arthritis," *Photodiagnosis and Photodynamic Therapy*, 7(1): 44-49.

Neupane J.; Ghimire S.; Shakya S.; Chaudhary L.; Shrivastava V.P., 2010; Effect of light-emitting diodes in the photodynamic therapy of rheumatoid arthritis. *Photodiagn. Photodyn. Ther*. 2010, 7, 44-49.

Nguyen A.L., Bobadova-Parvanova P., Hopfinger M., Fronczek F.R., Smith K.M., Vicente M.G., 2015; Synthesis and Reactivity of 4,4-Dialkoxy-BODIPYs: An Experimental and Computational study. *Inorg. Chem*., 54(1): 3228-3236.

Ni Y. and Wu J., 2014; Far-red and near-infrared BODIPY dyes: synthesis and applications for fluorescent pH probes and bio-imaging, *Org. Biomol. Chem*., 12(23): 3774-3791.

Nirmala M.J. and Nagarajan R., 2016; Microemulsions as potent drug delivery systems , *J. Nanomed. Nanotechnol*., 7(3): 139.

Noble GT, Stefanick JF, Ashley JD, Kiziltepe T, Bilgicer B. Ligand-targeted liposome design: challenges and fundamental considerations. *Trends Biotechnol*., 32(1): 32-45.

Oppermann M., Geilen C.C., Fecker L.F., Gillissen B., Daniel P.T., Eberle J., 2005; independent induction of apoptosis in human melanoma cells by the proapoptotic Bcl-2-related protein Nbk/Bik. *Oncogene*, 24(49): 7369-7380.

Ortiz M.J., Agarrabeitia A.R., Duran-Sampedro G., Prieto J.B., Lopez T.A., Massad W.A., Montejano H.A., Garcia N.A. and Arbeloa I.L., 2012; Synthesis and functionalization of new polyhalogenated BODIPY dyes. Study of their photophysical properties and singlet oxygen generation; *Tetrahedron*, 68(4): 1153-1162.

Ossio R., Roldán-Marín R., Martínez-Said H., Adams D.J. and Robles-Espinoza C.D., 2017; Melanoma: A Global Perspective. *Nat. Rev. Cancer*, 17(7): 393-394.

Ozdemir T., Bila J.L., Sozmen F., Yildirim L.T., Akkaya E.U., 2016; Orthogonal Bodipy Trimers as Photosensitizers for Photodynamic Action. *Org. Lett*., 18(): 4821-4823.

Ozlem S. and Akkaya E. U., 2009; Thinking outside the silicon box: Molecular and logic as an additional layer of selectivity in singlet oxygen generation for photodynamic therapy, *J. AM. Chem. SOC*., 131(1): 48-49.

Perenboom J A A J, Wyder P, and Meier P., 1981; Electronic properties of small metallic particles, *Phys. Rep*., 78(1): 173.

Pervaiz S., Olivo M., 2006; Art and Science of Photodynamic Therapy, *Clin. Exp. Pharmacol. Physiol*., 33(5-6), 551-556.

Pfaller M. A., Diekema D. J., Procop G. W. and Rinaldi M. G., 2007; Multicenter comparison of the VITEK 2 antifungal susceptibility test with the CLSI broth microdilution reference method for testing amphotericin B, flucytosine, and voriconazole against Candida spp. *J. Clin. Microbiol.*, 45(1): 3522-3528.

Pinheiro M.R.S., Lacerda H.R., Melo R.G.L., Maciel M.A., 2008; Pseudomonas aeruginosa infections: factors relating to mortality with emphasis on resistance pattern and antimicrobial treatment. *Braz. J. Infect. Dis*., 12(1): 509-515.

Pogue B.W., Braun R.D., Lanzen J.L., Erickson C., and Dewhirst M.W., 2001; Analysis of the heterogeneity of pO2 dynamics during photodynamic therapy with verteporfin, *Photochemistry, and Photobiology*, 74(5): 700-706.

Ranyuk E., Cauchon N., Klarskov K., Guérin B., Van Lier J.E., 2013; Phthalocyanine-peptide conjugates: receptor-targeting bifunctional agents for imaging and photodynamic therapy. *J. Med. Chem.*, 56(1): 1520-1534.

Reed J.C., 2000; Mechanisms of Apoptosis. *Amer. J. Pathol*., 157(5): 1415-1430.

Rodrigues C.F., Silva S., Henriques M., 2014; Candida glabrata: a review of its features and resistance. *Eur. J. Clin. Microbiol. Infect. Dis*. 33(1): 673-688.

Rohand T., Baruah M., Qin W., Boens N. and Dehaen W., 2006; Functionalisation of fluorescent BODIPY dyes by nucleophilic substitution. *Chem. Commun*., 266-268.

Rurack K., Kollmannsberger M., Daub J., 2001; A highly efficient sensor molecule emitting in the near-infrared (NIR): 3,5-distyryl-8-(p-dimethylaminophenyl)difluoroboradiaza-s-indacene. *New J. Chem*., 25(1): 289.

Sansonetti P., 2002; Phagocytosis of bacterial pathogens: Implications in the host response. *Seminars in Immunology*, 13(6): 381-90.

Schaller M., Borelli C., Korting H.C. and Hube B., 2005; Hydrolytic enzymes as virulence factors of Candida albicans. *Mycoses*, 48(6): 365-377.

Shaan L. Gellatly and Hancock R.E.W., 2013; Pseudomonas aeruginosa: new insights into pathogenesis and host defenses. *Pathogens and Disease*, 67(3): 159-173.

Shah Z.M., Thangaraj K., Soong M.-L., Wolford L.T., Boyer J.H., Politzer I.R., and Pavlopoulos T.G., 1990; Pyrromethene–BF_2 complexes as laser dyes:1, *Heteroat. Chem*., 1(1): 389.

Shain A.H. and Bastian B.C., 2016; From Melanocytes to Melanomas. *Nat. Rev. Cancer*, 16(1): 345-358.

Shanmugam S., Viswanathan B., and Varadarajan T.K., 2005; Polyoxometalate based soft chemical route for the preparation of Pt nanorods and self-assemblies. *Bull. Mater. Sci*., 28(6): 629-633.

Shao L. C., Sheng C. Q., and Zhang W. N., 2007; Recent advances in the study of antifungal lead compounds with new chemical scaffolds. *Yao Xue Bao*., 42(11): 1129-1136.

Sharma K.V. and Davids L.M., 2012; Depigmentation in melanomas increases the efficacy of hypericin-mediated photodynamic-induced cell death. *Photodiag. Photodyn. Therapy*, 9(2): 156-163.

Shirasu N., Nam S.O., and Kuroki M., 2013; Tumor-targeted photodynamic therapy. *Anticancer Res*., 33(1): 2823-2831.

Siegel R.L, Miller K.D, and Jemal A., 2016; Cancer Statistics, 2016. *CA Cancer J Clin*., 66(1): 7-30.

Silva M.T., 2012; Classical Labeling of Bacterial Pathogens According to Their Lifestyle in the Host: Inconsistencies and Alternatives. Frontiers in Microbiology, 3(71): 1-7.

Slominski A., Tobin D.J., Shibahara S., et al., 2004; Wortsman JMelanin pigmentation in mammalian skin and its hormonal regulation. *Physiol. Rev*., 84(1): 1155-1228.

Soengas M.S and Lowe S.W, 2003; Apoptosis and Melanoma Chemoresistance. *Oncogene*, 22(1): 3138-3151.

Sosa I.O., Noguez C., and Barrera R.G., 2003; Optical Properties of Metal Nanoparticles with Arbitrary Shapes. *J. Phys. Chem. B*, 107(26), 6269-6275.

Strateva T. and Mitov I., 2011; Contribution of an arsenal of virulence factors to pathogenesis of Pseudomonas aeruginosa infections. *Ann Microbiol*., 61(1): 717-732.

Stuart L.M., and Ezekowitz R.A., 2005; Phagocytosis: elegant complexity. Immunity, 22(1): 539-550.

Suedee R., 2013; The use of molecularly imprinted polymers for dermal. Drug delivery. *Pharma. Anal. Acta*., 4(8): 264.

Suhasini S. and Babu C.H.R., 2016; New trends: Delivery systems, *Rev. Pharma. Nanotechnol*., 4(1): 131-139.

Swain S., 2012; Mucoadhesive micro and nanoparticles for oral controlled drug delivery system for prolongation of gastric residence and its application, *Pharmaceut. Reg. Affairs*., 1(4): 115.

Swaminathan S and Jablonski M.M., 2012; Non-biological membranes as drug delivery systems, *J. Memb. Sci. Technol*., 2(3): 108.

Swavey S., and Tran M., 2013; Porphyrin and Phthalocyanine Photosensitizers as PDT Agents: A New Modality for the Treatment of Melanoma, In Tech. Recent Advances in the Biology, Therapy and Management of Melanoma.

Tahtaoui C., Thomas C., Rohmer F., Klotz P., Duportail G., Mely Y., Bonnet D., Hibert M., 2007; Convenient method to access new 4,4-Dialkoxy- and 4,4-Diaryloxy-diaza-s-indacene dyes: Synthesis and spectroscopic evaluation, *J. Org. Chem.,* 72(1): 269-272.

Tang Z.Y., Kotov N.A. and Giersig M., 2002; Spontaneous organization of single CdTe nanoparticles into luminescent nanowires, *Science*, 297(1): 237-240.

Taraszkiewicz A., Fila G., Grinholc M., and Nakonieczna J., 2013; Innovative strategies to overcome biofilm resistance. *Biomed. Res. Int*., 2013(5):150653.

Thevenot D.R., Toth K., Durst R.A., and Wilson G.S., 2001; Electrochemical biosensors: recommended definitions and classification, *Biosens Bioelectron*., 16(1):121-131.

Thompson J.F., Scolyer R.A., Kefford R.F., 2005; Cutaneous Melanoma, Lancet, 365(9460): 687-701.

Thudichum, J. L. 1867; Tenth report of the medical officer of the privy council. H.M. Stationery Office, London. pp. 152–233.

Tian R., Sun W., Li M., Long S., Li M., Fan J., Guo L., and Peng X., 2019; Development of a novel anti-tumor theranostic platform: a near-infrared molecular upconversion sensitizer for deep-seated cancer photodynamic therapy., *Chem. Sci*., 10(1): 10106.

Tian, N., Zhou, Z.-Y., Sun, S.-G., Ding, Y. and Wang, Z. L. (2007), "Synthesis of tetrahexahedral platinum nanocrystals with high-index facets and high electro-oxidation activity", *Science*, 316(5825), 732-735.

Tram K., Yan H., Jenkins H.A., Vassiliev S. and Bruce D., 2009; The synthesis and crystal structure of unsubstituted 4, 4-difluoro-4-bora-3a, 4a-diaza-s-indacene (BODIPY), *Dyes Pigm*., 82(3): 392-395.

Treibs A. and Kreuzer F.H, 1968; Difluorboryl-Komplexe von Di- und Tripyrrylmethenen, *Justus Liebigs Ann. Chem*., 718(1): 208-223.

Triesscheijn M., Baas P., Schellens J.H.M., and Stewart F.A., 2006; Photodynamic therapy in oncology. *Oncologist,* 11(9):1034-44.

Trofa D., Ga´cser A. and Nosanchuk J.D., 2008; Candida parapsilosis, an emerging fungal pathogen. *Clin. Microbiol. Rev*., 21(4): 606-625.

Tromberg, B. J.; Orenstein, A.; Kimel, S.; Barker, S. J.; Hyatt, J.; Nelson, J. S.; Berns, M. W. 1990; *In Vivo* tumor oxygen tension measurements for the evaluation of the efficiency of photodynamic therapy, *Photochemistry, and Photobiology*, 52(2): 375-85.

Ulrich G, Goze C, Guardigli M, Roda A, Ziessel R., 2005; Pyrromethene dialkynyl borane complexes for "Cascatelle" energy transfer and protein labeling, *Angew. Chem. Int. Ed*., 44(24): 3694-3698.

Ulrich G., Ziessel R., and Harriman A., 2008; The chemistry of fluorescent BODIPY dyes: Versatility Unsurpassed, *Angew. Chem. Int. Ed*., 47(7): 1184-1201.

Umezawa K., Matsui A., Nakamura Y., Citterio D. and Suzuki K., 2009; Bright, color-tunable fluorescent dyes in the Vis/NIR region: Establishment of new “Tailor-Made” multicolor fluorophores based on borondipyrromethene, *Chem. Eur. J*., 15(5): 1096-1106.

Vashist S.K., and Venkatesh A.G., 2012; Carbon nanotube-based electrochemical sensors and drug delivery systems: prospects and challenges, *J. Nanomed. Nanotechol*., 3(8): 121.

Vatansever F., de Melo D.C.M.A., Avci P., Vecchio D., Sadasivam M., Gupta A., Chandran R., Karimi M., Parizotto N.A., Yin R., Tegos G.P., Hamblin R.M., 2013; Antimicrobial strategies centered around reactive oxygen species - bactericidal antibiotics, photodynamic therapy and beyond. *FEMS Microbiol Rev*., 37(6): 955-989.

Venugopal V., 2002; Biosensors in fish production and quality control, *Biosens. Bioelectron*., 17(3): 147-157.

Wael E.V., d., Pardoen J.A., Koevering J.A., and Lugtenburg J., 1977; Pyrromethene-BF_2 complexes (4,4′-difluoro-4-bora-3a,4a-diaza-s-indacenes). Synthesis and luminescence properties. Recueil des Travaux Chimiques des Pays-Bas, 96(1): 306-309.

Wagner R.W., and Lindsey J.S., 1996; Boron-dipyrromethene dyes for incorporation in synthetic multi-pigment light-harvesting arrays, *Pure Appl. Chem*., 68(7): 1373-1380.

Wan M.T., Lin J.Y., 2014; Current evidence and applications of photodynamic therapy in dermatology, *Clinical, Cosmetic and Investigational Dermatology*, 7(1):145-163.

Wang J., 2008; Electrochemical glucose biosensors, *Chem Rev*., 108(1): 814-825.

Wang J., Guo X., Li L., Qiu H., Zhang Z., Wang Y. and Sun G., 2018; Application of the Fluorescent Dye BODIPY in the Study of Lipid Dynamics of the Rice Blast Fungus Magnaporthe oryzae. *Molecules*, 23(1): 1594.

Wang J., Tsung C.K., Hayward R.C., Wu Y. and Stucky G.D., 2004; Single-crystal mesoporous silica ribbons, *Angew. Chem., Int. Ed*., 44(2): 332-336.

Weiser J.N., and Nahm M.H., 2008; "Immunity to extracellular bacteria," in Fundamental Immunology, ed.W.E.Paul(Philadelphia: Lippincot Williams & Wilkins), 1182-1203.

Whiteley M., Bangera M.G., Bumgarner R.E., Parsek M.R., Teitzel G.M., Lory S., Greenberg E.P., 2001; Gene expression in Pseudomonas aeruginosa biofilms. *Nature*, 413(1): 860-864.

Wilcken N., 2016; The 'enablers': inhibitors of mTOR, PI3K and CDK that prolong endocrine sensitivity, *Cancer Forum*, 40(3): 16-19.

Wilcoxon, J. P. and Abrams, B. L., 2006; Synthesis, structure and properties of metal nanoclusters. *Chem. Soc. Rev*., 35(11), 1162-1194.

Wolf M.K., 1997; Occurrence, distribution, and associations of O and H serogroups, colonization factor antigens, and toxins of enterotoxigenic Escherichia coli. *Clin. Microbiol. Rev*., 10(1) :569-84.

Wood T.E and Thompson A, 2007; Advances in the chemistry of dipyrrins and their complexes, *Chem. Rev*., 107(5), 1831-1861.

World Health Organization (WHO), 2018; Antimicrobial resistance. (Accessed 16 January 2020). http://www.who.int/mediacentre/factsheets/fs194/en/.

Xia Y., Yang P., Sun Y., Wu Y., Mayers B., Gates B., Yin Y., Kim F. and Yan H., 2003; One-dimensional nanostructures: Synthesis, Characterization, and Applications. *Adv. Mater*., 15(1): 353.

Yamamura H., Ugawa S., Ueda T., Morita A., Shimada S.., 2008; TRPM8 Activation Suppresses Cellular Viability in Human Melanoma, *Am. J. Physiol. Cell Physiol*., 295(2): C296-301

Yano T., Muto M., Minashi K., Onozawa M., Nihei K., Ishikura S., Kaneko K., and Ohtsu A., 2011; Long-term results of salvage photodynamic therapy for patients with local failure after chemoradiotherapy for esophageal squamous cell carcinoma. *Endoscopy*, 43(1): 657- 63.

Ye X.C., Jin L.H., Caglayan H., Chen J., Xing Z.G., Zheng C., Doan-Nguyen V., Kang Y.J., Engheta N., Kagan C.R. and Murray C.B., 2012; Improved size-tunable synthesis of monodisperse gold nanorods through the use of aromatic additives, *ACS Nano*, 6(3): 2804-2817.

Yen Y., Liou J-P., and Liu T-R, Taipei Medical University, 2018; Compounds for inhibiting cancer and viruses. 2019 / 0016743 A1, (viewed 12 January 2020).

Yildiz F.H., 2007; Processes controlling the transmission of bacterial pathogens in the environment. *Research in Microbiology*, 158(3): 195-202.

Yin Y. and Alivisatos A.P., 2005; Colloidal nanocrystal synthesis and the organic-inorganic interface. *Nature*, 437(1): 664-670.

Ying S. and Chunyang L., 2012; Correlation between phospholipase of Candida albicans and resistance to fluconazole. *Mycoses,* 55(1): 50-55.

Yogo T., Urano Y., Ishitsuka Y., Maniwa F. and Nagano T., 2005; Highly Efficient and Photostable Photosensitizer Based on BODIPY Chromophore, *J. Am. Chem. Soc*., 127 (35), 12162-12163.

Yu C., Miao W., Wang J., Hao E. and Jiao J., 2017; Pyrrolyl-BODIPYs: syntheses, properties, and application as environment-sensitive fluorescence probes. *J. Am. Chem. Soc. ACS Omega*, 2(7): 3551-3561.

Zbytek B., Carlson J.A., Granese J., Ross J., Mihm M.C., Slominski J.., 2008; Current Concepts of Metastasis in Melanoma, *Expert. Rev. Dermatol*., 3(1): 569-585.

Zelickson BD., 2005; Mechanisms of action of topical aminolevulinic acid. In: Goldman MP, editor. Photodynamic Therapy. 1st ed. Philadelphia: Elsevier Saunders; 2005, 1-12.

Zhang D. K., Wang Y. C., Xiao Y., Qian S. X., Qian X. H., 2009; Long-wavelength boradiazaindacene derivatives with two-photon absorption activity and strong emission: versatile candidates for biological imaging applications. *Tetrahedron*, 65(35): 8099-8103.

Zhang G., Wang M., Ndung'U C., Bobadova-Parvanova P., Fronczek F.R., Smith K.M., and Vicente G.M.H., 2020; Synthesis and investigation of BODIPYs with restricted meso-8-aryl rotation. *J. Porphyrins and Phthalocyanines*, 24(5and7): 869-877.

Zhang Q., Li N., Goebl J., Lu Z., and Yin Y., 2011; A systematic study of the synthesis of silver nanoplates: Is Citrate a "Magic" reagent? *J. Am. Chem. Soc*., 133(46): 18931-18939.

Zhao J., Xu K., Yang W., Wang Z., and Zhong F., 2015; The triplet excited state of Bodipy: formation, modulation and application. *Chem. Soc. Rev*., 1(1): 1-36.

Zhao Q.A., Li F.Y. and Huang C.H., 2010; Phosphorescent chemosensors based on heavy-metal complexes, *Chem. Soc. Rev*., 39(8): 3007-3030.

Zhou Z., Song J., Nie L., and Chen X., 2016; Reactive oxygen species generating systems meeting challenges of Photodynamic Cancer Therapy. *Chem. Soc. Rev*., 45(23): 6597-6626.

Zhu Y., 2013; Mesoporous silica nanoparticles with a core-shell structure for drug delivery, *J. Bioanal. Biomed*., 5(3): 117.

Ziessel R., Bonardi L., Retailleau P. and Ulrich G., 2006; Isocyanate-, isothiocyanate-, urea-, and thiourea-substituted Boron Dipyrromethene dyes as fluorescent probes, *J. Org. Chem*., 71(8), 3093-3102.

Ziessel R., Ulrich G., and Harriman A., 2007; The chemistry of Bodipy: A new El Dorado for fluorescence tools, *New J. Chem*., 31(4): 496-501.

Zou J., Yin Z., Ding K., Tang Q., Li J., Si W., Shao J., Zhang Q., Huang W. and Dong X., 2017; BODIPY derivatives for photodynamic therapy: Influence of configuration versus heavy atom effect, *ACS Appl. Mater. Interfaces*, 9(1): 32475-32481.

CHAPTER 3

Experimental data

3.1 Reagents and Solvents used

The following list of reagents was used as received without any further purification during this study: 2,4-dimethyl pyrrole, 3-ethyl-2,4-dimethyl pyrrole, 4-isopropyl benzaldehyde, 4-ethyl benzaldehyde, 2,5-diaminobenzenesulfonic acid (DABSA), 3,4-diaminobenzoic acid (DABA), Sulfamoilbenzoic acid (SMBA), pyrrole-2-aldehyde, naphthalene-2-sulfonamide, 4-trifluoroacetylpyrrole, melamine, 1,3,5-tiriodo-4-aminobenzoic acid, 1,2,4-triiodobenzoic acid, Chloranil, sulfuric acid, N,N-diisopropylethylamine (DiPEA), boron trifluoro ethyl etherate ($BF_3.OEt_2$), trifluoroacetic acid (TFA), iodine solution, iodic acid, carboxylpyrrole, 3-carboxylbenzaldehyde and thionyl chloride. Precursors for synthesis were obtained from Sigma Aldrich South Africa. Solvents such as dichloromethane (DCM), ethyl acetate (EtAc), and methanol (MeOH) used for synthesis were dried before use using activated molecular sieves. Chromatographic purification with Chloroform, DCM, EtOAc, Hexane, dimethylformamide (DMF), dimethyl sulfoxide (DMSO), acetonitrile, Acetone, and ethanol (EtOH) was carried out using solvents as obtained. Reactions were carried under an inert atmosphere by purging the reaction mixture with argon. Thin-layer chromatography (TLC) was performed on Sigma silica gel TLC Al foil with 60 Å medium pore diameters. Silica gel high purity grade 60 Å pore size, 70 – 230 mesh, 63 – 200 µm, Sephadex LH-20, and bio beads particle size 40-80 µ were used as stationary phases for column chromatography from Sigma Aldrich. All BODIPYs were run through silica chromatography columns (10 times repeated elutions), bio beads, and Sephadex chromatography columns (3 times elutions) to get pure compounds. Other stationary phases which were later omitted for use from the study due to their clogging and blocking tendencies were: Alumina (both basic and acidic), cellulose, and silica gel with a larger pore size (these did not give the desired separation as the bands were clustering or the column would develop fissures).

3.2 Characterization techniques

The optical density properties of the synthesized complexes were observed using the UV-1800, UV-Vis spectrophotometer (Shimadzu), and fluorescence spectra were obtained from the RF-6000 Spectro fluorophotometer (Shimadzu). Perkin Elmer Spectrum 100 FT-IR spectrometer was used for FT-IR analysis. Mass spectrometer spectra were obtained from Agilent HRLC-

MS and the NMR spectra were obtained using Brucker XSN21 NMR. Nanoparticle size distribution and potential were obtained from DTS nano zeta sizer Malvern. TEM and SEM images were collected with FEI Tecnai T12 TEM and FEI Nova Nanolab 400 SEM. XRD patterns for both BODIPY PSs and nanoparticles were carried out with Phillips X‟Pert^3 XRD spectrometer respectively.

3.2.1 UV-Visible spectroscopy

UV-Vis spectroscopy uses visible light and near-ultraviolet (UV) light ranges to excite the chromophores and measure the light absorbed and the relationship between the concentration and the amount of light absorbed by dissolved molecules. Wavelengths (190-1100 nm) in the UV-Visible range is absorbed by most dissolved BODIPY compounds. Absorption spectroscopy correlates the type and amount of radiation absorbed by a material to its concentration, identity, and molecular structure. To obtain a spectrum, a deuterium (D2) lamp projects a light which is emitted and passes through a slit to a monochromator consisting of either a prism or a rotating metal grid (also known as grating) to the sample. The incoming light is then split by a prism according to its components by refraction to the detector and a spectrum is then generated. A schematic diagram for the UV-Vis principle is shown below. UV-Vis spectroscopy was employed to investigate the BODIPY PSs electronic transitions and their absorption and excitation profiles.

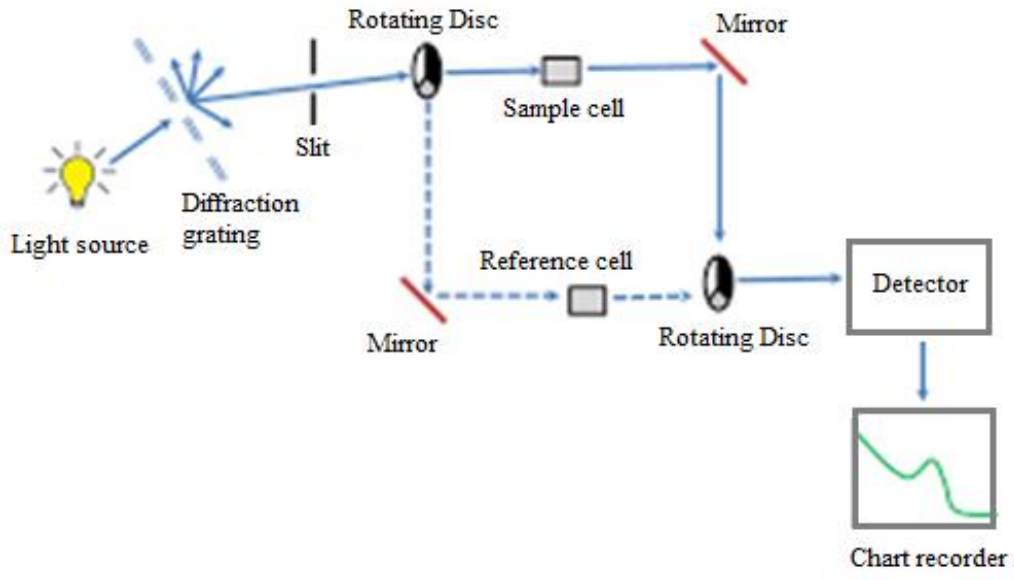

Scheme 3.1 Schematic representation of UV-Vis principles (Castro, 2013)

3.2.1.1 UV-Vis spectra acquisition method

Absorption spectra were recorded with Shimadzu the 1800 UV spectrophotometer mounted with a Czerny tuner mounting monochromator, a double beam photometric system, and a silicon photodiode detector. The spectra were recorded in the range of 350 – 1100 nm. All samples were prepared in their respective dissolution solvents. The optical density was recorded in the range of molar concentrations from 1×10^{-6} to 7×10^{-6} for BODIPY 1 to BODIPY 10 and 1×10^{-3} to 7×10^{-3} for BODIPY 11 to BODIPY 16 respectively towards molar extinction coefficients determination. A baseline was recorded before making the measurements in a quartz cuvette with 1 cm path length placed in a UV beam path.

3.2.2 Fluorescence spectroscopy

Fluorescence spectroscopy is widely used to measure the excitation and emission of the fluorophores. Fluorescence is itself the emission of light (electromagnetic radiation) by a molecule absorbed at different wavelength radiations. Fluorescence uses a variety of light sources to excite a molecule, these light sources vary from xenon lamps to light-emitting diodes (LED) (other lamps include: high-pressure mercury (Hg) lamps, Xe-Hg arc lamps, low-pressure Hg and Hg-Ar lamps, pulsed xenon lamps, quartz-tungsten halogen (QTH) lamps). Light passes through a monochromator (typically prism or directing gratings) and is filtered before it excites the sample, which emits radiative energy in the form of light. The emitted light of the excited molecule then passes through a monochromator which transmits a narrow band of light of specific wavelengths to the detector (InGaAs array is the standard detector used in many spectrofluorometers) which records the spectra of the analyzed sample.

Most spectrofluorometers can measure both emission and excitation spectra. Their main components consist of four parts: light sources, monochromators, optical filters, and a detector as shown in the **scheme. 3.2** below.

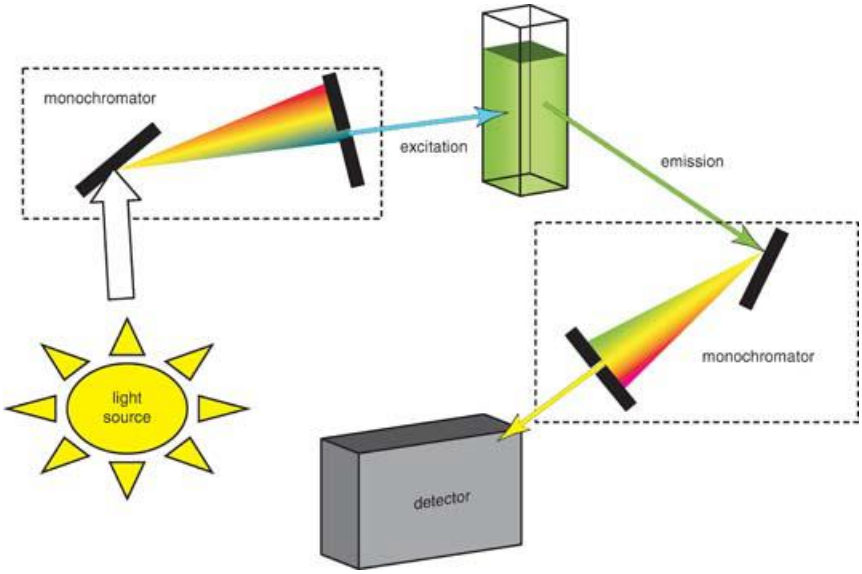

Scheme 3.2 A schematic presentation of the fluorescence spectrophotometer principle (Adapted from, Castro, 2013).

3.2.2.1 Emission spectra acquisition methods

Emission spectra were recorded by the use of a fluorescence quartz cuvette with a 1 cm path length using the Shimadzu RF-6000 Spectro fluorophotometer. Wavelength filters were used to allow the filtering of the excitation light to permit the light of specific wave lengths to pass through and to prevent the presence of any artifact peaks. Solutions used were excited in their diluted form mainly $1x10^{-6}$ M. The excitation wavelength was kept at <0.5 nm of the respective absorption wavelength of the studied BODIPY PSs.

3.2.3 Mass spectrometer

Mass spectrometry (MS) is a very powerful characterization technique used for the identification of a wide range of chemical compounds. Mass spectrometry is a tool for determining the molecular weight of the chemical species in a sample. In an electron impact (electron ionization source) ionization from a heated filament gives off electrons. These electrons are then accelerated to the anode and collide with the gaseous molecules, emanating from a vaporized sample as it is blasted through a beam of electrons. The high energy beam (typically 70 eV) of electrons from the sample molecules leaves positively charged radical species. The molecular ion typically undergoes decomposition or rearrangement to produce fragment ions. The ionized sample is separated in the mass spectrometer in the mass-to-charge ratio and detected in proportion to their abundance and a mass spectrum is displayed as an output (Hoffmann and Stroobantt, 2007). Because of this, electron impact is classified as a

"hard" ionization technique. On the other hand, the "soft" ionization technique requires negative chemical ionization, atmospheric pressure chemical ionization, chemical ionization, and field ionization (Abate *et al*., 2010; Hejazi *et al*., 2009). With metal-containing compounds, fragments in EI will almost always contain a metal atom. The Agilent high-resolution liquid chromatography-mass spectroscopy (Thermo scientific ultimate 3000 UHPLC coupled to a Bruker Compact Q-TOF high resolution mass spectrophotometer with soft innovative Captive EIS) provides more information related to the molecule analyzed with the advantage of giving information about the sample elemental composition. Below is a scheme demonstrating electron impact ionization in MS spectroscopy.

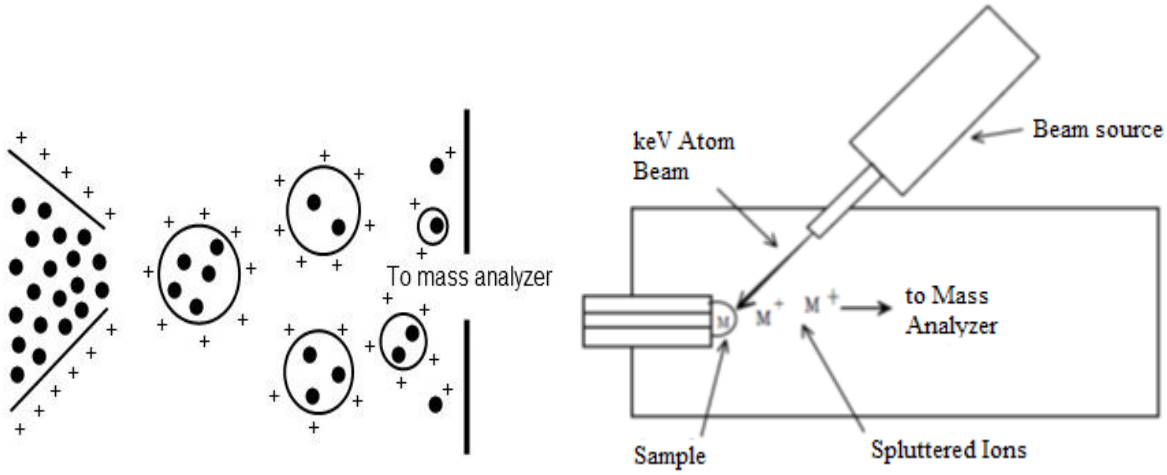

Scheme 3.3 Schematic diagram of electrospray mass analyzer (Adapted from Castro, 2013; van Bramer, 1998)

3.2.3.1 Mass spectrometer spectra acquisition method

Mass spectrometry analysis was performed with a Loop injection and UHPLC HRMS mass spectrometer. Samples were dissolved in acetonitrile and made up to an appropriate concentration (typically 10 ppm). The sample (A) 10 µL was directly injected into the UHPLC HRMS and eluted using a Gradient elution technique for 15 minutes. The starting elution solvent mixture was 95% - 5% solvent A consisting of 0.1% formic acid/water (v/v) and 5% - 95% solvent mixture solvent B consisting of 0.1% formic acid/Aetonitrile (v/v) through an acclaim RSLC 120 C18 column (2.2 µm 2.1 x 50 mm).

3.2.3.2 Elemental analysis and empirical formula acquisition

Elemental analysis and confirmation of the empirical formula of the analyzed BODIPY dyes were carried out; the COMPASS DATA analysis 4.3 from Bruker software predicts the

elemental composition by calculating the isotopic pattern obtained from data acquisition, this value is compared to the one calculated based on the (given molecular formula) and a score is given. All calculated hits are ranked by comparing the theoretical isotopic pattern of a sum formula suggestion to the measured pattern. The mSigma value visualizes the quality of the isotopic fit for measured vs Sum formula suggestion. The smaller the mSigma value, the better the fit, and the elemental (empirical) acquisition is deemed a fit.

3.2.4 Fourier Transform Infrared spectroscopy (FT-IR)

Fourier transform infrared spectroscopy is an analytical technique that gives details about qualitative and quantitative molecular features of the IR-active organic or inorganic molecules both for solid, liquid, or gas samples (King *et al*., 2013). A typical FTIR spectrometer is comprised of a light source, interferometer, sample component, detector, amplifier, analog to digital (A/D) converter, and a computer. Light is projected to an interferometer consisting of a beam splitter, which splits the incident infrared (IR) beam into two separate optical beams. One beam is reflected from a fixed mirror and the other from a moving mirror. The interferometer then measures all the frequencies of the sample simultaneously, while the light transmitting through the sample is refracted from the mirror to the detector. The instrument then acquires and digitizes the interferogram and performs the Fourier Transform function and provides an output of the spectrum (Smith, 1996).

Specific information about the vibrations (bending and stretching) and rotations of chemical bonds in a sample are obtained from the FTIR spectrum, making it a useful tool for analyzing organic and certain inorganic materials. An infrared spectrum represents a fingerprint of a sample with absorption peaks corresponding to the frequencies of vibrations of bonds between atoms making up the compound (Everhart and Thornley, 1960). A schematic diagram showing how the FT-IR instrument operates is presented in **scheme 3.4** below. Fourier transform infrared spectroscopy technique is very important in the elucidation of the structure of synthetic compounds. In this study, it was applied to determine and assign the functional groups of the synthesized BODIPY PSs.

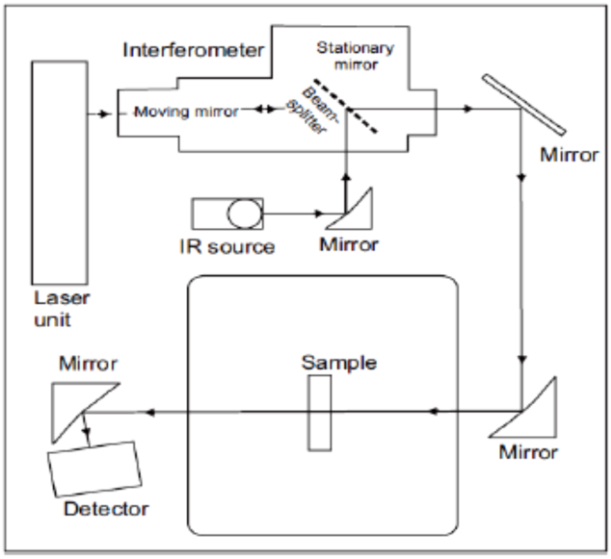

Scheme 3.4 Schematic diagram illustrating FTIR analysis to obtain a spectrum. (Adapted from King *et al*., 2013).

3.2.4.1 FT-IR spectra acquisition method

BODIPY functional group presence was confirmed using the Perkin Elmer Spectrum 100 Pike Technologies diamond crystal plate ATR unit FTIR spectrometer. The spectra obtained were collected from accumulated four scans with the pressure gauge of 100 KPa at a spectral range from 4000 to 500 cm^{-1}. Samples were dissolved in 1500 µL of methanol for BODIPY 1to10 and DMSO for BODIPY 6.1 to 6.6. Moreover, a sample drop was then placed on an ATR crystal, and analysis was carried out and a spectrum was collected.

3.2.5 Nuclear Magnetic Resonance (NMR) spectroscopy

Nuclear magnetic resonance spectroscopy is a powerful and widely used technique that makes use of the magnetic properties of analyzed nuclei. For the NMR analysis technique, samples are dissolved in deuterated solvents and the solutions transferred to NMR tubes which are transported into the machine so that the NMR tube containing the sample is placed within a magnet. The sample in the NMR magnet is surrounded by superconducting coils and is then subjected to a frequency from the radio waves source. In principle, when nuclei are exposed to an external magnetic field, they are compelled to exist in a specific nuclear spin state. The NMR spectrometer analyses the transitions between nuclear spin states that are specific to the chemical environment of the particular nuclei. In NMR spectroscopy, the instrument records the emitted frequency of the sample as it is excited with frequencies from 200 to 1000 Hz inside a stable magnetic field. The carbon NMR measures the frequencies at 100 Hz where proton

NMR is usually measured at 400 Hz depending on the sample signals. A detector then interprets the signals and sends them to the main console (Barron *et al*., 2013). The nuclear magnetic resonance response (a free induction decay) is received. This response is very weak and has to be picked up, a Fourier Transform is carried out to extract the frequency-domain from the raw-time domain free induction decay (FID). **Scheme 3.5** is a typical schematic diagram demonstration of the NMR instrument.

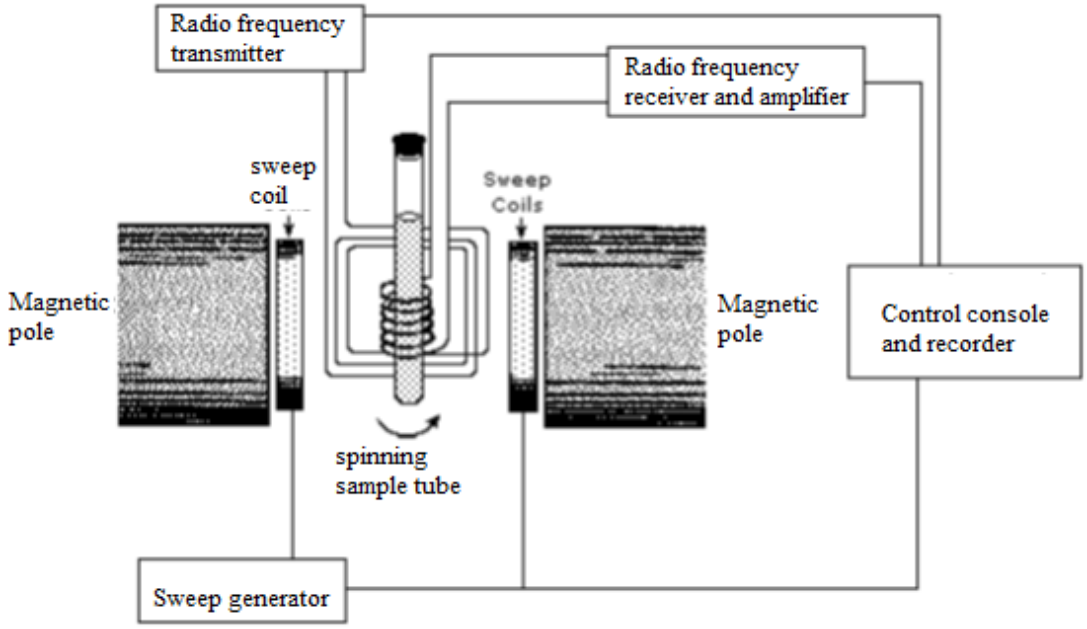

Scheme 3.5 Representation of NMR spectroscopy (adapted from Barron *et al*., 2013).

3.2.5.1 ^{1}H and ^{13}C spectra acquisition method

^{1}H and ^{13}C NMR spectra were obtained with Bruker XSN21 JEOL ECS-400 MHz NMR spectrometer. Chemical shifts for both ^{1}H and ^{13}C NMR spectra were referenced relative to the residual deuterated $CDCl_3$ and DMSO solvents. FID files were obtained and the spectra were used to elucidate the structure of the samples based on their chemical shifts.

3.2.6 X-ray Diffraction spectroscopy

X-rays are electromagnetic radiations with shorter wavelengths (of few Angstroms). X-rays are generated by a heated filament in a cathode ray tube producing electrons. These electrons are accelerated towards a target material by applying a voltage, where energy sufficient electrons dislodge inner shell electrons of the material and characteristic X-ray spectra are produced. The spectra contain specific components commonly referred to as the K_α and K_β (Bunaciu *et al*., 2015). Each crystalline material diffracts X-rays in a unique characteristic

pattern of diffraction order (Joshi *et al*., 2008). The K_{α} component consists of $K_{\alpha 1}$ and $K_{\alpha 2}$, with $K_{\alpha 1}$ having a shorter wavelength and twice the intensity of $K\alpha_2$. The specific wavelength carries characteristics of the targeted material (Cu, Fe, Mo, and Cr). Filtering with monochromators produces monochromatic X-rays needed for diffraction. These X-rays are then directed and collimated to the sample, after which the intensity of the reflected X-rays are recorded (Bunaciu *et al*., 2015). Below in **scheme 3.6** is a schematic representation of an X-ray spectrometer principle. X-ray diffraction spectroscopy was used to investigate the 2θ diffraction patterns for active BODIPY dyes and nanomaterials.

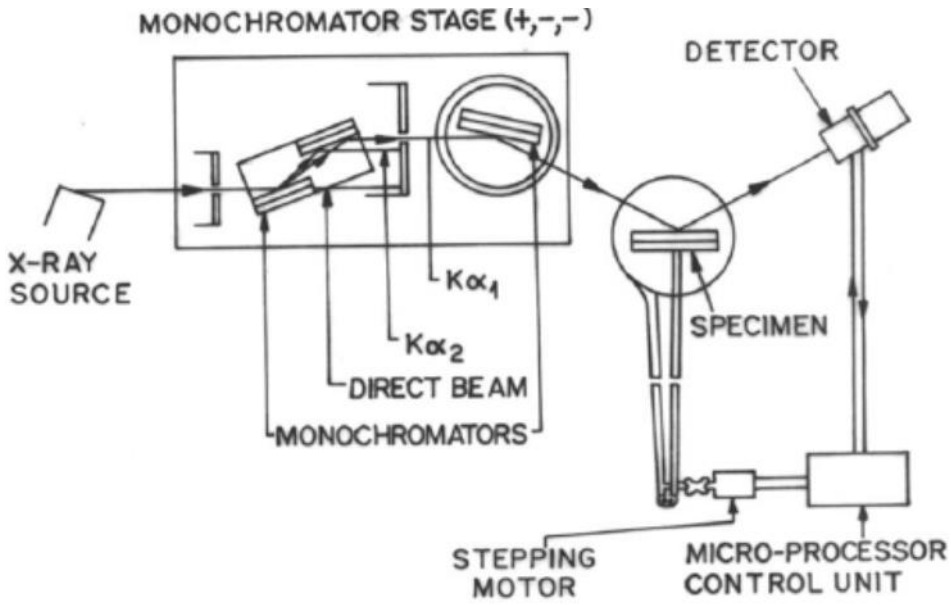

Scheme 3.6 Schematic representation of a typical XRD diffraction. (Adapted from Dhanaraj and Rajesh, 2009).

3.2.6.1 XRD spectra acquisition method

The X-ray patterns were obtained with Phillips X‟Pert^3 operated at 40 kV with the current of 40 mA, and delivering filtered Cu-Ka radiation of (1.54060 Å). The data was collected on a continuous mode starting from step size 2θ to 90θ scale of 4º to 80º respectively. The XRDML JCPDS files were used to compare the diffraction intensities of the synthesized nanoconjugates.

3.2.7 Transmission Electron Microscopy (TEM)

Transmission electron microscopy (TEM) is a fundamental analytical tool for the characterization of nanomaterials with direct imaging for the attainment of quantitative

measures of grain (particle) size, size distribution, morphology, and topology. In TEM imaging, electrons are produced either via field emission or thermionic emission. The electrons are then accelerated through condenser lenses and focused onto a thin sample (electron beam interaction with a sample). The beam of electrons generated from the electron gun passes through objective lenses where a fluorescent light (from the emission current) allows for image viewing. Images are collected using an electrostatic beam shift which displays the image onto sections of a CCD camera (Stach, 2008).

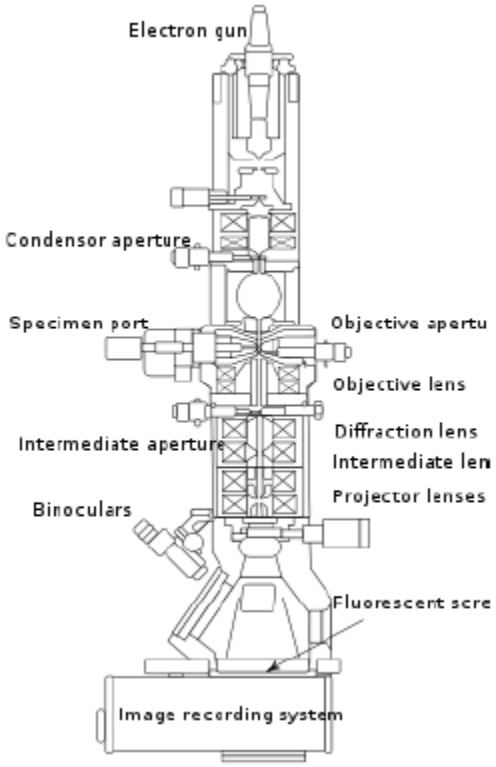

Scheme 3.7 illustration of TEM imaging. Adapted from (Bobji *et al*.2002).

3.2.7.1 TEM microgram (images) acquisition method

Transmission electron microscopy micrograms were obtained with FEI Technai T12 TEM mounted with FEI eagle 4k x 4k CCD camera operating at 120 kV. Sample images were acquired at a nominal magnification of 5000x to 50000x at pixel 0.25 nm/pixel. The electron dose of 1 – 45 e/Å2 was used with the nominal under the focus of -150 m (5000x) to -2 m (50000x). Particle selections were analyzed based on the clearly defined particle boundaries, particles contained in the field of view, and selected when contained in the copper grid holes for proper viewing and imaging.

3.2.8 Scanning Electron Microscopy (SEM)

The scanning electron microscope (SEM) is the most widely used technique for high-resolution imaging, allowing for observable size features of materials or objects at 1-5 nm. The electrons for SEM imaging emanating from a source (mostly heated tungsten wire) are accelerated through a column with a potential voltage and are gathered as an electron beam. This unfolds when the high energy electron beam is focused through a two-stage lens (the condenser and objective lenses) and a small electron probe is produced. These electrons are bombarded over the specimen surface. After this, either secondary electrons or backscattered incident electrons from the sample are amplified and detected, generating the image of the sample morphology (Argast and Tennis, 2004). A schematic diagram showing the operation of SEM is shown in **scheme 3.8** below.

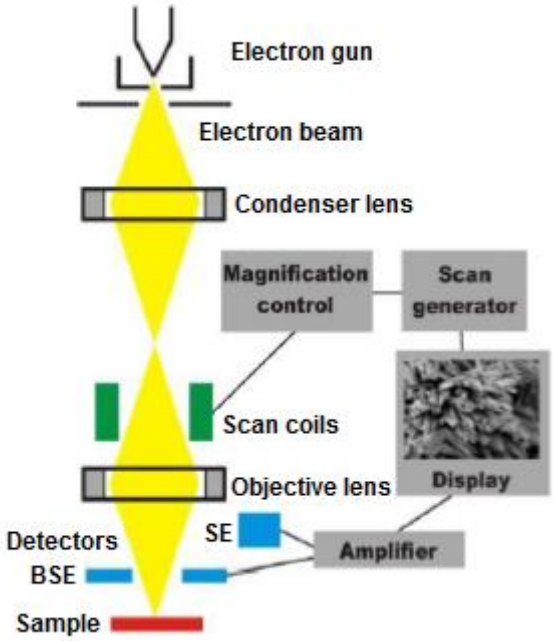

Scheme 3.8 Representation of a typical SEM microscopy. (Adapted from Krumeich, 2011).

3.2.8.1 SEM micrograph (images) acquisition method

The scanning electron microscope micrograms (images) were obtained with FEI Nova Nanolab 400 SEM. The accelerating voltage was set to 10 kV and the working distance was adjusted to 10 mm. The nanoparticles were first single coated with carbon for better contrast and view of the nanoparticles. The brightness and contrast of the images were adjusted to the optimum values to enhance the visibility of the nanoparticles. The image magnification was varied from 10 K and 500 k times.

3.2.9 Dynamic Light Scattering Spectroscopy (Zeta sizer)

Dynamic light scattering also is known as quasielastic light scattering (QELS) is a noninvasive and established analytical technique for the size of particles and molecules in the submicron region. The particles, molecules, and emulsion undergo Brownian motion which is induced by solvent molecules bombardment which themselves are moving due to thermal energy. When particles are illuminated with a laser, the scattered light intensity fluctuates at a rate depended on the size of the particles as smaller particles are "kicked" further by the solvent molecules and they rapidly move further. The analysis of these fluctuations analysis yields the velocity of the Brownian motion and the particle sizes (radius r_k) using the stoke-Eintein relationship as shown in equation 3.1.

$$r_k = \frac{kT}{6\pi\eta D} \qquad \text{equation 3.1}$$

Where K is the Blotzmans constant, T the temperature in K, η is the solvent viscosity, and D the diffusion coefficient. The later technology can analyze particles even at lower than 1-nanometer size. **Scheme 3.9** below shows the analysis principle for DLS respectively.

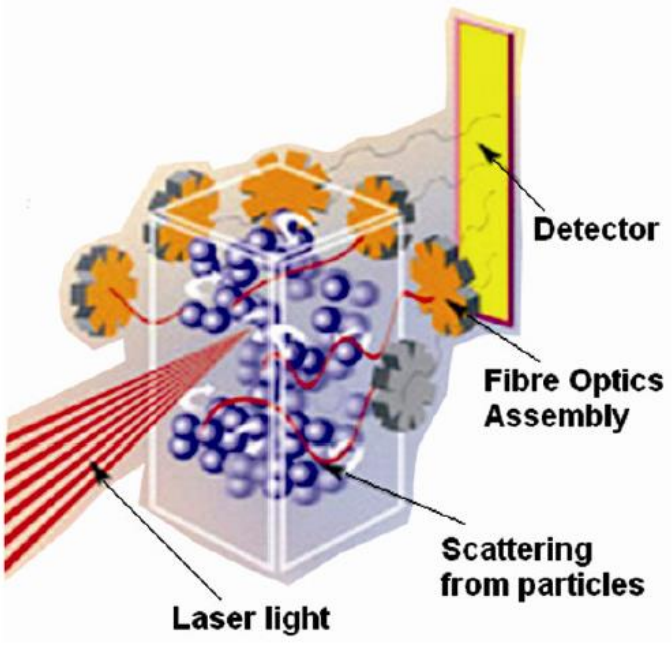

Scheme 3.9 Schematic presentation of Dynamic light scattering analysis (Adapted from Joshi *et al.*, 2008)

3.3 Synthesis

3.3.1 Synthesis of 2- pyrrole-naphthalene sulfonamide (2- Pyr-NSA) (Fessner and Walter, 1996)

A (10 mmol, 0.9 g) 2,4-dimethylpyrrole was placed in 100 mL three-necked round bottom flask, and to this 50 mL of methanol was added while stirring at 60 °C. Following this, (10 mmol, 20 g) of naphthalene-2-sulfonamide was slowly added, and subsequently, (excess catalyst) Bis(triphenylphosphine)palladium (II) dichloride (Pd^{2+}) (3 mL) was added to the reaction mixture. Then the reaction was left to stir overnight to allow for full conjugation of the pyrrole and naphthalene through C-C bond formation. A brownish product was obtained and separated on a silica column (DCM:EtAc 2:3 v/v) with a yield of 79%, $C_{18}H_{22}N_2O_2S$ calculated for m/z = 300.45 g/mol and obtained 301.91 g/mol $[M+1]^+$.

3.4 Synthesis of BODIPY PSs

3.4.1 Synthesis of 4,4-difluoro-2,6-diethyl-1,3,5,7-tetramethyl-8-[4-(isopropylbenzyl)]-3a,4a-diaza-s-indacene (BODIPY 1) **(Scheme 3.10)**

BODIPY dyes were prepared as per reported method (Galangau *et al*., 2010). In a reaction flask (250 mL three necked round bottom flask) containing 100 mL of dried dichloromethane (DCM), (5 mmol, 0.62 g) 3-ethyl-2,4-dimethylpyrrole was mixed with 4-isopropyl benzaldehyde (2.5 mmol, 0.31 g) followed by few drops of trifluoroacetic acid (TFA) added slowly. The reaction was heated to 30 ºC and left undisturbed for 48 hours. Following this, chloranil (10 mmol: 150 mg) was then added to the mixture and allowed to stir for a further 4 hours to allow full oxidation of the reaction product. After stirring, the reaction mixture was treated with N,N-diisopropylethylamine (DiPEA; 35 mmol, 5 mL, 7 eqv.) and left to stir further for 12 hours after which BF_3•OEt_2 (55.0 mmol, 6.78 mL) was added and the reaction was left to stir over night. A dark blue-black paste product was obtained. Column chromatography (silica gel (10x elution runs were carried out per band), followed by biobeads (3x runs) and sephadex (3x runs)) was used to purify the product and a highly fluorescent orange band was collected (2 Hexane: 5 Chloroform) with a yield of 42%, $C_{26}H_{33}BF_2N_2$ calculated for m/z = 422.81 g/mol obtained m/z = 423.28 g/mol, [M+H], elemental composition calculated for: C73.94%, H7.88%, B2.56%, F9.00%, N6.62% and Found: C73.82%, H7.55%, B2.55%, F8.91%, N6.63%. IR bands ascribed to ($\upsilon C=C_{Ar}$) 1400-1542 cm^{-1}, (υC-N) 1080-1190 cm^{-1}, (υB-F) 1603 cm^{-1}, (υC-$H_{bending}$) 1274-1363 cm^{-1}, (υC-$H_{stretch}$) 2853 -2958 cm^{-1}. ^1H NMR

($CDCl_3$, 400 Hz) δ[ppm]: 0.87(m, J=1.26Hz, 3H, CH_3); 1.05(d, 6H, 2x CH_3; 2,6-pyrrole); 1.25(s, 6H, 2x CH_3); 1.55(s, 2H, CH2); 2.16(d, J = 1.06Hz, 9H, 3x CH_3); 2.88(s, 2H, CH_2); 7.16(m, J=6.34Hz, 2H, Ar); 7.31(d, J=7.01Hz, 2H, Ar). ^{13}C NMR ($CDCl_3$, 100 Hz) δ[ppm]: 14.78; 14.80; 14.28; 12.60; 17.20; 17.41; 126.48; 151.50; 121.06; 114.10; 138.65; 147.17; 153.50; 133.08; 133.08; 127.05; 127.05; 147.70; 34.64; 23.88; 23.88

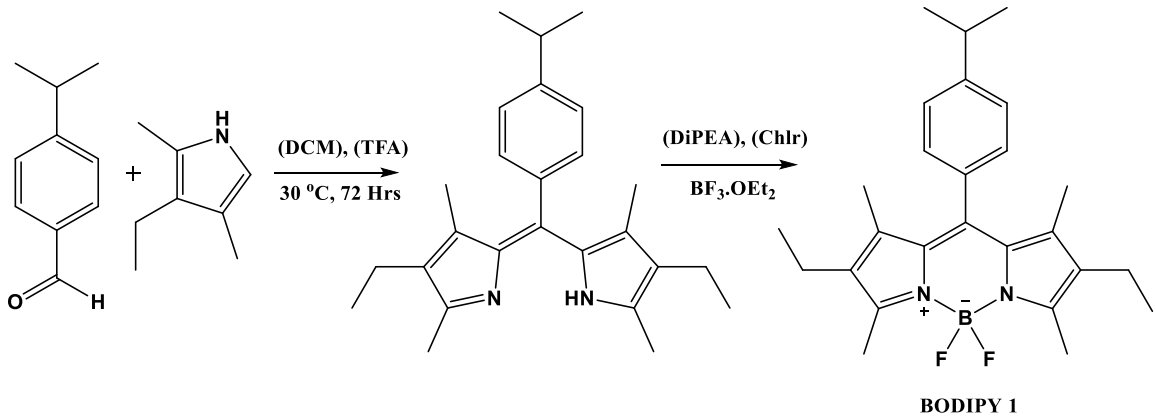

Scheme 3.10 BODIPY 1 synthesis schematic diagram

3.4.2 Synthesis of 4,4-difluoro-4-bora-2,6-diethylcarboxyl-1,3,5,7-tetramethylcarboxyl-8-[4-methylcarboxylbenzyl]-3a,4a-diaza-s-indacene (BODIPY 2) **(Scheme 3.11)**

BODIPY 2 is an oxidized counterpart of BODIPY 1. In a reaction flask (250 mL three necked round bottom flask) containing 1:4 chloroform: ethanol, 1:7 mole ratio of BODIPY1 to $KMnO_4$ (0.1 M) was added (Leen *et al*., 2010). The reaction was refluxed at 100 ºC and stirred for 8 hours uninterrupted. A brownish precipitate formed and then the mixture was dried in the oven at 70 ºC overnight. The resulting powder was then run on a silica column (DCM:MeOH) 1:4 v/v ratio followed by use of biobeads and sephadex as stationary phases, resulting in an orange oxidized BODIPY 2 obtained with a yield of 71%, ($C_{24}H_{15}N_2BF_2O_{14}$) calculated for m/z 604.19 g/mol found 605.37 g/mol, [M+H], elemental composition calculated for: C47.71%, H2.05%, B1.79%, F6.29%, N4.64%, O37.12% and Found: C47.76%, H2.35%, B1.97%, F5.31%, N4.76%, O37.25%. IR band ascribed to (υC=C_{Ar}) 1412 cm^{-1}, (υC-N) 1087-1190 cm^{-1}, (υB-F) 1624 cm^{-1}, (υC-H) 879 cm^{-1}, (υC-H) 1382 cm^{-1} and (υOH) vibrational peak at 3346 cm^{-1}. ^{1}H NMR ($CDCl_3$, 400 Hz) δ[ppm]: 7.32(d, J=5.61Hz, 2H, Ar); 7.54(s, 1H, 6-pyrrole); 7.71(d, J=6.01Hz, 2H, Ar); 9.82(s, 1H, 2,5Ar); 10.42(s, 1H, 1-pyrrole); 10.42(s, 1H 2-pyrrole); 10.76(s, 1H, Meso-Ar); 16.7(s, 1H, 6-pyrrole). ^{13}C NMR ($CDCl_3$, 100 Hz) δ[ppm]: 167.99; 129.93; 131.74; 129.97; 145.44; 138.58; 164.99; 155.34; 145.35; 138.58; 127.76; 142.76; 167.49; 121.22; 161.15; 169.89; 114.29.

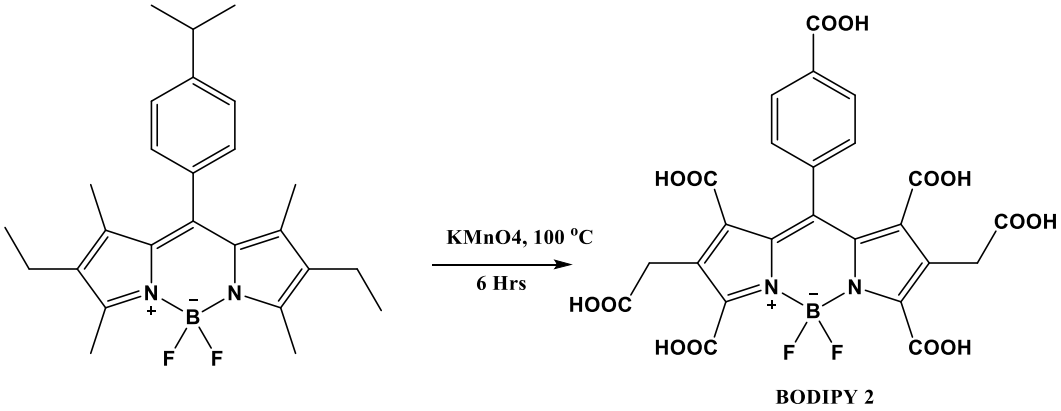

Scheme 3.11 BODIPY 2 synthesis schematic diagram

3.4.3 Synthesis of 4,4-difluoro-4-bora-1,3,5,7-tetramethyl-8-[4-ethylbenzyl]-3a,4a-diaza-s-indacene (BODIPY 3) **(scheme 3.12)**

A similar method as described for the synthesis of BODIPY 1 was carried out for the synthesis of BODIPY 3. In a reaction flask (250 mL three necked round bottom flask), 5 mmol, 0.78 g of 2,4-dimethylpyrrole was added in a dried DCM followed by addition of 4-ethylbenzaldehyde (2.5 mmol, 0.3 g), to this, few drops of trifluoroacetic acid was added and the reaction was left to stir 48 hours. Chloranil (150 mg) was then added slowly followed by N,N-diisopropylethylamine (DiPEA) (5 mL) and complexed with $BF_3.OEt_2$, (7 mL) a dark blue-black paste was obtained and a silica column, followed by use of cellulose, biobeads and sephadex stationary phases for column chromatography to separate the product. A lemon colored band was obtained (Hexane:Chloroform, 1:4 v/v) with a low yield (37%) $C_{21}H_{23}N_2BF_2$ calculated for m/z 352.19 g/mol found m/z 353.20 g/mol, [M+H], elemental composition calculated for: C71.08%, H6.78%, B3.07%, F10.72%, N7.95% and Found: C71.40%, H6.85%, B3.06%, F10.45%, N7.93%. IR bands ascribed to ($\upsilon C=C_{Ar}$) 1466-1547 cm^{-1}, (υC-N) 1082-1191 cm^{-1}, (υB-F) 1625 cm^{-1}, ($\upsilon C-H_{bending}$) 1301 cm^{-1}, ($\upsilon C-H_{stretch}$) 2853 -2957 cm^{-1}. ^{1}H NMR ($CDCl_3$, 400 Hz) δ[ppm]: 0.89(s, 3H, CH_3); 1.23(m, J= 4.98, 3H(2), CH_3); 2.17(m, J = 4.36Hz, 9H, 3x CH_3); 2.32(s, 2H, CH_2); 6.80(s, 1H(2), 2-pyrrole); 6.80(s, J=5.33Hz, 2H, Ar); 7.34(s, J=5.41Hz, 2H, Ar). ^{13}C NMR ($CDCl_3$, 100 Hz) δ[ppm]: 14.37; 28.78; 140.89; 124.61; 140.61; 133.20; 133.20; 12.81; 119.33; 127.33; 131.05; 156.43; 17.18; 14.26; 152.81; 113.36;142.46;18.24.

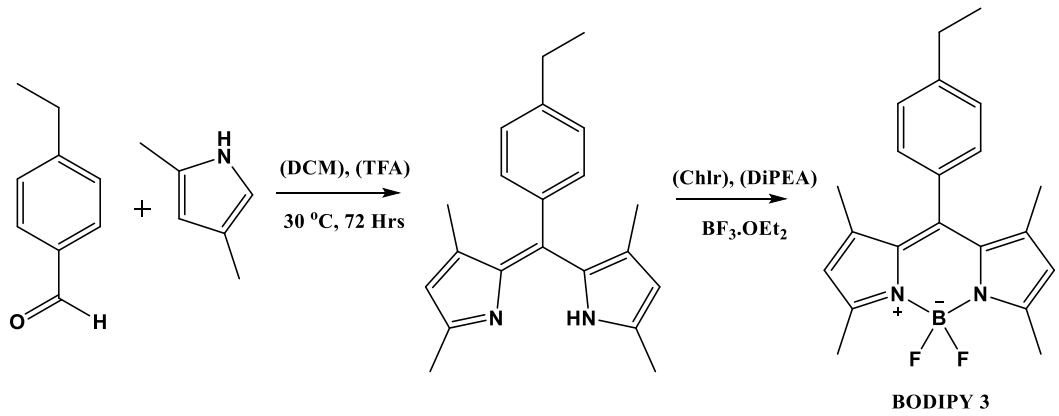

Scheme 3.12 BODIPY 3 synthesis schematic diagram

3.4.4 Synthesis of 4,4-difluoro-4-bora-1,3,5,7-tetramethylcarboxyl-8-[4-methylcarboxylbenzyl]-3a,4a-diaza-s-indacene (BODIPY 4) **(scheme 3.13)**

The oxidation method as described above was adapted as used for BODIPY 2, in a reaction flask (250 mL three-necked round bottom flask) containing 1:4 chloroform: ethanol. In a 1:5 mole ratio BODIPY 3 was added to $KMnO_4$ (0.1 M) (250 mg: 2.6 mL) and a brown precipitate was obtained and dried in the oven. Following this, column chromatography was used to purify the product (stationary phase silica gel, biobeads, and Sephadex) and a light orange-like colored solid was obtained with a high yield (88%), $C_{20}H_{11}N_2BF_2O_{10}$ calculated for m/z 488.12 found m/z 489.27g/mol [M+H], elemental composition calculated for: C49.21%, H2.27%, B2.21%, F7.78%, N5.74%, O32.78% and Found: C49.42%, H2.28%, B2.41%, F7.67%, N5.31%, O31.99%. IR bands ascribed to ($\upsilon C=C_{Ar}$) 1416 cm^{-1}, (υC-N) 1043-1086 cm^{-1}, (υB-F) 1624 cm^{-1}, (υ=C-H) 879 cm^{-1}, (υC-H) 1382 cm^{-1}, (υB-F) stretching at 1640 cm^{-1} and a broad band at (υO-H) 3342 cm^{-1} vibrations and (υC=O) at 1782 cm^{-1}. ^{1}H NMR ($CDCl_3$, 400 Hz) δ[ppm]: 5.68(s, 1H, 2-pyrrole); 5.97(s, 1H, 6-pyrrole); 7.18(d, J=7.51, 2H, Ar); 7.29(d, J=7.44, 2H, Ar); 12.21(s, 1H); 12.43(s, 1H). ^{13}C NMR ($CDCl_3$, 100 Hz) [δppm]: 161.15; 121.22; 119.22; 167.49; 124.11; 138.52; 145.44; 131.25; 132.27; 129.97; 169.99;167.87; 138.67; 130.0; 143.34; 167.19.

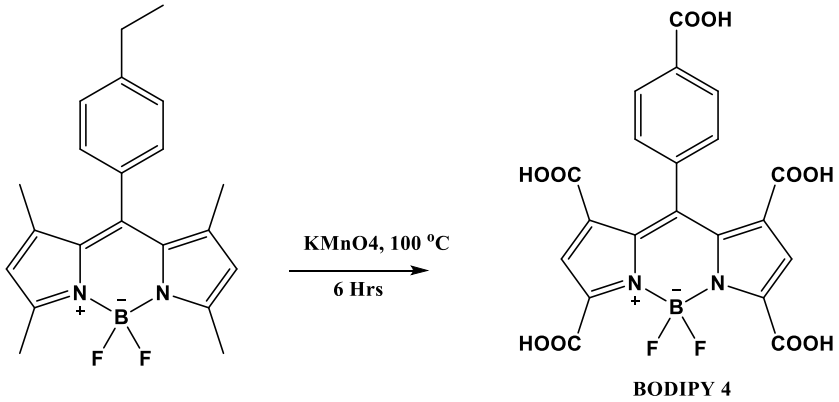

Scheme 3.13 synthetic route for BODIPY 4

A direct functionalization method was adapted for this study. BODIPY dyes 1 and 3 were functionalized using potassium permanganate to afford the oxidation of the synthesized parent BODIPY PSs to yield BODIPY 2 and 4 which are oxidized daughter compounds with carboxyl groups. Following the oxidation of BODIPY 1 and 3, the respective BODIPYs were further functionalized to introduce different functional groups to the periphery of the daughter BODIPY 3 respectively. To activate the carboxyl groups of BODIPY 3, thionyl chloride was used for acylation which afforded very active sides (acid chloride) for conjugation to amine groups containing small molecules. This allowed the addition or introduction of desired functionalities through carbonyl carbon-amine bond to yield BODIPY 8-10 respectively.

3.4.5 Synthesis of 4,4-difluoro-4-bora-3,5-ditrifluoroacetyl-8-[pyrrole]-3a,4a-diaza-s-indacene (BODIPY 5) **(scheme 3.14)**

In a three necked round bottom flask (250 mL), pyrrole-2-aldehyde and 4-trifluoroacetylpyrrole (10 mmol: 5 mmol; 0.21 : 0.24 g) were added in dried methanol, and the reaction was heated at 40 ºC and few drops of TFA were added and the mixture stirred for 72 hours. Following this, chloranil (150 mg) was added and left to stir for a further 4 hours, followed by addition of DiPEA (5 mL) and left to stir overnight and then complexed with BF_3•OEt_2 (7 mL). A dark brown-lemon paste was obtained and column (silica gel, sephadex, and biobeads stationary phases) chromatography was used to separate the mixture with a light brown BODIPY collected with a low yield (32%), $C_{17}H_8BF_8N_3O_2$ calculated for m/z 449.07 found m/z (447.35 g/mol), [M-2H], elemental composition calculated for: C45.47%, H1.8%, B2.41%, F33.85%, N9.56% O7.13% and Found: C42.46%, H1.90%, B2.61%, F34.79%, N9.87%, O7.62%. IR bands ascribed to ($\upsilon C=C_{stretch}$) 1702.97 cm^{-1}; ($\upsilon C=O_{stretch\ acetate}$) 1288 cm^{-1}; (υC-N) 1073 cm^{-1}; (υ N-H) 3362 cm^{-1}; (υC-Istretch) 636 cm^{-1}; ($\upsilon C-F_{stretch}$) 1396-1470 cm^{-1};

(υC-$N_{stretch}$) 2366 cm^{-1}.^{1}H NMR ($CDCl_3$, 400 Hz) δ[ppm]: 5.31(s, 1H, 6-pyrrole); 6.43(s, 1H, meso 3-pyrrole); 6.49(s,1H meso 2-pyrrole); 6.60(d, J=1.01, 2H, 1-pyrrole); 7.08(s, 1H, meso 4-pyrrole); 7.50(s, 1H, 2-pyrrole); 10.43(s, 1H, imine). ^{13}C ($CDCl_3$, 100 Hz) δ[ppm]: 118.04; 167.69; 130.85; 119.74; 111.15; 128.68; 136.83; 149.09; 118.04; 106.74; 151.06; 141.05; 119.02; 140.31; 202.53; 118.04.

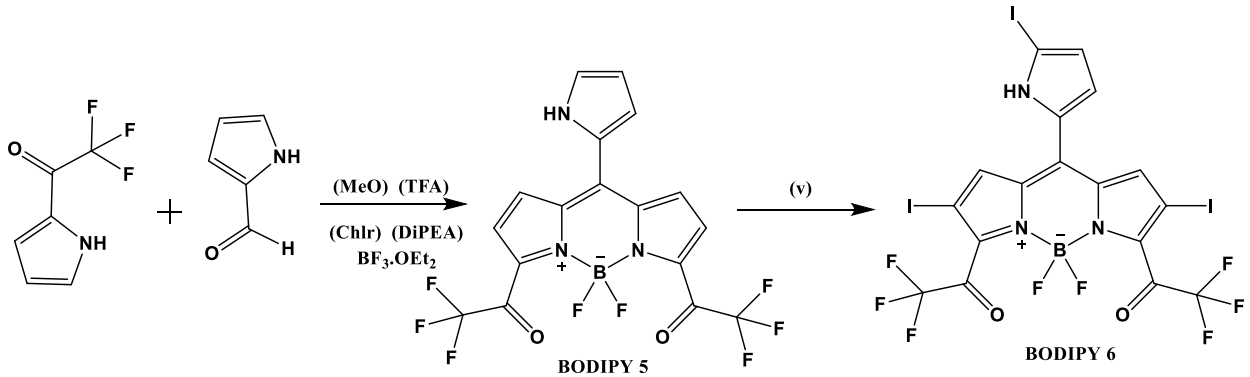

Scheme 3.14 BODIPY 5 and 6 synthesis schematic diagram, (v, HIO_3:I_2).

3.4.6 Synthesis of 4,4-difluoro-4-bora-2,6-diiodo-3,5-difluoroacetyl-8-[2-iodopyrrole]-3a,4a-diaza-s-indacene (BODIPY 6) **(scheme 3.15)**

The functionalization of BODIPY 5 to introduce heavy atoms (I_2) was also carried out. To achieve this, BODIPY 5 was treated with iodic acid and iodine solution at 100 ºC with a mole ratio of (1:3) to target the desired available pyrrolic sites for the addition of iodine molecules (Yogo *et al*., 2005).

Fluorinated BODIPY 5 was dissolved in dried DCM:EtOH (1:3; 25:75 mL v/v) and refluxed at 80 °C, with a subsequent addition of iodic acid and iodine (resulting in a 1:3:3 mole ratio, 250 mg; 0.434 g; 0.301 g) respectively. The reaction was stirred for 6 hours and then the resulting product was dried and separated using (silica, bio beads and sephadex stationary phases) column chromatography with a high yield (90%), $C_{17}H_5BF_8N_3O_2I_3$ calculated for m/z 826.76 g/mol found 803.50 g/mol, [M-F], elemental composition calculated for: C24.70%, H0.61%, B1.31%, F18.38%, I46.05%, N5.08%, O3.87% and Found: C23.05%, H0.29%, B1.34%, F19.11%, I46.13%, N5.01%, O4.21%. IR bands ascribed to (υC=$C_{stretch}$) 1993 cm^{-1}; (υC=$O_{stretch\ acetate}$) 1288 cm^{-1}; (υC-N) 1064 cm^{-1}; (υC-Istretch) 636 cm^{-1}; (υC-$F_{stretch}$) 1396-1504 cm^{-1}; (υC-$N_{stretch}$) 2357 cm^{-1}; (υB-F) 1644 cm^{-1}. ^{1}H NMR ($CDCl_3$, 400 Hz) δ[ppm]: 6.42(s, 1H, 1-pyrrole); 7.52(d, J=1.51 Hz, 1H, meso 2-pyrrole); 7.54(d, 1H, meso 3-pyrrole); 7.72(t, J=1.0 Hz, 1H); 8.14(d, 1H, amide). ^{13}C NMR ($CDCl_3$, 100 Hz) δ[ppm]: 115.77; 162.56; 132.74;

56.33; 108.05; 121.48; 137.51; 144.67; 110.93; 102.23; 85.03; 151.70; 149.67; 75.39; 144.26; 195.76; 113.33.

3.4.7 Synthesis of 4,4-difluoro-4-bora-1,3,5,7-tetramethyl-8-[4-isoprpylbenzyl]-2,6-dinaphthalene-2-sulfonamide-3a,4a-diaza-s-indacene (BODIPY 7) (**scheme 3.15**)

Briefly, (2.53 g, 0.0167 moles) of 2,4-dimethyl-3-naphthalene-2-sulfonamide (Fessner and Walter, 1996) was added to a solution containing (1.237 g, 0.00836 moles) of 4-isopropylbenzaldehyde followed by few drops of TFA and the reaction was left to stir for 48 hours. Chloranil was then added (200 mg) and left to stir for 6 hours after which (5 mL) of DiPEA was added and the reaction was left to stir for a further 12 hours. The resulting mixture was then complexed with $BF_3.OEt_2$ (7 mL) and stirred overnight and the brown product was separated using column chromatography (silica gel, biobeads and sephadex) with the moderate yield (43%), $C_{42}H_{39}BF_2N_4S_2O_4$ calculated for mz 776.23 g/mol and obtained mz 676.39 g/mol, cleaving (M - H_2NO_2SF, m/z 99.08) respectively, elemental composition calculated for: C64.95%, H5.06%, B1.39%, F4.89%, N7.21%, O8.24%, S8.26% and Found: C65.19%, H4.87%, B1.76%, F4.19%, N7.21%, O8.15%, S8.38%. IR bands ascribed to (υ=C-$H_{bending}$) 886 cm^{-1}; (υC=$C_{Ar\ stretch}$) 1511 cm^{-1}; (υC=$C_{stretch}$) 2098 cm^{-1}; (υS=$O_{sulfonamide}$) 1398 cm^{-1}; (υB-F) 1632 cm^{-1}; ($\upsilon NH_{2symetric}$) 3383 cm^{-1}; ($\upsilon CH_{3deformation}$) 1305.42 cm^{-1}; (υC-$H_{Ar,stretch}$) 3158.82 cm^{-1}; ($\upsilon OH_{sharp\ free}$) 3615.17 cm^{-1}. ^{1}H NMR ($CDCl_3$, 400 Hz) δ[ppm]: 0.88(s, H, 5pyrrolic); 2.25(s, H, 3-pyrrolic); 1.26(q, J=1.06Hz, 3H, CH_3), 2.71(d, J=2.55 Hz, 2H, 1,7-pyrrolic H), 5.10(m, 1H, isopropyl), 7.53(d, 1H, Ar); 7.70(s, 2H, 5,6Cnapht.); 7.72(s, 1H, Ar); 7.98(s, 1H, 5C napht.); 8.07(s, 1H, 3C naph.); 8.26(s,1H, 8Cnapht), 8.56(s, 1H, 3C napht.). ^{13}C NMR ($CDCl_3$, 100 Hz) δ[ppm]: 22.84, 33.98, 147.70, 127.55, 132.51, 11.09, 134.70, 134.51, 137.01, 129.01, 124.38, 136.90, 127.46, 124.11, 11.10, 155.29, 145.39, 116.42, 10.77, 127.86, 135.6, 124.11, 132.16.

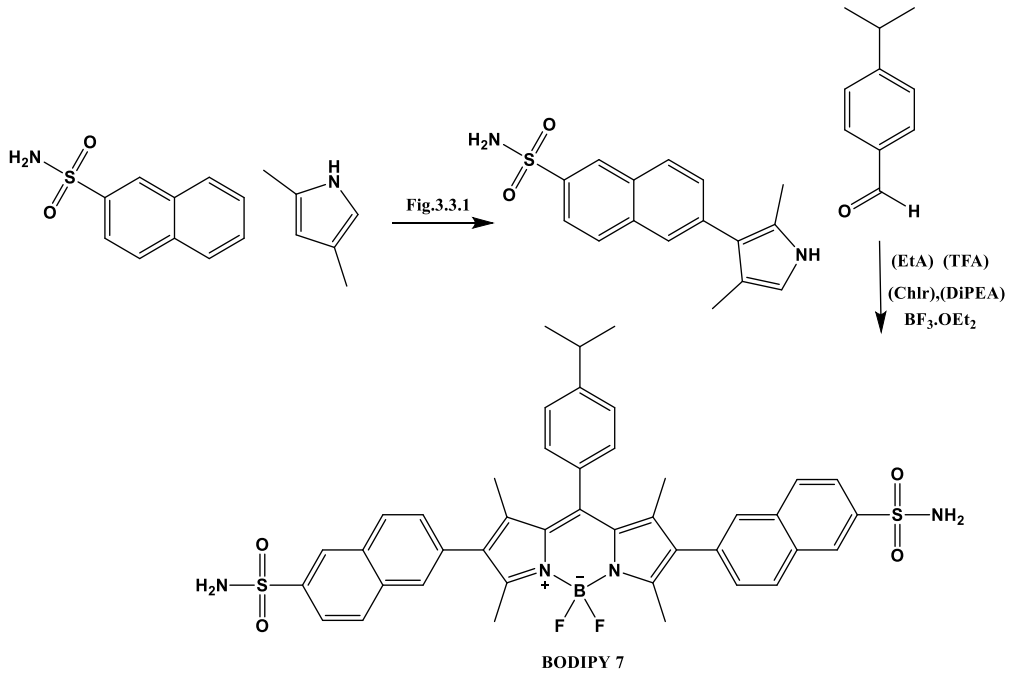

Scheme 3.15 BODIPY 7 synthesis schematic diagram.

3.4.8 Synthesis of 4-4difluoro-4bora-1,3,5,7,tetracarboxylamidebenzylsulfonamide-8[4-carboxylamidebenzylsulfonamide]-3a,4a-diaza-s-indacene (BODIPY 8) (**scheme 3.16**)

Diaminobenzylsalfonamide (DABSA) was dissolved in dimethylformamide (DMF) and left for 24 hours for complete dissolution. BODIPY 4 was dissolved in (chloroform:ethanol 1:4, 20:80 mL v/v) and stirred at room temperature. To this mixture, excess thionyl chloride was added slowly and a reddish color change was observed, and to this, a solution of DABSA was added (1:5 mol:mol ratio) and the reaction was left uninterrupted to stir over night. The resulting mixture was dried and separated using column chromatography (stationary phase silica gel, biobeads and sephadex) and a reddish-brown band was confirmed and product collected with a high yield (77%), $C_{52}H_{41}BF_2N_{12}S_5O_{20}$ calculated for m/z 1338.12 g/mol found m/z 1342 g/mol [M+4H], molecular cleavage found m/z 1176 [M - (HO_3S)*2, m/z 162)], elemental composition calculated for: C44.85%, H3.08%, B0.81%, F2.84%, N12.55%, O23.90%, S11.97% and Found: C46.29%, H2.91%, B0.83%, F2.84%, N12.62%, O23.78%, S4.81%. IR bands ascribed to (υC=O) 1728 cm^{-1}, (υC=C) 1643 cm^{-1}, (υC-N) 1307–1370 cm^{-1}, (υN-H_{amide}) 3340-3404 cm^{-1}, (υ$SO_3H_{sulfonic\ acid}$) 1495 cm^{-1}; (υ$OH_{sharp\ free}$) 3602 cm^{-1}, (υB-F) 1619 cm^{-1}, (υC-H_{Ar}) 3108 cm^{-1}, (υC-C_{Ar}) 1463-1546 cm^{-1}; (υN-$H_{stretch}$) 3428 cm^{-1}. ^1H NMR ($CDCl_3$, 400 Hz) δ[ppm]: 12.45(s, 1H,OH-DABSA); 3.02(s, 2H, amine); 3.07(s, 2H, amine); 3.10(s, 2H, amine); 3.22(s, 2H, amine); 3.25(s, 2H, amine); 6.31(s, 1H, pyrrolic H); 7.11(s,1H, 6-pyrrolic H); 7.69(s, 1H, Ph-DABSA); 7.99(d, 2H, meso-Ar); 8.09(m, 2H, meso-Ar); 9.46(s,

1H, NH linker); 9.61(s, 1H, NH linker); 9.89(s,1H,NH linker); 10.44(s, 1H, NH linker); 10.86(s, 1H, NH linker). ^{13}C NMR ($CDCl_3$, 100 Hz) δ[ppm]: 166.68, 124.44, 117.39, 133.42, 130.86, 125.37, 128.77, 143.36, 117.39, 119.08, 147.84, 125.37, 165.80, 172.05, 164.26, 161,06, 159.45.

3.4.9 Synthesis of 4-4difluoro-4bora-1,3,5,7,tetracarboxylamide-3-aminobenzoicacid-8[4-carboxylamide-3-aminobenzoic acid]-3a,4a-diaza-s-indacene (BODIPY 9) (**scheme 3.16**)

A similar protocol was followed as for the synthesis of BODIPY 8 with diaminobenzoic acid (DABA) as a substituent to form BODIPY 9 respectively, A silica column was used for the separation of BODIPY 9 (acetonitrile: methanol, 1:1 v/v), a reddish-pink band was confirmed and collected with a high yield (70%), $C_{56}H_{43}BF_2N_{12}O_{14}$ calculated for m/z 1150.31 g/mol found m/z 1117.55 g/mol [M^+-F_2], elemental composition calculated for: C57.01%, H3.57%, B0.93%, F3.28%, N14.5%, O20.71% and Found: C58.78%, H3.78%, B1.02%, F2.52%, N14.43%, O19.11%. IR band ascribed to (υC=O) 1687 cm^{-1}, (υC=C_{Ar}) 1456-1515 cm^{-1}, (υC-N) 1090-1380 cm^{-1}, (υN-H_{amide}) 3353 cm^{-1}, (υB-F) 1627 cm^{-1}, (υC-H_{Ar}) 3140 cm^{-1}. ^1H NMR ($CDCl_3$, 400 Hz) δ[ppm]: 3.22(s, 2H, amine); 6.74(s, 1H, 2-pyrrolic H); 7.52(d, J=4.16, 2H, mesoAr); 7.64(s, 1H, 6C-DABA); 7.69(s, 1H, 2C-DABA); 7,71(s, 1H, 3C-DABA); 7.76(s, 1H, 6-pyrrolic C); 7.95(d, J=6.01, 2H, mesoAr); 7.99(s, 1H, NH linker); 8.09(s, 1H, NH, linker); 10.39(s, 1H, NH linker); 10.86(s, 1H, carboxyl); 10.99(s, 1H, NH, linker); 11.40(s, 1H, NH, linker),. ^{13}C NMR ($CDCl_3$, 100 Hz) δ [ppm]: 193.14, 117.39, 121.25, 130.86, 124.44, 128.77, 143.36, 128.77, 136.89, 138.42, 125.42, 153.33, 153.01, 119.0, 161.06, 164.26, 165.80, 195.45, 157.93, 166.63.

3.4.10 Synthesis of 4-4difluoro-4bora-1,3,5,7,tetracarboxylamide-2-aminobenzenesulfonicacid-8[4-carboxylamide-2-aminobenzenesulfonicacid]-3a,4a-diaza-s-indacene (BODIPY 10) (**scheme 3.16**)

For the synthesis of BODIPY 10, sulfamoilbenzoic acid (SMBA) was used as a substituent. In a reaction flask (250 mL three necked round bottom flask), 1:5 mole ratio BODIPY4 and substituent was added and a reddish-brown product was obtained and a column (silica gel, biobeads and sephadex) was used to separate the components with a yield of 79%, $C_{55}H_{36}BF_2N_7O_{25}S_5$ calculated for m/z 1403.04 g/mol found m/z 1367.87 g/mol [M^+-F_2] and 1410.92 g/mol [M^++H_7], elemental composition calculated for: C47.05%, H2.55%, B0.77%, F2.71%, N6.95%, O28.49%, S11.42% and Found: C48.24%, H2.28%, B0.77%, F2.76%, N6.85%, O26.88%, S10.92%. IR bands ascribed to (υC=O) 1687 cm^{-1}, (υC=C_{Ar}) 1400-1549

cm^{-1}, (υC-N) 1087-1331 cm^{-1}, (υ-$OH_{sharp\ free}$) 3619 cm^{-1}, (υN-H) 3500-3741 cm^{-1}, (υB-F) 1609 cm^{-1}, (υC-H(Ar)) 3108 cm^{-1}. ^{1}H NMR ($CDCl_3$, 400 Hz) δ[ppm]: 6.17(s,1H, 2pyrrolic); 7.25(d, J=3.22, 2H, 3,5-meso); 7.54(d, J=4.01, 2H, 2-6meso); 7.93(s, 1H, 6pyrrolic), 7.95(d, J=2.59, 2H, Ar); 8.10(s, 1H, Ar); 8.13(s, 1H, Ar); 13.50(s, 1H, S-NH broad). ^{13}C NMR ($CDCl_3$, 100 Hz) δ[ppm]: 120.89, 120.94, 130.46, 134.23, 143.17, 122.28, 141.31, 145.27, 122.81, 143.4, 128.82, 127.27, 133.61, 127.27, 127.98, 122.81, 127.98,148.10, 127.98, 137.52, 132.62, 132.90, 166.79, 167.07, 169.03, 169.03, 166.98, 164.49.

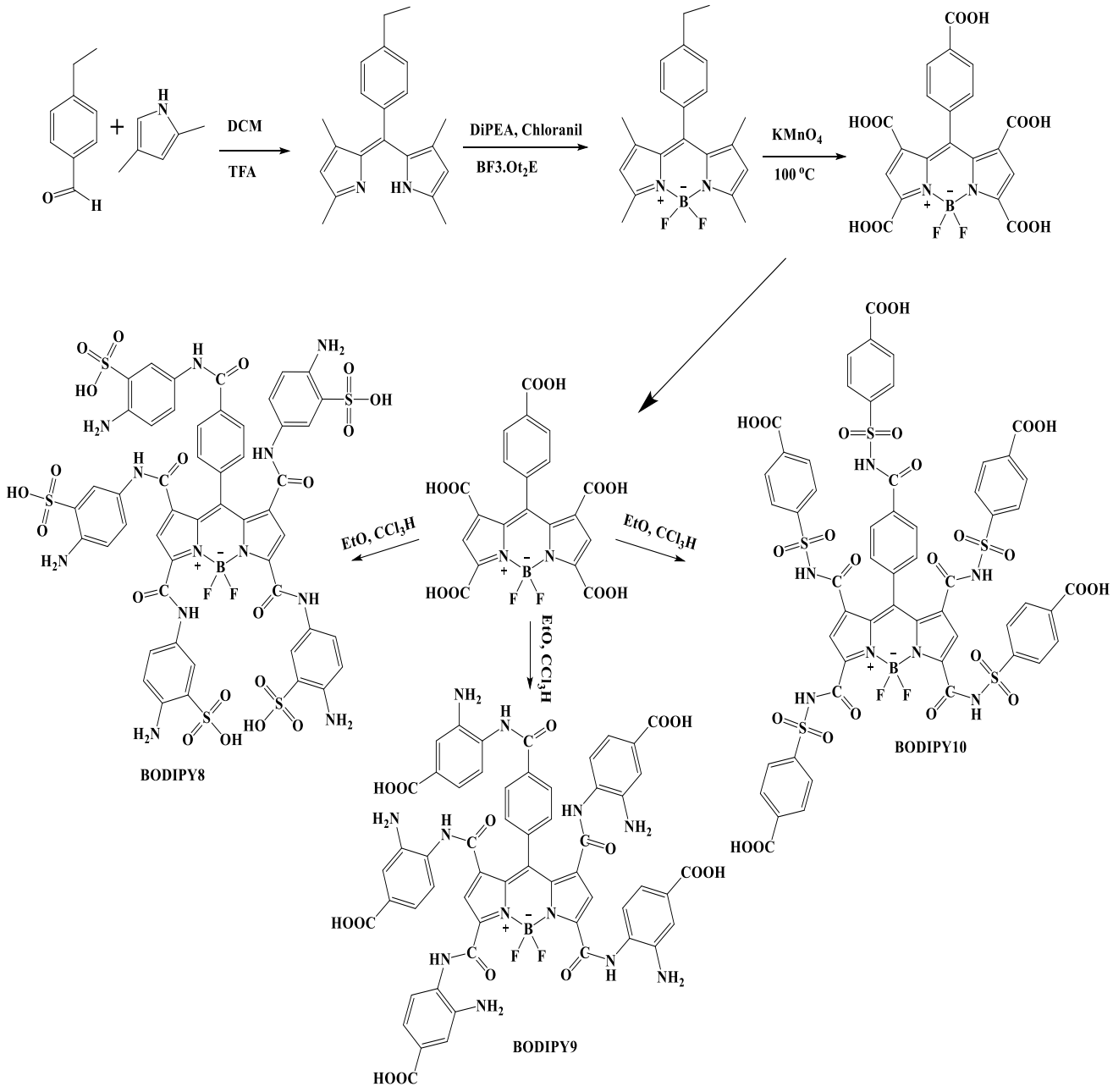

Scheme 3.16 synthesis method of BODIPY 8-10 schematic diagram

3.4.11 Synthesis of 4,4-difluoro-4-bora-4,5-dicarboxy-8[benzyl]-3a,4a-diaza-s-indacene (BODIPY 6.1) (**scheme 3.17**)

In a reaction vial (250 mL three-necked flask), 40 mmol: 80mmol (0.4g: 0.8g; 1:2) was dissolved in a 100 mL of ethyl acetate and stirred at room temperature, followed by the addition of few drops of TFA and the reaction was stirred for 24 hours uninterrupted. To this reaction, chloranil (150 mg) was added and the reaction was allowed to stir for 6 hours, after which (4 mL) of DiPEA was added and the reaction was left to stir for a further 12 hours. The resulting mixture was then complexed with $BF_3.OEt_2$ (5 mL) and stirred overnight and a dark purple product was separated with (silica gel, biobeads and Sephadex) with the low yield of (39%), $C_{17}H_{11}BF_2N_2O_2$ calculated for 356.09 g/mol and found 359.31 g/mol [M+3H], 338.34 g/mol [M-(F)], elemental composition calculated for: C56.98%, H3.47%, B3.04%, F10.67%, N7.87%, O17.97% and Found: C56.81%, H3.23%, B3.02%, F10.49%, N6.99%, O17.92%. IR bands ascribed to (υOHstretch) 3372 cm^{-1}, (υ-C-$H_{stretchAr}$) 3011 cm^{-1}, (υC=CstretchAr) 1410 cm^{-1}, (υ=C-Hbending)704 cm^{-1}, (υB-F) 1645 cm^{-1}, (υC-$N_{stretch}$) 1316 cm^{-1}.

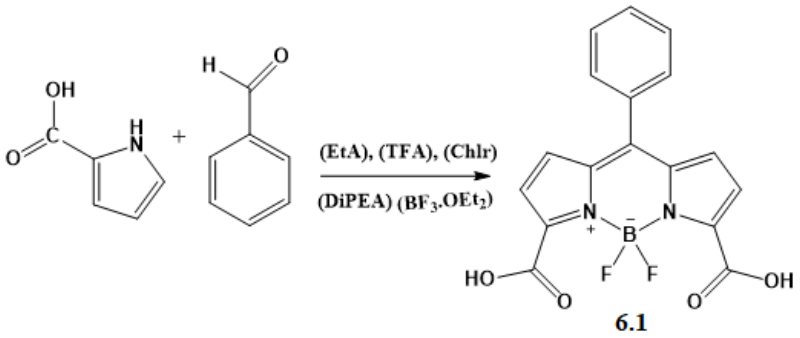

Scheme 3.17 synthetic schematic diagram of BODIPY 6.1

3.4.12 Synthesis of 4,4-difluoro-4-bora-3,5-ditrifluoroacetyl-8[pyrrole-1,2,4-triiodobenzoic acid]-3a,4a-diaza-s-indacene (BODIPY 6.2) (**scheme 3.18**)

In a 250 mL flask, 1,2,4-triiodobenzoic acid (TIBA, 0.741g 1.6 mM) was dissolved in EtOH:DMF (100 mL, 3:7 v/v) and stirred at room temperature. To this reaction, thionyl chloride (0.5 mL) was added drop-wise and allowed to stir for 60 minutes uninterrupted. The resulting product was used in the synthesis of BODIPY 6.2. In a general synthetic method for BODIPY5 see **section 3.4.5** respectively. BODIPY5 (150 mg, 1.5 mM) was dissolved in 100 mL of EtAc and to this 100 mL of acid, chloride-activated TIBA was added drop-wise while stirring at room temperature (1:1 mol:mol). The reaction was left uninterrupted for overnight. A dark blue product was purified with (silica gel, bio-beads and Sephadex) with the yield of

(61%), $C_{24}H_9BF_8N_3O_2I_3$ calculated for m/z 914.70 g/mol and found m/z 976.74 g/mol [M+Na], 897.60 g/mol [M-F_2], elemental composition calculated for: C33.54%, H0.98%, B1.16%, F16.33%, I40.80%, N4.52%, O3.44% and Found: C33.48%, H1.09%, B1.16%, F14.98%, I40.81%, N4.37%, O3.88%. IR bands ascribed to ($\upsilon C\text{-}H_{stretchAr}$) 3011 cm^{-1}, ($\upsilon C{=}C_{stretchAr}$) 1426 cm^{-1}, ($\upsilon{=}C\text{-}H_{bending}$) 939 cm^{-1}, ($\upsilon B\text{-}F$) 1645 cm^{-1}, ($\upsilon C\text{-}N_{stretch}$) 1316 cm^{-1}, ($\upsilon C\text{-}F$) 1034 cm^{-1}.

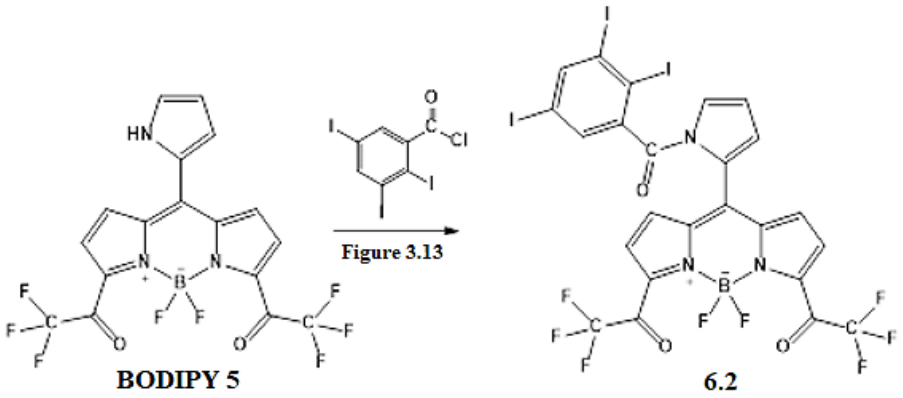

Scheme 3.18 synthetic schematic diagram of BODIPY 6.2

3.4.13 Synthesis of 4,4-difluoro-4-bora-1,5-carboxy-1,3,5-triiodobenzoic acid-8[benzyl]-3a,4a-diaza-s-indacene (BODIPY 6.3) (**scheme 3.19**)

In a 250 mL three necked reaction flask, BODIPY 6.1 (250 mg) was dissolved in 100 mL (MeOH:DMF, 1:4 v:v) and stirred at room temperature. To this reaction, excess thionyl chloride (3 mL) was added drop-wise and the reaction was stirred for 60 minutes. Following this, 1,3,5-triiodo-4-aminobenzoic acid (TIABA, 200 mg) dissolved in DMF (soaked for 24 hours) was added and the reaction was stirred over night without interruption. A reddish-orange band was obtained through a column chromatography (silica gel, biobeads and sephadex) with a yield of (78%), $C_{33}H_{15}BF_2N_4I_6O_{10}$ calculated for m/z 1437.73 g/mol found m/z 1527.29 g/mol [M+(Na_3,NH_4) and m/z 1418.55 g/mol [M-F], elemental composition calculated for: C27.37%, H1.05%, B0.75%, F2.64%, N3.90%, I52.96%, O11.13% and Found: C27.56%, H2.13%, B0.75%, F1.66%, I52.05%, N3.82%, O11.35%. IR bands ascribed to ($\upsilon N\text{-}H_{stretch}$) 3387 cm^{-1}, (υ $C\text{-}H_{strechAr}$) 2995 cm^{-1}, ($\upsilon B\text{-}F$) 1645 cm^{-1}, ($\upsilon C\text{-}N_{stretch}$) 1316 cm^{-1}, ($\upsilon C{=}C_{stretch}$) 1010 cm^{-1}, ($\upsilon{=}C\text{-}H_{bending}$) 955$cm^{-1}$.

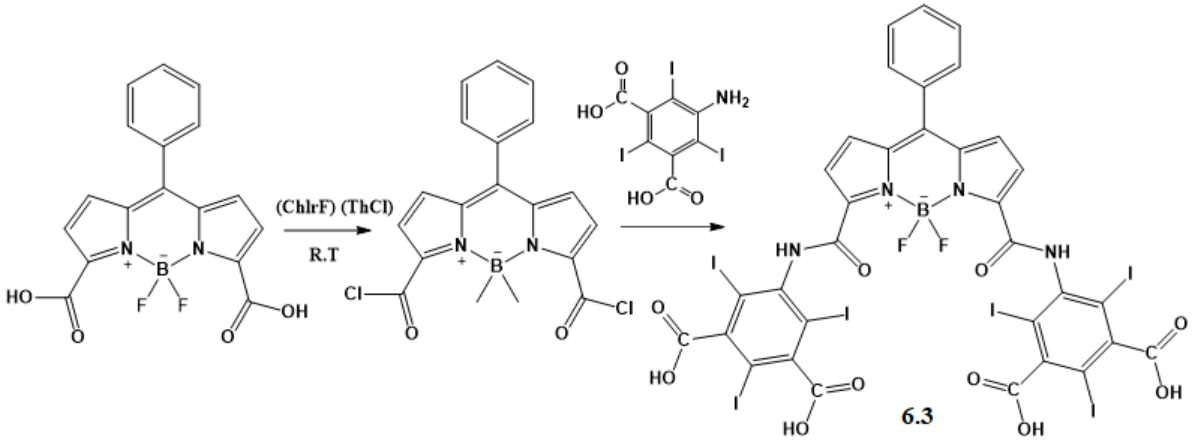

Scheme 3.19 synthetic schematic diagram of BODIPY 6.3

3.4.14 Synthesis of 4,4-difluoro-4-bora-3,5-dicarboxymelamine-2,4-(1,3,5-triiodobenzoicacid)-8[pyrryl]-3a,4a-diaza-s-indacene (BODIPY 6.4) (**scheme 3.20**)

In a three-necked reaction flask, (250 mg: 200 mg) of pyrrole-4-carboxylic acid and pyrrole carboxaldehyde acid were dissolved in ethyl acetate and stirred at room temperature followed by TFA and the reaction was stirred for 12 hours. Followed with, chloranil (150 mg) was added and stirred for 6 hours. After 6 hours DiPEA (5 mL) was added and stirred for 6 hours, followed by the addition of $BF_3.OEt_2$ and the reaction were left to stir for 12 hours. A light brown band was collected with column chromatography (silica gel, biobeads, and Sephadex) with a yield of (43%), $C_{15}H_{10}BF_2N_3O_4$ calculated for m/z 345.07 g/mol. Acid chloride formation reaction, 190mg of the BODIPY was dissolved in 100 mL of chloroform followed by drop-wise addition of thionyl chloride (3 mL) and the reaction was stirred for 60 minutes. To the reaction, melamine (dissolved in DMF 120 mg excess) was added and the reaction was left overnight, the resulting dark brown product was the separated with column chromatography (silica gel, biobeads, and Sephadex) to obtain, 81% of the melamine-BODIPY product m/z 561.28 g/mol wavelength λmax = 477.65 nm. The resulting melamine-BODIPY (300 mg) was dissolved in 100 mL of DMF, to this 250 mg of 1,3,5-triiodo-4-aminobenzoic acid (acid chloride activated benzoic acid) and the reaction was left to stir for 12 hours uninterrupted. The resulting brown product was then separated with column chromatography (Silica gel, biobeads and Sephadex) with the yield of (80%), $C_{53}H_{26}BF_2N_{19}I_{12}O_{14}$ calculated for m/z 2724.57 g/mol and obtained m/z 1359.54 g/mol [M/2], m/z 2146.88 g/mol [M-(TI-4-ABA+F)], m/z 2685.91 g/mol [M-F2], elemental composition calculated for: C23.36%, H0.76%, B0.40%, F1.39%, N9.77%, I55.89%, O8.22% and Found: C23.93%, H0.79%, B0.46%, F1.33%, I55.72%, N8.61%, O8.73%. IR bands ascribed to ($\upsilon N\text{-}H_{sym.stretch}$) 3418 cm^{-1}, ($\upsilon C\text{-}H_{stretch}$) 3011 cm^{-1}, (υB-F) 1677

cm^{-1}, (υC=$C_{stretch}$) 1426 cm^{-1}, (υC-$N_{stretch}$) 1316 cm^{-1}, (υC=$C_{stretchAr}$) 1065 cm^{-1}, (=C-$H_{bending}$) 955 cm^{-1}.

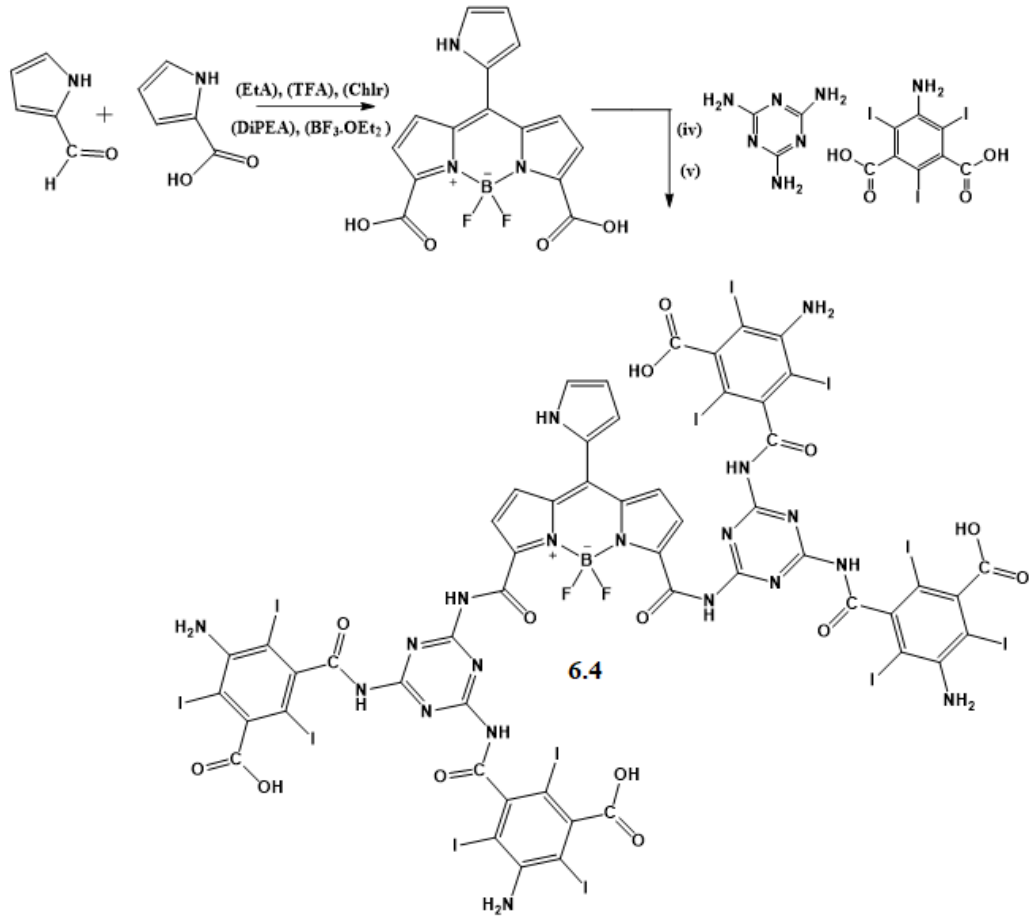

Scheme 3.20 synthesis schematic diagram of BODIPY 6.4**,** (iv) melamine, (v) 1,3,5-triiodo-4-aminobenzoic acid

3.4.15 Synthesis of 4,4-difluoro-4-bora-1,3,5,7-tetracarcoxylamide-1,3,5,-tetratriiodocarboxylicacid-8[(4-carboxylamide-1,3,5-triiodobenzoicacid)benzyl]-3a,4a-diaza-s-indacene (BODIPY 6.5) (**scheme 3.21**)

The synthetic reaction was carried in a 250mL round bottom flask. In a reaction flask, 250mg of BODIPY 4 was dissolved in chloroform:methanol solvent mixture (4:1 v/v) and stirred at room temperature. To this excess (3 mL) of thionyl chloride was added (solution changed from orange-yellow to red) followed by DMF (2 mL) and stirred at 250 rpm for 60 minutes at room temperature. To this, 300 mg of 1,3,5-triiodobenzoic acid (in 50 mL DMF) was slowly added and the color changed from red to brown and the reaction was left to stir for 24 hours. The resulting product was then separated in a column EtOH:DMF (2:3 v/v) (silica gel, diobeads and sephadex) with the yield of (77%), $C_{62}H_{21}BF_2N_7I_{15}O_{27}$ calculated for m/z 3248.20 g/mol

and found m/z 3260.58 g/mol [M+H_{12}], m/z 1627.21 g/mol [M/2], m/z 2787.72 g/mol [M-$C_8H_3I_3O_4$], m/z 3275.91 g/mol [M+Na_2-F], elemental composition calculated for: C22.93%, H0.65%, B0.30%, F1.17%, N3.02%, I58.60%, O13.30% and Found: C23.01%, H0.97%, B0.29%, F1.15%, I57.92%, N2.85%, O13.21%. IR bands ascribed to ($\upsilon N\text{-}H_{sym.stretch}$) 3434 cm^{-1}, ($\upsilon C\text{-}H_{stretch}$) 3011 cm^{-1}, ($\upsilon B\text{-}F$)1660 cm^{-1}, ($\upsilon C{=}C_{stretch}$) 1426 cm^{-1}, ($\upsilon C\text{-}N_{stretch}$) 1316 cm^{-1}, ($\upsilon C{=}C_{stretchAr}$) 1065 cm^{-1}, ($\upsilon{=}C\text{-}H_{bending}$) 970 cm^{-1}.

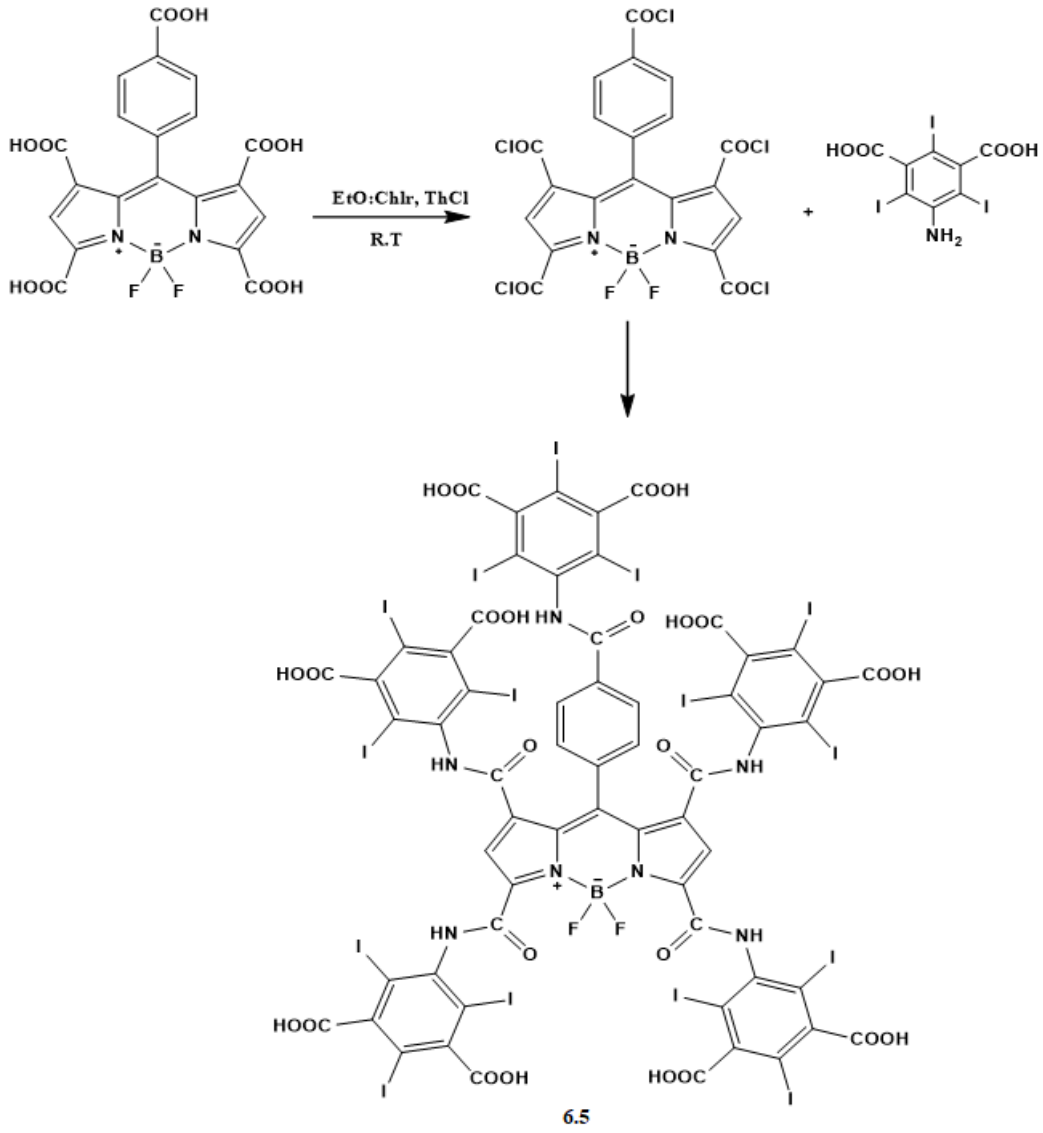

Scheme 3.21 synthetic schematic diagram of BODIPY 6.5

3.4.16 Synthesis of 4,4-difluoro-4-bora-1,3,5,7-tetracarboxylamidemelamine-2,4-octacarboxylamide-1,2,4-octatriiodobenzoicacid-8[(4-carboxylamidemelamine-2,4-dicarboxylamide-1,2,4-ditriiodobenzoicacid)benzyl]-3a,4a-diaza-s-indacene (BODIPY 6.6) (**scheme 3.22**)

In a three-necked 250 mL round bottom flask, BODIPY4 was dissolved in chloroform: methanol (4:1 v/v) and the reaction was stirred at room temperature. To this, thionyl chloride (in excess, 3 mL) was added followed by DMF (0.5 mL) and the reaction stirred for further 60 minutes to allow for full acid chloride formation. Following this, melamine (200 mg, in DMF) was slowly added and the reaction was allowed to stir for 24 hours. A reddish-brown product 81% absorbance 512.35 nm was purified with column chromatography (silica gel, biobeads, and Sephadex). After drying the product, 300 mg was dissolved in DMF 100 mL and to this, 350 mg of 1,2,4-triiodobenzoic acid (dissolved in ethylacetate:ethanol 1:1 v/v and activated with thionyl chloride (3 mL) catalyzed with DMF (0.5 mL)) and the reaction was stirred at room temperature undisturbed for 24 hours. A dark blue-brown product was then purified with a column chromatography (silica gel, biobeads and Sephadex) with a yield of (74%), $C_{105}H_{41}BF_2N_{32}I_{30}O_{15}$ calculated for m/z 5846.63 and found m/z 5864.83 g/mol [M+18], 1948.24 [M/3], 1169.71 g/mol [M/5], 4759.32 g/mol [M-$C_{17}H_7I_6N_6O_2$], elemental composition calculated for: C21.57%, H0.71%, B0.18%, F0.65%, N7.67%, I65.12%, O4.10% and Found: C21.65%, H1.07%, B0.18%, F0.65%, I64.09%, O4.03%. IR bands ascribed to (vN-$H_{sym.stretch}$) 3434 cm^{-1}, (υC-$H_{stretch}$) 3011 cm^{-1}, (υB-F) 1660 cm^{-1}, (υC=$C_{stretch}$) 1441 cm^{-1}, (υC-$N_{stretch}$) 1318 cm^{-1}, (υC=$C_{stretchAr}$) 1049 cm^{-1}, (υ=C-$H_{bending}$) 939 cm^{-1}.

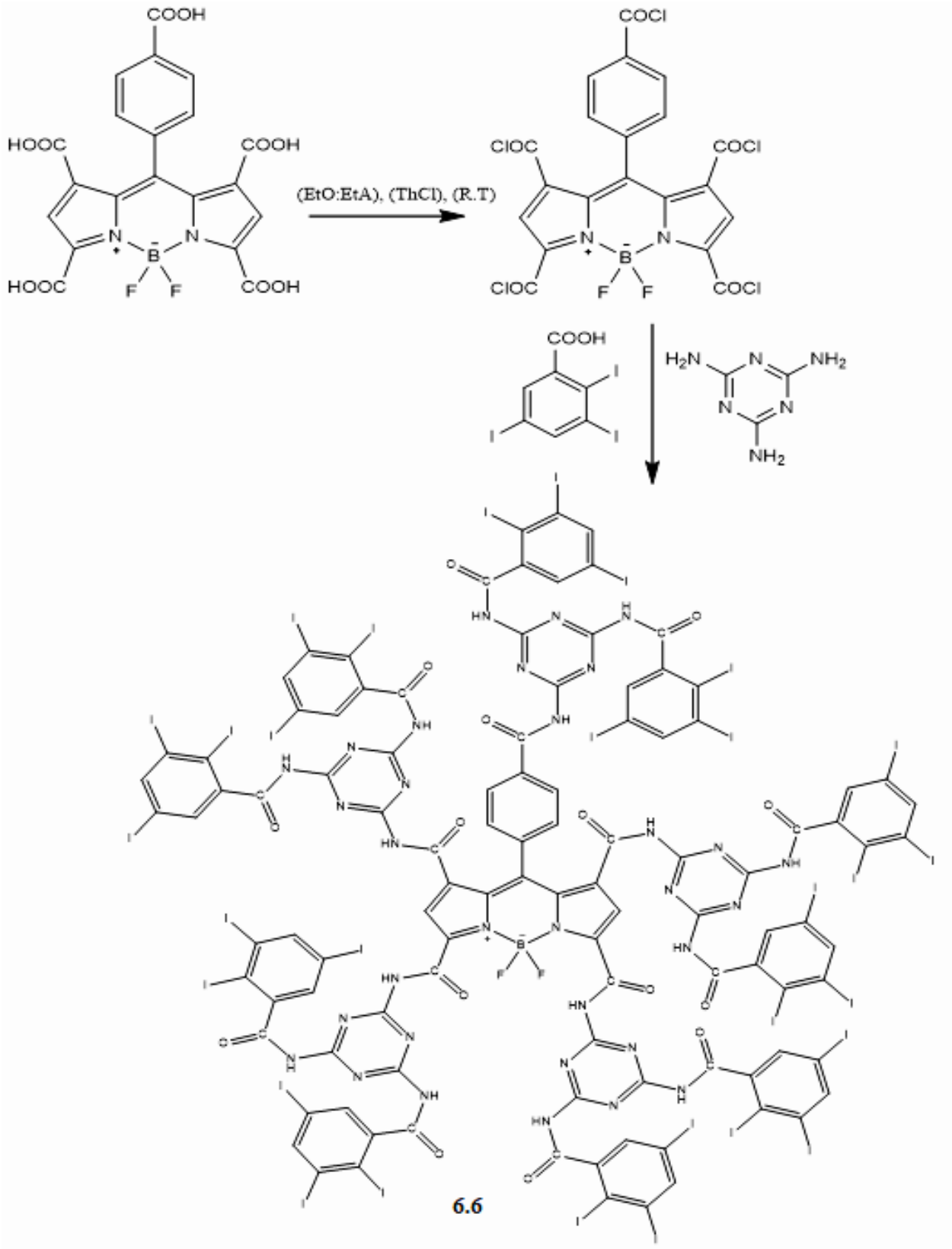

Scheme 3.21 synthetic schematic diagram for BODIPY 6.6

3.5 Synthesis of Au and Pt nanoparticles

3.5.1 Synthesis of Au NRs with the seed-mediated method (Adapted from Nikoobakht and El-Sayed, 2003)

3.5.1.1 Seed solution preparation

A seeding solution was prepared from Au salt. Briefly, in a 25 mL conical flask, a solution containing 2 mM tetrachloroauric acid was added and stirred at room temperature. Ice cold 1 mM sodium borohydride solution 50 µL was added and the nanoparticles solution was used immediately for nanorods synthesis.

3.5.1.2 Synthesis of Gold nanorods

A solution containing 20 mL of 2.0 mM CTAB, 15 mL 2 mM tetrachloroauric acid $HAuCl_4$ was allowed to stir for 60 minutes at 30 °C. Thereafter, subsequent addition of silver nitrate 1.8 mL 10 mM to the solution was carried out and the reaction was left to stir 10 minutes. After few minutes, the addition of a seed solution 200 µL was carried out followed by the addition of, 140 µL of 10 mM ascorbic the reaction mixture was left to stir for 4 hours resulting in a colorless solution which subsequently changed color after 20 to 30 seconds from yellow resulting in a purple/deep red color change. After 4 hours the reaction was stopped and stored in the dark for 72 hours which allowed for the growth of Au NRs.

3.5.2 Synthesis of Pt NRs (Scheme 3.23)

3.5.2.1 Pt seed solution preparation

Platinum seed solution was prepared from chloroplatinic acid. Briefly, in a 25 mL conical flask, 20 mL of 2 mM chloroplatinic acid was added and stirred at room temperature. After which ice-cold sodium borohydride 75 µL was added and the resulting nanoparticles were used immediately for the synthesis of Pt NRs.

3.5.2.2 Synthesis of Platinum nanorods (Adapted from Nikoobakht and El-Sayed, 2003)

A solution containing (2 mM, 20 mL) chloroplatinic acid was placed in a 100 mL round-bottomed flask while heated at 80 °C and stirred at 350 rpm. To this, 20 mL of 2 mM CTAB solution was added and the reaction was left to stir for 5 minutes. 1.5 mL solution of silver nitrate was added and stirred for 30 minutes. Followed by the addition of 200 µL of 2 mM chloroplatinic acid seed solutions, the reaction was left to stir for 30 minutes uninterrupted.

Following the seeding reaction, ascorbic acid 10 mM, 2 mL was then added as the reducing agent for the formation of Pt NRs. After 4 hours the reaction was stopped and the resulting solution was stored in the dark for 72 hours to allow for complete growth of Pt NRs.

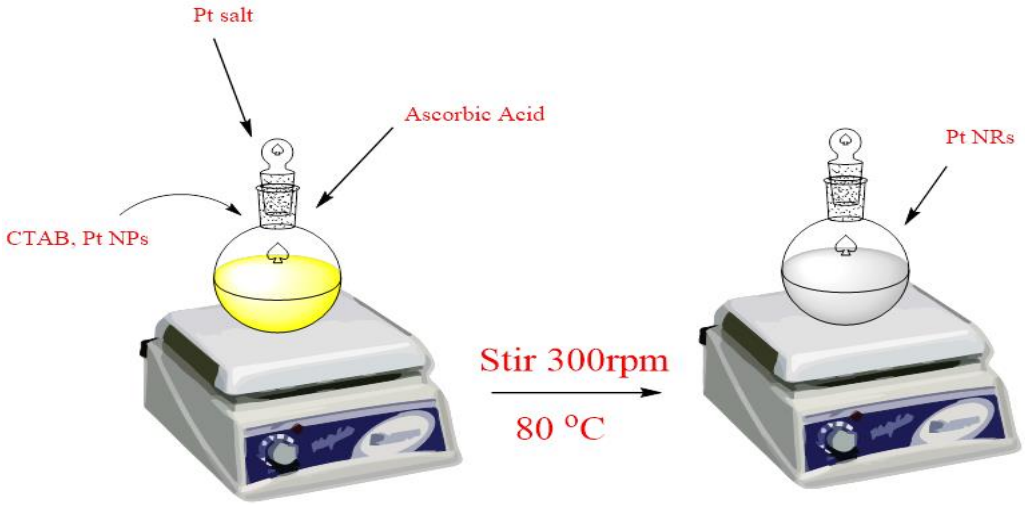

Scheme 3.23 prepared schematic diagram for the synthesis of Pt NRs.

3.5.3 Synthesis of spherical NPs and nanotubes (Adapted from Iqbal *et al*., 2016)

3.5.3.1 Synthesis of spherical Au and Pt NPs

Tetrachloroauric acid (25 mg) was dissolved in 50 mL of water in a 100 mL one necked round bottom flask and stirred at 300 rpm at room temperature. Sodium borohydride (0.1 µM, 1 mL) was then added drop-wise and the reaction stirred for 5 minutes. The color changes from yellow to solid-pink were observed and the NPs were stored in the dark at room temperature.

3.5.3.2 Synthesis of spherical Pt NPs

A similar procedure was followed in the synthesis of Pt NPs. Platinic acid (25 mg) was dissolved in 50 mL of water and stirred in one necked round bottom flask at room temperature. Sodium borohydride (2 mM, 1 mL) was added in the reaction flask and the color changes from yellow to black were observed and the reaction was stirred for 5 minutes and stored in the dark.

3.5.3.3 Synthesis of cubic Au NPs (Adapted from Wu *et al*., 2010)

In a one necked round bottom flask (100 mL), 25 mg of Au salt was dissolved in water and CTAB (0.1 µM, 1 mL) was added to this solution and stirred 80 ºC. To this mixture, 2 mL of Ascorbic acid (5 µM) was added and the reaction was left to stir for 3 hours uninterrupted. The reaction was left to cool at room temperature for 24 hours in the dark. The resulting solution

(purple) was then centrifuged twice at 10000 rpm for 10 minutes to remove the excess of CTAB and the NPs were stored in water at room temperature.

3.5.3.4 Synthesis of cubic Pt NPs

Similarly, 25 mg of Pt salt was dissolved in 50 mL of water in a one necked round bottom flask, followed by the addition of CTAB (0.1 µM, 1 mL) and the reaction was heated at 120 ºC then ascorbic acid (5 µM, 5mL) was added and the reaction was left to stir for 15 minutes. The resulting solution was then cooled at room temperature for 24 hours and centrifuged at 10000 rpm for 10 minutes twice. The NPs were stored in the dark at room temperature.

3.6 Photodynamic inactivation of microorganisms

Methods and Materials

3.6.1 Test compounds

BODIPY photosensitizers were prepared according to the literature as described in chapter 3 section 3.3.1 to 3.4.16 of this thesis in the methods subsection. The solvents for the test compounds (BODIPY PSs) were prepared as a mixture of acetone/dimethylsulfoxide (DMSO) and water (1:3 or 25% to 75%) depending on the solubility of the test compounds. The efficacy of solvent concentrations was tested before the reconstitution of the samples to serve as negative controls. The concentrations as stipulated above were mixed to eradicate the solvent effect that it would not affect the growth of the microorganisms or inoculum. Furthermore, the working starting concentration of the test compound was adjusted to be 66.67 mg/mL throughout the experiments. The white LED light source (65 mW/cm^2) was used for photodynamic inactivation (PDI) experiments.

3.6.2 Bacterial and fungal cultures

Staphylococcus aureus (ATCC 25923), Streptococcus pyogenes (ATCC 8668), *E. coli* (ATCC 25922), and *Pseudomonas aeruginosa* (ATCC 27853) cultures were obtained from the department of oral biological sciences, University of the Witwatersrand. An ethical clearance waiver was granted by the Human Ethics Research Committee for the use of all the strains used in this study (Refer to appendix 5). The cultures were grown on blood agar before their use for any study. A sterile loop was used to subculture the organisms on the blood agar and the plates were incubated at 37^{o}C for 24 hours. The inoculums for drug test experiments were prepared

in Mueller Hinton broth. A known volume of broth was placed in 5 mL disposable plastic vials; a loop full of culture was dissolved in the broth to a concentration of 0.5 McFarland standards.

Candida albicans (ATCC 90028), *Candida tropicalis* (ATCC 750), *Candida glabrata* (ATCC 2850) and *Candida parapsilosis* (ATCC 22019) were obtained from the University of the Witwatersrand. All fungal strains were cultured on the sabouraud dextrose agar (SAB) plate. Preparation of cultures was carried out by sub-culturing the fungal strains with a sterile loop. The culture plates were then incubated at 37^{o}C for 24-48 hours to allow for the complete growth of cultures. The experimental inoculums were prepared in a disposable plastic vial; a loop full of fungal culture was dissolved in a SAB broth to a concentration of 0.5 McFarland standards before the test experiments.

3.6.3 Disk diffusion test

The disk diffusion tests were carried out for both bacterial and fungal species to determine the zone of inhibition before the studies of minimum inhibitory concentration (Balouin *et al*., 2016). The sterilized blank discs (BD0680W/C) were obtained from (Davies diagnostics) with an average diameter of 6.13 mm and were used as supplied.

For Fungal species, Sabouraud dextrose (SAB) agar, and for the bacterial cultures, blood agar plates were used. Using a swab, culture inoculum was spread onto the agar plate surface. Disks were placed on to the seeded surfaces and the samples were placed onto the disks (test compound: 40 µL containing 2 mg/mL). Similarly, two more plates were prepared, one plate was not exposed to light and the other two were exposed to light for 30 minutes, 45 minutes, and 60 minutes then incubated. After incubation, the zones of inhibition were manually measured using a Callipers and Vernier Scale. This experiment was repeated three times for each compound and each organism.

3.6.4 Minimum inhibitory concentration (MIC) assay

The minimum inhibitory concentration assays were carried out in 96 well plates (Mah, 2014). To measure the MICs for the fungal species, Sabouraud dextrose broth (SAB) and for the bacterial cultures Mueller Hinton broth was used.

A serial two-fold dilution of test compounds was carried out using an appropriate broth with a starting concentration of 66.67 mg/mL. A 100 µL of each dilution was added into the wells. Following this, 100 µL of inoculum was added to each well and the plates were incubated at

37^{o}C for 24 hours. After incubation, the plates were read. The first concentration without a visible growth in the well was recorded as MIC. Wells were subcultured on agar plates and incubated for further 24 hours under the same conditions. The first concentration with no growth on the agar plate was recorded as minimum bactericidal/fungicidal concentration (MBC/MFC).

3.6.5 Photodynamic inactivation (PDI) studies

A typical PDI setup was used. Briefly, an LED light holder (32 white LED lights mounted on a light stand, (65 mW/cm^2)) was hooked at 5 cm away from the sample plates. A 96 well plate containing a test compound and an organism under study were first incubated for 6 hours to allow the absorption or adsorption of the test compound and its internalization or surface attachment, and then the plate was placed under the PDI setup and irradiated for 45 minutes. The plate was then incubated for further 24 hours and the wells were read for MIC and subcultured for MBC/MFC. The test chemicals and the work flow chart are described in **Appendix 4,** see also **Chapter 5**

3.6.6 Preparation of Nanoconjugates

The synthesis or preparation of nanoparticles is outlined in **section 3.5** of this chapter. Different shapes of both gold and platinum nanoparticles were prepared and centrifuged for 10 minutes at 10000 rpm (three times) to eliminate the excess surfactant. Spherical, cuboidal, and rod-shaped nanoparticles were obtained. The nanoparticles were then tested for their toxicity with the disc diffusion test method. From the results obtained, we observed that Pt NRs had more activity (larger zone of inhibition) towards all the test organisms. Platinum NRs were selected for further studies as drug carriers and to enhance drug activity against selected bacterial and fungal strains.

BODIPY Pt nanoconjugates were prepared from the compounds that showed antimicrobial activity. The loaded BODIPY PSs were selected from the most photoactive antimicrobial PSs drugs. To load nanoparticles with drugs, 1 mL of Pt NRs solution (10 µg/mL) in water was placed in a 25 mL volumetric flask and stirred at room temperature. To this solution, 50 mg of the most active BODIPY dyes (BODIPY 6 and 6.4) in 15 mL of DMSO were slowly added and the reaction was stirred overnight. The resulting mixture was then centrifuged for 10 minutes at 10000 rpm with 45 mL of water twice to remove the unattached BODIPY dyes.

Then the nanoconjugates were stored for later use. The loading was confirmed with UV-Vis, TEM, and XRD (refer to **Figures 4.10 to 4.13** in chapter 4 **section 4.3.2 to 4.4**).

3.7 Photodynamic therapy of normal HaCat and UCT Mel-1 cancer cell lines

Material and methods

3.7.1 BODIPY photosensitizers and Cell cultures

BODIPY photosensitizers and their nanoconjugates were synthesized and characterized. The procedures for the synthesis and the characteristics observed are described in chapter 3 section 3.3 – 3.16.

The HaCat and UCT Mel-1 melanoma cells were a gift from Dr. E.L Wilson, Department of Haematology, at the Groote Schuur Hospital, Cape Town. Dulbecco's Modified Eagle's Medium (DMEM) was obtained as a Lonza product from WhiteHead Scientific, Johannesburg, South Africa, fetal bovine serum (FBS) and antibiotics were obtained from Sigma Aldrich, P3032/S91370, St. Louis, Missouri, United States, MycoAlert mycoplasma detection kit was purchased from Lonza, LT07-318, Basel, Switzerland. All the solvents were purchased from Sigma Aldrich, Johannesburg.

Cell lines were cultured in Dulbecco's Modified Eagle's Medium supplemented with 10% (v/v) heat-inactivated FBS, penicillin (100 U/mL), and streptomycin (100 mg/mL) and incubated at 37 ºC, 5% CO_2 until 90% confluence was reached. All cells were routinely checked for mycoplasma contamination with the Hoechst 33342 nuclear stain or with a MycoAlert mycoplasma detection kit. Cells were cultured to 90% confluency for all experiments to obtain similar pigmentation levels.

3.7.2 Experimental procedure

Hypericin (Hyp), which was used as a positive control was obtained from Sigma Aldrich (South Africa). Hypericin was used as a positive control as it is known to induce apoptotic and necrotic cell death at 3 μM concentration (Kleeman *et al*., 2014; Sharma and Davids, 2012; Davids and Kleeman, 2011). Working solutions were prepared fresh at a concentration of 50 mM in phosphate-buffered saline (PBS) and then further diluted in microtiter plates using a complete cell culture medium containing 10% (v/v) FBS. Hypericin (3 μM) working concentration for the positive control (PC3) was decided after obtaining its efficacy to induce cell killing (Davids *et al*., 2009; Davids and Kleeman, 2011; Sharma and Davids, 2012, Kleeman *et al*., 2014). The

cells were covered with lids and irradiated from above in PBS. It was activated with ~1.5 J/cm^2 UVA, using a lightbox with two F15T8 15W/UVA PUVA lamps (emitting between 320-410 nm range, with optimal emission at 351 nm, Waldmann, 451415530, Villingen-Schwenningen, Germany). The controls included negative control 1 (cells with no treatment), positive control (cells treated with Hyp + irradiation). Human pigmented/melanotic (UCT Mel-1) cells were exposed to 4 h of Hyp in complete media to maximize uptake, followed by light ~1.5 J/cm^2 irradiation for 20 minutes.

The working solutions of BODIPYs and BODIPY nanoconjugates were freshly prepared in DMSO at a concentration of 50 mM and then further diluted to 0.7, 3, 5, 7 µM (BODIPY 6) and to 3, 5, 10, and 30 µM (BODIPY 16) in complete cell culture medium (DMEM) containing 10% (v/v) FBS. Each plate was prepared as follows, cells were seeded into 96-well plates at a density of 2 x 10^4 cells per well and incubated at 37ºC in an incubator with 5% CO_2 for 24 h to allow the cells to adhere to the surface of the plates. Each dilution was applied to the confluent growth of cells in each of the microtitre plate wells. Cells were exposed to 4 hours of BODIPYs solutions in complete media to maximize uptake, followed by the removal of the excess BODIPY PSs that may have not attached to the cells or been absorbed by the cells. Cells seeded into 96-well plates were covered with plate leads and irradiated from above for 20 minutes. BODIPY PSs were excited with ~1.5 J/cm^2 using a lightbox with two F15T8 15W/UVA PUVA lamps (wavelength 320-410 nm/ peak 351 nm, Waldmann, 451415530, Villingen-Schwenningen, Germany). Controls were sham-irradiated by covering the dish with foil to block the irradiation beam. For the dark toxicity controls (cells, BODIPY treated cells and Hypericin treated cells), were added but not irradiated with light. The plates were incubated for 24 h and cell viability assay was performed.

3.7.3 Cell viability assay

Cell viability were evaluated using a tetrazolium salt XTT (2,3-bis(2-methoxy-4-nitro-5-sulphophenyl)-5-carboxanilide-2H-tetrazolium, monosodium salt), a colorimetric method after the PDT experiments. The assay relies on the ability of viable cells to reduce the yellow XTT tetrazolium salts to an orange formazan salt which is then read at an absorbance of 490 nm. XTT (100 µL/well) solution was then added and left for 2 hours at 37ºC and the plates read at an absorbance of 490-560 nm using a multi-well reader (VERSAmax tunable microplate reader, Labotec Molecular, USA) associated with SOFTmaxPRO 4.3.1 software. The readings of absorbance were recorded by subtracting the value for 0.5% DMSO/DMEM solution which

was included in every plate read. Readings were then converted into percentages of untreated control values. The results were then reported as the mean ± SD of four experimental repeats.

Data were statistically analyzed by the Student t-test for independent samples with a $p < 0.05$ as criteria for statistical significance. The IC50 was determined from the log value of concentration for viable cell plot. The cell viability was calculated according to the formula below:

$$Viable\ cells = \frac{Abs_s - Abs_b}{Abs_c - Abs_b} \times 100\% \qquad \text{Equation 3.2}$$

Where Abs (s, b, and c) are the absorbance of sample, blank and control respectively.

3.8 Conclusion

All the synthetic precursors as well the solvents were used as received. Purging of solvents for the BODIPY synthesis method setup did not have any significant changes compared to those without purging with argon gas. All BODIPY PSs were successfully synthesized with the yields ranging from 30% to 80% respectively. Purity problems persisted for BODIPY dyes synthesized; first, the BODIPYs were purified using the recrystallization method but this resulted in very small yields of the re-crystallized BODIPYs. The search for better separation and purification methods is still ongoing for BODIPYs. Scaling up BODIPY PSs remains a challenge and further optimization is required.

Similarly, the synthesis of Pt and Au NRs was carried out successfully with high yields of uniform Pt NRs compared to their Au NRs counterpart. Centrifugation of NRs more than 4 times resulted in the NRs being unstable. There was a need for optimization of the synthetic method for the synthesis of Au NRs because they yielded NPs with a mixture of shapes and sizes.

Following the synthesis of BODIPY PSs, these compounds were then studied for their antimicrobial effect. The methods to evaluate the BODIPY PSs cell killing capacity and for their cytotoxicity study were optimized. All the studies were carried out in triplicates for antimicrobial study to ascertain the statistical significance of data obtained. Similarly, cytotoxicity studies on normal and cancer cells were carried out in quadruplicates for statistical significance in comparison to their counterpart hypericin PS.

3.9 References

Abate S., Ahn Y.G., Kind T., Cataldi Tri. And Fiehn O.; 2010; Determination of elemental compositions by gas chromatography/time-of-flight mass spectrometry using chemical and electron ionization, *Rapid Commun. Mass Spectrom.*, 24(1): 1172.

Argast A. and Tennis C.F., 2004; A web resource for the study of alkali feldspars and perthitic textures using Light Microscopy, Scanning Electron Microscopy, and Energy Dispersive X-ray Spectroscopy, *J. Geosci. Edu*., 52(3): 213-217.

Barron A.R and Raja P.M.V., 2013; *Physical methods in chemistry and nanoscience, Barron and Raja, Connexions*, (visited on 02-2020)

Bobji M.S., Nirhali P., Chavan N., Powor C. and Kadam M. 2002; Report on transmission electron microscopy: Materials and structural property correlations., www.mecheng.iisc.net.in/~bobji/mspc/assign/TEM.doc. (Accessed 10-2018).

Bunaciu A.A., Udriştioiu E.G., and Aboul-Enein H.Y., 2015; X-ray diffraction: instrumentation and applications., *Critic. Rev. Anal. Chem*., 45(1): 258-299.

Castro A.M., 2013; Organic spectroscopy international, orgspectroscopyint., 02-2020. https://orgspectroscopyint.blogspot.com/p/basics-of-uv-visible-spectroscopy.html.

Davids L.M. and Kleemann B., 2011; Combating Melanoma: The Use of Photodynamic Therapy as a Novel, Adjuvant Therapeutic Tool. *Canc. Treatment Rev*., 37(1): 465-475.

Dhanaraj Pv., and Rajesh N.P., 2009; Growth and characterization of nonlinear optical γ-glycine single crystal from lithium acetate as solvent. *Materials Chemistry and Physics* 115(1):413-417.

Everhart E.T. and Thornley R.F.M., 1960; "Wide-band detector for micro-microampere low-energy electron currents, *J. Scientific Instrument*, 37(1): 246-248.

Fessner W-D., and Walter C., 1996; Enzymatic C-C bond formation in asymmetric synthesis. In: Schmidtche F.P. (ed), in current chemistry, vol. 184. Springer, Berlin, Heidelberg.

Galangau O., Méallet-Renault R., Cécile Dumas-Verdes C., and Clavier G., 2010; Rational design of visible and NIR distyryl-BODIPY dyes from a novel fluorinated platform. *Org. Biomol. Chem.*, 8(20):4546-4553.

Hejazi L., Ebrahimi D., Hibbert D.B. and Guilhaus M., 2009; Compatibility of electron ionization and soft ionization methods in gas chromatography/orthogonal Time-Of-Flight Mass Spectrometry. *Rapid Commun. Mass Spectrom*., 23(14): 2181-2189.

Hoffmann E. de. and Stroobantt V., 2007; *Mass spectrometry: Principles and Applications*, 2007, 3rd Ed. ISBN 978-0-470-03313-4, 2007.

Iqbal M., Usanase G., Oulmi K, Aberkane F., Bendaikha T., Fessia H., Zine N., Agusti G., Errachid E-S., Elaissari A., 2016; Preparation of gold nanoparticles and determination of their particles size via different methods. *Mater. Res. Bull.*, 79(1): 97-104.

Joshi M., Bhattacharyya A. and Ali S.W., 2008; Characterization techniques for nanotechnology applications in textiles, *Indian J. Fibr. Text. Res*., 33(1): 304-317.

King, P.L., and Larsen, J.F. (2013) A micro-reflectance IR spectroscopy method for analyzing volatile species in basaltic, andesitic, phonolitic, and rhyolitic glasses. *Am. Min.*, 98, 1162–1171.

Kleemann B., Loos B., Scriba T.J., Lang D. and Davids L.M., 2014; St John's Wort (Hypericum perforatum L.) Photomedicine: Hypericin-Photodynamic Therapy Induces Metastatic Melanoma Cell Death. *PloS ONE*, 9(7): e103762.

Krumeich F, Müller E, Wepf RA and Nesper R (2011) Characterization of catalysts in an aberration-corrected scanning transmission electron microscope. *J. Phys. Chem. C*., 115, 1080-1083.

Leen V., Gonzalvo V.Z., Deborggraeve W.M., Boens M., and Dehaen W., 2010; Direct functionalization of BODIPY dyes by oxidative nucleophilic hydrogen substitution at the 3, or 3,5-positions. Chem. Commun., 46(27): 4908-4910.

Leggio A., Belsito E.L., de Luca G., di Gioia L.M., Leotta V., Romio E., Siciliano C., and Liquori A., 2016; One-pot synthesis of amides from carboxylic acids activated using thionyl chloride. RSC advances, 6(41): 34468-34475.

Mah T-F., 2014; Establishing the Minimal Bactericidal Concentration of an Antimicrobial Agent for Planktonic Cells (MBC-P) and Biofilm Cells (MBC-B). *J. Vis. Exp*., 83(1): 50854.

Nikoobakht B., and El-Sayed M.A., 2003; Preparation and growth mechanism of gold nanorods (NRs) using seed-mediated growth method. *Chem. Mater*., 15(10): 1957-1962.

Sharma K.V. and Davids L.M., 2012; Depigmentation in melanomas increases the efficacy of hypericin-mediated photodynamic-induced cell death, *Photodiag. Photodyn. Therapy*, 9(2): 156-163.

Smith W., and Dent G.; Introduction, basic theory and principles, and resonance Raman scattering. Modern Raman spectroscopy, John Wiley and Sons, LTD, England, 2005; 1-7 and 93-97.

Stach E.A., 2008; Real-time observations with electron microscopy, microscopy special issue, materials today, ISSN: 13697021, p. 50-58.

Van Bramer S.E., 1998; http://science.widener.edu/~svanbram. (visited 10-2018).

Wu H-L., Kuo C-K., and Huang M.H., 2010; Seed-Mediated Synthesis of Gold Nanocrystals with Systematic Shape Evolution from Cubic to Trisoctahedral and Rhombic Dodecahedral Structures, *Langmuir*, 26(14): 12307-12313.

Yogo T., Urano Y., Ishitsuka Y., Maniwa F., and Nagano T., 2005; Highly efficient and photostable photosensitizersbased on BODIPY chromophores. *J. Am. Che. Sci*., 127(5): 12162-12163.

CHAPTER 4

Synthesis and Spectroscopic Characterization

4.1 Introduction

Synthesis of novel compounds is of great importance, as there are global challenges encountered with the existing and clinically approved antimicrobial, anticancer, and antiviral drugs. In recent years there is a challenge of anticancer resistance to drugs as highlighted by WHO, (2018). BODIPY structural modifications are of importance as they give way to overcome challenges including but not limited to: solubility, resistance to drugs, bioavailability, long sensitivity experienced from the use of other photosensitizers, ROS species production and triplet state photosensitization, etc. (Kamkew *et al*, 2013). This study focuses on extended conjugation of BODIPY PSs to enhance intersystem crossing, which encourages triplet state photosensitization. This leads to enhanced ROS production while lowering fluorescence capacity and increasing solubility. The addition of heavy halogen atoms in the pyrrole rings increases the triplet state quantum yields and allows the molecules to function as PSs (Kamkew *et al*, 2013).

Therefore, the characterization of these molecules is necessary to study their electronic characteristics. In this study, BODIPY PSs are characterized to examine and confirm their synthesis, structural modifications, structural elucidation, crystallinity, photochemical characteristics and to determine their potential activity on Mel-1 cancer cells and selected microbial species. Moreover, the synthesized nanoconjugates formed from loading BODIPY PSs onto nanorods were characterized using techniques and methods discussed in chapter 3 sections 3.2 to 3.12.

4.2 List of synthesized BODIPY Photosensitizers

This study demonstrates BODIPY PSs synthesis using the acid-catalyzed condensation of aryl aldehydes with pyrroles (Adapted from Boens *et al*., 2012). The adapted method of choice was selected because of the ease of the synthesis procedure, its production of fewer byproducts and its cost-effectiveness. Furthermore, this method affords an easy platform for the functionalization of the BODIPY PSs to the desired final product. **Table 4.1** below shows a list of the synthesized BODIPY PSs for this study.

Table 4.1 Synthesized BODIPY PSs nomenclature and their novelty (This work)

BODIPY	Name	Novelty	Reference	BODIPY	Name	Novelty	Reference
Alkyl and carboxyl substituted BODIPY PSs				**BODIPY PSs with bulky substituents**			
1	4,4-difluoro-2,6-diethyl-1,3,5,7-tetramethyl-8-[4-(isopropylbenzyl)]-3a,4a-diaza-s-indacene	No	Trieflinger *et al*., 2005	**7**	4,4-difluoro-4-bora-1,3,5,7-tetramethyl-8-[4-isoprpylbenzyl]-2,6-dinaphthalene-2-sulfonamide-3a,4a-diaza-s-indacene	Novel	This work
2	4,4-difluoro-4-bora-2,6-diethylcarboxyl-1,3,5,7-tetramethylcarboxyl-8-[4-methylcarboxylbenzyl]-3a,4a-diaza-s-indacene	Novel	This work	**8**	4-4difluoro-4bora-1,3,5,7, tetracarboxylamidebenzylsulfonamide-8[4-carboxylamidebenzylsulfonamide]-3a,4a-diaza-s-indacene	Novel	This work
3	4,4-difluoro-4-bora-1,3,5,7-tetramethyl-8-[4-ethylbenzyl]-3a,4a-diaza-s-indacene	No	Kollmannsberger *et al*., 1998	**9**	4-4difluoro-4bora-1,3,5,7, tetracarboxylamide-3-aminobenzoicacid-8[4-carboxylamide-3-aminobenzoic acid]-3a,4a-diaza-s-indacene	Novel	This work
4	4,4-difluoro-4-bora-1,3,5,7-tetramethylcarboxyl-8-[4-methylcarboxylbenzyl]-3a,4a-diaza-s-indacene	Novel	This work	**10**	4-4difluoro-4bora-1,3,5,7, tetracarboxylamide-2-aminobenzenesulfonicacid-8[4-carboxylamide-2-aminobenzenesulfonicacid]-3a,4a-diaza-s-indacene	Novel	This work
Halogenated BODIPY PSs				**BODIPY PSs with extended iodine moieties**			
5	4,4-difluoro-4-bora-3,5-ditrifluoroacetyl-8-[pyrrole]-3a,4a-diaza-s-indacene	Novel	This work	**6.4**	4,4-difluoro-4-bora-3,5-dicarboxymelamine-2,4-(1,3,5-triiodobenzoicacid)-8[pyrryl]-3a,4a-diaza-s-indacene	Novel	This work
6	4,4-difluoro-4-bora-2,6-diiodo-3,5-difluoroacetyl-8-[2-iodopyrrole]-3a,4a-diaza-s-indacene	Novel	This work	**6.5**	4,4-difluoro-4-bora-1,3,5,7-tetracarcoxylamide-1,3,5, -tetratriiodocarboxylicacid-8[(4-carboxylamide-1,3,5-triiodobenzoicacid) benzyl]-3a,4a-diaza-s-indacene	Novel	This work
BODIPY PSs with extended iodine moieties							
6.1	4,4-difluoro-4-bora-4,5-dicarboxy-8[benzyl]-3a,4a-diaza-s-indacene	Novel	This work	**6.6**	4,4-difluoro-4-bora-1,3,5,7-tetracarboxylamidemelamine-2,4-octacarboxylamide-1,2,4-octatriiodobenzoicacid-8[(4-carboxylamidemelamine-2,4-dicarboxylamide-1,2,4-ditriiodobenzoicacid) benzyl]-3a,4a-diaza-s-indacene	Novel	This work
6.2	4,4-difluoro-4-bora-3,5-ditrifluoroacetyl-8[pyrrole-1,2,4-triiodobenzoic acid]-3a,4a-diaza-s-indacene	Novel	This work				
6.3	4,4-difluoro-4-bora-1,5-carboxy-1,3,5-triiodobenzoic acid-8[benzyl]-3a,4a-diaza-s-indacene	Novel	This work				

The images are shown in **Figure 4.1** shows the synthesized BODIPY PSs before light irradiation and **Figure 4.2** the ones under blue UV light. The selected BODIPY demonstrates the physical observations of the PSs. The BODIPYs shown in **Figure 4.1** and **Figure 4.2** consists of different functional groups including meso-phenyl-isopropyl (BODIPY 1), meso-phenyl-ethyl (BODIPY 3), 3,5-trifluoride (BODIPY 5) and 2,6-diiodo-2-meso-pyrryliodo (BODIPY 6) see **Table 4.1**.

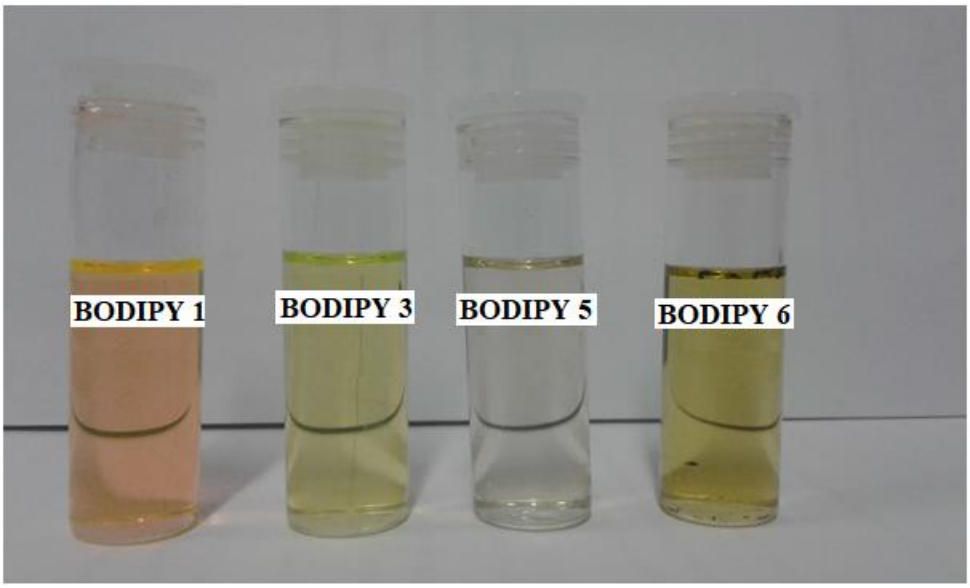

Figure 4.1 BODIPY PSs in ethanol ($1x10^{-6}$ M) without light exposure

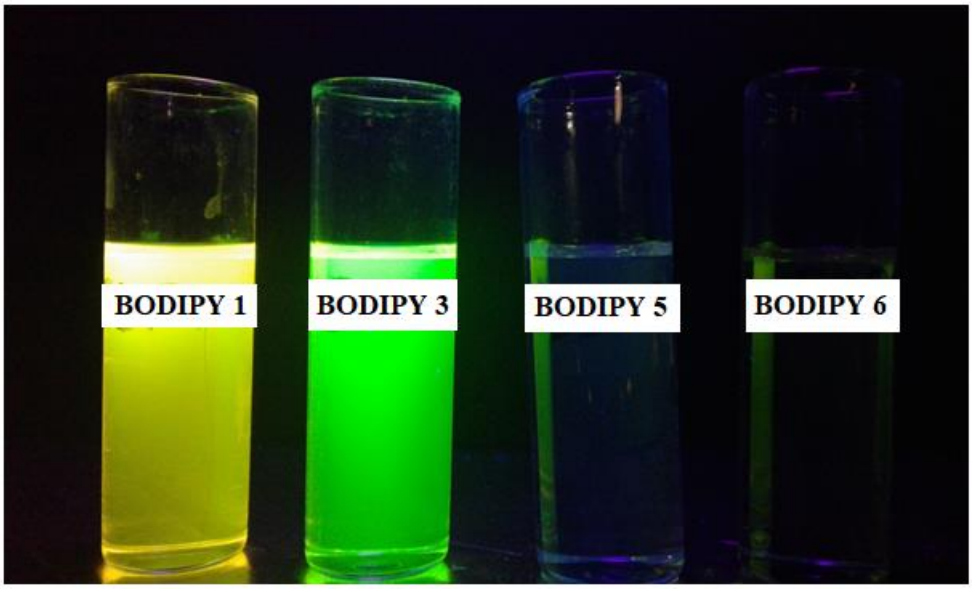

Figure 4.2 BODIPY PSs in ethanol ($1x10^{-6}$ M) with blue light exposure

4.3 Results and discussion

4.3.1 Optical properties

UV-Vis spectroscopy was used to acquire the electronic absorption spectra of BODIPYs 1 – 10 in ethanol concentration (1×10^{-6} M) and characterized by absorption bands in the range of 200 – 1100 nm. The electronic absorption spectra of BODIPY 6.1 to 6.6 in DMSO concentration (1×10^{-2} M) were characterized by absorption bands in the range of 200 – 1100 nm respectively. **Table 4.2** demonstrates BODIPY 1 to 4 photochemical properties in different solvents. BODIPY 1 showed electronic absorption spectra at 520 nm which is the characteristic of the synthesized BODIPY PS. Upon oxidation of BODIPY 1 to form a daughter BODIPY 2 with carboxyl functional groups, we observed a negligible hypsochromic shift of 1.5 nm which was due to the meso-phenyl isopropyl functional group cut-off to form a methyl-carboxylic acid functional group (Choi *et al*., 2014). Similar observations were noticed with BODIPY 3, when oxidized there was a carboxylic acid formation to form BODIPY 4.

Table 4.2 Photochemical properties of BODIPY 1 to 4 acquired in EtOH, DMF, and DMSO (concentration 10^{-6} M)

					Fluorescence Quantum Yields		
BODIPY	**λmax**	**λem**	**Log ε**	**Δλ stokes Shifts (nm)**	**EtOH**	**DMF**	**DMSO**
1	520	534	4.77	14	0.29	0.27	*
2	518.5	530	4.65	10	0.24	0.20	*
3	500	506	4.94	06	0.30	0.27	*
4	498.5	538	4.80	40	0.22	0.18	*

* did not dissolve (undefined)

The BODIPYs 1 to 4 showed high extinction coefficients which were recorded above 50000 $cm^{-1}M^{-1}$ respectively. This high extinction coefficient suggests that the BODIPY 1 to BODIPY 4 absorbs more light compared to their conjugated counterparts (Kukoyi, 2017). Summers *et al*., 2016, suggested that this high extinction coefficient is attributed by the π-π* transition of the BODIPY PSs. The stokes shifts were low for BODIPY 1 to 3 and quite larger for BODIPY 4. The fluorescence quantum yields which were recorded at 0.18 to 0.3 were quite low compared to the standard Rhodamine B (0.65, in ethanol). All four samples did not dissolve in polar solvent dimethyl sulfoxide (DMSO). These carboxylic acid groups facilitate the functionalization of BODIPY PSs through conjugation reactions.

The fluorescence quantum yields (Petrushenko *et al*., 2017) for BODIPY PSs 1-10 and BODIPY 6.1 (in EtOH and DMF) were calculated with the formula below: Rhodamin B (quantum yields 0.65) was used as a reference standard for the calculations of the fluorescence quantum yields for all the samples.

$$\Phi_S = \Phi_{ref} \times \frac{F_S A_{ref} \eta_S^2}{F_{ref} A_S \eta_{ref}^2} \qquad \text{equation 4.1}$$

Where, Φ_s and Φ_{ref} are the quantum yields of the sample and reference standard, the F_s and F_{ref} are the integrated fluorescence intensity, A is the optical density and η is the solvent refractive index.

The equation 4.2 (Niyangoda *et al*., 2017) was used to determine the fluorescence quantum yields for the BODIPYs 5, 6, 7, 6.2 to 6.6. The fluorescence quantum yields were extracted from the linear plot of the absorbance/emission according to the equation below:

$$\Phi_S = \Phi_{ref} \frac{S_S}{S_{ref}} \qquad \text{equation 4.2}$$

where Φ_s is the fluorescence quantum yield of the sample (BODIPYs), Φ_{ref} is the fluorescence quantum yield of the reference (Rhodamine B, Φ_{ref} = 0.65 in ethanol; Kubin and Fletcher, 1982; Divya *et al*., 2014) and S_s/S_{ref} are the slopes of the sample vs the slope of the reference.

The spectroscopic properties of BODIPYs 1 – 4 are demonstrated in **Figure 4.3** below. The BODIPYs 1 to 4 all showed the spectroscopic characteristic of BODIPY PSs which is characterized by two absorption peaks associated with the absorption maxima and excitation shoulder peaks (Laine *et al*., 2017). **Figure 4.3 B** and **C** demonstrate the fluorescence spectra of BODIPY 1 to 4. It was observed that upon oxidation, the fluorescence quantum yield was quenched significantly due to the presence of the carboxylic acid on the BODIPY surfaces.

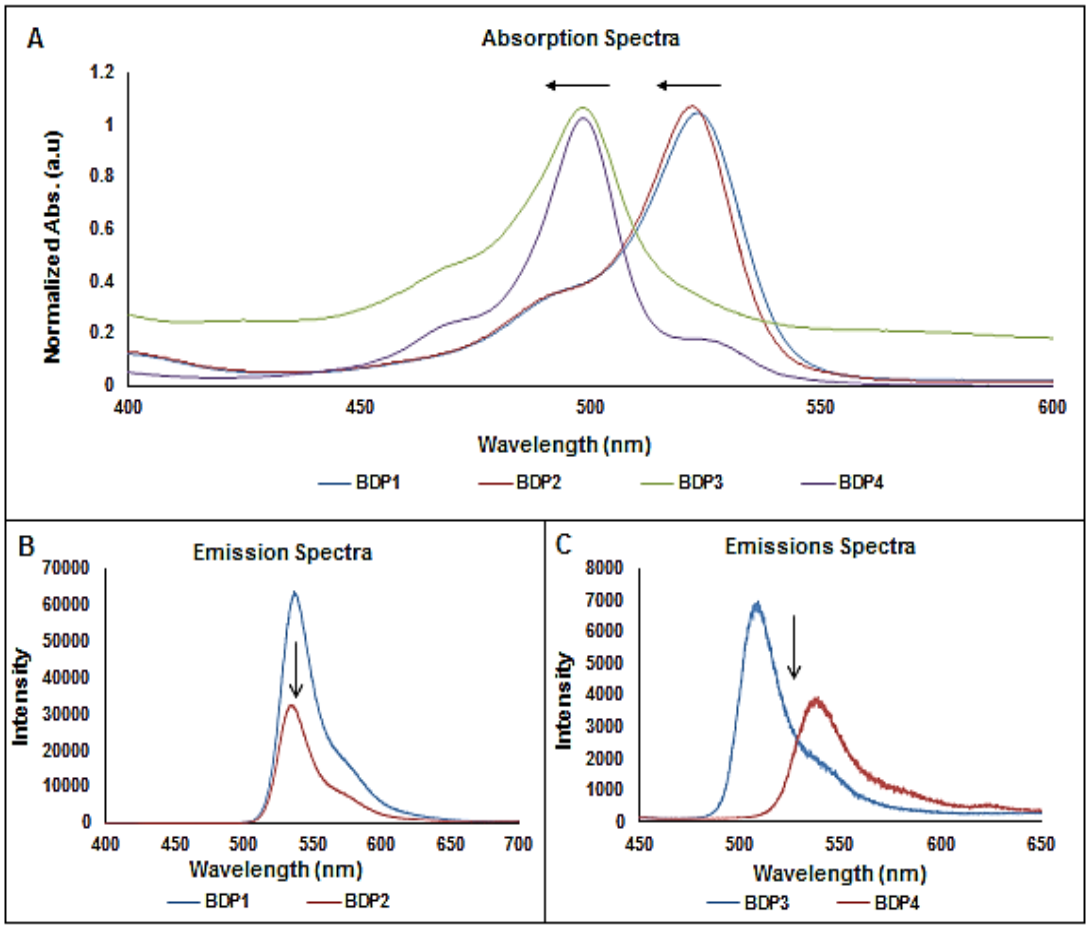

Figure 4.3 (A) the absorption spectra BODIPY 1 – 4, and (B and C) the emission spectra of BODIPY 1 – 4, recorded in ethanol at room temperature (concentration of 1×10^{-6} M).

The effect of functional groups was further investigated by looking at the effect of fluoride substitution at the 3,5-pyrrolic position of BODIPY 5 and the effect of iodine functionalization on 2,6-pyrrolic positions and 4-meso-pyrrolic carbon of BODIPY 5 to form BODIPY 6. **Table 4.3** demonstrates the electronic spectroscopic properties of BODIPY 5 to BODIPY 7. BODIPY 5 showed absorption λmax at 422 nm for both ethanol and dimethylformamide. Upon the functionalization of BODIPY 5 with iodine, there was a bathochromic shift of 2 nm from λmax of 422 nm to λmax at 424 nm comparing BODIPY 5 and 6. This suggested a structural change due to the attachment of iodine moieties on the BODIPY 5 structure confirming the successful functionalization of BODIPY 5 to BODIPY 6. BODIPY 7 showed absorption maxima at 508 nm. This redshift was attributed to the direct functionalization of the BODIPY core structure with naphthaline-2-sulfonamide groups at the 2,6-pyrrolic positions respectively.

Moreover, the BODIPY PSs demonstrated very low extinction coefficients as shown in **Table 4.3**. The fluorescence capacity of the synthesized BODIPY PSs was very low due to the heavy

atom effect for BODIPY 5 and BODIPY 6. Furthermore, BODIPY 7 also demonstrated very low fluorescence quantum yields, as a result of the bulk substituents on the 2,6-pyrrolic positions. The stokes shift values were fairly small for these BODIPY PSs.

Table 4.3 Photochemical properties of BODIPY 5 to 7 acquired in EtOH, DMF, and DMSO (concentration 10^{-6} M)

					Fluorescence Quantum Yields		
BODIPY	**λmax**	**λem**	**Log ε**	**Δλ stokes Shifts (nm)**	**EtOH**	**DMF**	**DMSO**
5	422	427	2.32	5	$<1\times10^{-4}$	$<1\times10^{-4}$	*
6	424	428	2.24	4	$<1\times10^{-4}$	$<1\times10^{-4}$	**
7	508	515	2.63	7	5.00×10^{-4}	5.90×10^{-4}	*

* did not dissolve (undefined), **partially dissolve

Figure 4.4 demonstrates the electronic absorption spectra of BODIPY 5 to 7 acquired in ethanol. The effect of iodine substitution was noted by the bathochromic shift of the absorption spectra (small resolution which may be ascribed to instrumental and solvatochromic factors). Both BODIPY 5 and 6 showed a broad peak at 422 and 424 nm respectively. Moreover, BODIPY 7 showed a characteristic absorption peak at 508 nm with excitation shoulder peaks at 479 and 491 nm respectively. Furthermore, BODIPY 7 showed a sharp absorption peak which is a characteristic of BODIPY PSs. The emission spectra are not shown since the intensity of the spectra obtained was insignificant because the BODIPY PSs had poor emission properties (as shown in **Figure 4.2** above). This is made evident in the value of the fluorescence quantum yields obtained and shown in **Table 4.3**.

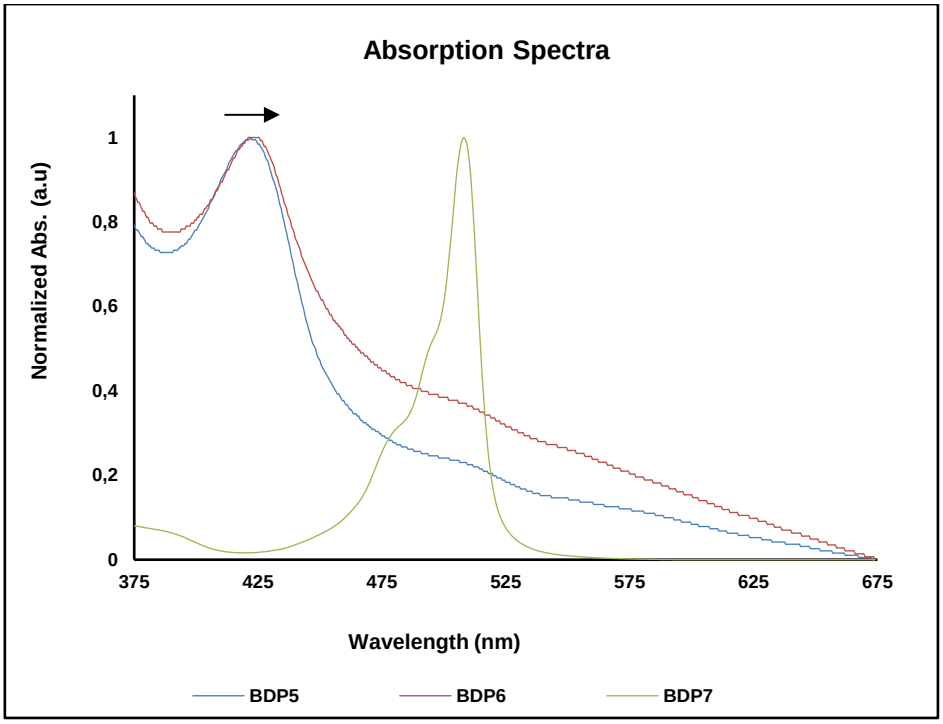

Figure 4.4 shows absorption spectra of BODIPY 5 – 7 recorded in ethanol at room temperature (concentration 1×10^{-6} M)

BODIPY 4 was further functionalized to introduce bulky functional groups including diaminobenzylamine, diaminobenzylsulfonic acid and sumfamoilbenzoic acid on the BODIPY periphery. **Table 4.4** shows the photochemical properties of the resulting functionalized BODIPY PSs. Upon the introduction of bulk functional groups, there was a bathochromic shift of 1.5 nm to 5.5 nm respectively. This bathochromic shift confirmed the formation of new bonds and extended conjugation from the introduction of bulk moieties (Descalzo *et al.*, 2008). A study by Descalzo and co-workers, (2008) made similar observations that substitution of bulk moieties enhance red shift and bright fluorescence. The synthesized BODIPY PSs demonstrated fairly high extinction coefficients. The fluorescence quantum yields did not improve after functionalization. A slight drop in fluorescence quantum yields was encountered in DMF solvent and may be due to the solvent effect which may hinder the emission of the BODIPY PSs (Zhou et al., 2017). The group discovered that the fluorescence quantum yields follow the sequence of viscosity, hence quantum yields are quenched in high polar solvents (Zhou et al., 2017). The BODIPYs 8 to 10 did not dissolve in DMSO.

Table 4.4 Photochemical properties of BODIPY 8 to 10 acquired in EtOH, DMF, and DMSO (concentration 10^{-6} M)

					Fluorescence Quantum Yields		
BODIPY	**λmax**	**λem**	**Log ε**	**Δλ stokes shifts (nm)**	**EtOH**	**DMF**	**DMSO**
4	498.50	538	4.80	40	0.22	0.18	*
8	500.00	517	4.58	17	0.21	0.17	**
9	502.00	515	4.32	13	0.21	0.15	**
10	504.00	518	4.41	14	0.23	0.17	**

***** did not dissolve (undefined), ******partially dissolves

Absorption and emission spectra for BODIPY 8 to 10 are shown in **Figure 4.5** below. In **Figure 4.5 A,** broad absorption spectra are shown and the broadness observed may be a result of hydrogen bonding facilitated by the sulfonamide, amine, and many carboxyl moieties found in BODIPY 8, 9, and 10 respectively (Ryu *et al*., 2018; Matarranz *et al*., 2018). It is also possible that the envisaged hydrogen bonding could lead to the aggregation of these BODIPY dyes in solution further worsening the broadness of the absorption spectral peaks (Matarranz *et al*., 2018). Also, Matarranz and co-workers reported that substitution with bulk moieties may induce the formation of translationally slipped π-stacks. The group envisaged that the dimerization of the carboxylic groups further stabilizes the assembly via intermolecular hydrogen bonds. This behavior suggests the initiation of the aggregation process which leads to broadening of the absorption peaks as observed in this study (Matarranz *et al*., 2018). Furthermore, **Figure 4.5 B** shows the emission profile of the functionalized BODIPY 8, 9, and 10. It can be observed that the different functional groups resulted in different photochemical properties for the BODIPYs with the sulfumoilbenzoic acid moiety (BODIPY 10) showing higher fluorescence quenching properties followed by diaminobenzylsulfonic acid and lastly the diaminobenzoic acid functionalized (BODIPY 9) PSs (Descalzo *et al*., 2008).

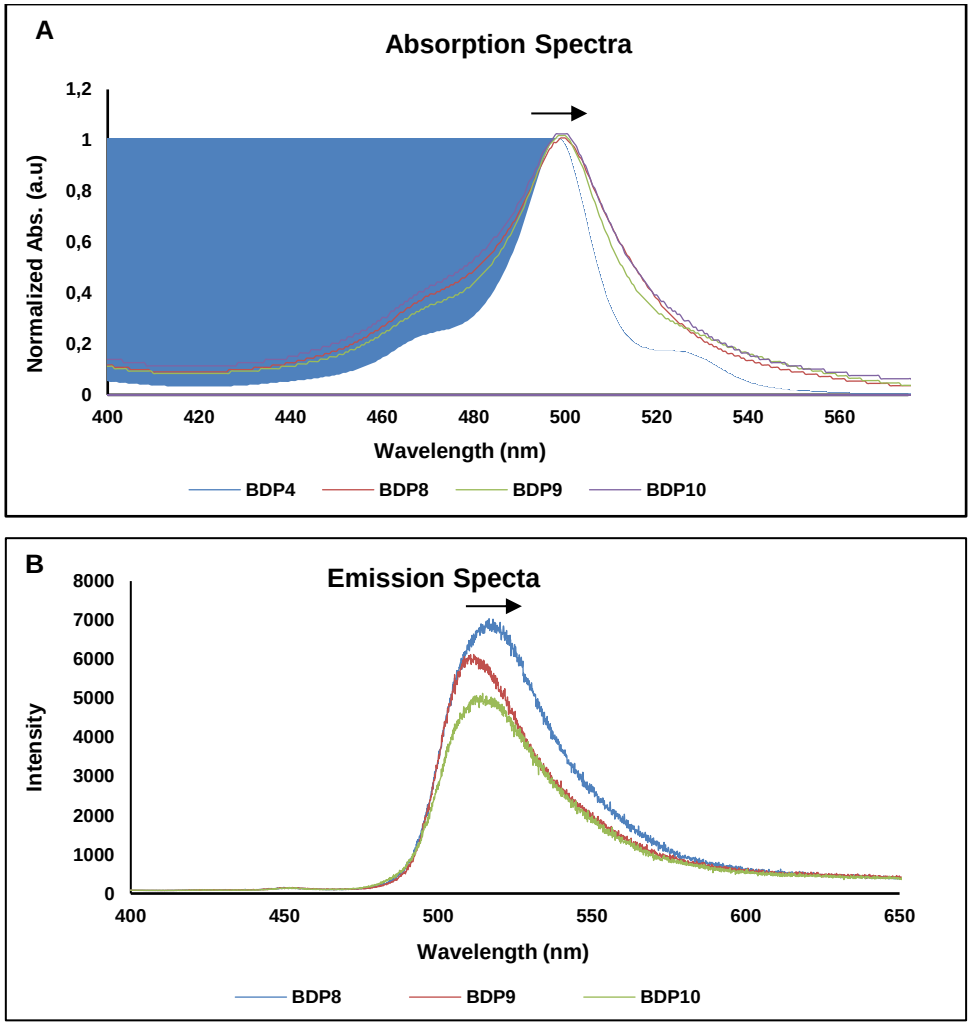

Figure 4.5 (A) absorption spectra of BODIPY 4 and 8 to 10 recorded in ethanol at room temperature (concentration 1×10^{-6} M), (B) is the emission spectra of BODIPY 8 to 10 recorded in ethanol (concentration 1×10^{-6} M) excited at 435 nm.

BODIPY PSs with increased iodine functional moieties were prepared using the amide (acid chloride-amine bond) linker. The BODIPY 4 PS was acylated to introduce the acid chloride active moiety, which was further functionalized with amine-functionalized benzene with iodine functional groups to increase the number of iodine moieties. **Table 4.5** shows the photochemical properties of the synthesized novel BODIPY PSs. BODIPY 6.1 to 6.6 exhibited low absorption extinction coefficients at very low concentrations (1×10^{-6} M) during UV-Vis analysis and showed solubility in polar solvents, therefore the concentration was increased to 1×10^{-2} M respectively. This is attributed to the attachment of bulky moieties on the BODIPY external structure and heavy atom effect (Matarranz *et al.*, 2018; Tao *et al.*, 2019). BODIPY 6.1 was synthesized with carboxylic acid groups at positions 3,5-pyrrolic groups as a precursor for the synthesis of BODIPY 6.3 which contained six iodine functional groups. BODIPY 6.3

showed a bathochromic shift of 26 nm compared to the precursor BODIPY 6.1. Moreover, all the iodo containing BODIPYs showed low extinction coefficients as shown in **Table 4.5**.

BODIPY 6.2 was prepared as a daughter BODIPY PS derived from BODIPY 5 with extended conjugation at the meso-pyrrolic nitrogen. There was an observed electronic bathochromic shift of 5 nm from 422 nm to 427 nm. This redshift of the absorption wavelength suggested successful structural modification. BODIPY 6.4 showed a much red-shifted BODIPY PS with an absorption maxima at 508 nm and 12 iodo functional moieties bonded through the amide linker (facilitated through functionalization with melamine).

Furthermore, BODIPY 4 was acylated with thionyl chloride and functionalized with 1,3,5-tiiodo-4-aminobenzoic acid to afford BODIPY 6.5. Upon functionalization, there was a high electronic bathochromic shift of 12.5 nm and the extinction coefficient also was decreased dramatically. Moreover, the fluorescence quantum yields were very low due to the extended conjugation as well as the availability of more iodine moieties.

BODIPY 4 was further functionalized with melamine forming an intermediate BODIPY (Mel.), with a redshift of 58.5 nm on the electronic absorption spectrum of the functionalized BODIPY(Mel.) PS compared to BODIPY 4. BODIPY (Mel.) was further functionalized with 1,2,4-triiodobenzoic acid to form BODIPY 6.6. There was an electronic absorption hypsochromic shift of 42 nm, which is possibly due to autofluorescence from the carboxyl functional groups (Esnal *et al*., 2013). Introduction of phenyl groups with carboxyl moieties resulted to the blue shift of the electronic spectrum of BODIPY-Mel. A study by Esnal and co-workers (2013), demonstrated that substitution with heteroatoms (specifically N and O) at the meso-position of the BODIPY PSs resulted in the hypsochromic shift. This is evident with other carboxyl group functionalized BODIPY PSs which showed a hypsochromic shift on the electronic absorption wavelength due to autofluorescence of the BODIPY PSs (Ramírez-Ornelas *et al*., 2018). The group reported that electron withdrawing functional groups (like carboxylates) directly lower the fluorescence efficiencies. Which is attributed to the intramolecular charge transfer (Ramírez-Ornelas *et al*., 2018). In contrast, all these BODIPYs 6.1 to 6.6 demonstrated very low fluorescence quantum yields due to their lack of emission (with the intensity value $< 1\times10^{-4}$ nm) which can be said that these novel dyes are non-emissive. This is due to the effect of heavy atoms as well at the carboxyl functional groups respectively.

Furthermore, BODIPY 6.1 to BODIPY 6.6 with extended conjugation and iodine heavy atoms showed similar broad absorption spectra ascribed to the S_0-S_n transition (where $n \geq 2$). These

broad absorption spectra are attributed to the heavy atom effect as well as the existence of many carboxyl and carbonyl functional groups. A study by Adarsh and co-workers, (2010) concluded that the intersystem crossing probability ($S_1 \rightarrow T_1$) transition can be enhanced through spin-orbit by the incorporation of heavy atoms. Moreover, the broadening spectra of these BODIPY PSs can also be an effect of the hydrogen bonding facilitated by the amide bridges and many carboxylic moieties on these BODIPY structures.

Table 4.5 Photochemical properties of BODIPY 6.1 to 6.6 acquired in EtOH, DMF, and DMSO (concentration 10^{-2} M)

					Fluorescence Quantum Yields		
BODIPY	**λmax**	**λem**	**Log ε**	**Δλ stokes shifts (nm)**	**EtOH**	**DMF**	**DMSO**
6.1	465	472	2.99	7	0.043	0.030	0.027
6.2	427	443	2.30	16	*	0.0021	0.0021
6.3	491	513	2.31	22	*	0.0021	0.0022
6.4	508	523	2.28	15	*	1.7×10^{-4}	2×10^{-4}
6.5	511	529	2.23	18	*	$<1\times10^{-4}$	$<1\times10^{-4}$
6.6	515	536	2.22	21	*	$<1\times10^{-4}$	$<1\times10^{-4}$
Mel	557	573	2.54	15	*	5.1×10^{-4}	5×10^{-4}

The electronic absorption spectra for BODIPY 6.1 to 6.6 are demonstrated below in **Figure 4.6**. In **Figure 4.6 A**, all the BODIPY PSs showed broad spectral properties due to the $S_1 \rightarrow S_n$ (where $n \geq 2$) electronic state (Tao *et al*., 2019). BODIPY 6.3 and 6.4 showed red-shifted spectral absorption maxima in comparison to BODIPY 6.1 and BODIPY 6.2 which confirmed structural configuration. The observations were further quantified by the results obtained from mass spectroscopy and FTIR analysis (section 4.3.2 and 4.3.3) respectively. Also, in **Figure 4.6 B** showed broad spectral absorption band, with the BODIPY (Mel) showing a low energy shoulder peak at 619 nm. Similar observations are made with BODIPY 6.6 which showed a broad blue-shifted daughter peak at 372 nm. BODIPY 6.5 also showed a weak shoulder peak around 380-402 nm.

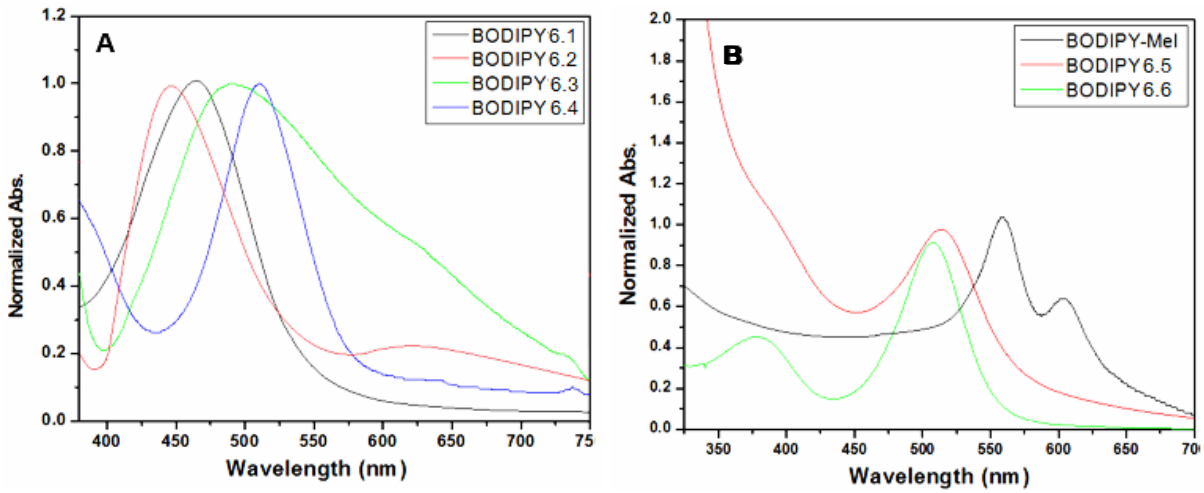

Figure 4.6 shows (A) absorption spectra of BODIPY 6.1 to 6.4 recorded in DMF at room temperature (concentration 1×10^{-2}M), (B) is the absorption spectra of BODIPY Mel and BODIPY 6.5 to 6.6 recorded in DMF (concentration 1×10^{-2}M).

Overall BODIPY 5, 6, 7 (in EtOH and DMF), and 6.2 to 6.6 (in DMF and DMSO) showed negligible to no fluorescence quantum yields respectively. The lowering of the fluorescence quantum yields resulted from substitution with bulky moieties as well as the heavy atom effect on the BODIPY PSs.

4.3.2 Mass spectrometry and elemental analysis

The mass to charge ratios of the synthesized BODIPY PSs were determined by using the high-resolution mass spectrometry coupled with ultra-high-resolution liquid chromatography (HRMS-UHPLC) spectrometer. The analysis was carried out as described in Chapter 3 section 3.3. **Table 4.6** shows the mass to charge ratios of BODIPY 1 to BODIPY 4. All these BODIPY PSs showed a match of the theoretical and experimental peaks. As shown in **Table 4.6**, BODIPY 1, 2, 3, and 4 showed the expected parent ion peaks ascribed as [M+H] ions. The data is in agreement with the elemental data that was computed for all the BODIPY PSs confirming the molecular weights of the BODIPY dyes. **Table 4.6** shows the molecular formula and the corresponding molecular weights with the accompanying elemental data, which in turn matched the calculated empirical composition.

Table 4.6 Mass spectrometer data acquired for BODIPY 1 to BODIPY 4

BODIPY	Mol. Formula	Product Yields (%)	Calc. m/z (g/mol)	Found m/z (g/mol)	Elemental Composition (%)
1	$C_{26}H_{33}BF_2N_2$	42	422.81	423.28	Calc.: $C_{73.94}$, $H_{7.88}$, $B_{2.56}$, $F_{9.00}$, $N_{6.62}$ Found: $C_{73.82}$, $H_{7.55}$, $B_{2.55}$, $F_{8.91}$, $N_{6.63}$
2	$C_{24}H_{15}BF_2N_2\ O_{14}$	71	604.19	605.37	Calc.: $C_{47.71}$, $H_{2.05}$, $B_{1.79}$, $F_{6.29}$, $N_{4.64}$, $O_{37.12}$ Found: $C_{47.76}$, $H_{2.35}$, $B_{1.97}$, $F_{5.31}$, $N_{4.76}$, $O_{37.25}$
3	$C_{21}H_{23}BF_2\ N_2$	37	352.19	353.20	Calc.: $C_{71.08}$, $H_{6.78}$, $B_{3.07}$, $F_{10.72}$, $N_{7.95}$ Found: $C_{71.40}$, $H_{6.85}$, $B_{3.06}$, $F_{10.45}$, $N_{7.93}$
4	$C_{20}H_{11}N_2BF_2O_{10}$	88	488.12	489.27	Calc.: $C_{49.21}$, $H_{2.27}$, $B_{2.21}$, $F_{7.78}$, $N_{5.74}$, $O_{32.78}$ Found: $C_{49.42}$, $H_{2.28}$, $B_{2.41}$, $F_{7.67}$, $N_{5.31}$, $O_{31.99}$

The analysis of BODIPY 5 to BODIPY 10 showed cleaving of some functional groups and with some undergoing protonation. The presence of the halogens on BODIPY PSs periphery showed that these BODIPY PSs tend to undergo protonation and/or react with other adducts. Having highlighted that, BODIPY 5 was calculated for 449.07 g/mol but a weight of 447.35 g/mol was obtained which was due to the deprotonation ascribed as [M-2H]. Moreover, BODIPY 6 showed a cleaving of -F atom, and calculated for 826.7 g/mol while the weight obtained was 803.50 g/mol ascribed to [M-F]. Cleaving was observed with BODIPY 7. Due to the extended conjugation with naphthalene-2-sulfonamide (N_2SA), BODIPY 7 showed the cleaving of the sulfonamide (SO_2NH_2) bond on one of the N_2SA moieties and a fluoride moiety of the B-F bond. BODIPY 7 molecular weight was calculated for 776.23 g/mol and 676.39 g/mol was obtained, which was ascribed to [M-(SO_2NH_2+F)] respectively (Kolemen and Akkaya, 2018). It is worth noting that BODIPY PSs tend to cleave mostly on the B-F bond due to the weaker bond between the boron and fluorine atoms (Qi et al., 2015; Wei et al., 2013; Rosario et al., 1998; Mosley et al., 2011). **Table 4.7** shows the mass to charge ratio of the synthesized BODIPY 5 to 7 and their corresponding computed elemental composition which was a close match to the elemental composition obtained from analysis.

Table 4.7 Mass spectrometer data acquired for BODIPY 5 to BODIPY 7

BODIPY	Mol. Formula	Product Yields (%)	Calc. m/z (g/mol)	Found m/z (g/mol)	Elemental Composition (%)
5	$C_{15}H_8BF_8N_3O_2$	32	449..07	447.35	Calc.: $C_{45.47}$, $H_{1.8}$, $B_{2.41}$, $F_{33.85}$, $N_{9.56}$ $O_{7.13}$ Found: $C_{42.46}$, $H_{1.90}$, $B_{2.61}$, $F_{34.79}$, $N_{9.87}$, $O_{7.62}$
6	$C_{15}H_7BF_8N_2O_2I_3$	90	826..76	803.50	Calc.: $C_{24.70}$, $H_{0.61}$, $B_{1.31}$, $F_{18.38}$, $I_{46.05}$, $N_{5.08}$, $O_{3.87}$ Found: $C_{23.05}$, $H_{0.29}$, $B_{1.34}$, $F_{19.11}$, $I_{46.13}$, $N_{5.01}$, $O_{4.21}$
7	$C_{42}H_{39}BF_2N_4S_2O_4$	43	776.23	676.39	Calc.: $C_{64.95}$, $H_{5.06}$, $B_{1.39}$, $F_{4.89}$, $N_{7.21}$, $O_{8.24}$, $S_{8.26}$ Found: $C_{65.19}$, $H_{4.87}$, $B_{1.76}$, $F_{4.19}$, $N_{7.21}$, $O_{8.15}$, $S_{8.38}$

BODIPY 8 showed both cleaving patterns and protonation, the calculated molecular mass was 1338.12 g/mol and 1342.00 g/mol was obtained which was ascribed to protonation [M+4H].

There was also the cleaving of the DABSA and amine functional groups having molecular masses of 1117.68 g/mol [M-(DABSA+$(NH_2)_2$]. Furthermore, BODIPY 10 was calculated for 1403.04 g/mol and the obtained molecular weight of 1410.92 g/mol was ascribed to the protonation [M+7H], and 1367.86 g/mol which could have resulted from cleaving ascribed to [M-2F] respectively. The protons already exist in solution and they are transferred in gas phase during ES hence samples are protonated (Gaskel, 1997). The elemental composition obtained from the analysis corresponded to the theoretical and calculated elemental analysis of the synthesized BODIPY PSs as shown in **Table 4.8** below.

Table 4.8 Mass spectrometer data acquired for BODIPY 8 to BODIPY 10

BODIPY	Mol. Formula	Product Yields (%)	Calc. m/z (g/mol)	Found m/z (g/mol)	Elemental Composition (%)
8	$C_{52}H_{41}BF_2N_{12}S_5O_{20}$	77	1338.12	1342.00	Calc.: $C_{44.85}$, $H_{3.08}$, $B_{0.81}$, $F_{2.84}$, $N_{12.55}$, $O_{23.90}$, $S_{11.97}$ Found: $C_{46.29}$, $H_{2.91}$, $B_{0.83}$, $F_{2.84}$, $N_{12.62}$, $O_{23.78}$, $S_{4.81}$
9	$C_{56}H_{43}BF_2N_{12}O_{14}$	70	1156.93	1117.55	Calc.: $C_{57.01}$, $H_{3.57}$, $B_{0.93}$, $F_{3.28}$, $N_{14.5}$, $O_{20.71}$ Found: $C_{58.78}$, $H_{3.78}$, $B_{1.02}$, $F_{2.52}$, $N_{14.43}$, $O_{19.11}$
10	$C_{55}H_{36}BF_2N_7O_{25}S_5$	79	1403.04	1410.92	Calc.: $C_{47.05}$, $H_{2.55,}$ $B_{0.77}$, $F_{2.71}$, $N_{6.95}$, $O_{28.49}$, $S_{11.42}$ Found: $C_{48.24}$, $H_{2.28}$, $B_{0.77}$, $F_{2.76}$, $N_{6.85}$, $O_{26.88}$, $S_{10.92}$

The analysis of BODIPY 6.1 to BODIPY 6.6 showed more cleaving patterns during the mass spectrometry analysis. Additionally, due to the bulkiness of some BODIPY PSs there was a mass to charge transfer that was observed resulting in the m/x where "x" is a fraction of the charge transfer. BODIPY 6.1 was calculated for m/z 356.09 and the obtained m/z 359.31 g/mol ascribed to [M+3H], while another cleaving m/z 338.34 g/mol was ascribed to [M-F]. Moreover, BODIPY 6.2 was calculated for m/z 930.89 g/mol, and the obtained m/z 948.71 g/mol ascribed to [M+NH_4] coming from the instrumental adducts produce during gassification. Other BODIPY cleavages were m/z 976.74 g/mol ascribed to [M+$(Na)_2$], m/z 925.63 g/mol ascribed to [M-4H] and m/z 897.60 g/mol ascribed to [M-F_2]. BODIPY 6.3 was calculated for m/z 1437.73 g/mol and obtained 1450.73 g/mol ascribed to [M+13H]. Other cleaving patterns obtained were m/z 1418.55 g/mol ascribed to [M-F], and m/z 1527.29 g/mol ascribed to [M+(Na_3 + NH_4)] (Appendix 1A).

Furthermore, BODIPY 6.4 was calculated for m/z 2724.57 g/mol, and the obtained m/z 2685.91 g/mol was ascribed to [M-2F]. The other cleaving observed included m/z 2146.85 g/mol ascribed to [M-($C_8H_4O_4NI_3$+F)] and m/z 1359.54 g/mol ascribed to [M/2] due to charge transfer. BODIPY 6.5 was calculated for m/z 3248.20 g/mol while the obtained m/z 3260.58 g/mol was ascribed to [M+12H] due to protonation. Other cleaving patterns m/z 2787.72 g/mol

ascribed to [M-($C_8H_3O_4I_3$] and m/z 1627.21 g/mol ascribed to [M/2] due to charge transfer respectively. Danell and Parks (2003), who studied the role of a donor-acceptor BODIPY analog on the fluorescence resonance energy transfer (FRET) in trapped oligonucleotide ions, displayed consistent characteristics with intermediate state related to dissociation dynamics into single strands of oligonucleotides. The group also reported that the thermally controlled experiments resulted in electron autodetachment with the fluorescence and mass spectrometer analysis. They concluded that the fluorescence intensities corrected for the decaying population of ions were due to electron autodetachment and resulted in conformational changes with change in charge state (Danell and Parks, 2003). It is with this reason that BODIPY PSs may display electron autodetachment during mass spectrometer analysis resulting in charge transfer which leads to fragments associated with the formation of the charges measured. In contrast, BODIPY 6.6 was calculated for m/z 5846.63 g/mol and found m/z 5864.89 g/mol ascribed to [M+18H] due to protonation (see Appendix). Other cleaving patterns were obtained including m/z 4759.32 g/mol ascribed to [M-($C_{17}H_7N_6O_2I_6$)], m/z 1948.24 g/mol ascribed to [M/3], and m/z 1169.21 g/mol [M/5] which were due to charge transfer. More studies for experiments to provide the bases for the dynamics of conformational changes as well as autodetachment of electrons need to be explored to explain the charge transfer experienced during analysis. **Table 4.9** below summarizes the observations made as well as the elemental analysis obtained for the synthesized BODIPY PSs. All elemental composition analysis values corresponded with the theoretical or calculated elemental composition respectively.

Table 4.9 Mass spectrometer data acquired for BODIPY 6.1 to BODIPY 6.6.

BODIPY	Mol. Form.	Yield (%)	Calc. m/z (g/mol)	Found m/z (g/mol)	Elemental Composition (%)
6.1	$C_{17}H_{11}BF_2N_2O_2$	39	356.09	359.31	Calc.: $C_{56.98}$, $H_{3.47}$, $B_{3.04}$, $F_{10.67}$, $N_{7.87}$, $O_{17.97}$ Found: $C_{56.81}$, $H_{3.23}$, $B_{3.02}$, $F_{10.49}$, $N_{6.99}$, $O_{17.92}$
6.2	$C_{26}H_9BF_8N_3O_2I_3$	61	930.89	976.74	Calc.: $C_{33.54}$, $H_{0.98}$, $B_{1.16}$, $F_{16.33}$, $I_{40.80}$, $N_{4.52}$, $O_{3.44}$ Found: $C_{33.48}$, $H_{1.09}$, $B_{1.16}$, $F_{14.98}$, $I_{40.81}$, $N_{4.37}$, $O_{3.88}$
6.3	$C_{33}H_{15}BF_2N_4I_6O_{10}$	78	1437.73	1450.72	Calc.: $C_{27.37}$, $H_{1.05}$, $B_{0.75}$, $F_{2.64}$, $N_{3.90}$, $I_{52.96}$, $O_{11.13}$ Found: $C_{27.56}$, $H_{2.13}$, $B_{0.75}$, $F_{1.66}$, $I_{52.05}$, $N_{3.82}$, $O_{11.35}$
6.4	$C_{53}H_{26}BF_2N_{19}I_{12}O_{14}$	80	2724.57	2685.91	Calc.: $C_{23.36}$, $H_{0.76,}$ $B_{0.40}$, $F_{1.39}$, $N_{9.77}$, $I_{55.89}$, $O_{8.22}$ Found: $C_{23.93}$, $H_{0.79}$, $B_{0.46}$, $F_{1.33}$, $I_{55.72}$, $N_{8.61}$, $O_{8.73}$
6.5	$C_{62}H_{21}BF_2N_7I_{15}O_{27}$	77	3248.20	3260.58	Calc.: $C_{22.93}$, $H_{0.65}$, $B_{0.30}$, $F_{1.17}$, $N_{3.02}$, $I_{58.60}$, $O_{13.30}$ Found:$C_{23.01}$, $H_{0.97}$, $B_{0.29}$, $F_{1.15}$, $I_{57.92}$, $N_{2.85}$, $O_{13.21}$
6.6	$C_{105}H_{41}BF_2N_{32}I_{30}O_{15}$	74	5846.63	4759.63	Calc.: $C_{21.57}$, $H_{0.71}$, $B_{0.18}$, $F_{0.65}$, $N_{7.67}$, $I_{65.12}$, $O_{4.10}$ Found: $C_{21.65}$, $H_{1.07}$, $B_{0.18}$, $F_{0.65}$,$N_{7.99}$, $I_{64.09}$, $O_{4.03}$

4.3.3 Fourier Transform Infrared (FTIR) Spectroscopy

The structural-functional groups of the synthesized BODIPY PSs were successfully identified using FTIR spectroscopy analysis. **Table 4.10** summarizes the functional groups of BODIPY 1 to BODIPY 4. All BODIPY PSs demonstrated a characteristic vibrational peak at 1603 cm^{-1} to 1625 cm^{-1} which is assigned to the B-F functional group (Krumova and Cosa, 2010). BODIPY 2 and BODIPY 4 showed an intense broad peak around 3340 cm^{-1} which was ascribed to the hydroxyl functional group. **Appendix 2** shows the BODIPY spectral changes before and after functionalization to introduce carboxylic acid groups.

Table 4.10 Infra-red vibration signals data acquired for BODIPY 1 to BODIPY 4**.**

BODIPY 1	Wavelength (cm^{-1})	Vibrations	BODIPY 2	Wavelength (cm^{-1})	Vibrations
	1400-1542	C=CAr		1412	C=CAr
	1080-1190	C-N		1087-1190	C-N
	1603	B-F		1624	B-F
	1274-1363	C-Hbend		1382	C-Hbend
	2853-2958	C-Hstr		2859-2967	C-H str
				3346	OH
BODIPY 3	**Wavelength (cm^{-1})**	**Vibrations**	**BODIPY 4**	**Wavelength (cm^{-1})**	**Vibrations**
	1466 - 1547	C=CAr		1416	C=CAr
	1082 - 1191	C-N		1043 - 1086	C-N
	2853 - 2957	C-Hstr		1624	B-F
	1301	C-Hbend		3342	OH
	1625	B-F		1782	C=O
				879	H-C=

Ar (aromatic), bend (bending), str (stretching)

The infra-red vibrational signals for BODIPY 5 to BODIPY 8 functional groups are summarized in **Table 4.11**. The BODIPY PSs showed a characteristic peak at 1619 to 1644 cm^{-1} which is a characteristic peak assigned to the BODIPY B-F functional group. Moreover, BODIPY 5 and BODIPY 6 showed a peak at 1396 cm^{-1} which was assigned to the C-F moiety of the triflouro acetic acid group at the 3,5-pyrrolic positions. However, there was a peak at 636 cm^{-1} for BODIPY 6 that was observed which is ascribed to the C-I functional group, suggesting a successful iodine moiety on the BODIPY PS. Furthermore, BODIPY 7 and BODIPY 8 showed a sharp peak at 3602 cm^{-1} and 3615 cm^{-1} respectively, which was assigned to free OH groups. BODIPY 7 showed a peak at 1398 cm^{-1} which was assigned to the S=O functional group respectively. In contrast, BODIPY 8 showed two peaks at 1495 cm^{-1} assigned to SO_3H and a peak at 3404 cm^{-1} ascribed to the amide bond respectively.

Table 4.11 Infra-red vibration signals data acquired for BODIPY 5 to BODIPY 8.

BODIPY 5	Wavelength (cm^{-1})	Vibrations	BODIPY 6	Wavelength (cm^{-1})	Vibrations
	1702	C=C		1993	C=C
	1288	C=Ostr		1288	C=Ostr
	1073	C-N		1064	C-Nstr
	2366	C-Nstr		636	C-I
	3362	N-H		1396	C-F
	1396	C-F		2357	C-Nstr
	1639	B-F		1644	B-F
BODIPY 7	**Wavelength (cm^{-1})**	**Vibrations**	**BODIPY 8**	**Wavelength (cm^{-1})**	**Vibrations**
	886	C-Nbend		1728	C=O
	1511	C=CAr		1643	C=C
	2098	C=Cstr		1307-1370	C-N
	1398	S=O		3340-3404	N-Hamide
	1631	B-F		1495	SO_3H
	3382	NH_2 sym		3602	OHsharp free
	1305	CH_3def.		1619	B-F
	3158	C-HAr str		3108	C-HAr
	3615	OHsharp free		1463-1546	C-CAr

Ar (aromatic), bend (bending), str (stretching), Def. (deformed)

The Infra-red vibrational signals for BODIPY 9 and BODIPY 10 functional groups are summarized in **Table 4.12**. BODIPY 9 and BODIPY 10 showed peaks ascribed to the amide bond which confirmed the attachment of the bulky functional groups. These observations corroborate the observations made with UV-Vis which showed a redshift in the absorption wavelength maxima (λmax) of these BODIPY PSs following functionalization and the diminished fluorescence quantum yields compared to BODIPY 4. Mass spectrometry analysis also showed an increase in the molecular weights of the PSs obtained after functionalization as shown in **sections 4.3.1** and **4.3.2**.

Table 4.12 Infra-red vibrational signals for BODIPY 9 and BODIPY 10**.**

BODIPY 9	Wavelength (cm^{-1})	Vibrations	BODIPY 10	Wavelength (cm^{-1})	Vibrations
	1687	C=O		1687	C=O
	1456 – 1515	C=CAr		1400 - 1549	C=CAr
	1090 – 1380	C-N		1087 - 1330	C-N
	3353	N-Hamine		3500	N-Hamide
	1627	B-F		1610	B-F
	3140	C-HAr		3108	C-Nstr
				3471	OH

BODIPY 6.1 to BODIPY 6.6 which contained extended iodine moieties were the expansion of BODIPY 6 to study the effect of increased Iodine moieties on BODIPY PSs. These BODIPY PSs were synthesized through the amide bridge linker. Benzene rings with triiodo functional groups were used as precursors for the synthesis.

Infra-red vibrational signals were recorded to confirm the attachment of the iodine functionalized benzene rings. All these BODIPY PSs showed a characteristic peak of the B-F bond at 1647 cm^{-1} and 1663 cm^{-1} respectively. Moreover, the BODIPY PSs showed a peak at 3390 ccm-1 and 3437 cm^{-1} which was attributed to the amide bridge linker. Furthermore, the BODIPY 6.2 to BODIPY 6.6 which contained iodine moieties showed a characteristic peak at 676 cm^{-1} to 707 cm^{-1}, attributed to the C-I vibrational signals.

These results were also confirmed by other analyses including UV-Vis which showed a significant shift towards the red region of the visible spectrum. Also, these BODIPY PSs did not show emission capacity as their fluorescence intensity was recorded between 140 and 200 when compared to their parent BODIPY 4 due to the heavy atom effect. **Table 4.13** below summarizes the BODIPY 6.1 to BODIPY 6.6 vibrational signals and their corresponding wavenumbers.

Table 4.13 Infra-red vibrational signals for BODIPY 6.1 to BODIPY 6.6**.**

BODIPY 6.1	Wavelength cm^{-1}	Vibrations	BODIPY 6.2	Wavelength cm^{-1}	Vibrations	BODIPY 6.3	Wavelength cm^{-1}	vibrations
	3390	OH		3390	N-Hamide		3390	N-Hamide
	3020 - 2912	C-HAr		3020 - 2927	C-HAr		3020 -2912	C-HAr
	1663	B-F		1663	B-F		1647	B-F
	1447	C=Ostr		1431	C=Ostr		1417	C=Ostr
	1309	C-Nstr		1324	C-Nstr		1309	C-Nstr
	1032	H-Cbend		1000	C=C		1016	C=C
				676	C-I		707	C-I
BODIPY 6.4	**Wavelength cm-1**	**Vibrations**	**BODIPY 6.5**	**Wavelength cm^{-1}**	**Vibrations**	**BODIPY 6.6**	**Wavelength cm^{-1}**	**vibrations**
	3421	N-Hamide		3421	N-Hamide		3437	N-Hamide
	2989 - 2912	C-HAr		2984 - 2912	C-HAr		3005	C-Hstr
	1663	B-F		1663	B-F		1648	B-F
	1417	C=Ostr		1432	C=Ostr		1432	C=Ostr
	1309	C-Nstr		1309	C-N		1309	C-N
	1016	C=C		1046	C=C		1046	C=C
	954	H-C=bend		938	H-C=bend		938	H-C=bend
	691	C-I		691	C-I		676	C-I

Ar (aromatic), bend (bending), str (stretching)

4.3.4 Nuclear Magnetic Resonance (NMR) Spectroscopy

The structural characterization and elucidation of the synthesized BODIPY PSs were achieved by using proton (^{1}H) and carbon (^{13}C) NMR spectroscopy (**Appendix 3**). The characteristic spectra obtained for BODIPY dyes, the samples were dissolved in deuterated chloroform ($CDCl_3$) (BODIPY 1 – 10) and deuterated dimethyl sulfoxide (DMSO-d_6) (BODIPY 6.1 – 6.6). The chemical shifts for protons 400 MHz and carbons 100 MHz were observed in their expected regions in the ^{1}H and ^{13}C NMR spectra. However, BODIPY 6.1 to BODIPY 6.6 analysis did not provide good spectra as anticipated due to the high noise to signal ratio (Appendix 3). Therefore, triangulation from all the techniques employed in this work was necessary for the elucidation of these BODIPY PSs. The high noise to signal ratio challenge encountered in this study has been shown to result from a variety of factors that include but are not limited to: the number of spectral acquisitions, magnetic field strength, transmission, receiving coils, sample concentration, and the scan parameters (Hyberts, 2013).

In the ^{1}H NMR analyses, it is confirmed that the intensity of a peak is directly proportional to the number of nuclei causing the signal (provided that some conditions are met) (Reich, 2020, University of Wisconsin, 17 February). Therefore, the integrated ^{1}H NMR signals were used to confirm the number of hydrogens per sample to elucidate the structure of the BODIPY PSs. All the synthesized BODIPY PSs were elucidated using a method described by (Reich, 2020) as follows: Example BODIPY 8 ($C_{52}\mathbf{H_{41}}BF_2N_{12}S_5O_{20}$)

Coupling signals: 0.99 : 1.79 : 1.06 : 0.73 mm

Sum of Integral signals = 4.57, then we showed the ratio of the signals

Divide by the smallest value of the signal intensities: 1.36 : 2.45 : 1.45 : 1 (×2)

(3/5/3/2) H/peak for a pure compound

The integral per peak = 4.57/41(the number of hydrogen) = 0.11

Therefore, 0.99/0.11 = 9H, **total # of <u>H = 42</u> equivalents to BODIPY 8 Hs.**

1.75/0.11 = 16H,

1.06/0.11 = 10H,

0.73/0.11 = 7H

This method was very helpful in determining the number of hydrogens for each synthesized compound. All the samples showed equivalent protons for each of the BODIPY PSs as summarized in **Table 4.14** below. The ^{1}H NMR spectra for all BODIPY PSs are shown in **Appendix 3**.

Table 4.14 Calculated the number of hydrogens for BODIPY PSs using J-coupling values from ^{1}H NMR data.

BODIPY	Mol. Form.	Sum of coupling signals	H/peak	Integral/peak	Number of H/Integral
1	$C_{26}\mathbf{H_{33}}BF_2N_2$	16.67	(6/7/1/2)	0.51	32
2	$C_{24}\mathbf{H_{15}}BF_2N_2O_{14}$	14.74	((4/4/2)	0.98	14
3	$C_{21}\mathbf{H_{23}}BF_2N_2$	20.08	(4/4/3/3)	0.87	23
4	$C_{20}\mathbf{H_{11}}BF_2N_2O_{10}$	14.95	(2/2)	1.36	11
5	$C_{15}\mathbf{H_8}BF_8N_3O_2$	1.01	(1)	0.13	8
6	$C_{15}\mathbf{H}_5BF_8N_3O_2I_3$	2.83	(4/3)	0.4	7
7	$C_{42}\mathbf{H_{39}}BF_2N_4S_2O_4$	3.61	(2/5/4/6)	0.093	38
8	$C_{52}\mathbf{H_{41}}BF_2N_{12}S_5O_{20}$	4.57	(3/5/3/2)	0.11	42
9	$C_{56}\mathbf{H_{43}}BF_2N_{12}O_{14}$	3.09	(9/9/1/1)	0.064	43
10	$C_{55}\mathbf{H_{36}}BF_2N_7S_5O_{25}$	5.33	(3/3/4)	0.15	36

In $CDCl_3$, the isopropyl methyl hydrogens' of BODIPY 1 showed an up-field peak at 1.25 ppm. The meso-phenyl(aryl) hydrogens were observed as doublets at 7.16 ppm (J = 6.34 Hz) and 7.31 ppm (J = 7.01 Hz). Furthermore, the 1,7-pyrrolic methyl protons showed an upfield doublet peak at 2.16 ppm (J 1.06 Hz) which is due to the shielding of the phenyl ring (Gibbs et al., 2013). The methyl protons at the 3-pyrrolic atoms were observed at 2.51 ppm, while the protons at 5-pyrrolic atoms were observed at 0.87 ppm chemical shift which was due to the partially positively charged nitrogen. Moreover, the 3,5-pyrrolic methyl hydrogens showed multiplet peaks (J = 1.26 Hz) (Savoldeli *et al*., 2018; Leen, 20110). Additionally, the 2,6-pyrrolic methyl protons were observed as an upfield singlet at 1.55 ppm and the ethyl singlet at 1.05 ppm for CH_2.

However, upon functionalization to form BODIPY 2, there was a downfield peak from 7.16 ppm to 7.71 ppm of the meso-phenyl 3,5-aromatic protons due to the carboxylic acid at the 4-phenyl position. A similar downfield peak from 7.31 ppm to 7.32 ppm was observed for

BODIPY 4 proton shift. Furthermore, a downfield chemical shift at the 1,7-pyrrolic protons from 2.16 ppm to 10.76 ppm, which confirmed the presence of an acidic proton was noted. Moreover, the 2,6-pyrrolic protons also showed similar downfield singlet peaks at 10.42 ppm and 16.70 ppm.

Carbon NMR was also carried out to study the ^{13}C chemical shifts. The aromatic carbons for BODIPY 1 were observed at 127.05 ppm to 147.17 ppm. The isopropyl methyl carbons showed chemical shifts at 23.88 ppm and the center isopropyl carbon was observed at 34.64 ppm. The 2,6-pyrroli ethyl carbons were observed at 17.20 ppm and 17.41 ppm whereas, the 2,6-pyrrolic methyl carbons at 12.60 ppm and 14.78 ppm. In addition, the 2,6-pyrrolic carbons showed downfield chemical shifts at 114.10 ppm and 121.60 ppm due to the π system of the BODIPY core structure. A similar observation was made for the 3,5-pyrrolic carbons with chemical shifts at 126.48 and 151.50 ppm and chemical shifts for the 1,7-pyrolic carbons were obtained at 153.50 ppm and 136.33 ppm respectively. Again, the chemical shift at 5-pyrrolic position showed a downfield chemical shift due to the partial positive charge of the nitrogen.

After oxidation of BODIPY 1 forming BODIPY 2 there was a disappearance of the two isopropyl carbons at the meso-phenyl position. However, the peak at 4-meso-phenyl position showed a chemical shift at 140.89 ppm which indicated the formation of the carboxylic acid. This corroborated with the proton chemical shit respectively. Furthermore, the chemical shifts at 3,5-pyrrolic carbons showed downfield chemical shifts from 126.48 ppm to 156.43 ppm and 151.50 to 152.81 ppm. Similarly, the 2,6-pyrrolic carbons showed similar observations with downfield chemical shifts from 114.10 ppm to 131.0 ppm however the partial positive nitrogen-carbon demonstrated a downward (upfield) chemical shift due to the electron-withdrawing carboxylic acid carbonyl group with chemical shits at 121.60 ppm to 113.36 ppm.

Similarly, with BODIPY 3, the methyl protons (-CH_3) were observed at an upfield chemical shift as multiplets (J = 4.98 Hz) at 1.23 ppm while 4-phenyl ethyl protons were showed as a singlet at 2.32 ppm respectively. The phenyl (aryl) protons were observed at the expected chemical shifts at 7.34 ppm doublet (J = 5.41 Hz) and 6.80 ppm doublets (J = 5.33 Hz). Moreover, the 1,7-pyrrolic protons showed an upfield multiplet at 2.17 ppm and 1.98 ppm which is due to the shielding as observed with BODIPY 1. Similar observations were made with the 3,5-pyrrolic methyl protons with an upfield chemical shift at 0.89 ppm and 2.17 ppm respectively. Additionally, the 2,6-pyrrolic hydrogens were observed at 6.80 ppm and 6.01 ppm due to the π-system of the BODIPY core.

Furthermore, the ^{13}C for BODIPY 2 showed an upfield chemical shift of the ethyl carbons at 14.37 ppm and 28.76 ppm. The phenyl carbons were showed at their expected chemical shift at 124.61 ppm to 140.89 ppm respectively. 1,7-pyrrolic carbons were observed at 124.61 ppm and 142.46, the 2,6-pyrrolic position carbons were showed at 131.05 ppm and 113.36 ppm respectively. Moreover, the 3,5-pyrrolic carbons were showed a downfield at 156.43 ppm and 152.81 ppm. However, upon oxidation, the phenyl hydrogens showed a doublet (J = 7.44 Hz) downfield of 0.5 ppm respectively. Similarly, the 1,7-pyrrolic protons showed a downfield at 12.20 ppm and 12.10 ppm respectively. However, the protons at 2,6-pyrrolic positions showed an upfield of 0.83 ppm, this is due to the carboxylic effect at the 3,5- and 1,7-pyrrolic carbons in the adjacent sides. Gibbs also reported a similar observation, that the upfield is partly due to the shielding of the meso-phenyl ring (Gibbs *et al*., 2013).

BODIPY 5 and BODIPY 6 ^{1}H NMR spectra showed similar downfield chemical shifts at 10.43 ppm and 8.14 ppm which were ascribed to the N-H of the meso-pyrrole. Other pyrrolic hydrogens of the meso-pyrrole were observed as a singlet at 6.21 ppm to 7.08 ppm for BODIPY 5 respectively. The protons at 1,7-pyrrolic positions showed a downfield chemical shift at 6.60 ppm and 6.21 ppm, similar to the 2,6-pyrrolic position protons which showed a downfield chemical shift at 6.49 ppm and 5.31 ppm. However, upon iodine functionalization, there was a disappearance of the chemical shifts at 2,6-pyrrolic positions as well at the 4-meso-pyrrolic carbons which confirms the loading of the iodine moiety respectively (Gibbs *et al*., 2013).

Furthermore, the ^{13}C NMR for BODIPY 5 showed a 4-meso-phenyl carbon downfield chemical shift at 118.04 ppm, due to iodine functionalization, this peak showed an upfield chemical shift at 85.03 ppm which is in agreement with the observations on ^{1}H NMR for the formation of the I-C- bond. In addition, there was a significant upfield chemical shift for the 2,6-pyrrolic carbons from 130.85 ppm and 119.22 ppm to 56.33 ppm and 75.39 ppm. This confirmed the successful iodine functionalization of the BODIPY core structure of BODIPY 6. There was no significant change in the chemical shifts of the corresponding 3,5-pyrrolic positions of both BODIPY 5 and BODIPY 6.

BODIPY 7 ^{1}H NMR showed a multiplet peak at 7.26 ppm to 7.72 ppm (J = 3.25 Hz) naphthalene chemical for the naphthalene sulphonamide at the 2-pyrrolic position. Similar multiplet peaks at 7.02 ppm to 7.43 ppm (J = 2.98 Hz) downfield chemical shifts were observed for the 6-pyrrolic position naphthalene substituted BODIPY core. Moreover, the downfield NH_2 singlet peak was also showed at 7.26 ppm. The 3,5-pyrrolic protons were observed at 2.15

ppm and 1.83 ppm upfield chemical shifts. The isopropyl methyl protons were observed as multiplets at 1.26 ppm (J = 1.06 Hz) whereas the 1,7-pyrrolic protons were observed as a doublet at 2.71 ppm (J = 2.55 Hz) respectively. Furthermore, in ^{13}C NMR all the naphthalene carbons were observed at their expected chemical shifts at 124 ppm to 137 ppm respectively. Similarly, the meso-phenyl carbons were observed at 127.55 to 147.70 ppm. Moreover, 1,7-pyrrolic carbon were observed at 116.42 ppm and 131.70 ppm respectively, 2,6-pyrrolic carbons both showed at 121.20 ppm.

BODIPY 8 to BODIPY 10 were synthesized through the amide bond from the parent BODIPY 4. The NMR spectra were recorded in $CDCl_3$ for BODIPY 8 and DMSO for BODIPY 9 and BODIPY 10. BODIPY 8 showed a new downfield peak at 8.09 ppm which was ascribed to the amide bond. Furthermore, there was a downfield at 6.74 ppm which ascribed to the amine groups of the extended functional groups. This confirmed the successful attachment of diaminobenzoic acid moiety on the BODIPY structure. Moreover, BODIPY 8 showed doublet (J = 0.73 Hz) peaks for 1,7-pyrrolic protons at 7.99 ppm and 7.69 ppm, the doublet (J = 1.79 Hz) at 7.51 ppm and 7.26 ppm was ascribed to the 2,6-pyrrolic protons, the protons ascribed to the 3,5-pyrrolic carbon showed a multiplet (J = 1.06 Hz) at 7.97 ppm and 7.71 ppm. A doublet (J = 0.99 Hz) peak at 6.97 ppm to 6.76 ppm was ascribed to the phenyl protons respectively. Additionally, there was a downfield peak of the ^{13}C NMR at 159.45 ppm that was ascribed to the amide bridge carbon respectively. These results support the results observed with the ^{1}H NMR analysis.

^{1}H NMR for BODIPY 9 showed a downfield shifted peak at 13.08 ppm which is ascribed to the amide bond. A similar peak is also visible for BODIPY 8 and BODIPY 10 respectively. The amine chemical shift was observed at 13.31 ppm to 13.38 ppm as a singlet peak. The 3,5-phenyl protons showed a doublet (J= 1.38 Hz) at 8.02 ppm and 8.04 ppm, 2,6-phenyl protons also showed a doublet (J = 1.39 Hz) at 7.88 ppm and 7.79 ppm respectively. The amide bridge peak on the ^{13}C NMR was observed at 157.93 ppm respectively. The other 13C chemical shifts were observed at their expected positions.

In contrast, the ^{1}H NMR of BODIPY 10 showed a downfield peak at 13.50 ppm which was ascribed to the –OH groups of the phenyl substituted BODIPY PSs. The aromatic peaks were showed at 8.13 ppm to 8.10 ppm as a doublet (J = 1.61 Hz). The 3,5-phenyl protons were observed at 6.17 ppm, the 2,6-phenyl protons were showed at 6.09 ppm. The amide-sulfamoyl bridge protons were observed at 7.21 ppm to 7.95 ppm respectively. Similar to BODIPY 8 and

BODIPY 9, the ^{13}C NMR showed the amide bridge chemical shift at 164.49 ppm. These observations ascertain the formation of the desired BODIPY PSs.

4.3.5 X-ray diffraction (XRD) analysis

The characterization of the BODIPY PSs with XRD was based on the selected BODIPY 6 and BODIPY 6.6 after these were shown to have activity on both microorganisms and the Mel-1 cell line. The Pt NRs patterns were referenced with the online electronic library file (JCPDSICSD4-802). The XRD patterns for BODIPY PSs were studied and compared with the XRD patterns in the literature (Nwahara *et al*., 2018, Ooyama *et al*., 2014; Liu *et al*., 2019).

The crystallinity of the synthesized BODIPY 6 and BODIPY 6.6 before loading onto nanorods was determined using X-ray powdered diffraction. The XRD measurements with the powdered BODIPY PSs exhibited diffraction peaks at 2θ = 24º and 30º, demonstrating the crystal lattices ascribed to well defined microcrystalline structures (Ooyama *et al*., 2014) as shown in **Figure 4.7A**. A broadening diffraction peak observed at 2θ = 25º confirms the small size of the BODIPY microcrystals. Moreover, BODIPY 6.6 showed more intense diffraction peaks, confirming extended conjugation in this BODIPY PS (Nwahara et al., 2018; Liu et al., 2019). Also noted was a diffraction peak at 2θ = 64º which is ascribed to the BODIPY microcrystalline nature (Nwahara *et al*., 2018; Liu *et al*., 2019).

Furthermore, The XRD patterns of the synthesized Pt nanorods loaded with BODIPY PSs are shown in **Figure 4.7B**. The comparison of the diffraction patterns of the synthesized Pt NRs with those reported in the (JCPDSICSD4-802) show distinctive peaks at 2θ values = 39.84º (111), 46.20º (200), 68.01º (220). These patterns are due to the Pt NRs fingerprint peaks, also shown with the ICSB number 76951 database for monometallic Pt nanorods systems (Yang and Xia, 2013; Aritenang *et al*., 2014). Additionally, the small peak at 82.94 º (311) according to ICSB7695 database may be attributed to the Pt NRs but it was not pronounced due to the BODIPY peaks also observed in the same region. BODIPY diffraction patterns in the BODIPY loaded NP counterparts were observed at their respective 2θ positions, demonstrating the successful loading of BODIPY PSs onto Pt NRs respectively. **Figure 4.7** demonstrates the diffractograms of the synthesized BODIPY PSs (A) and platinum nanorods (B).

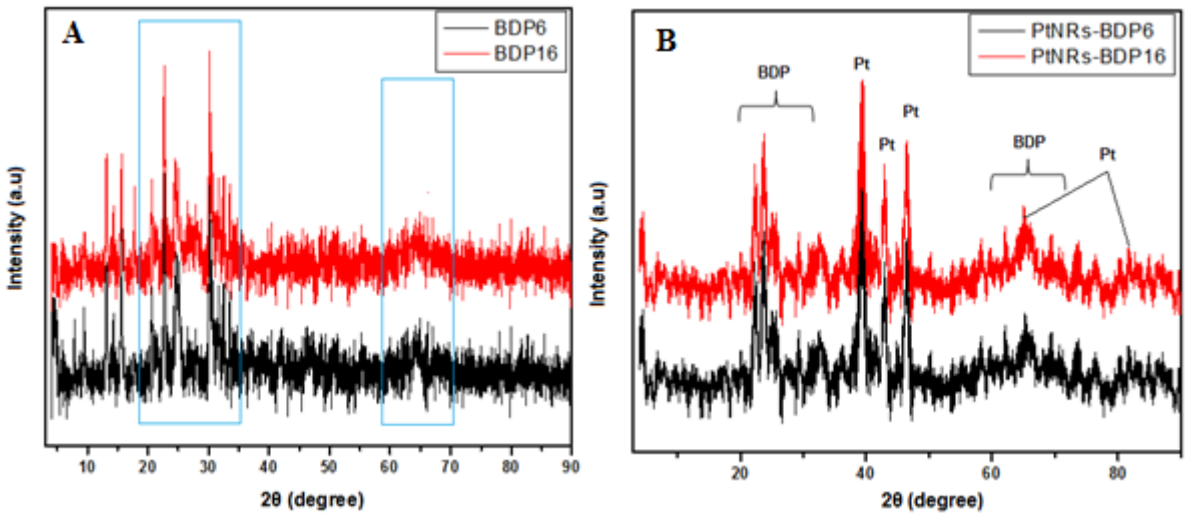

Figure 4.7 powder XRD patterns for powdered (A) BODIPY 6 and BODIPY 6.6 without nanorods and (B) BODIPY PSs loaded onto Pt nanorods.

4.3.6 UV Vis Spectroscopy for Platinum Nanorods (Pt NRs)

UV-Vis spectroscopy was used to determine the nanoparticles' plasmon and absorption spectra. **Figure 4.8** represents the Pt and Au NRs surface plasmon bands. The two bands show the longitudinal oscillating plasmons at the wavelength of 548 nm and 458 nm for gold (Au) NRs and platinum (Pt) NRs, whereas the transverse oscillating plasmon band was observed at 271 and 296 nm respectively (Feng et al., 2008). The two plasmon bands suggest that there was a successful synthesis of Pt NRs. The broadening of the peaks on the other hand is indicative of the size distribution (Feng *et al*., 2008). A study by Feng *et al*., (2008) show that by deposition of Pt on Au NRs (coating of Au NRs with Pt) leads to the broadening of the longitudinal plasmonic peak and reduction in the spectral intensity. The broadening of the peak is reported as due to the damping of the Pt respectively (Feng *et al*., 2008).

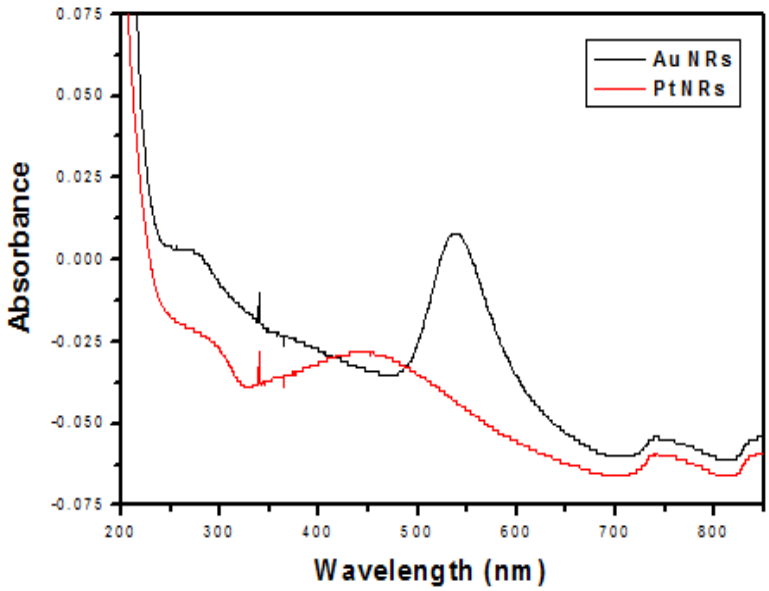

Figure 4.8 Surface plasmon resonance of Au NRs and Pt NRs in water 2×10^{-5} M

4.3.7 Scanning Electron Microscopy (SEM) analysis of nanorods

Figure 4.9 shows SEM images of Pt (left) and Au (right) NRs obtained by the seeding synthetic method. Platinum nanorods were frequently observed to have formed even aggregated nanorods with uniform topographic surfaces. Yoon et al., (2012) reported the synthesis of the aggregated five-fold twinned Pt nanorods with enhanced electrostatic activity. It is suspected that the white spots observed in **Figure 4.9** are the cetyltrimethylammonium bromide (CTAB) molecules that remained after washing and centrifugation. This can be explained by the negative surface charge of the Pt nanorods. It has been shown that for Pt NRs it is difficult to achieve monodispersity in aqueous solution, because of aggregation tendencies mostly due to the attractive van der Waals interactions (which are particularly shown to be strong) for Pt nanoparticles (Krishnaswamy *et al.*, 2006). On the contrary, the Au NRs prepared were observed to form a mixture of shapes and sizes of nanoparticles. This mixture contained rods, spheres, and cubes of different sizes respectively.

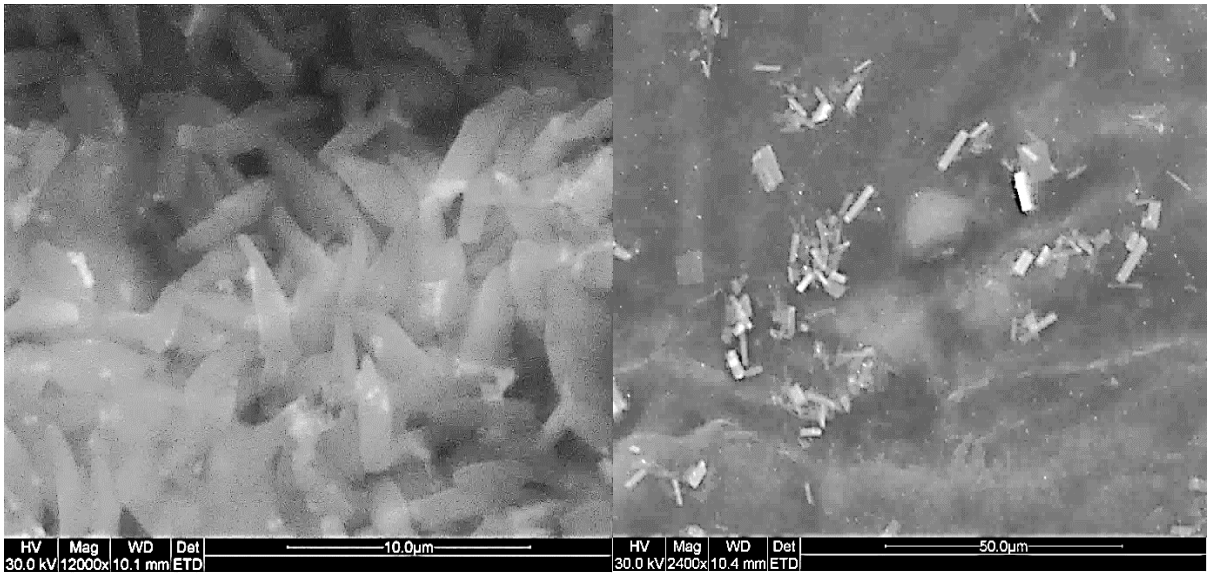

Figure 4.9 Images for (left) SEM for Pt NRs and (right) SEM for Au NRs, the magnification of 1200x, and the scale at 10 µm and 50 µm respectively.

4.3.8 Transmission Electron Microscopy (TEM) analysis of Pt nanorods

The Pt NRs analysis with TEM microscopy was conducted after their screening for microorganisms activity to enable the determination of the most suitable nanoparticles. The novel application of Pt NRs as the delivery mechanism was decided on because they showed less photothermal activity and adequate solubility after loading the synthesized BODIPY PSs under study. Having said that, Pt nanorods were the best candidates for the loading of selected PSs, and further studies for their efficiency to enhance activity and delivery of BODIPY PSs were conducted. **Figure 4.10** below shows Pt NRs images acquired at 50 nm and 100 nm respectively. The images show that the Pt NRs were aggregated and even in size. The seeding method resulted in particles with crystal planes (111), (200), (220) and (311) as described by the (JCPDSICSD4-802) and ICSB number 76951databases respectively. Similar findings were made by Chen *et al*., (2004) and Krishnaswamy *et al*., (2006).

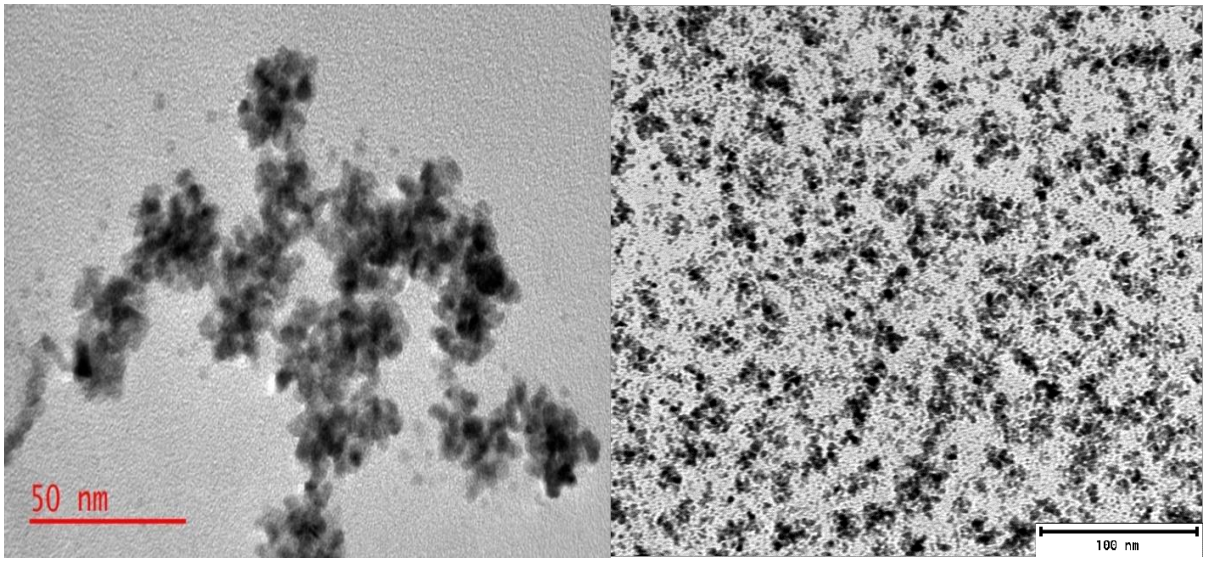

Figure 4.10 TEM images for Pt nanorods acquired at (left) 50 nm and (right) 100 nm.

4.3.9 Dynamic light scattering (zeta sizer and zeta potential) analysis of Pt nanorods

The size distribution was investigated with DLS. In **Figure 4.11 A**, a size distribution plot is shown. The diagram shows that the majority of NRs had an average of 90 nm with fewer showing an average of 255 nm respectively. However, the results showed that the majority of the nanorods average between 100 nm and 120 nm respectively. Removing CTAB with the centrifugation technique destabilizes nanoparticles and thus excessive washing of NRs was avoided (the nanoparticles were washed only three times with water). The zeta potential analysis showed that the surface charge of the nanorods was between -6.7 to -12 for pH6 to pH9 respectively. Moreover, the negative charge we observed on the NRs indicates that there is less CTAB on the NRs surfaces. This is further explained by the study done by Gao *et al*., (2003) and Grzelzak *et al*., (2006) who reported the role of the silver ions which may influence the formation of the Ag-Br on the surface of the nanorods. Furthermore, the effect of the negative charge may be as a result of the presence of negatively charged seeds respectively (Nikoobakht *et al*., 2003; Murphy *et al*., 2005; Gao *et al*., 2003; Grzelzak *et al*., 2006). The histogram in **Figure 4.11 B** shows the statistical graph measurement of Pt NRs average size diameter (nm) which shows that the average diameter of the nanorods was between 90 nm to 120 nm.

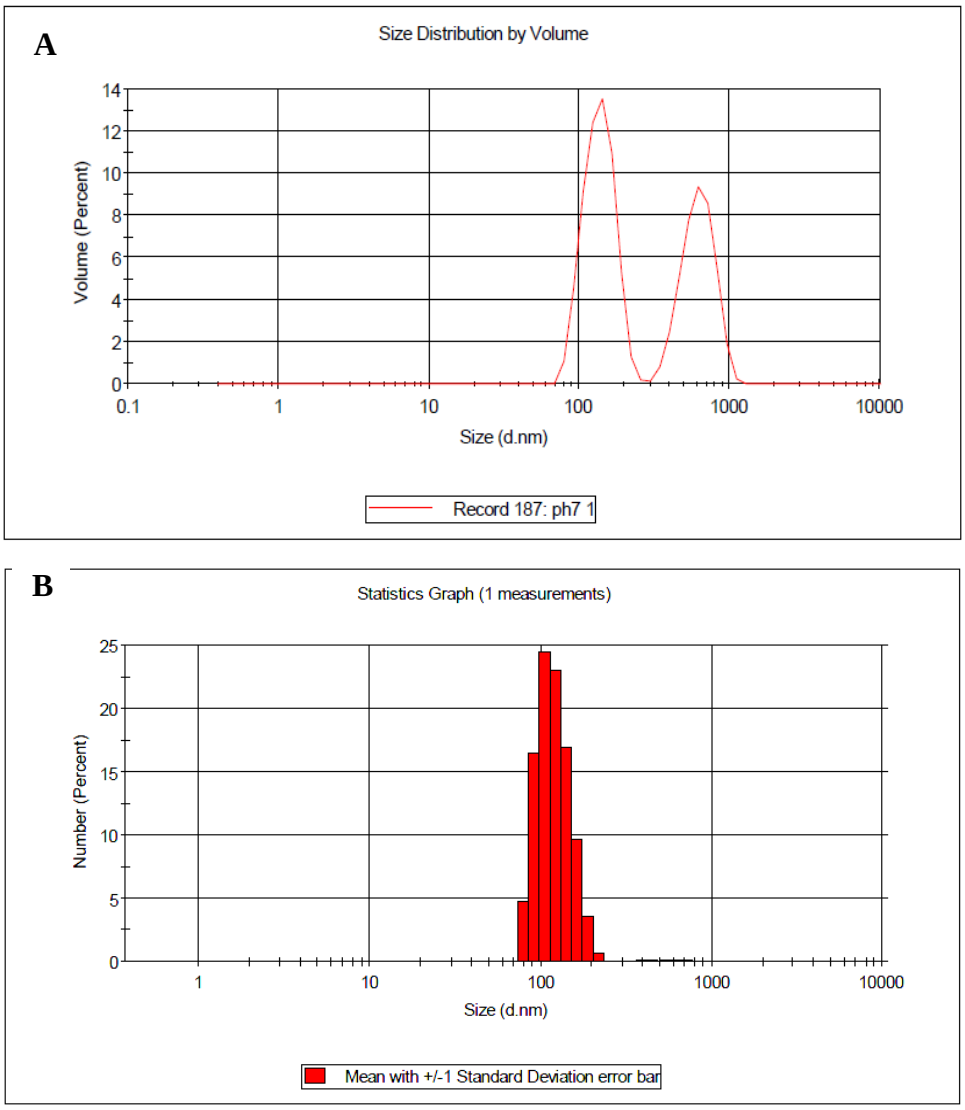

Figure 4.11 The size distribution and the statistical histogram of Pt NRs in water, pH7.2

Figure 4.12 shows the nanorods surface charge before (A) and after removal (B) of CTAB through centrifugation. As observed in **Figure 4.12A**, the surface charge of Pt NRs before centrifugation was +32 $C.m^{-2}$, this confirmed the capping agent available on the surface of the NRs. However, after the NRs were centrifuged with water three times the surface charge was on the negative area respectively. As shown in **Figure 4.12B**, the surface charge was found to be -11 $C.m^{-2}$ at pH 8 this may be justified by the effect of the negative charge as a result of the presence of negatively charged seeds.

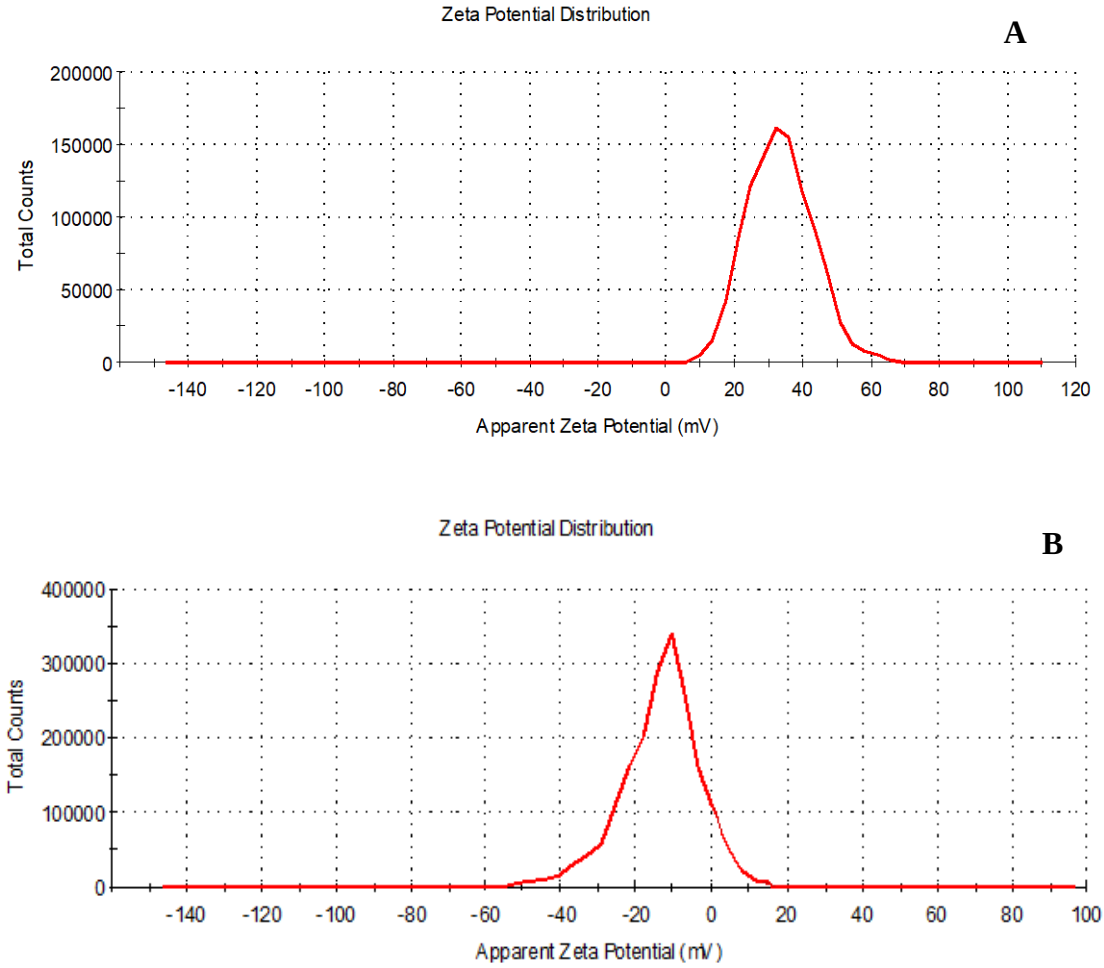

Figure 4.12 shows the changes in zeta potential after centrifugation of Pt NRs in water pH 8.

4.4 BODIPY PSs loading onto Pt NRs

Platinum nanorods were used as loading materials for the concentration of BODIPY PSs to the targeted cells. The reaction was monitored by measuring the absorbance hourly for 12 hours. Inorganic nanoparticles have widely used gold and silver nanoparticles due to their surface plasmon resonance (SPR) (Patra *et al*., 2018). A physical absorption for the loading of BODIPY PSs was adopted (Kong *et al*., 2017). **Figure 4.13 A** below shows a reduction in the absorbance of BODIPY 6.6 in solution. There was a significant drop in the absorbance intensity, which is due to the reduced free BODIPY PSs in the solution. This is because the BODIPY PSs were attaching to the Pt NRs. The results in **Figure 4.13 B** shows that there was a high rate of adsorption during the first hour of the reaction. This is because there is the free availability of the absorption site on the Pt NRs surface. Similar observations were discussed by (Kong *et al*., 2017). BODIPY 6.6 showed more absorption to the Pt NRs compared to BODIPY 6. This may be due to the interactions of the functional groups on the BODIPY

structure with the Pt NRs surfaces. The formula for the estimation of the adsorbed BODIPY PSs onto Pt NRs surfaces is shown below.

Figure 4.14 A shows the absorption profile of BODIPY 6 onto Pt NRs. In the first hour there was a significant drop in the absorption spectra as seen with BODIPY 6.6 (Figure 4.13A). This suggests that BODIPY PSs are absorbed onto the Pt NRs walls more rapidly compared to four and above hours later. Also noted in Figure 4.14 B, as time approaches 10 hours, the reaction was slower, which signifies that there is little to no binding sights on Pt NRs. Similar results were observed with BODIPY 6.6 discussed above in Figure 4.13 A and B.

$$\%Loaded = \frac{A_i - A_f}{A_i} \times 100 \qquad \text{equation 4.3}$$

Where A_i And A_f are the initial absorbances before the reaction and final absorbance after 12 hours respectively.

The loading efficiency was determined using the formula below (adapted from Sebelemetja *et al*., 2019)

$$Loading\ efficiency = \frac{A_i - A_f}{amount\ of\ Pt\ NRs} \times 100\% \qquad \text{equation 4.4}$$

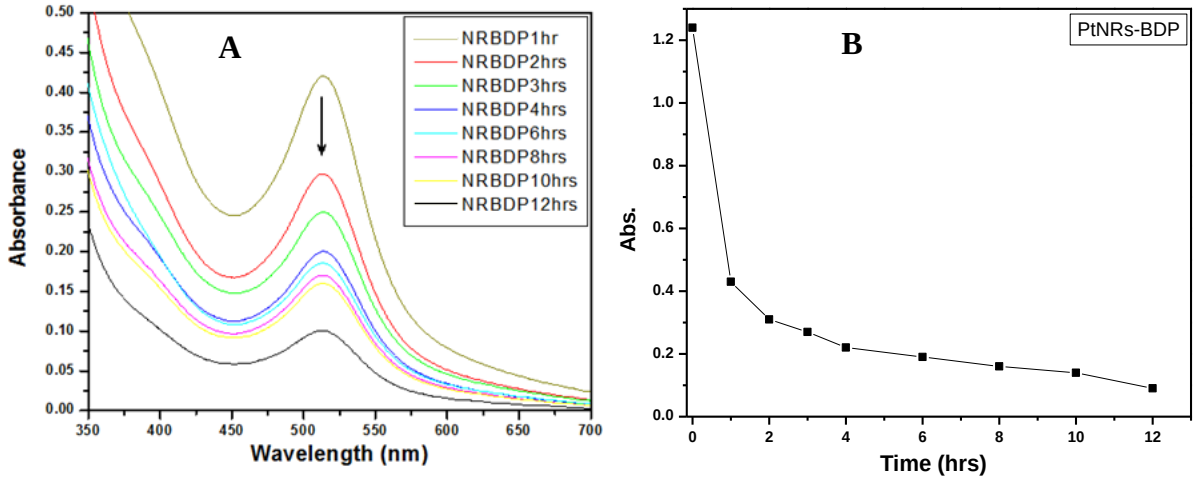

Figure 4.13 BODIPY 6.6 loading onto Pt NRs at room temperature in water/DMSO solution (physical absorption method) (A) UV-Vis spectra showing absorbance and (B) absorption efficiency of loading to Pt NRs.

The loading efficiency for BODIPY 6.6 was determined as follows:

$$loading\ efficiency = \frac{BDP_{initial} - BDP_{final}}{NRs_{amount}} \times 100$$

$$loading\ efficiency = \frac{50\ mg - 8.3\ mg}{2\ mg} \times 100\%$$

$$loading\ efficiency = 20.85 \times 100\% = \mathbf{2085}\%$$

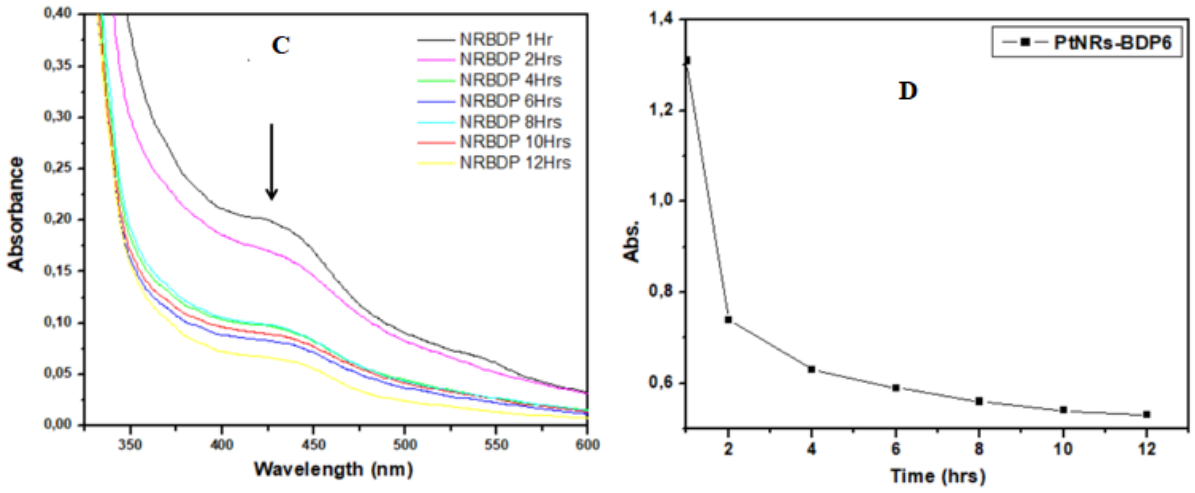

Figure 4.14 BODIPY 6 loading onto Pt NRs at room temperature in water/DMSO solution (physical absorption method) (A) UV-Vis spectra showing absorbance and (B) absorption efficiency of loading to Pt NRs.

The loading efficiency for BODIPY 6:

$$loading\ efficiency = \frac{50_{mg} - 12.9_{mg}}{2_{mg}}$$

$$loading\ efficiency = 18.55\ \times 100\% = \mathbf{1855}\%$$

Based on the equation above, BODIPY 6.6 showed more absorption capacity compared to BODIPY 6. The loading capacity indicates that Pt NRs have a greater surface to volume ratio which is the characteristic known for metallic/inorganic nanoparticles. Moreover, it can be observed that BODIPY 6.6 (with NH_2 functional groups) had a greater loading capacity, which may be attributed to the BODIPY functional groups since these permit attachments to the Pt NRs surfaces respectively. Furthermore, it is clear from the data that the first hour of the

reaction shows more adsorption of the drugs onto Pt NRs due to the availability of adsorption sites (Laletina *et al*., 2017).

4.5 Discussion

The functionalized BODIPY 2 and BODIPY 4 PSs with carboxyl moieties showed quenched fluorescence quantum yields. The observed quenching of the fluorescence quantum yields for BODIPY 2 and 4 (**Table 4.2**) and blue shifting of the absorption spectra suggest transitional changes or photo-induced electron transfer (PET) during radiation (Choi *et al*., 2014; Kee *et al*., 2005). The fluorescing capacity of some BODIPY dyes (as shown in **Fig. 4.3 C**) for BODIPY 3, 4, 8, 9, and 10 was rather low. This lower fluorescent capacity is attributed to the carboxyl moieties on BODIPY 4 as well as the bulk substituents (diaminobenzoic acid, diaminobenzenesulfonic acid, sulfamoilbenzoic acid located on the periphery of the BODIPYs) used for functionalization of BODIPY 8, 9, and 10 (Espinoza *et al*., 2019). Hydrogen bonding (which in turn may encourage aggregate formation by the virtue of substituents used for functionalization) may contribute to the observed diminished fluorescing capacity for BODIPY 4, 8, 9, and 10.

Espinoza and coworkers (2019) highlighted that the substituted BODIPY systems can undergo either H- or J-type aggregates according to different supramolecular organizations (Espinoza *et al*., 2019). Based on this theory, BODIPY 2 and 4 are suspected to undergo H-type aggregation; this arrangement gives rise to hypsochromic absorption and partial fluorescence. Moreover, a J-type aggregation can be assigned for BODIPY 8, 9, and 10 which is associated with red-shifted absorptions and emissions respectively (Kumar *et al*., 2017).

The effect of the electron pulls towards the benzene rings through the amide-carbonyl bridge on BODIPYs 8, 9, and 10 results in the electron-rich BODIPY surfaces which further results in high energy transitions (Zhao *et al*., 2017; Sutradhar and Misra, 2018). Aside from the fluorescence quantum yield being quenched from oxidation effects, there are other reasons why it could have been observed for BODIPY 2, 4, 8, 9, and 10. Some of these reasons include the possibility of forbidden transitions from the singlet excited state to the triplet excited state of the functionalized BODIPY dyes (Zhao *et al*., 2015).

As shown in **Table 4.3**, absorption and fluorescence data for the photosensitizers BODIPY 5, 6, and 7 demonstrated negligible emission properties (or no emission at all) where this may be due to the heavy atom effect for BODIPY 5 and 6 or because of the bulky naphthalene

sulfonamide substituents on the BODIPY core structure for BODIPY 7. The emissions for BODIPY 5, 6, and 7 dyes (in ethanol) were extracted from the linear plot of absorbance. Similar results were observed with BODIPY PSs 6.1 to BODIPY 6.6 with extended iodine moieties, as these were shown to be non-emissive PSs as shown in **Table 4.5**. Additionally, the Infrared spectroscopy analysis for BODIPY PSs was conducted and all the expected peaks were observed in their expected regions.

Moreover, the elemental composition analyses were carried out with COMPASS data analysis 4.3 from Bruker. On the mass spectra of individual m/z peaks of the corresponding BODIPY PS, a calculated prediction of the elemental composition and the signal sensitivity was improved by increasing the peaks tolerance from 4 to 100 to generate the possible elemental data. All identified mass peaks and estimated elemental compositions were recorded on a high-resolution positive ion electrospray mode (charge of 1). The charged molecular ions presented isotopic patterns (see **Appendix 1 B**). There were no significant differences between the theoretical molecular weights and the experimental molecular weight obtained from analysis for the prepared BODIPY PSs. This indicated that the final products from the synthesis matched those that were designed and expected confirming the success of the synthesis and functionalization of the BODIPYs to obtain the desired BODIPY PSs, and corroborating NMR and FTIR analysis. However, NMR for BODIPY 6.1 to 6.6 was not obtained as mentioned in Appendix 3.

Some BODIPYs were prone to fragmenting during Mass spectrometry analysis (BODIPY 7 to 10). A similar observation was reported by Gao and co-workers (2018) who also observed that analysis of BODIPY PSs with mass spectrometry (a Bruker Autoflex speed TOF/TOF spectrometer) resulted in the cleaving of fluorine atoms at the boron center and where this is attributed to the weak bonds between the boron and fluoride. Similar findings were demonstrated by Qi and co-workers (2015) who have reported that during the electron spray ionization (ESI) process, BODIPY PSs formed isotopes and generate molecular ions relating to the parent and daughter peaks in the form $[M+H]^+$ and $[M]^{+\bullet}$ radical ions were formed during electron ionization (EI). Furthermore, these isotopic patterns ($[M+H]^+$ and $[M]^{+\bullet}$ radical ions) were also observed in high energy collision-induced dissociation (CID) (Rosario *et al*., 1998), deposition or ionization technique such as fast atom bombardment (FAB) (Morris,1981) and ion-electron dissociation technique (Wei *et al*., 2013; Mosely *et al*., 2011). The group speculated that the electron-loss oxidation process observed occurred during ESI process, it has been shown for large polynuclear aromatic systems that $[M]^{+\bullet}$ was formed by unimolecular

decomposition of $[M+H]^+$ ions (Morris,1981; Qi *et al*., 2015). Similar observations in this study were made with large molecular weight BODIPY 7 to BODIPY 6.6 respectively. The M/2 mass to charge ratios observed may be due to the bulkiness of the BODIPY compounds. This is a consequence of electron autodetachment of the substituents as discussed in section 4.3.2 respectively.

The chemical shifts for protons 400 MHz and carbons 100 MHz were observed in their expected regions in the ^{1}H and ^{13}C NMR spectra. The integration of the proton NMR peaks quantifies the appropriate number of H contained under the integrated peak. There was a downfield shift at 7.6 – 8.3 ppm on the spectra for the protons of all the BODIPY PSs (BODIPY 1 to 6.6) at position 8 of the BODIPY meso-phenyl groups. This is attributed to the deshielding fast rotation of the meso-phenyl ring for these BODIPY PSs (Epelde-Elezcano *et al*., 2016; Leen, 2010). There is no literature to support the effect of pyrrole substituted BODIPY on the meso-position. The protons ascribed at positions 1 and 7 were also observed in the upfield region at 2.0 - 2.2 ppm of the ^{1}H NMR due to the shielding effect of the phenyl electrons around the benzyl ring, similar observations were reported by (Liu *et al*., 2019). Moreover, the protons ascribed to the methyl groups at positions 3 and 5 were observed at 2.13-0.8 ppm, where the upfield peak corresponding to protons at position 5 is obtained due to the partial positive nitrogen atom which was observed to induce an upfield chemical shift for all BODIPY PSs (Savoldelli *et al*., 2018). Furthermore, the effect of the B-F bond on the adjacent methyl protons results in the upfield chemical shift which is attributed to the electron-withdrawing nature of the fluorine atoms (Leen, 2010).

The formation of the oxidized BODIPY 2 and BODIPY 4 was also confirmed by the disappearance of the methyl proton chemical shift at an upfield position of 0.8 and 2.15 ppm and the emergence of a peak downfield at 11.0-12.75 ppm. These downfield chemical shifts are attributed to the carboxylic acid hydrogens (Ambroz *et al*., 2019). Furthermore, BODIPY 6 showed an upfield chemical shift at the 4-pyrrolic carbon position (from downfield of 118.04 to 85.03 ppm) which is due to the iodine effect on the meso-4pyrrolic carbon. Similar observations were made with 2,6-meso-pyrrolic carbons, which saw an upfield chemical shift from (130.85, 119.74 to 75.39, 56.33 ppm) respectively. Similar observations were made by Kritskaya and co-workers, (2017) who reported that the introduction of the heavy atoms induces an upfield shift due to heavy atom effect on the carbon. Moreover, BODIPY 8 -10 showed an upfield proton chemical shift that is attributed to the amide bridge hydrogens at 7.11 and 8.09 ppm. This confirmed the formation of the desired conjugation of the BODIPY 4 and

the disappearance of the carboxylic acid proton shift at 12.75 ppm. The carbon spectra of the synthesized BODIPY PSs also confirmed the functionalization (BODIPY 1 and 3) and conjugation (BODIPY 8 to 10), the chemical shifts were recorded at their expected positions as shown in **section 4.3.4**, and **appendix 3**.

It is worth mentioning that there is minimal literature on the characterization of multiple iodine substituents on the periphery of BODIPY PSs. There were challenges of high signal to noise ratio encountered in the NMR analysis of BODIPY 6.1 to BODIPY 6.6 which are all Iodine substituent containing PSs. The high signal to noise challenge is a frequently observed issue noted with some BODIPY PSs (Kumar *et al*., 2017) and this may be attributed to the sampling schedule which is very important for detection sensitivity. However, Hybert and co-workers (2013), demonstrated how to elucidate NMR spectral data with high noise to signal ratio using the Non-Uniformly Sampled Multi-Dimensional NMR Spectra. The high signal to noise ratio challenge faced in this work for BODIPY 6.1 to BODIPY 6.6 is thought to have resulted from many factors including but not limited to the number of acquisitions, magnetic field strength, transmission and receiving coils, sample concentration, and the scan parameter (Hybert and Roberts, 2013).

4.6 Conclusion

The synthesis of BODIPY PSs, synthesis of nanoparticles and their nanoconjugates was successfully achieved. Characterization of the resultant compounds and their nanoconjugates were characterized to study their optical and photochemical properties as well as their structural elucidation. The results obtained demonstrated that upon functionalization, the chemical and optical properties of these compounds can be tuned by the introduction of various functional groups on their skeletal structure. The structural elucidation of the BODIPY PSs confirmed the desired structures as anticipated. However, mass spectrometer analysis showed that substitution of BODIPY PSs with bulky substituents may result in the formation of different ions which leads to the detection of many ion peaks. This study opened a gap into studying the mass to charge ratio fragmentation patterns of BODIPY PSs synthesized through the amide linker. There is no literature to support this observation, however, Danell and Park, 2003 have shown that attachment of double-strand oligonucleotides to the BODIPY PSs leads to electron autodetachment hence splitting the latter to a single strand BODIPY-oligonucleotide conjugates. This phenomenon may apply to the observation made in this study which showed m/z $[M/x]^+$ where $x > 1$. NMR study showed a ^1H and ^{13}C chemical shift at their expected

regions. However, BODIPY 6.1 to 6.6 did not show NMR results, which was attributed to poor spectral acquisition and/or instrumental defaults. Analysis of the NPs and their resultant nanoconjugates was confirmed with XRD, SEM, and TEM analysis which showed the desired loading of the PSs onto the nanostructures.

4.7 References

Adarsh N., Shanmugasundaram M., Avirah R.R., and Ramaiah D., 2012; AzaBODIPY derivatives: enhanced quantum yields of triplet excited states and the generation of singlet oxygen and their role as facile sustainable photooxygenation catalysts. Chem. - Eur. J. 18, 12655-12662.

Boens N., Leen V., and Dehaen W., 2012; Fluorescent indicators based on BODIPY, *Chem. Soc. Rev*., 2012, 41(1): 1130-1172.

Chen J., Herricks T., Geissler M., and Xia Y., 2004; Single-Crystal Nanowires of Platinum Can Be Synthesized by Controlling the Reaction Rate of a Polyol Process. J. Am. Chem. Soc., 126(1): 10854-10855.

Choi, S., Bouffard, J., and Kim, Y. (2014). Aggregation-induced emission enhancement of a meso-trifluoromethyl bodipy via j-aggregation. Chem. Sci. 5, 751–755.

Danell A.S. and Park J.H., 2003; Fraying and electron autodetachment dynamics of trapped gas phase oligonucleotides. *J. Am. Soc. Mass Spectrom*., 14(1): 1330-1339.

Descalzo, A. B.; Xu, H. J.; Xue, Z. L.; Hoffmann, K.; Shen, Z.; Weller, M. G.; You, X. Z.; Rurack, K., Phenanthrene-fused boron-dipyrromethenes as bright long-wavelength fluorophores. Org. Let., 10, 1581-1584.

Divya K.P., Savithri S., and Ajayaghosh A., 2014; A fluorescent molecular probe for the identification of zinc and cadmium salts by excited-state charge transfer modulation, *Chem. Commun*., 50(1): 6020-6022.

Epelde-Elezcanoa N., Martínez-Martínez V., Peña-Cabrera E., Gómez-Durán C.F.E., Arbeloa I.L., and Lacombe S., 2016; Modulation of singlet oxygen generation in halogenated BODIPY

dyes by substitution at their meso position: towards a solvent-independent standard in the vis region. RSC Adv., 6(1): 41991-41998.

Esnal I., Valois-Escamilla I., Gómez-Durán C.F.A., Urías-Benavides A., Betancourt-Mendiola M.L., López-Arbeloa I., Bañuelos J., García-Moreno I., Costela A. and Peña-Cabrera E., 2013; Blue-to-Orange color-tunable laser emission from tailored boron-dipyrromethene dyes, *Chem. Phys. chem.*, 14(1): 4134-4142.

Espinoza M.M.I., Sori L., Pizzi A., Terraneo G., Moggio I., Arias E., Pozzi G., Orlandi S., Dichiarante V., Metrangolo P., Cavazzini M., and Bombelli F.B., 2019; BODIPY Dyes Bearing Multibranched Fluorinated Chains: Synthesis, Structural, and Spectroscopic Studies. Chem. Eur. J., 25(1): 9078-9087.

Feng L., Wu X., Ren L., Xiang Y., He W., Zhang K., Zhou W., and Xie S., 2008; Well-controlled synthesis of Au@Pt nanostructures by gold-nanorod-seeded growth, *Chem. Eur. J.*, 14: 9764-9771.

Gao H., Gao Y., Wang C., Hu D., Xie Z., Liu L., Yang B., and Ma Y., 2018; Anomalous Effect of Intramolecular Charge Transfer on the Light Emitting Properties of BODIPY. *ACS Appl. Mater. Interface*, 10(1): 14956-14965.

Gao J., Bender C.M., and Murphy C.J., 2003; Dependence of the gold nanorods aspect ratio on the nature of the directing surfactant in aqueous solution, *Langmuir*, 19(21): 9065-9070.

Gaskel, 1997; Electrospray: Principles and Practice. J. Mass Spectrom., 32(1): 677-688.

Gibbs J.H., Robins L.T., Zhou Z., Bobadova-Parvanova P., Cottam M., McCandlessa G.T., Fronczek F.R., and Vicente M.G.H, 2013; Spectroscopic, computational modeling and cytotoxicity of a series of meso-phenyl and meso-thienyl-BODIPYs. *Bioorg Med Chem*., 21(18): 5770-5781.

Grzelzak M., Peerez-Juste J., Rodriguez-Gonzalez B., and Liz-Marzan L.M., 2006; Influence of silver ions on the growth mode of platinum on gold nanorods, *J. Mater. Chem.*, 16(40): 3946-3951.

Hyberts S.G., Robson S.A. and Wagner G.,2013; Exploring signal-to-noise ratio and sensitivity in non-uniformly sampled multi-dimensional NMR spectra, *J. Biomol. NMR*, 55(1), 167-178.

Kamkaew A, Lim SH, Lee HB et al (2013) BODIPY dyes in photodynamic therapy. *Chem Soc Rev*, 42(1): 77-88.

Kee H.L., Kirmaier C., Yu L., Thamyongkit P., Youngblood W.J., Calder M.E., Ramos L., Noll B.C., Bocian D.F., Scheidt W.R., Birge R.R., Lindsey J.S., and Holten D., 2005; Structural Control of the Photodynamics of Boron-Dipyrrin Complexes. *J. Phys. Chem. B*, 109(1): 20433-20443.

Kolemen S. and Akkaya E.U., 2018; Reaction-based BODIPY probes for selective bio-imaging. Coordination Chemistry Reviews, 354(1): 121-134.

Kong F-Y., Zhang J.W., Li R-F., Wang Z-X., Wang W-J., and Wang W., 2017; Unique roles of gold nanoparticles in drug delivery, targeting and imaging applications Molecules, 22(1): 1445-1455.

Krishnaswamy R., Remita H., Imperor-Clerc M., Even C., Davidson P., and Pansu B., 2006; Synthesis of single-crystalline platinum nanorods within a soft crystalline surfactant–PtII Complex. *Chem. Phys. Chem*., 7(1): 1510-1513.

Kritkaya A.Y., Bumagina N.A., Antina E.V., Ksenofontov A.A., Berezin M.B., Semeikin A.S., 2017; Synthesis and Photochemical Properties of 2,3;5,6-bis(cyclohexano)-BODIPY. *J. fluorescence, springer*, DOI: 10.1007/s10895-017-2201-4.

Krumova K. and Cosa G., 2010; Bodipy Dyes with Tunable Redox Potentials and Functional Groups for Further Tethering: Preparation, Electrochemical, and Spectroscopic Characterization. *J. American Chem. Soc*., 132(1): 17560-17569. Doi: 10.1021/ja1075663.

Kubin R.F. and Fletcher A.N., 1982; Fluorescence quantum yields of some Rhodamine dyes, *J. Lumin*., 27(1): 455-462.

Kukoyi A. A., 2017; Red emissive BODIPY Dyes as sensitizers for near-Infrared emission of lanthanide complexes & structural & spectroscopic studies of quinoline-functionalized BODIPY Dyes, Masters Theses. 2910. https://thekeep.eiu.edu/theses/2910.

Kumar S., Thorat K.S. and Ravikanth M., 2017; Synthesis and Properties of Covalently Linked AzaBODIPY-BODIPY Dyads and AzaBODIPY-(BODIPY)2 Triads. *J. Org. Chem*., 82(1): 6568-6577.

Liu Z., Jiang Z., Yan M. and Wang X., 2019; Recent progress of BODIPY dyes with aggregation-Induced emission, *Front. Chem*., 7:712.

Matarranz B., Sampedro A., Daniliuc C.G. and Fernández G., 2018; Self-assembly of a carboxyl-functionalized BODIPY dye via hydrogen bonding, *Crystals*, 8(1): 436-446.

Morris H.R.,1981; Soft Ionization Biological Mass Spectrometry. Heyden, London.

Mosely A.J., Smith J.M.P., Prakash A.S., Sims M., and Bristow A.W.T., 2011; Electron-induced dissociation of singly charged organic cations as a tool for structural characterization of pharmaceutical type molecules. *Anal. Chem*., 83(11): 4068-4075.

Murphy C.I., Sau T.K, Gole A.M., Orendorff C.J., Gao J., Guo L., Hanyadi S.E., and Li T., 2005; Anisotropic metal nanoparticles synthesis, assembly, and optical applications, *J. Phys. Chem. B*,109(29): 13857-13870.

Ni Y., Zeng L., Kang N-Y., Huang K.W., Zeng L.W.Z., Chang Y.T., and Wu F., 2014; meso-Ester and Carboxylic Acid Substituted BODIPYs with Far-Red and Near-Infrared Emission for Bioimaging Applications. Chem. Eur. J. 2014, 20, 2301-2310.

Nikoobakht B and El-Sayed M.A., 2003; Preparation and growth mechanism of gold nanorods (NRs) using seed-mediated growth method. *Chem. Mater*., 15(10): 1957-1962.

Niyangoda C., Miti T., Breydo L., Uversky V., Muschol M., 2017; Carbonyl-based blue autofluorescence of proteins and amino acids, *Plos ONE*, 12(5): 1-15.

Nwahara N., Nkhahle R., Ngoy B.P., Mack J., Nkhahle R., and Nyokong T., 2018; Synthesis and photophysical properties of BODIPY-decorated graphene quantum dot–phthalocyanine conjugates. *New J. Chem*., 00(1-3): 1-14.

Ooyama Y, Hagiwara Y., Oda Y., Fukuoka H. and Ohshita J., 2014; BODIPY dye possessing solid-state red fluorescence and green metallic luster properties in both crystalline and amorphous states, *RSC Adv*., 4, 1163-1167.

Petrushenko K.B., Petrushenko I.K., Petrova O.V., Sobenina L.N., Ushakov I.A., and Trofimov B.A.; Environment-responsive 8-CF_3-BODIPY dyes with aniline groups at the 3 position: Synthesis, optical properties, and RI-CC_2 calculations, *Asian J. Org. Chem*., 2017, 6(1): 852-861.

World Health Organization, 2018; Pricing of cancer medicines and its impacts. Geneva: License: CC BY-NC-SA 3.0 IGO.

Qi Y., Bortoli S., and Volmer D.A.; 2015; Determining the Binding Sites of β-Cyclodextrin and Peptides by Electron-Capture Dissociation High-Resolution Tandem Mass Spectrometry. J. Am. Soc. *Mass Spectrom*. 25(1): 1143–1149.

Qi Y., Geib T., Huynh A-M., Jung G., and Volmer D.A., 2015; Fragmentation patterns of boron-dipyrromethene (BODIPY) dyes by electrospray ionization high-resolution tandem mass spectrometry. Rapid Commun. *Mass Spectrom*., 29(1): 885-890.

Ramírez-Ornelas D.E., Sola-Llano R., Bañuelos J., Arbeloa I.L., Martínez-Álvarez J.A., Mora-Montes H.M., Franco B., and Peña-Cabrera E., 2018; Synthesis, photophysical study, and biological application analysis of complex Borondipyrromethene Dyes. ACS Omega, 3(1): 7783-7797.

Reich H., University of Wisconsin, 5-HMR-1 Integration of Proton NMR Spectra. https://organicchemistrydata.org/hansreich/resources/nmr/?page=05-hmr-01-integration%2F, (visited, 17 February 2020).

Rosario M., Domingues M., Nemirovskiy O.V., Graço M., Marques O.S., Neves M.G., Cavaleiro A.J.S., Ferrer-Correia A.J., Gross M.L. High- and low-energy collisionally activated decompositions of octaethylporphyrin and its metal complexes. Journal of the American Society for Mass Spectrometry 1998, 9(8): 767-774.

Ryu I.S., Liu X., Jin Y., Sun J. and Lee Y.J., 2018; Stoichiometric analysis of competing for intermolecular hydrogen bonds using infrared spectroscopy, RSC Adv., 2018, 8, 23481-23488.

Sebelemetja M., Moeno S., and Patels M., 2019; Anticariogenic properties of Dodonaea viscosa var. angustifolia derived flavone stabilized nanoparticles. Masters dissertation, Submiitted to the Faculty of Health Sciences, University of the Witwatersrand, Johannesburg, 2019.

Summers G.H., Lefebvre J-F. Black F.A., Davies E.S., Gibson E.A., Christopher T.P., Wooda J. and Zidek K., 2016; Design and characterization of bodipy sensitizers for dye-sensitized NiO solar cells, Phys. Chem. Chem. Phys., 2016, 18, 1059-1070.

Sutradhar T., and Misra A., 2018; Role of Electron-Donating and Electron-Withdrawing Groups in Tuning the Optoelectronic Properties of Difluoroboron-Napthyridine Analogues. J Phys Chem A, 122(16): 4111-4120.

Tao J., Sun D., Sun L., Li Z., Fu B., Liu J., Zhang L., Wanga S., Fang Y., and Xua H., 2019; Tuning the photo-physical properties of BODIPY dyes: Effects of 1, 3, 5, 7-substitution on their optical and electrochemical behaviors. *Dyes and Pigments*, 168(1): 166-174.

Wei J., Li H., Barrow M., and O'Connor P., 2013; Structural characterization of chlorophyll-a by high-resolution tandem mass spectrometry. *J. Am. Soc. Mass Spectrom*., 24(5): 753-760.

Yang M., and Xia J., 2013; Preparation and Characterization of Platinum Nanorods Using Ascorbic Acid as the Reducing Agent. Advanced Materials Research, 774-776(1): 577-580.

Yang T., Du M., Zhang M., Zhu H., Wang P., and Zou M., 2015; Synthesis and immobilization of Pt nanoparticles on Amino-Functionalized halloysite nanotubes toward highly active catalysts. Nanomater. Nanotechnol., 5(4): 1-9.

Yoon J., Khi N.T., Kim H., Kim B., Baik H., Back S., Lee S., Lee S-W., Kwon S.J., and Lee K., 2013; High yield synthesis of catalytically active five-fold twinned Pt nanorods from a surfactant-ligated precursor, *Chem. Commun*. (Camb), 21, 49(6):573-5

Zhao J., Xu K., Yang W., Wanga Z., and Zhong F., 2015; The triplet excited state of Bodipy: formation, modulation and application. Chem. Soc. Rev., 44(24): 8904-8939.

Zhao N., Williams T.M., Zhou Z., Fronczek R.F., Sibrian-Vazquez M., Jois S.D. and Vicente G.H., 2017; Synthesis of BODIPY-Peptide Conjugates for Fluorescence Labeling of EGFR Overexpressing Cells. Bioconjug. Chem., 28(5): 1566-1579.

Zhou Q., Zhou M., Wei Y., Zhou X., Liu X., Zhang S., and Zhang B., 2017; Solvent effects on the triplet–triplet annihilation upconversion of diiodo-Bodipy and perylene. Phys. Chem. Chem. Phys., 19(2): 1516-1525.

CHAPTER 5

Anti-microbial properties of novel boron dipyrromethene (BODIPY) photosensitizers

5.1 Introduction

Chapter 5 the results of the antimicrobial activity of the synthesized BODIPY PSs and their platinum nanorods and nanoconjugates are showed. The tables of results are shown and the corresponding figures showing the analysis of the results obtained for this study. Furthermore, the statistical data are shown and discussed in this chapter.

5.2 Results

5.2.1 Disk diffusion test

Test compounds were screened using a disk diffusion test method for their antimicrobial activity. The results are shown in **Table 5.1** and **Table 5.1**. The results showed that BODIPY 6 and BODIPY 10 which contained heavy atoms and sulfonamide groups had antimicrobial activity against all tested bacteria and fungi. BODIPY 7, 8, and 9 also had some antimicrobial activity against specific bacteria. The recorded zones of the inhibition were the ones used to decide on the further studies of the test compounds to determine the minimum inhibitory concentrations of the compounds. These results demonstrated the heavy atom effect of BODIPY6 on microorganisms understudy, where this dye had greater activity on the organisms respectively. The test studies were carried out in triplicates.

In **Figure 5.1**, it can be seen that BODIPY 6 showed better activity and generally the light exposure did not improve the efficacy against bacterial species. This figure also showed that BODIPY 6 has a better fungicidal activity and the activity improved with the length of light exposure.

The study demonstrated that functional groups play a pivotal role in the activity of BODIPY dyes. Moreover, BODIPY dyes with heavy atoms were more active than the sulfonamide moiety compared to those with other functional groups. The finding resulted in further studies of the BODIPY PSs containing the iodine moiety and sulfonamide groups.

Table 5.1 Antibacterial activity of BODIPY 1 to 10 using disk diffusion test (screening)

Organism	**Compound**	**Concentration (2mg/mL/disk) Zone of inhibition in mm Mean (range) n=3**		
		Unexposed	**30 min**	**60 min**
S. aureus	1	0	0	0
	2	0	0	0
	3	0	0	0
	4	0	0	0
	5	0	0	0
	6	11.1 (9.8-12.2)	11.2 (9.7-12.5)	11.5 (9.9-12.8)
	7	0	0	0
	8	0	0	0
	9	8.5 (8.3-8.6)	9.1 (8.7-9.7)	8.8 (8.3-9.1)
	10	10.2 (9.7-10.6)	10.2 (9.9-10.4)	11.0 (10.1-12.2)
S. pyogenes	1	0	0	0
	2	0	0	0
	3	0	0	0
	4	0	0	0
	5	0	0	0
	6	12.0 (9.4-13.6)	12.5 (10.4-13.7)	12.9 (11.3-14.1)
	7	5.7 (0-8.7)	5.8 (0-8.9)	5.9 (0-9.1)
	8	0	0	0
	9	8.2 (8.1-8.2)	8.4 (8.3-8.4)	8.8 (8.7-9.0)
	10	11.3 (9.4-12.5)	12.3 (11.6-12.9)	12.8 (12.1-13.4)
E. coli	1	0	0	0
	2	0	0	0
	3	0	0	0
	4	0	0	0
	5	0	0	0
	6	12.5 (10-14.8)	12.3 (9.2-15.1)	13.1 (11-15.6)
	7	0	0	0
	8	23.9 (22.8-25.8)	24.4 (23.5-26)	25.5 (24.2-27.3)
	9	0	0	0
	10	9.3 (8.6-10.1)	9.1 (8.8-9.3)	9.1 (8.4-9.7)
P. aeruginosa	1	0	0	0
	2	0	0	0
	3	0	0	0
	4	0	0	0
	5	0	0	0
	6	19.4 (8.3-25.4)	14.4 (9-25.1)	14.0 (8-25.9)
	7	0	0	0
	8	0	0	0
	9	0	0	0
	10	7.6 (7.3-8.2)	9.4 (7.9-11.8)	8.3 (7.6-9.0)

Table 5.2 Antifungal activity of BODIPY 1 to 10 using disk diffusion test (screening)

Organism	Compound	Conc. (2mg/mL/disk) Zone of inhibition in mm Mean (range) n=3		
		Unexposed	**30 min**	**60 min**
C. albicans	1	0	0	0
	2	0	0	0
	3	0	0	0
	4	0	0	0
	5	0	0	0
	6	40.5 (40.3-40.7)	51.8 (51.6-52.0)	65.8 (65.5-66.1)
	7	0	0	0
	8	0	0	0
	9	0	0	0
	10	20.9 (19.2-23.4)	21.8 (20.6-23.9)	24.3 (23.7-25.0)
C. tropicalis	1	0	0	0
	2	0	0	0
	3	0	0	0
	4	0	0	0
	5	0	0	0
	6	22.0 (20-23.6)	30.7 (29.1-32.8)	33.6 (32.4-34.9)
	7	0	0	0
	8	0	0	0
	9	0	0	0
	10	10.6 (9.3-12.4)	12.4 (10.9-13.8)	12.2 (11.5-12.9)
C. glabrata	1	0	0	0
	2	0	0	0
	3	0	0	0
	4	0	0	0
	5	0	0	0
	6	29.2 (28.1-30.1)	28.2 (15.7-38.6)	30.8 (16.7-39.9)
	7	0	0	0
	8	0	0	0
	9	0	0	0
	10	16.1 (15.7-16.4)	17.0 (16.8-17.4)	19.4 (19.1-19.8)
C. parapsilosis	1	0	0	0
	2	0	0	0
	3	0	0	0
	4	0	0	0
	5	0	0	0
	6	38.8 (38.2-39.4)	40.2 (35.4-43.7)	42.2 (41.2-43.1)
	7	0	0	0
	8	0	0	0
	9	0	0	0
	10	9.5 (9.1-10.0)	10.4 (9.8-11.3)	12.8 (12.6-13.1)

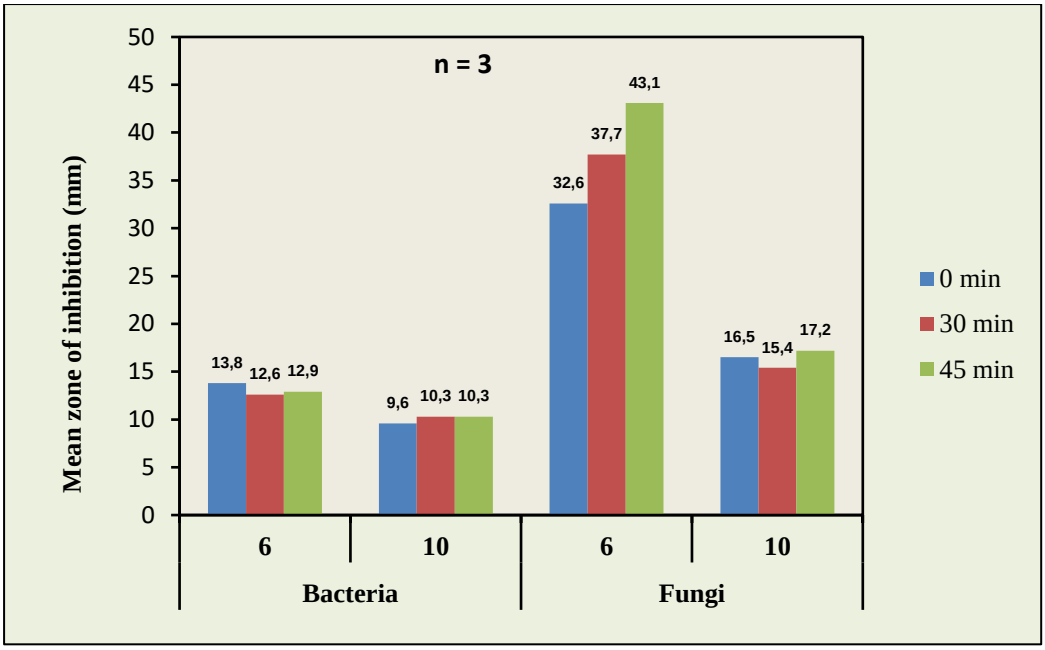

Figure 5.1 Antimicrobial activity of BODIPY 6 and 10 with (30 min and 45 min) and without (0 min) a 65 mW/cm^2 light exposure using disk diffusion test (screening)

5.2.2 Antimicrobial activity of BODIPY 6 and 10 using a micro-dilution technique

Table 5.3 and Fig. 5.2 demonstrate the MIC results of freshly reconstituted BODIPY 6 and BODIPY 10 for both selected bacterial and fungal species without the exposure to light. The results showed that for the bacteria, the MIC values for BODIPY 10 were lower than for BODIPY6 whereas, for the fungi, BODIPY 6 showed a better activity with MIC ranging from 0.25 to 1 mg/mL. For this reason, it was decided to further develop iodine-rich BODIPY derivatives.

Table 5.3 MIC, MBC, and MFC results of compound 6 and 10 (Freshly reconstituted in Acetone:water (1:3 v/v)

Organism	Compound	Median (range) in mg/ml n=3	
		MIC	MBC/MFC
S. aureus	6	8.33 (8.33-8.33)	16.67 (16.67-16.67)
S. pyogenes	6	8.33 (8.33-8.33)	16.67 (16.67-16.67)
E. coli	6	16.67 (16.67-16.67)	33.33 (33.33-33.33)
P. aeruginosa	6	16.67 (16.67-16.67)	33.33 (33.33-33.33)
C. albicans	6	0.25 (0.25-0.25)	0.50 (0.50-0.50)
C. tropicalis	6	0.25 (0.25-0.25)	0.50 (0.50-0.50)
C. glabrata	6	1.04 (1.04-1.04)	2.08 (2.08-2.08)
C. parapsilosis	6	0.25 (0.25-0.25)	0.50 (0.50-0.50)
S. aureus	10	4.17 (4.17-4.17)	8.34 (8.34-8.34)
S. pyogenes	10	2.08 (2.08-2.08)	4.17 (4.17-4.17)
E. coli	10	8.33 (8.33-8.33)	16.67 (16.67-16.67)
P. aeruginosa	10	16.67 (16.67-16.67)	33.33 (33.33-33.33)
C. albicans	10	4.17 (4.17-4.17)	8.34 (8.34-8.34)
C. tropicalis	10	8.34 (8.34-8.34)	16.67 (16.67-16.67)
C. glabrata	10	8.34 (8.34-8.34)	16.67 (16.67-16.67)
C. parapsilosis	10	4.17 (4.17-4.17)	8.34 (8.34-8.34)

Figure 5.2 is a graphical visual representation of MIC studies for BODIPY 6 and 10 against bacterial and fungal species without any exposure to light. It demonstrates the activity of these BODIPYs on bacterial strains, we observed that BODIPY 10 showed more activity on gram-positive bacteria compared to the negative bacteria strains (**5.2 A**). Some resistance was observed for gram-negative bacteria with iodine substituted and sulfonamide substituted BODIPY PSs. Whereas on fungal species, BODIPY 6 showed enhanced activity compared to BODIPY 10 as shown in **Figure 5.2 B**. This significant change is due to the favorable activity of different functional groups.

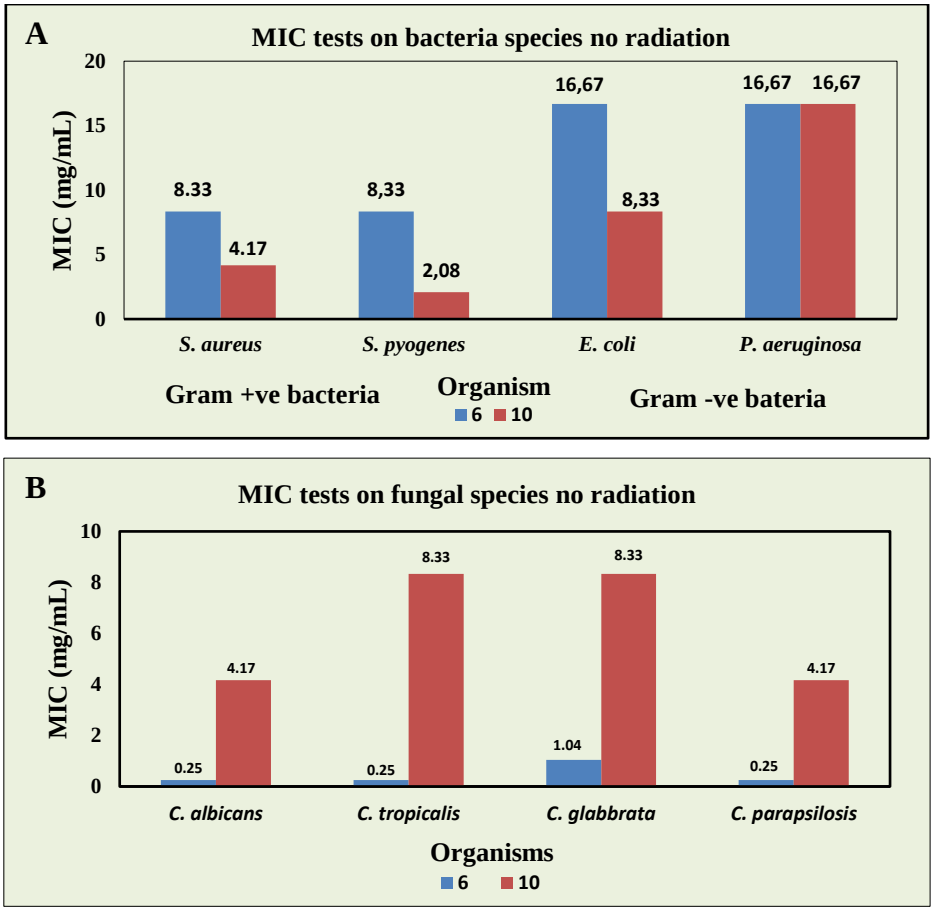

Figure 5.2 Antimicrobial activities of compound 6 and 10 constituted in 1:3 acetone:water mixture (against bacteria (A) and fungi (B)

While performing these MIC experiments, it was noted that BODIPY 6 was unstable in a solution form when constituted for more than 24 hours. Therefore, MIC experiments were also repeated on a 1 – 5 days constituted solutions. **Table 5.4** shows the MIC results of these experiments. The results showed an unusual observation concerning BODIPY 6 against Candida species. The activity of the compound was recorded to be < 0.25 pg/mL. It was decided to further purify BODIPY 6 using a column chromatography technique to further investigate if the purity influenced the findings. Synthesis of multi-iodine substituted derivatives was carried out to understand the trend of iodine substituents on the periphery of the BODIPY PS.

Table 5.4 demonstrates MIC results for BODIPY6 and 10 after 24-hour suspension to determine their stability. There were no changes as per the activity of BODIPY 10 which suggests the compound was stable in solution even after 24 hours suspension. A significant change was observed with BODIPY 6 which demonstrated some enhanced activity after 24 hrs. suspensions. The tests were conducted three times to see if there was going to be some

stability with the compound but similar behavior was observed. These observations suggested that the compound clusters forms dimers or trimers in solution after 24 hours suspension. This called for the synthesis of more iodine substituted BODIPY PSs to determine if a similar trend would be observed.

Table 5.4 MIC, MBC, and MFC results of compound 6 and 10 (24 hr suspension constituted in 1:3 acetone:water mixture)

Compounds	Organism	Median (range) in mg/ml n=3	
		median MIC	median MBC
Compound 6	***S. aureus***	0.52 (0.52-0.52)	1.04 (1.04-1.04)
	S. pyogenes	0.26 (0.26-0.26)	0.52 (0.52-0.52)
	E. coli	1.04 (1.04-1.04)	2.08 (2.08-2.08)
	P. aeruginosa	0.52 (0.52-0.52)	1.04 (1.04-1.04)
	C. albicans	**	**
	C. tropicalis	**	**
	C. glabrata	**	**
	C. parapsilosis	**	**
Compound 10	***S. aureus***	4.17 (4.17-4.17)	8.34 (8.34-8.34)
	S. pyogenes	2.08 (2.08-2.08)	4.17 (4.17-4.17)
	E. coli	8.34 (8.34-8.34)	16.67 (16.67-16.67)
	P. aeruginosa	16.67 (16.67-16.67)	33.33 (33.33-33.33)
	C. albicans	4.17 (4.17-4.17)	8.34 (8.34-8.34)
	C. tropicalis	8.34 (8.34-8.34)	16.67 (16.67-16.67)
	C. glabrata	8.34 (8.34-8.34)	16.67 (16.67-16.67)
	C. parapsilosis	4.17 (4.17-4.17)	8.34 (8.34-8.34)
** (conc. >$2.5x10^{-12}$/mL) MIC of <0.25 pg/mL			

5.2.3 A time effect on the antimicrobial activity of BODIPY 6 against *Candida albicans* (MIC/MFC)

A new batch of BODIPY6 was generated and a time effect of a suspension against *C. albicans* was studied. **Table 5.5** demonstrated a stability test on BODIPY 6, to investigate the effect of the compound on C. *albicans* over five days without radiation. The results showed that there was a fluctuation in the MIC readings over the test days which suggested that the compound

was unstable; this may be due to the fact that the molecules turned to agglomerates or interlock with each other in the solvent when left in solution.

Table 5.5 Time effect study (on a new batch) of compound 6 against *Candida albicans*

Compound	**Organism**	**Day**	**MIC (mg/mL)**	**MFC (mg/mL)**
6	***C. albicans***	1	0.521	1.042
		2	0.065	0.13
		3	0.065	0.13
		4	0.13	0.26
		5	0.13	0.26

5.2.4 Antimicrobial activity of BODIPY6 with increased iodine moieties

To improve the antifungal activity, observed with BODIPY 6, the number of iodine moieties on the surface of the BODIPY PSs was increased generating BODIPY**6.1 to 6.6**. **Table 5.6** demonstrates the activity of BODIPY 6.1 – 6.6 against bacterial strains over a light exposure time of 45 min and with no exposure. There was no considerable antibacterial activity for BODIPY 6.1-6.6 noted with the MIC ranging from 0.5 to 33.33 mg/mL. The results of the antifungal activity of BODIPY 6.1 to 6.6 are shown in **Table 5.7** and **Figure 5.3**. There was no significant activity on BODIPY 6.1, 6.2, and 6.3 which had the carboxyl groups and the pyrrolic amino conjugated triiodo-benzene substituent. Furthermore, the most activity was observed with BODIPY6.6, containing triiodo groups and with conjugation at the positions 1,3,5,7 and 8 (total iodine groups of 30) of the BODIPY structure. Moreover, we observed negligible dark toxicity compared to the photo-activated studies. This showed that the BODIPY PSs were active upon irradiation and suggesting the production of ROS species was evident by the microbial cell death respectively. BODIPY 6.6 proved to have the lowest MIC value particularly after irradiation with white LED light. There was observed resistance with *C. glabrata* and C. *parapsilosis* when compared to C. *albicans* and *candida tropicalis* respectively. Therefore, we had to further purify the compound to ensure that the effects were not due to the impurities but the activity of the compound itself.

Table 5.6 MIC and MBC of improved BODIPY 6 with additional iodine molecules Iodine functionalized BODIPY 6.1-6.6 against Bacteria species.

Compound	organism	0 min exposure		45 min exposure	
		MIC mg/mL	MBC mg/mL	MIC mg/mL	MBC mg/mL
6.1	***S. aureus***	33.33	33.33	16.67	33.33
	S. pyogenes	8.33	16.67	1.08	2.08
	E. coli	33.33	33.33	>33.33	>33.33
	P. aeruginosa	33.33	33.33	>33.33	>33.33
6.2	***S. aureus***	16.67	33.33	4.17	8.33
	S. pyogenes	4.17	8.33	2.08	4.17
	E. coli	33.33	33.33	16.67	33.33
	P. aeruginosa	33.33	33.33	>33.33	>33.33
6.3	***S. aureus***	8.33	16.67	2.08	4.17
	S. pyogenes	4.17	8.33	0.52	1.04
	E. coli	33.33	33.33	>33.33	>33.33
	P. aeruginosa	33.33	33.33	>33.33	>33.33
6.4	***S. aureus***	33.33	>33.33	>33.33	>33.33
	S. pyogenes	>33.33	>33.33	>33.33	>33.33
	E. coli	>33.33	>33.33	>33.33	>33.33
	P. aeruginosa	>33.33	>33.33	>33.33	>33.33
6.5	***S. aureus***	8.33	16.67	4.17	8.34
	S. pyogenes	2.08	4.17	0.52	1.04
	E. coli	33.33	>33.33	16.67	33.33
	P. aeruginosa	>33.33	>33.33	>33.33	>33.33
6.6	***S. aureus***	8.33	16.67	2.08	4.17
	S. pyogenes	2.08	4.17	0.13	0.26
	E. coli	33.33	>33.33	16.67	33.33
	P. aeruginosa	33.33	>33.33	16.67	33.33

Table 5.7 MIC and MFC of improved BODIPY 6 with additional iodine molecules Iodine functionalized BODIPY 6.1-6.6 against *Candida species*

Compound	***Candida spp.***	**0 min exposure**		**45 min exposure**	
		MIC (mg/mL)	**MFC (mg/mL)**	**MIC (mg/mL)**	**MFC (mg/mL)**
6.1	***C. albicans***	33.33	66.67	16.67	33.33
	C. tropicalis	8.33	16.67	1.08	2.17
	C. glabrata	66.67	66.67	66.67	66.67
	C. parapsilosis	66.67	66.67	66.67	66.67
6.2	***C. albicans***	8.33	16.67	2.08	4.17
	C. tropicalis	4.17	8.33	2.08	4.17
	C. glabrata	4.17	8.33	2.08	4.17
	C. parapsilosis	8.33	16.67	8.33	16.67
6.3	***C. albicans***	2.08	4.17	2.08	4.17
	C. tropicalis	2.08	4.17	2.08	4.17
	C. glabrata	4.17	8.33	4.17	8.33
	C. parapsilosis	2.08	4.17	2.08	4.17
6.4	***C. albicans***	1.04	2.08	0.52	1.08
	C. tropicalis	2.08	4.17	0.52	1.08
	C. glabrata	2.08	4.17	2.08	4.17
	C. parapsilosis	4.17	8.332	1.04	2.08
6.5	***C. albicans***	2.08	4.17	0.52	1.08
	C. tropicalis	2.08	4.17	0.52	1.08
	C. glabrata	1.042	2.083	0.521	1.083
	C. parapsilosis	2.083	4.166	1.042	2.083
6.6	***C. albicans***	4.166	8.333	0.0325	0.065
	C. tropicalis	4.166	8.333	0.0325	0.065
	C. glabrata	4.166	8.333	0.13	0.26
	C. parapsiolsis	2.083	4.166	0.521	1.042

Figure 5.3 demonstrates the graphical presentation of BODIPY6.1-6.6 activity against *Candida* species irradiated for 45 minutes and with no irradiation. Significant activity as demonstrated in the graph was observed with BODIPY 6.4-6.6 respectively. BODIPY 6.1 containing –COOH moieties on the 3 and 5 pyrrolic carbons of the BODIPY structure showed little to no activity. These observations were noted with BODIPY 2 and 4 too. Noticeable

activity was observed with BODIPY 6.2 showing some activity with initial MIC of 8.33 mg/mL without irradiation to 2.08 mg/mL after irradiation for 45 minutes, which demonstrates that there were visible photosensitization and a level of inactivation of *Candida* species.

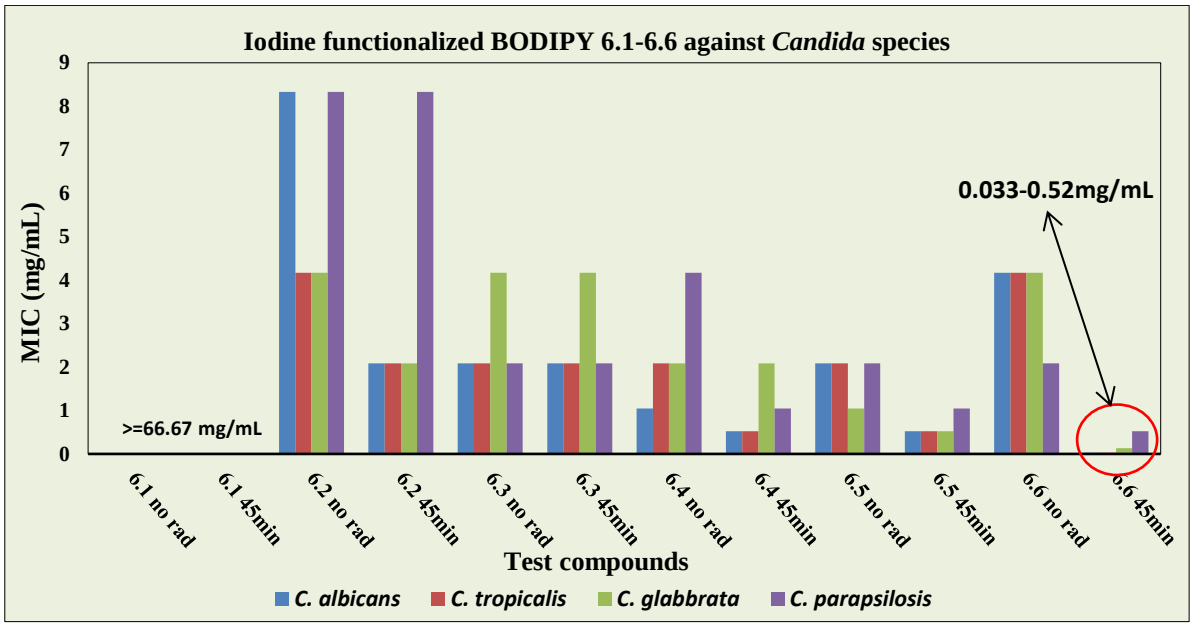

Figure 5.3 Antifungal activity of Iodine functionalized BODIPY 6.1 to 6.6

5.2.5 Fractionation of compound 6.6 and its antimicrobial activity

BODIPY 6.6 was selected for further analysis. Four sub-fractions (6.6.1 to 6.6.4) were obtained from column chromatography. The screening of the fractions containing the actual photosensitizer **BODIPY 6.6** with 30 iodine moieties on the periphery of the conjugated structure was carried out. The MIC, **Table 5.8,** demonstrated some activity towards bacteria understudy with fraction **6.6.4** (MIC 0.5 mg/mL) which came out as the last band from separation and confirmed with TLC plate. The results demonstrated the activity of the photosensitizer that there were some suspicions of ROS production. Hence the much-anticipated activity may be due to intersystem crossing taking place during activation of the photosensitizers with light. The less activity observed with other subfractions is a result of the synergistic effect that may be taking place due to band separations.

Table 5.9 demonstrates the activity of the subfractions of BODIPY 6.6 against the *Candida* species at various light exposures. As observed in the test results, the subfraction 6.6.4 was found to be the actual BODIPY PSs as it was observed on the TLC plate. Furthermore, the results demonstrated the activity of BODIPY6.6.4 activity against all fungal species upon illumination with light (MIC ranging from 0.065 to 4.17 mg/mL) with the best activity against

C. albicans and *C. tropicalis* (**Figure 5.4**). Further tests were conducted with this subfraction and it was further loaded onto nanoparticles for drug delivery studies and to enhance the activity of this compound.

Table 5.8 Antibacterial activity of subfractions of BODIPY 6.6 (6.6.1 - 6.6.4)

		0 min exposure		**45 min exposure**		**Internalized**	
Fraction	**organism**	**MIC (mg/mL)**	**MBC/MFC (mg/mL)**	**MIC (mg/mL)**	**MBC/MFC (mg/mL)**	**MIC (mg/mL)**	**MBC/MFC (mg/mL)**
6.6.1	***S. aureus***	16.67	33.33	16.67	33.33	8.33	16.67
	S. pyogenes	4.17	8.34	1.08	2.08	4.17	8.34
	E. coli	16.67	33.33	16.67	33.33	16.67	33.33
	P. aeruginosa	16.67	33.33	16.67	33.33	16.67	33.33
6.6.2	***S. aureus***	16.67	33.33	4.17	8.33	4.17	8.33
	S. pyogenes	16.67	33.33	2.08	4.17	8.33	16.67
	E. coli	16.67	33.33	16.67	33.335	16.67	33.33
	P. aeruginosa	16.67	33.33	>33.33	>33.33	16.67	33.33
6.6.3	***S. aureus***	8.33	16.67	2.08	4.17	8.33	16.67
	S. pyogenes	4.17	8.33	0.52	1.04	4.17	8.33
	E. coli	16.67	33.33	>33.33	>33.33	16.67	33.33
	P. aeruginosa	16.67	33.33	>33.33	>33.33	16.67	33.33
6.6.4	***S. aureus***	16.67	33.33	2.08	4.17	2.08	4.17
	S. pyogenes	4.17	8.33	0.52	1.08	2.08	4.17
	E. coli	8.33	16.67	1.08	2.08	4.17	8.33
	P. aeruginosa	8.33	16.67	2.08	4.17	8.33	16.67

Table 5.9 Antifungal activity of sub fractions of compound 6.6 (6.6.1 - 6.6.4)

Fraction	organism	0 min exposure		45 min exposure		Internalized	
		MIC (mg/mL)	MBC/MFC (mg/mL)	MIC (mg/mL)	MBC/MFC (mg/mL)	MIC (mg/mL)	MBC/MFC (mg/mL)
6.6.1	***C. albicans***	>33.33	>33.33	>33.33	>33.33	16.67	33.33
	C. tropicalis	>33.33	>33.33	>33.33	>33.33	8.33	16.67
	C. glabbrata	>33.33	>33.33	>33.33	>33.33	>33.33	>33.33
	C. parapsilosis	>33.33	>33.33	>33.33	33.33	>33.33	>33.33
6.6.2	***C. albicans***	16.67	33.33	16.67	33.33	8.33	16.67
	C. tropicalis	8.33	16.67	8.33	16.67	8.33	16.67
	C. glabbrata	>33.33	>33.33	>33.33	>33.335	>33.33	>33.33
	C. parapsilosis	>33.33	>33.33	>33.33	>33.33	>33.33	>33.33
6.6.3	***C. albicans***	16.67	33.33	16.67	33.33	8.33	16.67
	C. tropicalis	8.33	16.67	8.33	16.67	4.17	8.33
	C. glabbrata	16.67	33.33	16.67	33.33	16.67	33.33
	C. parapsilosis	16.67	33.33	16.67	33.33	16.67	33.33
6.6.4	***C. albicans***	4.17	8.33	1.04	2.08	0.13	0.26
	C. tropicalis	0.26	0.52	0.26	0.52	0.065	0.13
	C. glabbrata	8.33	16.67	2.08	4.17	2.08	4.17
	C. parapsilosis	8.33	16.67	8.33	16.67	4.17	8.33

From T**able 5.9** it was observed that there was photoactivity after irradiation of BODIPY6.6.4 with a white light dose for 45 minutes. This photoinactivation was evident from the lowered MIC readings. Enhanced photoactivity was observed with *C. albicans* and *C. tropicalis*, whereas the *C. glabrata* and *C. parapsilosis* demonstrated some resistance which is not a surprise as these have more antifungal resistance as reported in the literature.

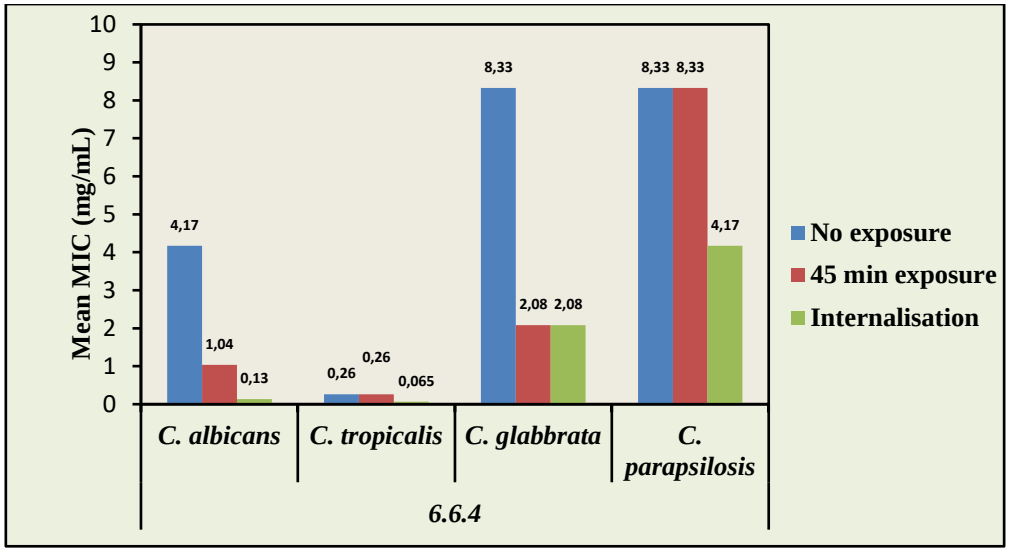

Figure 5.4 Antifungal activity of subfraction 6.6.4 constituted in 1:3 DMSO:water with and without the exposure of light

In **Figure 5.4** the reduced MIC signifies the best activity of the BODIPY PSs under study and the enhancement of the activity after irradiation and internalized studies suggest the production of the ROS species which contributes to microbial photoinactivation.

5.2.6 Antimicrobial activity of BODIPY nanoconjugates (Pt NRs) for both BODIPY 6 and BODIPY 6.6.4

The results of the antimicrobial activity of nanoconjugates for BODIPY 6 and 6.6.4 are shown in **Table 5.10**. A general trend was noted. Both the nanoconjugates were more effective against fungi compared to the bacteria and an increase in activity with light exposure and internalization being the most effective was observed.

Table 5.10 MIC, MBC, and MFC of Pt NRs-6.0 and Pt NRs-6.6.4

Fraction	organism	Median (range) in mg/ml n=3					
		0 min exposure		45 min exposure		Internalized	
		MIC	MBC/MFC	MIC	MBC/MFC	MIC	MBC/MFC
Pt NRs-6	***S. aureus***	0.13 (0.065-0.13)	0.26 (0.13-0.26)	0.065 (0.065-0.065)	0.13 (0.13-0.13)	0.033 (0.033-0.065)	0.065 (0.065-0.13)
	S. pyogenes	0.008 (0.008-0.008)	0.016 (0.016-0.016)	0.008 (0.008-0.008)	0.016 (0.016-0.016)	0.008 (0.008-0.008)	0.016 (0.016-0.016)
	E. coli	4.17 (4.17-4.17)	8.33 (8.33-8.33)	1.04 (1.04-1.04)	2.08 (2.08-2.08)	0.26 (0.26-0.521	0.52 (0.52-1.04)
	P. aeruginosa	4.17 (4.17-4.17)	8.33 (8.33-8.33)	0.52 (0.52-0.52)	1.04 (1.04-1.04)	0.26 (0.26-0.26)	0.52 (0.52-0.52)
	C. albicans	1.04 (1.04-1.04)	2.08 (2.08-2.08)	0.52 (0.52-1.04)	1.04 (1.04-2.08)	0.065 (0.065-0.065)	0.13 (0.13-0.13)
	C. tropicalis	0.065 (0.065-0.065)	0.13 (0.13-0.13)	0.065 (0.065-0.065)	0.13 (0.13-0.13)	0.016 (0.016-0.033)	0.033 (0.033-0.065)
	C. glabrata	0.52 (0.52-1.04)	1.04 (1.04-2.08)	0.52 (0.52-0.52)	1.04 (1.04-1.04)	0.26 (0.26-0.26)	0.52 (0.52-0.52)
	C. parapsilosis	2.08 (2.08-2.08)	4.17 (4.17-4.17)	0.52 (0.52-0.52)	1.04 (1.04-1.04)	0.13 (0.13-0.13)	0.26 (0.26-0.26)
Pt NRs-6.6.4	***S. aureus***	0.52 (0.52-0.52)	1.04 (1.04-1.04)	0.065 (0.065-0.065)	0.13 (0.13-0.13)	0.033 (0.033-0.033)	0.065 (0.065-0.065)
	S. pyogenes	0.008 (0.008-0.008)	0.016 (0.016-0.016)	0.008 (0.008-0.008)	0.016 (0.016-0.016)	0.008 (0.008-0.008)	0.016 (0.016-0.016)
	E. coli	2.08 (2.08-2.08)	4.17 (4.17-4.17)	0.52 (0.52-0.52)	1.04 (1.04-1.04)	0.26 (0.26-0.26)	0.52 (0.52-0.52)
	P. aeruginosa	8.33 (8.33-8.33)	16.67 (16.67-16.67)	2.08 (2.08-2.08)	4.17 (4.17-4.17)	1.04 (1.04-1.04)	2.08 (2.08-2.08)
	C. albicans	0.52 (0.52-0.52)	1.04 (1.04-1.04)	0.52 (0.52-0.52)	1.04 (1.04-1.04)	0.26 (0.26-0.26)	0.52 (0.52-0.52)
	C. tropicalis	0.13 (0.13-0.13)	0.26 (0.26-0.26)	0.008 (0.008-0.008)	0.016 (0.016-0.016)	0.008 (0.008-0.008)	0.016 (0.016-0.016)
	C. glabrata	0.26 (0.26-0.26)	0.52 (0.52-0.52)	0.26 (0.26-0.26)	0.52 (0.52-0.52)	0.26 (0.26-0.26)	0.52 (0.52-0.52)
	C. parapsilosis	0.52 (0.52-0.52)	1.04 (1.04-1.04)	0.26 (0.26-0.26)	0.52 (0.52-0.52)	0.013 (0.013-0.013)	0.033 (0.033-0.033)

5.2.6.1 Antimicrobial activity of BODIPY nanoconjugates for BODIPY 6

The results on antimicrobial activity of nanoconjugates for BODIPY 6 are shown in (**Figure 5.5 A, B & C**). An improvement on the activity of the compounds upon loading them to the nanoparticles was observed. Generally, it can be observed that the antifungal effect is better than the antimicrobial effect. For all the organisms, the light exposure experiments improved the antimicrobial activity. It can also be observed that internalization further improved the activity.

This study has demonstrated again the high activity of the compounds on gram-positive bacteria species with the lowest MIC of 0.0082 mg/mL (8.2 µM). This improvement may be due to the concentrated number of drugs due to the loading of BODIPYs onto the nanorods. Furthermore, it was notable that both *E. coli* and *P. aeruginosa* which are gram-negative bacteria had low activity. Similar observations were made with the activity of the nanoconjugates with fungal species. *C. albicans* and *C. tropicalis* showed better efficacy compared to *C. glabrata* and *C. parapsilosis*.

As observed in **Figure 5.5 C**, the nanoconjugates, and internalized experiments after irradiation for 45 minutes showed a great improvement in the activity of the drugs. These observations suggest that there is some adsorption or absorption of the nanoconjugates onto or into the microorganism's cells. Fungal studies showed more activity compared to their counterpart bacterial species.

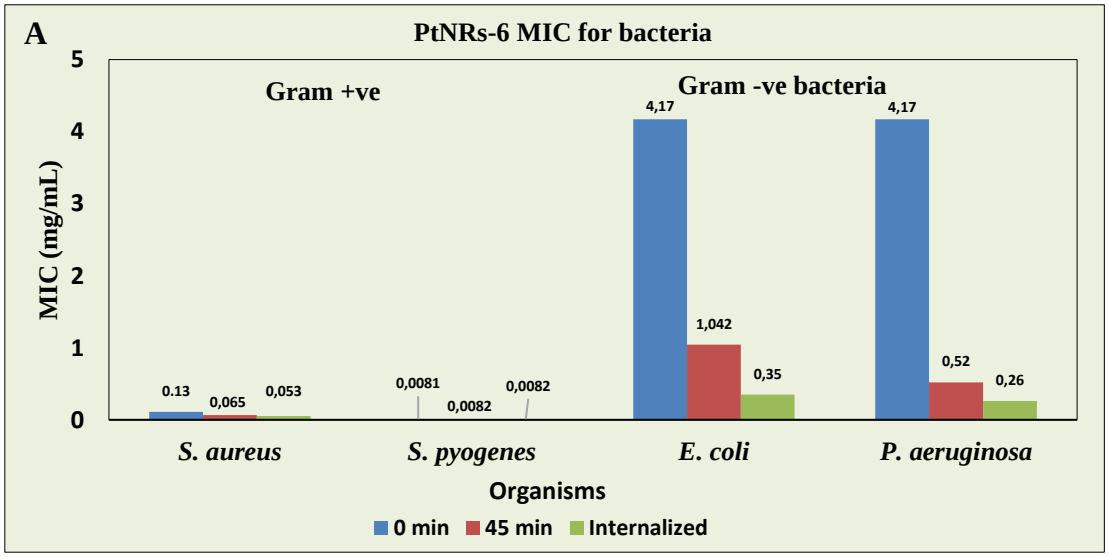

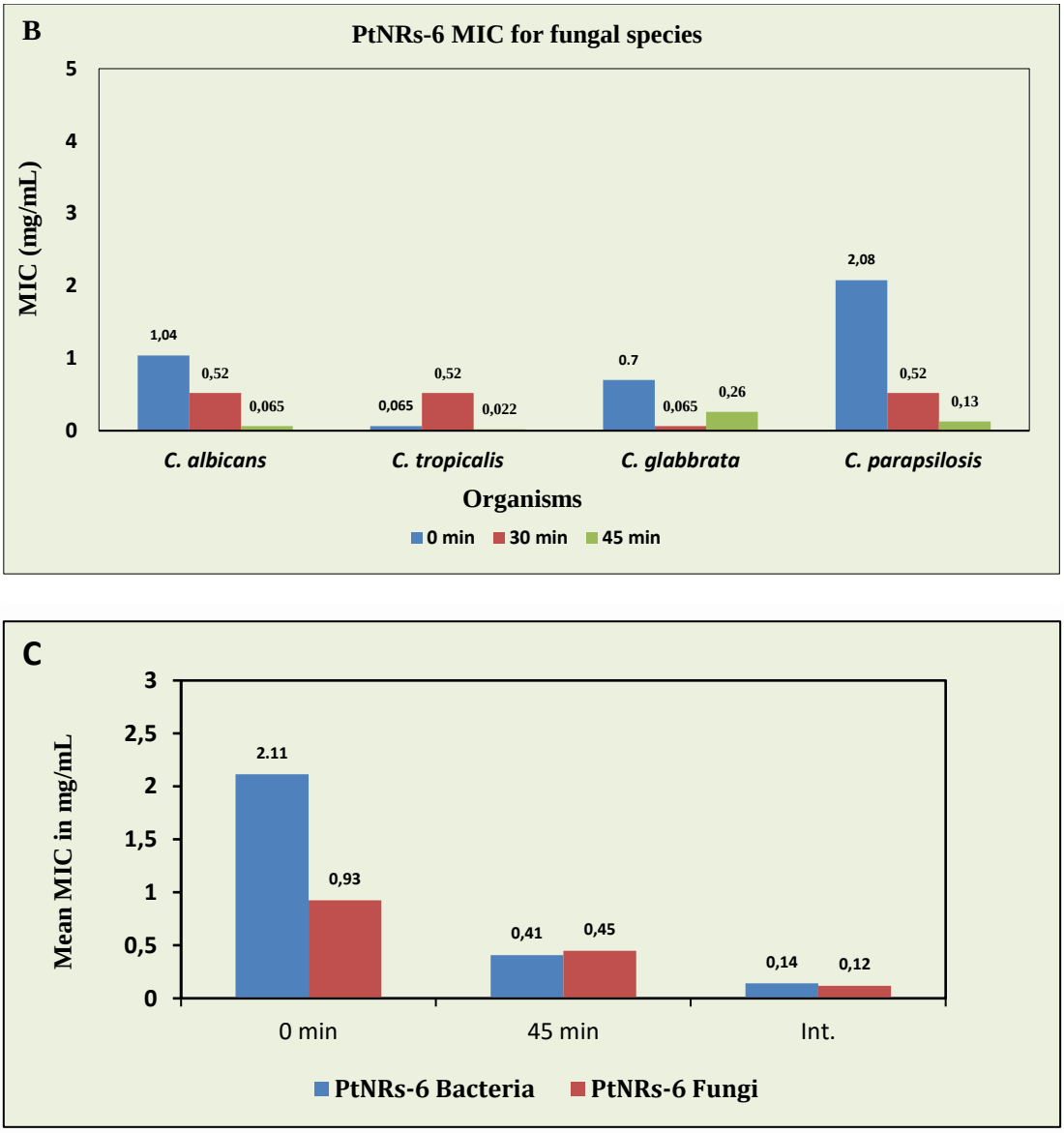

Figure 5.5 Antimicrobial activity of nanoconjugates of BODIPY 6 (A: bacterial species, B: Fungal species, C: species combined)

5.2.6.1 Statistical analysis of both bacteria and fungi considering nanoconjugates of BODIPY 6

Statistical analysis of the results of the nanoconjugates of BODIPY 6 was conducted and the results are shown in (**Figure 5.6, A: bacteria, B: fungi**). A descriptive statistical t-test analysis for grouped comparisons between the means was carried out with a p-value of <0.05 considered statistically significant. The paired t-tests were conducted to see the significant differences between the test compounds' activity on bacteria and fungi with the varied exposure times. For the antibacterial activity (**Figure 5.6 A**) the efficacy of Pt NRs-6 significantly improved from

no light exposure to 45-minute exposure (p-value of 0.013) and internalization (p-value of 0.0043). It further significantly improved when the compound was internalized (p-value of 0.052) compared to the direct 45-minute exposure. For fungi (**Figure 5.6 B**), the efficacy of Pt NRs-6 did not significantly improve from no light exposure to 45-minute exposure (p of 0.59). However, it significantly improved with internalization (p-value of 0.0018). It also significantly improved when the compound was internalized (p-value of 0.0007) compared to the value obtained at direct 45-minute exposure.

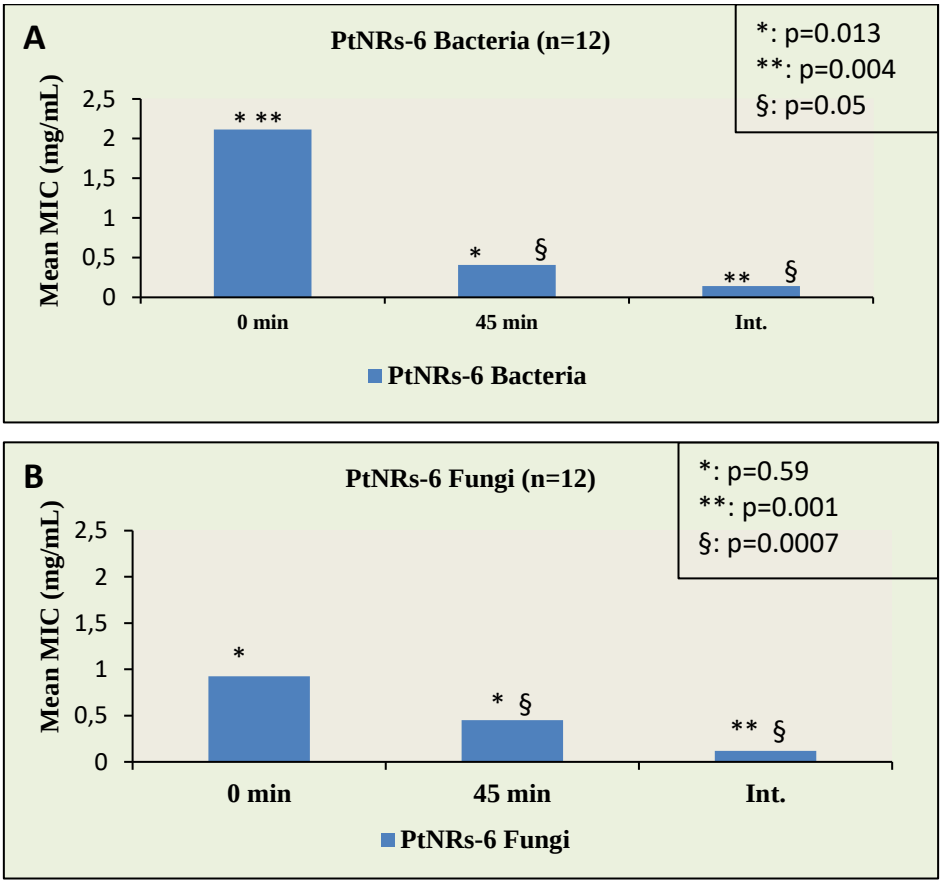

Figure 5.6 Antimicrobial activity of BODIPY6-nanoconjugates of (**A**: bacteria, **B**: Fungi)

5.2.6.2 Antimicrobial activity of BODIPY nanoconjugates for BODIPY 6.6.4

The results for antimicrobial activity of BODIPY6.6.4-nanoconjugates are shown in **Figure 5.7 A, B & C**. Again, an improvement in the activity of the compounds upon loading to the nanoparticles was observed. Generally, it was observed that the antifungal effect is better than the antibacterial effect. For all the organisms, light exposure improved the activity. It can also be seen that internalization further improved the activity suggesting the surface or internal cell damage. This study has demonstrated again the high activity of the compounds on gram-positive bacteria species with the lowest MIC of 0.0082 mg/mL (**Figure 5.7 A**). This much

improvement may be due to the concentrated amount of the BODIPY 6.6.4 due to its loading onto nanorods. Furthermore, it was noticed that both *E. coli* and *P. aeruginosa* which are gram-negative bacteria had low activity. There was not much difference in the MIC values of PtNRs6.6.4 against all the test fungal species.

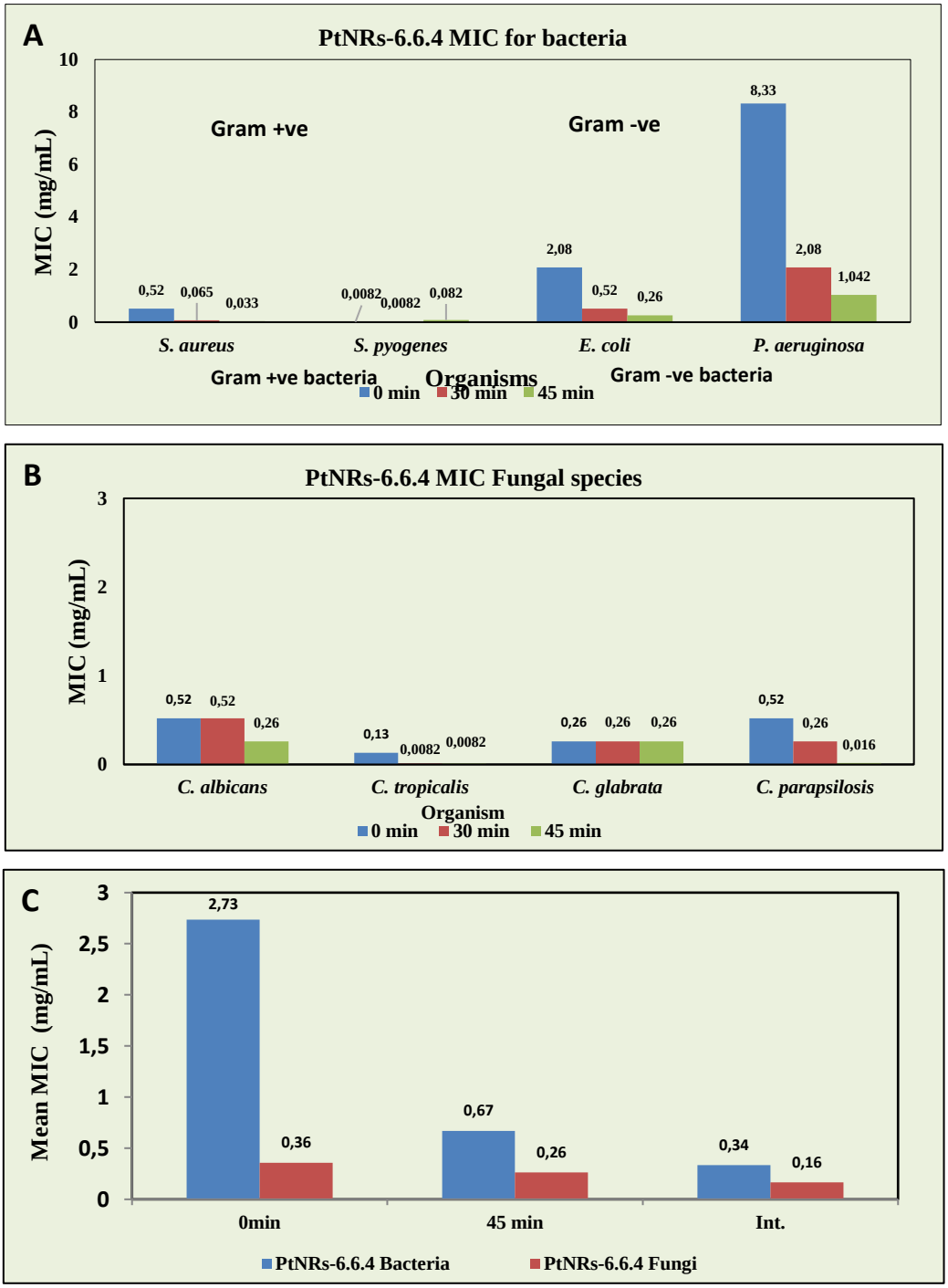

Figure 5.7 Antimicrobial activity of nanoconjugates of BODIPY 6.6.4 (A: bacterial species, B: Fungal species, C: species combined)

5.2.6.2.1 Statistical analysis of both bacteria and fungi nanoconjugates of BODIPY 6.6.4

Statistical analysis of the results of the nanoconjugates of BODIPY 6.6.4 was conducted and the results are shown in **Figure 5.8** (**A: bacteria, B: fungi**). A descriptive statistical t-test analysis for grouped comparisons between the means was done. The paired tests were conducted to see the statistically significant differences between the test compounds' activity on bacteria and fungi with the varied exposure times. For the antibacterial activity (**Figure 5.8 A**) the efficacy of Pt NRs-6.6.4 significantly improved from no light exposure to 45-minute exposure (p-value of 0.05) and internalization (p-value of 0.02). However, there was no significant difference in MIC when 45 minutes of exposure was compared to the internalization (p-value of 0.2). For fungi (**Figure 5.8 B**), the efficacy of Pt NRs-6.6.4 did not significantly improve from non-irradiated to 45-minute exposure (p-value of 0.21). However, it significantly improved with internalization ($p < 0.01$). There was no difference in MIC when 45 minutes of exposure was compared to the internalization (p-value of 0.14).

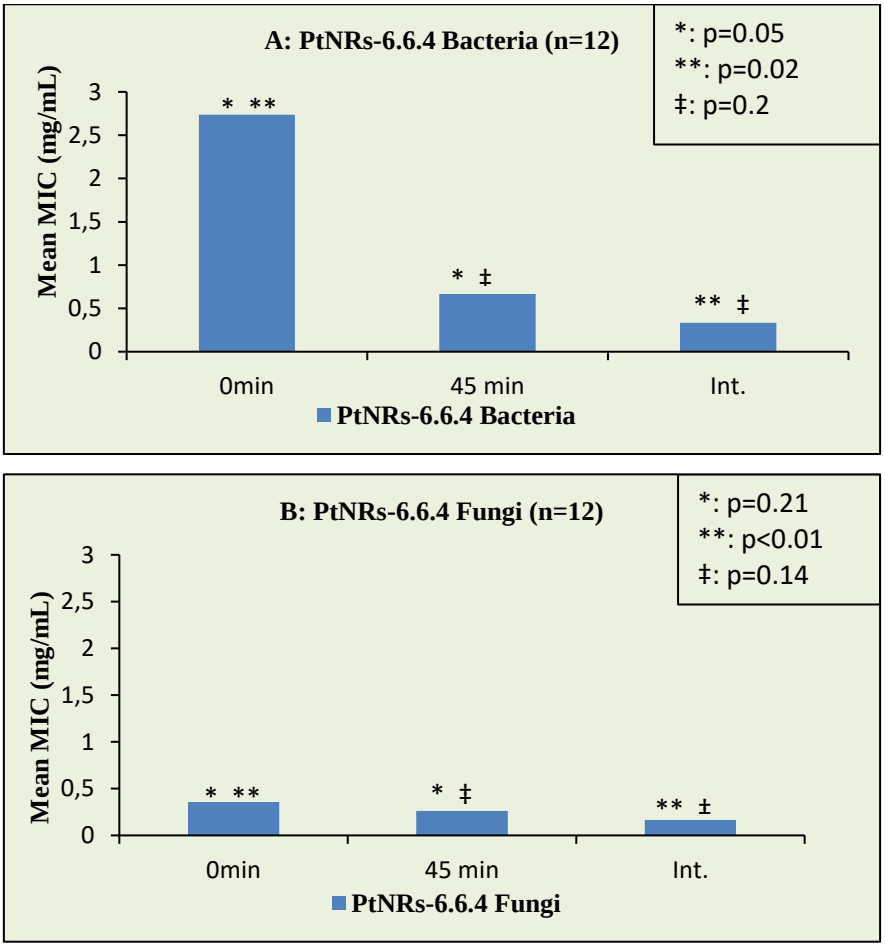

Figure 5.8 Antimicrobial activity of nanoconjugates of BODIPY 6.6.4 (A: bacteria, B: Fungi)

5.2.6.3 BODIPY6, BODIPY6.6.4, and nanoconjugates statistical analysis on bacterial and fungal species

Figure 5.9 shows statistical analysis of the results for photodynamic inactivation of *S. aureus*, *S. pyogenes*, *E. coli*, and *P. earugenosa* bacterial strains against the iodized BODIPY 6, BODIPY 6.6.4 and their corresponding platinum nanoconjugates. **Figure 5.9 A** and **Figure 5.9 B** demonstrates the statistical comparison study under no photodynamic effect (no irradiation) to determine the dark toxicity of the compounds. A downward trend was observed which indicated that the BODIPY PSs with enhanced iodine moieties showed more dark toxicity against bacterial strains. Moreover, loading of these PSs onto Pt nanorods, not only increased their solubility but also enhanced their antibacterial activity. A significant statistical difference was observed when comparing BODIPY 6 and BODIPY 6.6 (p-value of 0.14), whereas for the comparison of BODIPY 6.6 and BODIPY 6.6.4 there was no significant difference (p-value of 0.039). Similarly, on comparison of BODIPY 6.6.4 and their nanoconjugates counterpart, no difference in the statistical mean values tests (p-value <0.01) was observed respectively. The standard deviation of the data demonstrated that the data was widely spread apart from the mean MIC values for BODIPY 6, 6.6.4-NRs, and 6-NRs, wherein for BODIPY 6.6 and 6.6.4 the standard deviations were clustered by the mean values.

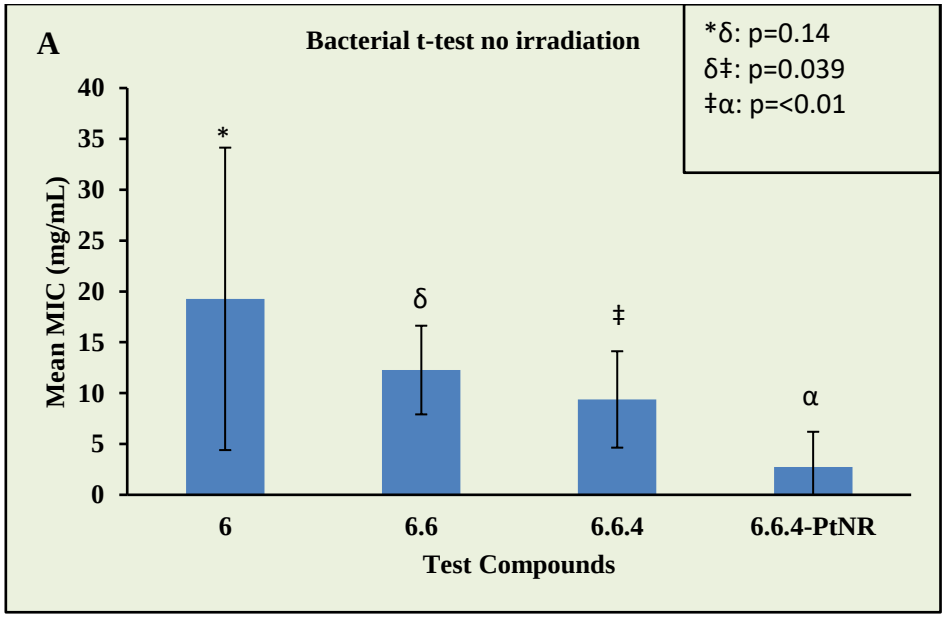

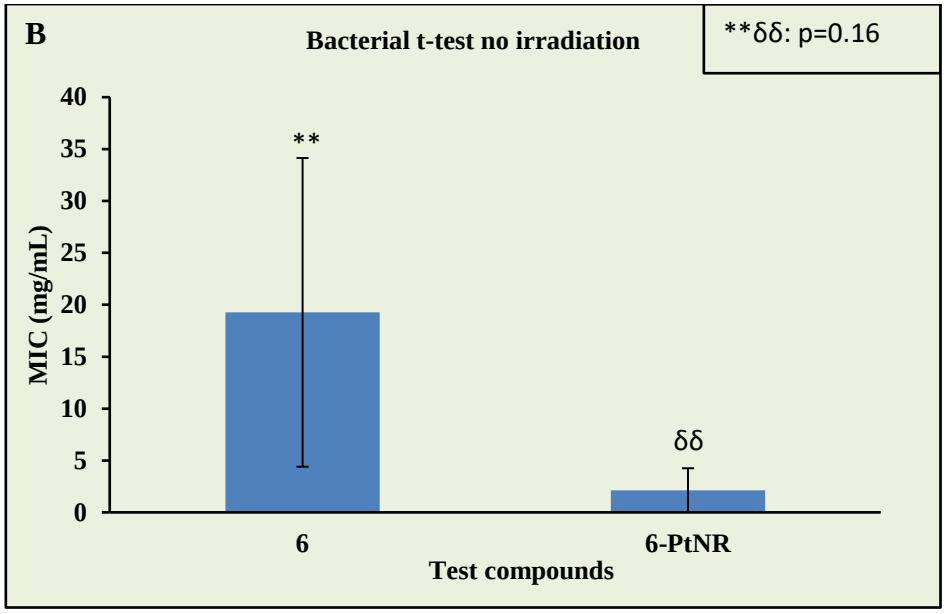

Figure 5.9 Non-irradiated comparative statistical analysis for bacterial species.

Figure 5.10 shows statistical analysis of the results for photodynamic inactivation activity of *C. albicans*, *C. tropicalis*, *C. glabrata* and *C. parapsilosis* against BODIPY 6, BODIPY 6.6, BODIPY 6.6.4, and their resulting nanoconjugates. In **Figure 5.10 B** we observed a synergistic effect from BODIPY 6.6 to BODIPY 6.6.4 which demonstrated high activity before extended column chromatography purification experiments. The lower MIC demonstrates more activity respectively. The statistical analysis demonstrated no statistically significant difference between BODIPY 6 and BODIPY 6.6 (p-value <0.05). Furthermore, a comparison study between BODIPY 6.6 and BODIPY 6.6.4 showed a significant difference between the mean values (p-value of 0.14) which can be attributed to the synergistic effect due to extensive column chromatographic purification of the compounds. Also, upon loading BODIPY PSs onto nanorods, there was a significant improvement in the antifungal activity, which suggested the drug intake by the microorganisms. The statistical study demonstrated a significant difference between the mean values (p-value <0.01) respectively. Moreover, there was no noticeable statistical difference between the mean values for BODIPY 6 and BODIPY 6-PtNRs (p-value of 0.022). The standard deviation for the antifungal test showed the mean values were clustered for BODIPY 6, BODIPY 6.6, and BODIPY 6.6.4-PtNRs, whereas for BODIPY 6-PtNRs and BODIPY 6.6.4 the mean values were widely spread. This is due to some resistance to the *C. glabrata* and *C. parapsilosis* respectively.

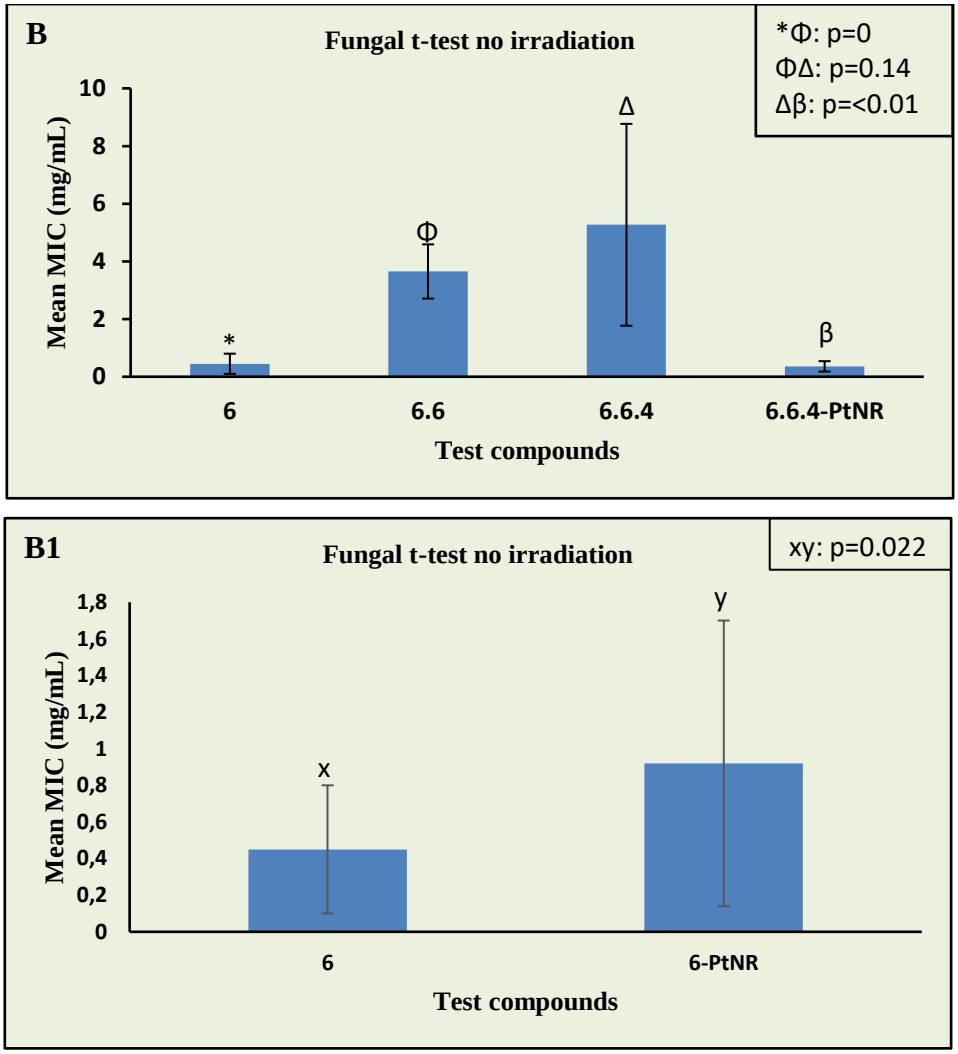

Figure 5.10 Non-irradiated comparative statistical analysis for fungal species.

5.3 Discussion

Boron dipyrromethene (BODIPY) photosensitizers have been commonly reported as new emerging PSs with promising antimicrobial properties which have led to extensive research interests for antimicrobial photodynamic therapy (aPDT/PDI) application. Sixteen different BODIPY PSs with different functional groups were tested in this study to select the most active PSs with phototoxicity against pathogenic bacteria *S. aureus, S. pyogenes, E. coli, and P. aeruginosa,* and unicellular fungal pathogens *C. albicans, C. tropicalis, C. glabrata, and C. parapsilosis.*

5.3.1 Disk diffusion test (screening)

BODIPY 6 and 10 were found to have antimicrobial activity with and without light irradiation against all the test microorganisms. Therefore, they were further investigated. BODIPY 9, 7

and 8 also showed some antibacterial activity against only *S. aureus, S. pyogenes,* and *P. aeruginosa* but the zones of inhibitions were very low. Due to this limited activity, BODIPY 1, 2, 3, 4, 5, 7, 8, and 9 were not further investigated. The results of this study can be rationalized by the different functional groups on the PSs and the binding capacity to the surface of the microorganisms. Disk diffusion is a crude, cheap, and simple technique that can be used as a screening of therapeutic compounds, and therefore it can provide limited information. It can show that a specific test concentration has any antimicrobial effect or not. Nevertheless, this technique has its advantages and is therefore frequently used (Bomanda *et al*., 2018).

5.3.2 MIC/MBC/MFC study of BODIPY 6 and 10

MIC study showed that compound 6 had good antifungal activity before further purification with the lowest MIC being $25x10^{-12}$ mg/mL. The significant activity of BODIPY 6 PSs was due to the iodine moieties on the periphery of the compound and the extended fluorine atoms. The observed effect is in line with the literature findings which have reported that the presence of heavy atoms enhances intersystem crossing affording triplet state photosensitization (Zhao *et al*., 2015; Yogo *et al*., 2005). Moreover, the heavy atom effect has been shown by different researchers to enhance the production of reactive oxygen species responsible for cell damage and cell death (Zhao *et al*., 2015; Yogo *et al*., 2005). The other intriguing observation as evidenced by some instability concerning BODIPY 6 suggesting that dimerization or another form of aggregation resulting in trimmers may be possible.

A review of studies carried out by Durantini *et al*., (2018), demonstrated a wide variety of iodine bearing BODIPY PSs enhanced the antimicrobial PDI effect. Durantini and his group synthesized compounds whose antimicrobial MIC ranged between 0.1 µM against gram-positive bacteria and 10 µM against gram-negative bacteria. They observed that the BODIPY PSs PDT activity was 0.25 µM against *A. baumanni,* 0.5 µM against *P. aeruginosa*, 1 µM against *K. pneumonia* and 10 µM against *E. coli* (gram-negative strains), 0.1 µM against *E. faecium* and 0.1 µM against *S. aureus*. The synthesized BODIPY PSs also demonstrated sensitive activity against fungal strains with concentrations of 0.1 µM against *C. Albicans,* 0.5 µM against *Cryptococcus neoformans* and 0.1 µM against *C. glabrata* irradiated with 171 J/cm^2 light source. In this study, similar results to those by Durantini et al. (2018) were observed in that MIC values up to 0.0082 mg/mL (8.2 µM) for gram-positive bacteria and poor activity of 260 µM MIC against gram-negative bacteria. This suggests that more studies have

to be carried out with BODIPY analogs to further study the effect of different substituents including iodine moieties on the antimicrobial activity of these dyes. Further studies will help to find ways to curb the resistance which is developing in gram-negative bacterial strains. This comes as a reason why attention has to be directed to the PDT drug agent charge as gram-negative microorganisms have high resistance towards neutral and negatively charged drug structures (Bourre *et al*., 2010).

5.3.3 Iodine functionalized BODIPYs 6.1 to 6.6

BODIPY structures are modified by attaching substituents (where some of these include heavy atoms) directly on the s-indacene ring (Yogo *et al*., 2005). When substituents contain heavy atoms, they tend to facilitate intersystem crossing and triplet state photosensitization producing long-lived electronic excited triplet state affording the production of reactive oxygen species (Durantini *et al*., 2018). Iodine substituents are considered heavy atoms and they are expected to facilitate triplet state photosensitization and enhance ROS generation, leading to reduced fluorescence quantum yields (Zhao *et al*., 2015; Yogo *et al*., 2005).

From the MIC experiment, the BODIPY with conjugation through phenyl substituent bearing iodine moieties demonstrated enhanced antimicrobial activity with a MIC of 0.13 mg/mL (130 µM) for *S. pyogenes* and 0.033 mg/mL (33 µM) for *C. Albicans* which are comparable observations even at low irradiation energy with other research groups. These findings are in agreement with the findings made by Frimannsson and co-worker (2010) who observed photoinactivation at a high irradiation energy of 16 J/cm^2 at 4.5- µM concentration against *Staphylococcus xylosus* and *E. coli*. Orlandi et al. (2014) also made similar observations with high irradiation energy of 171 J/cm^2 with a concentration of 2.5-80 µM cell deactivation of *P. aeruginosa*. These findings are in line with observations noted by Durantini and co-workers in that, direct iodine functionalization of the BODIPY core structure with positively charged moieties affords triplet state photosensitization hence more activity is realized. It is shown that the carbonyl moieties have played a major role in the reduced BODIPYs antimicrobial activity. The low activity observed for BODIPY 6.6 may be explained by conjugation chemistry since the amide bonds formed tend to have an electron-withdrawing capacity which in turn leads to low photoactivity (Durantini *et al*., 2018). However, BODIPY6 demonstrated more activity on Gram-positive bacterial species compared to that of fungal species. This is because the compound did not possess electron-withdrawing functional groups (carbonyl) on its outer

structure. This effect plays a major role in terms of BODIPY activity as indicated in a study carried by Durantini and co-workers (2018).

5.3.4 Antimicrobial effect of BODIPY 6.6 after further purification

Fractionation of BODIPY6.6 comes after the observations made with BODIPY 6 PSs. These observations were in line with the synergistic effect suspected or observed with BODIPY6. As specified previously, purity plays a pivotal role in drug and synthetic chemistry. After the first microbial activity test and the results observed, there was a need to verify that there were no synergistic effects taking place (as these could influence the observed activity of these compounds). Having done more purification, there was no considerable improvement in the activity of the BODIPY 6 to BODIPY 6.6.4 as shown in **Figure 5.10**. Moreover, the results indicated that the purity of the compounds plays an important role in the activity of drugs. Thorough purification was carried out while striving to maintain the structure of the synthetic compounds and preventing possible fragmentation. This study showed that BODIPY 6 possibly had underlying synergistic effects (from impurities) for the observed antimicrobial activity on fungal strains used in this study. The possible evidence that impurities may have led to the high activity observed with BODIPY 6 is shown in **Table 5.4**. After further purification, there was a significant drop in the activity of BODIPY 6 which conformed to the finding made on the stability test against *candida* species shown in **Table 5.5**. This demonstrated that the compound after its further purification studies the compound was stable in its pure form.

The challenge with these BODIPY PSs (6.1 to 6.6.4) was the conjugation chemistry for their synthetic strategy. The four fragments (from BODIPY 6.6) were tested for antimicrobial effect under irradiation for 45 minutes. The most effective and bactericidal and fungicidal fragments were observed with sub-fraction 6.6.4 (the structure was confirmed with MS, FTIR, TLC, elemental composition) and the microbial efficacy was also studied). BODIPY6.6.4 was loaded onto Pt NRs and the successful loading was confirmed with UV-Vis, TEM, and XRD techniques.

The novelty of this study comes into light by the synthesis of the BODIPY PSs, the use of Pt NRs as drug carriers for BODIPY PSs. It is worth mentioning that the study demonstrated the adsorption of about ±80% of the BODIPYs 6 and 6.6.4 on the Pt NRs surfaces which can be improved by further studies for drug delivery using Pt NRs.

5.3.5 Antimicrobial activity of BODIPY 6.6.4 and the resulting nanoconjugates

As mentioned in **section 5.3.4**, BODIPY 6 and BODIPY 6.6.4 were the most active PSs in this work and were studied for their antimicrobial and antifungal activity and loaded onto Pt nanorods. The novelty of these BODIPY PSs and their application is of great interest and serves as potential antimicrobial agents. There is a lack of information concerning BODIPY-PtNRs antimicrobial efficacy. Platinum nanoparticles have been synthesized and studied by other research groups with their application in environmental monitoring, catalysis, and energy, but there is no much information available concerning the use of Pt NRs in PDT. In this study, we chose Pt NRs because of their large surface to volume ratio and their non-photothermal activity, which makes them a potential candidate for this study. The nanoconjugates demonstrated an enhanced antimicrobial activity against *S. pyogenes* with the MIC of 0.0082 mg/ml (8.2 µM) and 0.0082 mg/mL against *C. tropicalis* after 45 minutes irradiation studies. Nanoparticles have been applied in many fields of study due to their promising properties which granted them their attention in a variety of research fields. This study demonstrated the effect of nanoparticles in enhancing the solubilisation of synthesized dyes against microbial organisms understudy

In contrast, there was a great improvement in the activity of the BODIPY PSs when comparing the dark toxicity (no light irradiation) and phototoxicity (with light irradiation) studies. Furthermore, as demonstrated in **Figure 5.5 C** and **Figure 5.7 C**, an improvement of about 90% was observed with BODIPY6 compared to 86% improvement with BODIPY 6.6.4. This shows that conjugation plays a role in BODIPY activity and in this case, it led to a slight lowering of activity.

5.3.6 Implications of the results and possible application

BODIPY photosensitizers are macromolecular compounds with promising properties and having a wide range of applications ranging from biology to physics. Most of the commercially available antimicrobial drugs have challenges of anti-drug resistance by microorganisms. Hence, new therapeutic compounds are required. BODIPY PSs and photodynamic therapy emerge as a promising method to solve the aforementioned challenge. A wide range of antimicrobial drugs are used intravenously due to their solubility and targeting capacity, but their activity remains a limiting factor. Research still needs to be done to determine the intravenous use of BODIPYs and their mode of transport to the targeted site. However, due to the short wavelength of BODIPY PSs under study, it may not be ideal for these compounds to be applied intravenously and for PDT purposes. The short wavelength range (<530 nm

wavelength) does not afford the application for deep-seated infections (microbial or tumor-related). Having said that, the results obtained from this study suggest that these BODIPYs and their nanocomposites will be suited for external applications.

The synthesized BODIPY PSs may also be suitable for the treatment of dental infections, where they may be applied superficially. Furthermore, nanofibre technology has made it very easy to develop skin antiseptic bandages for burn wounds to prevent possible wound infections. These BODIPY PSs can be impregnated and/or pasted/sprayed onto the surface of the biodegradable polymeric bandage after which they can be photosensitized with commercially available LED lights to activate the dyes. This would be a novel approach and affordable therapeutic modality which could be used in local clinics, hospitals, and/or households. Furthermore, because of their ability to be excited with white light which is more penetrable, they can be activated with domestic LED white light devices. Also, another possible and potential application of these compounds would be health care surgical equipment sterilization to avoid any cross-contamination during surgery.

5.3.7 BODIPY inactivation and interaction with microbial cells

Antimicrobial photodynamic therapy of bacterial and fungal cells varies depending on the microbial cell wall structure. In photodynamic therapy, cell death is triggered by the lethal oxidative stress that is induced by irradiation of the infected area with the light of resonant visible wavelength range of 400 nm to 900 nm (Liu *et al*., 2015). While cell killing depends on the microbial cell membrane susceptibility to drugs, Gram-positive bacteria possess a thick and porous cell wall with an interconnected peptidoglycan layer that surrounds a cytoplasmic membrane (Bourre *et al*., 2010; Harmbert *et al*., 2002). Gram-negative bacteria on the other hand have a thin outer peptidoglycan layer and a cytoplasmic membrane (Bourre *et al*., 2010). This means that a Gram-positive bacterium possesses a porous layer of peptidoglycan and a single lipid bilayer, while a Gram-negative bacterium possesses a double lipid bilayer that sandwiches a peptidoglycan layer and another outer layer of lipopolysaccharide which is as a reason for its low degree of permeability of lipophilic small molecules (Sharma *et al*., 2011). Furthermore, concerning fungal species, the cell wall of *Candida* fungal yeast shows an intermediate permeability between gram-positive and Gram-negative bacteria (Sperandio *et al*., 2013).

This explains the observations about this study. In this study, the Gram-positive bacterial species experienced more cell killing compared to Gram-negative counterparts. The BODIPY

PSs in this work has shown little to minor dark toxicity which suggests that they possess some good qualities for possible application for PDT of microorganisms. Moreover, after photosensitization with LED light for 45 minutes before incubation, we observed enhanced cell killing activity. This suggests that there was oxidative stress or interaction with the cell wall of the microorganisms. Furthermore, our internalization study has demonstrated some interesting observations, which may render some important aspects as to the adsorption or surface attachment of the BODIPY PSs with the microbial cell walls. We observed that incubation of the BODIPY PSs and microorganisms for six hours either affords adsorption and/or absorption of the drugs onto the surfaces of the microorganisms. This theory is explained by enhanced cell death after irradiation with light after incubation for six hours. In contrast, Gram-negative bacteria and *Candida parapsilosis* and *Candida glabrata* still showed some level of resistance. This is explained in the literature that some Gram-negative bacterial species tend to resist PSs with negative or neutral molecular structure (Sperandio *et al*., 2013). In contrast, the reported BODIPY PSs showed more activity against gram-positive bacteria. This is due to the variations in the bacterial cell walls; it was reported by Erdem *et al*., (2014) that cell interaction with gram-positive bacteria may be through the binding of the antimicrobial agent with peptidoglycan transpeptidases (PGTP). In this study, BODIPY-cell interaction may be due to cell wall attachments or cell penetration through PGTP binding or by other internalization mechanisms. Flow cytometry studies and fluorescence microscopy should be carried to help underpin the localization of BODIPY PSs and understand their mechanism of cell mortality.

5.4 Conclusion

A series of ten photo-stable functionalized BODIPY PSs bearing carboxylic acid, amine, sulfamoyl, sulfonamide at 1, 3, 4, 5, 7, and 8 positions, fluorine, and iodine functional groups at the 2, 3, 5 and 6, positions were synthesized to investigate their photodynamic therapy effect on microbial species. BODIPY 6 PSs bearing iodine moieties were further improved to introduce more iodine functional groups through conjugation to substituent groups to form BODIPY6.1 to BODIPY6.6. Moreover, the study investigated the effects of purity which lead to further purification of BODIPY6.6 to obtain BODIPY6.6.4 (one of four sub-fractions) which was the purest form of BODIPY6.6 respectively. The structures for the synthesized compounds were characterized and elucidated successfully with FTIR, mass spectrometry; elemental analysis, UV-Vis, and fluorescence (refer to chapter 4). This study demonstrated the activity of the newly synthesized BODIPY PSs in an *in vitro* experimental setup. The results were

measured and interpreted as the minimum inhibitory concentration and minimum bactericidal/fungicidal concentrations.

Also, the study has shown that there was no significant dark toxicity (no light exposure) on microorganisms with the synthesized BODIPY PSs. The BODIPY PSs were soluble in polar solvents which are desired for possible PSs in aPDT applications setup. Moreover, we further showed that BODIPY PSs bearing sulfamoyl and iodine groups demonstrated more activity on microbial organisms. BODIPY 10 demonstrated activity without light irradiation with the MIC between 2.08 and 16.70 mg/mL for bacteria and 0.28 and 8.33 mg/mL for fungal species. MIC of BODIPY 6 was between 8.33 and 16.70 mg/mL for bacteria and 0.25 and 1.04 mg/mL for fungal species. BODIPY 6 was further purified to study the synergistic effect on microorganisms. The activity dropped from 0.25 *p*M to between 65 µg/mL and 130 µg/mL against *C. Albicans* after further purifications (running a silica column chromatography for 10 runs, Sephadex 3 runs, and biobeads 3 runs) which suggested there were existing impurities. It was also observed that BODIPY 6 solution when left for further 120 hours, the compound became stable with the MIC of 130 µg/mL.

Daughter compounds of BODIPY 6 with extended iodine groups were synthesized giving BODIPY6.1 to BODIPY6.6. Consequently, BODIPY6.6 showed more activity on *S. pyogenes* strain with the MIC 2.08 mg/mL without light irradiation and 0.13 mg/mL with light irradiation, and 4.17 mg/mL for *C. Albicans* without light, 0.325 mg/mL with light irradiated for 45 minutes. Subsequently, BODIPY 6.6 was purified further resulting in the isolation of BODIPY 6.6.4 with MIC 4.17 mg/mL against *S. pyogenes* no light and 0.52 mg/mL after 45 minutes light irradiation. Moreover, the MIC against *C. Albicans* was 4.17 mg/mL without light and 1.04 mg/mL light irradiated for 45 minutes, and 0.13 mg/mL incubated for 6 hours (internalization study) and then irradiated for 45 minutes. Moreover, upon loading the BODIPY PSs onto Pt nanorods, the study demonstrated an improvement in the antimicrobial photodynamic therapy inactivation activity.

These improvements suggest that there was a better interaction of the BODIPY PSs with the microorganisms after loading to the nanoparticles with these PSs. Moreover, this shows that nanoparticles serve as good drug carriers of the photoactive agents for an improved photodynamic inactivation of both bacterial and fungal species.

5.5 References

Adler-Shohet F., Waskin H. and Lieberman J.M., 2001. Amphotericin B lipid complex for neonatal invasive candidiasis. *Arch. Dis. Child Fetal Neonatal ed*. 84(1):131-133.

Aires de Sousa M. and Lencastre H., 2004; Bridges from hospitals to the laboratory: genetic portraits of methicillin-resistant *Staphylococcus aureus* clones. *FEMS Immunol Med Microbiol*, 40(1): 101-111.

Ali S., 2013; http://www.austincc.edu/microbio/2421f/mrsa.htm.

Allison R.R., Bagnato V.S., and Sibata C.H., 2010; Future of oncologic photodynamic therapy. *Future Oncol*., 6(6): 929-940,

Ann Chai L.Y., Denning D.W., and Warn P., 2010; *Candida tropicalis* in human disease. *Crit. Rev. Microbiol*., 36(4): 282-298.

Arendrup M. C., Fuursted K., Gahrn-Hansen B., Jensen I. M., Knudsen J. D., Lundgren B., Schønheyder H. C., and Tvede M., 2005; Seminational surveillance of fungemia in Denmark: notably high rates of fungemia and numbers of isolates with reduced azole susceptibility. *J. Clin. Microbiol*., 43(1): 4434-4440.

Atsay A., Gül A., and Koçak M.N., 2014; A new hexadeca substituted non-aggregating zinc phthalocyanine. *Dyes Pigments*, 100(1): 177-183.

Awuah S.G. and You Y., 2012; Boron dipyrromethene (BODIPY)-based photosensitizers for photodynamic therapy. *RSC Adv*., 2(1): 11169-11183.

Bailey R., 2018; A guide to different types of pathogens, http://www.thoughtco.com/types-of-pathogens-4135656 (Accessed, 18 05 2018).

Batchtiar B.M., 1997; Some factors affecting virulence pathogenicity of *Candida albicans* candidiasis in the mouth. *J. Dent. Univ. Indonesia*, 4(1): 704-706.

Bialkova A. and Šubík J., 2006; Biology of the pathogenic yeast *Candida glabrata.* Folia *Microbiol*., 51(1): 3-20.

Bien J, Sokolova O, Bozko P., 2011; Characterization of virulence factors of *Staphylococcus aureus*: Novel function of known virulence factors that are implicated in activation of airway epithelial proinflammatory response. *J. Pathog*., 601905(1): 1-13.

Bisno, A. L. 1995. *Streptococcus pyogenes*, p. 1786–1799. In G. L. Mandell, R. G. Bennett, and R. Dolin (ed.), Principles and practice of infectious diseases, vol. 2. Churchill Livingstone, New York, N.Y.

Blaess M., Bibak N., Claus R.A., Kohl M., Bonaterra G.A., Kinscherf, Laufer S., DeignerH. -P., 2017; NB 06: From a simple lysosomotropic aSMase inhibitor to tools for elucidating the role of lysosomes in signaling apoptosis and LPS-induced inflammation. *Eur. J. Med. Chem*., 153(1): 73-104.

Boens N., Leen V., Dehaen W., 2012; Fluorescent indicators based on BODIPY. *Chem. Soc. Rev*., 41(1): 1130-1172.

Bomanda B.T., Waudo W., Ngoy B.P., Muya J.T., Mpiana P.T., Mbala M., Openda I., Mack J. and Nyokong T., Photophysical and in vitro antimicrobial studies of 2,6-dibromo-BODIPY Dyes substituted with diethienylenevinylene at 3,5-positions., *Macroheterocycles*, 11(4): 429-437. Doi:10.6060/mhc180898n.

Bourre L., Giuntini F., Eggleston I.M., Mosse C.A., Marcobert A.J. and Wilson M., 2010; Effective photoactivation of Gram-positive and Gram-negative bacterial strains using an HIV-1 Tat peptide-porphyrin conjugate, *Photochem. Photobiol., Scie*., 9(1): 1630-1620.

Brooks G.F., Carroll K.C., Butel J.S., Morse S.A., Jawetz, Melnic, Adelberg'c Medical Microbiology. 24th Ed. McGraw-Hill: 1995. P.608-610.

Brubaker R.R., 1985; Mechanisms of bacterial virulence. *Annu. Rev. Microbiol*., 39(1): 21-50.

Carr K., 2001; Phthalocyanine ink-jet dyes. US 6190422 B1, Google Patents (2001), http://www.google.ch/patents/US6190422 (Accessed 24.01.2017).

Chaffin W.L., Lopez-Ribot J.L., Casanova M., Gozalbo D. and Martínez JP., 1998; Cell wall and secreted proteins of *Candida albicans*: identification, function, and expression. *Microbiol. Mol. Bio. Rev*., 62(1): 130-180.

Chang Y., Zhou S., Li E., Zhao W., Ji Y., Wen X., Sun H., Yuan H., 2017; Fragment-based discovery of novel pentacyclic triterpenoid derivatives as cholesteryl ester transfer protein inhibitors. *Eur. J. Med. Chem*., 126(1): 143-153. doi: 10.1016/j.ejmech.2016.09.098.

Clements A., Young J.C., Constantinou N. and Frankel G., 2012; Infection strategies of enteric pathogenic *Escherichia coli*. *Gut Microbes* 3(2): 71-87.

Cohen M.L., Morpholino end-capped, hindered amine substituted amino triazine and their use as light stabilizers. US 6096886 A, Google Patents (2000), https://www.google.ch/patents/US6096886 (Accessed 24.01.2017).

Collins T.L., Markus E.A., Hassett D.J. and Robinson B.J., 2010; The effect of a cationic porphyrin on *Pseudomonas aeruginosa* biofilms. *Curr. Microbiol*., 61(1): 411-416.

Colombo A.L., Guimaraes T., Silva L.R., de Almeida Monfardini L.P., Cunha A.K., Rady P., Alves T. and Rosas R.C., 2007; Prospective observational study of candidemia in São Paulo, Brazil: incidence rate, epidemiology, and predictors of mortality. *Infect. Control Hosp. Epidemiol*., 28(5): 570-576.

Colombo A.L., Nucci M., Park B.J, Nouer A.S., Arthington-Skaggs B., da Matta D.A., Warnock D. and Morgan J., 2006; Epidemiology of candidemia in Brazil: a nationwide sentinel surveillance of candidemia in eleven medical centers. *J. Clin. Microbiol*. 44(1):2816-2823.

Cordeiro R. de-A., Sales J.A., Collares D. de-S., Castelo-Branco M., Brilhante R.S.N., de Ponte Y.B., Araújo G. dos-S., Mendes P.B.L., Pereira V.S., de Alencar L.P., Pinheiro A. de-Q., Sidrim J.J.C., Rocha M.F.G., 2017; *Candida parapsilosis* complex in veterinary practice: A historical overview, biology, virulence attributes, and antifungal susceptibility traits. *Veterinary Microbio*., 212 (1): 22-30.

Costa-de-Oliveira S., Pina-Vaz C., Mendonca D. and Goncalves Rodrigues A., 2008*;* A first Portuguese epidemiological survey of fungemia in a university hospital. *Eur. J. Clin. Microbiol. Infect. Dis*., 27(5): 365-374.

Courtney, H. S., J. B. Dale, and D. L. Hasty. 1999. Strategies for prevention of group A streptococcal adhesion and infection, p. 553–579. In Y. H. An and R. J. Friedman (ed.), Handbook of bacterial adhesion: principles, methods, and applications. Humana Press, Totowa, N.J.

Croxen M.A., and Finlay B.B., 2010; Molecular mechanisms of *Escherichia coli* pathogenicity. *Nat. Rev. Microbiol*., 8(1): 26-38; PMID:19966814.

Cunningham M.W., 2000; Pathogenesis of group A *streptococcal* infections. *Clin. Microbiol.Rev*., 13(3): 470-511.

Dan M., Poch F., and Levin D., 2002; High rate of vaginal infections caused by non-*C. albicans Candida* species among asymptomatic women *Med. Mycol*., 40(1): 383-386.

Desai C., Mavrianos J. and Chauhan N., 2011; *Candida glabrata* Pwp7p and Aed1p are required for adherence to human endothelial cells. *FEMS Yeast Res*., 11(1): 595-601.

Diamond R.D., 1993; Interactions of phagocytic cells with *Candida* and other opportunistic fungi. *Arch. Med. Res*., 24(1): 361-369.

Dichiara M., Prezzavento O., Marrazzo A., Pittal V., Salerno L., Rescifina A., Amata E., 2017; Recent advances in drug discovery of phototherapeutic non-porphyrinic anticancer agents. *Eur. J. Med. Chem*., 142(1): 459-485.

Dixon, D.M.; Walsh, T.J. Chapter 76: Antifungal agents. In Medical Microbiology, 4th ed; Baron, S., Ed.; University of Texas Medical Branch at Galveston: Galveston, TX, USA, 1996.

Donnenberg M.S. and Whittam T.S., Pathogenesis and evolution of virulence in enteropathogenic and enterohemorrhagic *Escherichia coli*, J. Clinic. Investigation., 107(5): 539-548.

Durantini A.M., Heredia D.A., Durantini J.E., Durantini N.E., 2018; BODIPYs to the rescue: potential applications in photodynamic inactivation. *Euro. J. Med. Chem*., 144(1): 651-661.

Eggimann P., Garbino J. and Pittet D., 2003; Epidemiology of *Candida* species infections in critically ill non-immunosuppressed patients. *Lancet Infect. Dis*., 3(1): 685-702.

Erdem S.S., Khan S., Palanisami A. and Hasan T., 2014; Rapid, low-cost fluorescent assay of β-lactamase-derived antibiotic resistance and related antibiotic susceptibility., *J. Biomed. Opt*., 19(10): 105007-11. Doi:10.11171/1.JB).19.10.105007.

Espinel-Ingroff A., Canton E., Peman J., Rinaldi M. G., and Fothergill A. W., 2009; Comparison of 24-Hour and 48-Hour Voriconazole MICs as determined by the clinical and laboratory standards institute broth microdilution method (M27-A3 Document) in Three Laboratories: Results Obtained with 2,162 Clinical Isolates of Candida spp. and Other Yeasts *J. Clin. Microbiol.*, 47(1): 2766-2771.

Evans J.L., Maddux B.A., and Goldfine, I. D., 2005; The molecular basis for oxidative stress-induced insulin resistance, *Antioxid. Redox Signal*, 7(1): 1040-1052.

Felden B., Vandenesch F., Bouloc P., and Romby P., 2011; The *Staphylococcus aureus* RNome and its commitment to virulence. *PLoS Pathog*., 7(1): e1002006.

Ferreira A.J.G., Carr J.H., Starling C.E.F., de Resende A.E., and Donlan R.M., 2009; Biofilm formation and effect of caspofungin on biofilm structure of *Candida* species bloodstream isolates. *antimicrob. Agents chemother*., 53(10): 4377-4384.

Fidel P.L., Vazquez J.A., Sobel J.D., 1999; *Candida glabrata*: a review of epidemiology, pathogenesis, and clinical disease with comparison to *C. Albicans*. *Clin. Microbiol. Rev*., 12(1): 80-96.

Finnan S., Morrissey J.P., O'Gara F., Boyd E.F., 2004; Genome diversity of *Pseudomonas aeruginosa* isolates from cystic fibrosis patients and the hospital environment. *J. Clin. Microbiol*., 42(1): 5783-5792.

Fonzi W.A. and Calderon R.A., 2001; Virulence factors of *Candida albicans*. *Trends Microbiol*., 327(1): 333-339.

Frimannsson D.O., Grossi M., Murtagh J., Paradisi F., and O'Shea D.F., 2010; Light-induced anti-microbial properties of a brominated boron difluoride (BF_2) chelated tetraarylazadipyrromethene photosensitizer, J. Med. Chem. 53 (2010): 7337e7343.

Fuchs T.M., Eisenreich W., Heesemann J., and Goebel W., 2012; Metabolic adaptation of human pathogenic and related nonpathogenic bacteria to extra- and intracellular habitats. *FEMS Microbiol. Rev*. 36(1): 435-462.

Gellatly S.L. & Hancock R.E.W., 2013; *Pseudomonas aeruginosa*: new insights into pathogenesis and host defenses. *Pathogens and Disease*, 67(1), 159-173.

Goodpasture E.W., 1919; The significance of certain pulmonary lesions in relation to the etiology of influenza. Am. J. Med. Sci., 158(1):863-870.

Hambert P.A., 2002; Cellular impermeability and uptake of biocides and antibiotics in Gram-positive bacteria and mycobacteria. *Sym. Ser. Soc. Appl. Microbiol*., 1(1): 46S-54S.

Hancock R.E.W., 1997; the bacterial outer membrane as a drug barrier. *Trends Microbiol*., 5(1): 37-42.

Hossler F., https://visualsunlimited.photoshelter.com/image/I0000fEbrbYy0LKU.

Meurman J.H., Siikala E., Richardson M. and Rautemaa R., 2007; Non-Candida albicans Candida yeasts of the oral cavity. A. Méndez-Vilas (Ed.): 719-731.

Jia X., Yang F.F, Li J., Liu J.Y. and Xue J.P., 2013; Synthesis and in Vitro Photodynamic Activity of Oligomeric Ethylene Glycol–Quinoline Substituted Zinc(II) Phthalocyanine Derivatives. *J. Med. Chem*., 56(1): 5797-5805.

Joachim H. and Polayes S., 1940; Subacute endocarditis and systemic mycosis (monilia). JAMA 205-208.

Johnson E.M., Warnock D.W., Luker J., Porter S.R. and Scully C., 1995; Emergence of azole drug resistance in Candida species from HIV-infected patients receiving prolonged fluconazole therapy for oral candidosis. *J. Antimicrob. Chemother*., 35(1): 103-114.

Junqueira J.C., Jorge A.O.C., Barbosa O.J., Rossoni R.D., Vilela S.F.G., Costa A.C.B.P., Primo F.L., Gonçalves J.M., Tedesco AC., and Suleiman J.M.A.H., 2012; Photodynamic inactivation of biofilms formed by *Candida spp., Trichosporon mucoides*, and *Kodamaea ohmeri* by cationic nanoemulsion of zinc 2,9,16,23-tetrakis(phenylthio)-29H, 31H-phthalocyanine (ZnPc).*Lasers Med. Sci*., 27(1): 1205-1212,

Kamkaew A., Lim S.H., Lee H.B., Kiew L.V., Chung L.Y., Burgess K., 2013; BODIPY dyes in photodynamic therapy. *Chem. Soc. Rev*., 42(1): 77-88.

Kaper J.B., Nataro J.P., Mobley H.L., 2004; Pathogenic *Escherichia coli. Nat. Rev. Microbiol*., 2(1): 123-40.

Karen Shaw, 2016; http-publichealthmatters.blog.gov.uk-2016-10-16-beating *E. coli* - what are you doing to break the chain of infection (Accessed 2017-09-20).

Ke M.R., Eastel J.M., Ngai K.L.K., Cheung Y.Y., Chan P.K.S., Hui M., Ng D.K.M, Lo P.C., 2014; Photodynamic inactivation of bacteria and viruses using two monosubstituted zinc(II) phthalocyanines. *Eur. J. Med. Chem*., 84(1): 278–283.

Knodler L.A., and Celli J., 2011; Eating the strangers within host control of intracellular bacteria via xenophagy. *Cell. Microbiol*., 13(9): 1319-1327.

Knops P.E., Kramer J.H., and Frohberger W.; Morpholino propanol derivatives, fungicidal compositions, and use. US 4495184 A, Google Patents (1985), pathogens (Goodpasture, 1936; Brubaker, 1985). http://www.google.ch/patents/US4495184 (Accessed 24.03.2017).

Kon Kateryna, 2005-2018; https://www.123rf.com/photo_69859619_stock-illustration-bacteria-staphylococcus-aureus-on-the-surface-of-skin-or-mucous-membrane-3d-illustration.html.

Kothavade R.J., Kura M.M., Valand A.G., and Panthaki M.H., 2010; *Candida tropicalis:* its prevalence, pathogenicity, and increasing resistance to fluconazole. *J. Med. Microbiol*., 59(8): 873-880.

Kudrevich S.V., and van Lier J.E., 1996; Azaanalogs of phthalocyanine: syntheses and properties. *Coord. Chem. Rev*., 156(1): 163-182.

Kurlenda J, Grinholc M., 2012; Alternative therapies in *Staphylococcus aureus* diseases. *Acta. Biochim. Pol*., 59(2):171-184.

Leng B-F, Qiu J-Z, Dai X-H, Dong J, Wang J-F, Luo M-J, *et al*., 2011; Allicin reduces the production of α-toxin by *Staphylococcus aureus*. *Molecules*, 16(1): 7958-7968.

Li L., Redding S. and Dongari-Bagtzoglou A., 2007; *Candida glabrata*: an emerging oral opportunistic pathogen. *J. Dent. Res*., 86(1): 204-215.

Liu D, 2014; Molecular detection of human fungal pathogens. Taylor and Francis CRC Press, Boca Raton, Florida, USA. ISBN: 9781439812402.

Liu Y., Qin R., Zaat S.A.J., Brenkink E. and Heger M., 2015; Anti-microbial photodynamic therapy: Review of a promising approach to fight antibiotic-resistant bacterial infections, *J.Clinic. Transl. Res*., 1(3): 140-167.

Loudet A., and Burgess K., 2007; BODIPY dyes and their derivatives: syntheses and spectroscopic properties, Chem. Rev. 107 (1): 4891-4932.

Ma Y, Xu Y, Yestrepsky BD, Sorenson RJ, Chen M, Larsen SD, Sun H., 2012; Novel inhibitors of *Staphylococcus aureus* virulence gene expression and biofilm formation. *PloS One*, 7(1): e47255. doi: 10.1371/journal.pone.0047255.

Mack J., and Kobayashi N., 2011; Low symmetry phthalocyanines and their analogs. *Chem. Rev*., 111(2):281-321.

Mah T-F., 2014; Establishing the minimal bactericidal concentration of an anti-microbial agent for planktonic cells (MBC-P) and biofilm cells (MBC-B). *J. Vis. Exp*. 83(1): 1-6, e50854.

Makhseed S., Al-Sawah M., Samuel J., Manaa H., 2009; Synthesis, characterization, and nonlinear optical properties of nonaggregating hexadeca-substituted phthalocyanines. *Tetrahedron Lett*., 50(1): 165-168.

Mathews R.C., 1994; Pathogenicity determinants of *Candida albicans*: potential targets for immunotherapy? *Microbiol.,* 140(1): 1505-1511.

Mayer F.L., Wilson D., and Hube B., 2013; *Candida albicans* pathogenicity mechanisms, *Virulence,* 4(2): 119-128.

Messer S.A., Jones R.N., and Fritsche T.R., 2006; International surveillance of *Candida* spp. and *Aspergillus spp*.: Report from the SENTRY antimicrobial surveillance program (2003) *J. Clin. Microbiol*., 44(1):1782-1787.

Moulder J.W., 1962; The biochemistry of intracellular parasitism. Chicago: The University of Chicago Press (Accessed 05.03.2017).

Moulder J.W., 1985; Comparative biology of intracellular parasitism. *Microbiol. Rev*., 49(1): 298-337.

Nahm M.H., Apicella M.A., and Briles D.E., 1999; "Immunity to extracellular bacteria," in Fundamental Immunology, ed.W.E. Paul (Philadelphia, PA, Lippincott Raven),1373-1386.

Nasution A.I., 2013; Virulence factor and pathogenicity of *Candida albicans* in Oral Candidiasis. *World J. dent*., 4(4): 267-271.

Nataro J.P. and Kaper J.B., 1998; Diarrheagenic *Escherichia coli*. *Clin. Microbiol. Rev.,* 11(1):142-201.

Negri M., Silva S., Henriques M. and Oliveira R., 2012; Insights into *Candida tropicalis* nosocomial infections and virulence factors. *Eur J Clin Microbiol Infect Dis*., 31(7): 1399-412.

Orlandi V.T., Rybtke M., Caruso E., Banfi S., Tolker-Nielsen T., and Barbieria P., 2014; Antimicrobial and anti-biofilm effect of a novel BODIPY photosensitizer against Pseudomonas aeruginosa PAO1, Biofouling, 30(1): 883-891.

Pamer E, 2008; "Immune responses to intracellular bacteria," in Fundamental Immunology, ed.W.E. Paul (Philadelphia: Lippincott Williams &Wilkins), 1165-1181.

Peveler W.J., Noimark S., Al-Azawi H., Hwang G.B., Crick C.R., Alan E., Edel B.J., Ivanov A.P., AmcRobert A.J., and Parkin I., 2019; Low-dimensional systems and nanostructures. *ACS Appl. Mater. Interface*. 10(1): 98-104.

Pfaller M. A., Diekema D. J., Procop G. W., and Rinaldi M. G., 2007; Multicenter comparison of the VITEK 2 antifungal susceptibility test with the CLSI broth microdilution reference method for testing amphotericin B, flucytosine, and voriconazole against *Candida spp*. *J. Clin. Microbiol*., 45(1): 3522-3528.

Pinheiro M.R.S., Lacerda H.R., Melo R.G.L., Maciel M.A., 2008; *Pseudomonas aeruginosa* infections: factors relating to mortality with an emphasis on resistance pattern and anti-microbial treatment. *Braz. J. Infect. Dis*., 12(1): 509-515.

Ranyuk E., Cauchon N., Klarskov K., Gue K., van Lier J.E., 2013; Phthalocyanine–Peptide conjugates: Receptor-targeting bifunctional agents for imaging and photodynamic therapy. *J. Med. Chem*., 56(4): 1520-1534.

Riera M., Mogensen E., d'Enfert C., Janbon G., 2012; New regulators of biofilm development in *Candida glabrata*. *Res. Microbiol*., 163(4): 297-307.

Rodrigues C.F., Silva S., Henriques M., 2014; *Candida glabrata*: a review of its features and resistance. *Eur. J. Clin. Microbiol. Infect. Dis*. 33(1): 673-688.

Sansonetti, P., 2001; Phagocytosis of bacterial pathogens: implications in the host response. *Semin. Immunol*., 13(1), 381-390.

Schaller M., Borelli C., Korting H.C. and Hube B., 2005; Hydrolytic enzymes as virulence factors of *Candida albicans*. *Mycoses*, 48(6): 365-377.

Shao L. C., Sheng C. Q., and Zhang W. N., 2007; Recent advances in the study of antifungal lead compounds with new chemical scaffolds. *Yao Xue Xue Bao*., 42(11): 1129-1136.

Sharma S.K., Chiang L.Y. and Hamblin M.R., 2011; Photodynamic therapy with fullerenes in vivo: Reality or a dream? *Nanomedicine* (Lond), 6(1): 1813-1835.

Shirasu N., Nam S.O. and Kuroki M., 2013; Tumor-targeted photodynamic therapy. *Anticancer Res.*, 33(1); 2823-2832.

Silva M.T., 2012; Classical labeling of bacterial pathogens according to their lifestyle in the host: inconsistencies and alternatives. *Front. Microbiol*. 3(1):71.

Silva, A.P., Miranda, I.M., Guida, A., Synnott, J., Rocha, R., Silva, R., Amorim, A., Pina-Vaz, C., Butler, G., Rodrigues, A.G., 2011. Transcriptional profiling of azole-resistant *Candida parapsilosis* strains. *Antimicrob. Agents Chemother*. 55(1): 3546-3556.

Sperandio F.F., Huang Y-Y., Hamblin M.R., 2013; Anti-microbial photodynamic therapy to kill Gram-negative bacteria. Recent Patents on Antimicrobial infective drug discovery., 8(2):105-120.

Strateva T. and Mitov I., 2011; Contribution of an arsenal of virulence factors to pathogenesis of *Pseudomonas aeruginosa* infections. *Ann Microbiol*., 61(1): 717-732.

Stuart L.M., and Ezekowitz R.A., 2005; Phagocytosis: elegant complexity. *Immunity*, 22(1): 539-550.

Suter E., 1956; Interaction between phagocytes and pathogenic microorganisms. *Bacteriol. Rev*., 20(1): 94-132.

Tam P., Gee K., Piechocinski M. and Macreadie I., 2015; *Candida glabrata*, Friend and Foe. *J. Fungi*. 1(1): 277-292.

Taraszkiewicz A., Fila G., Grinholc M. and Nakonieczna J., 2013; Innovative strategies to overcome biofilm resistance. *BioMed Res. Int. Hindawi*., 1(1): 1-13.

Tavares A., Carvalho C.M.B., Faustino M.A., Neves M.G.P.M.S., Tome J.P.C., Tome A.C., Cavaleiro J.A.S., Cunha A., Gomes N.C.M., Alves E. and Almeida A., 2010; Anti-microbial photodynamic therapy: Study of bacterial recovery viability and potential development of resistance after treatment. *Mar. Drugs*, 8(1): 91-105.

Trofa D., Ga´cser A. and Nosanchuk J.D., 2008; *Candida parapsilosis*, an emerging fungal pathogen. *Clin. Microbiol. Rev*., 21(4): 606-625.

Ulrich G., Ziessel R., Harriman A., 2008; The chemistry of fluorescent BODIPY dyes: versatility unsurpassed. *Angew. Chem. Int. Ed. Engl*., 47(1): 1184-1201.

Vatansever F., de Melo W.C.M.A., Avci P., Vecchio D., Sadasivam, M. Gupta A., Chandran R., Karimi M.A, Parizotto N.A., Yin R., Tegos G.P., and Hamblin M.R., 2013; Anti-microbial strategies centered around reactive oxygen species--bactericidal antibiotics, photodynamic therapy, and beyond. *FEMS Microbiol. Rev.*, 37(1): 955-989.

Volkov K.A., Avramenko G.V., Negrimovskii V.M., and Luk'yanets E.A., 2008; Phthalocyanines and related compounds: XLVII. Nucleophilic replacement of chlorine atoms in Tetrachlorophthalonitrile. synthesis of Phenyl(alkyl) amino-substituted Phthalonitriles and some Phthalocyanines based thereon. *Russ. J. Gen. Chem.*, 78(1): 1787-1793.

Wannamaker, L. W. 1970; Differences between streptococcal infections of the throat and of the skin. I., *N. Engl. J. Med*, 282(1):23-31.

Weiser J.N., and Nahm M.H., 2008; "Immunity to extracellular bacteria," in Fundamental Immunology, ed.W.E. Paul (Philadelphia: Lippincott Williams & Wilkins), 1182-1203.

Whiteley M., Bangera M.G., Bumgarner R.E., Parsek M.R., Teitzel G.M., Lory S., Greenberg E.P., 2001; Gene expression in *Pseudomonas aeruginosa* biofilms. *Nature,* 413(1): 860-864.

Wierzchowski M., Sobotta L., Skupin-Mrugalska P., Kruk J., Jusiak W., Yee M., Konopka K., Düzgünes N., Tykarska E., Gdaniec M., Mielcarek J. and Goslinski T., 2013; Phthalocyanines functionalized with 2-methyl-5-nitro-1H-imidazolylethoxy and 1,4,7-trioxanonyl moieties and the effect of metronidazole substitution on photocytotoxicity. *J. Inorg. Biochem.*, 127(1): 62-72.

Wolf M.K., 1997; Occurrence, distribution, and associations of O and H serogroups, colonization factor antigens, and toxins of enterotoxigenic *Escherichia coli*. *Clin. Microbiol. Rev*., 10(1) :569-84; PMID:9336662.

Wood T.E. and Thompson A., 2007; Advances in the chemistry of dipyrrins and their complexes. *Chem. Rev*., 107(1): 1831-1861.

Working Group on Severe Streptococcal Infections. 1993. Defining the group A streptococcal toxic shock syndrome: rationale and consensus definition. JAMA 269(1):390-391

Yano S., Hirohara S., Obata M., Hagiya Y., Ichiro Ogura S., Ikeda A., Kataoka H., Tanaka M., Joh T., 2011; Current states and future views in photodynamic therapy. *J. Photochem. Photobiol*. C, Photochem. Rev., 12(1): 46-67.

Yildiz F.H., 2007; Processes controlling the transmission of bacterial pathogens in the environment. *Res. Microbiol*. 158(3): 195-202.

Ying S. and Chunyang L., 2012; Correlation between phospholipase of *Candida albicans* and resistance to fluconazole. *Mycoses*, 55(1): 50-55.

Yogo T., Urano Y., Ishitsuka Y., Maniwa F. and Nagano T., 2005; Highly efficient and photostable photosensitizer based on BODIPY chromophore, *J. Am. Chem. Soc*., 127(35): 12162-12163.

Zhao J., Xu k., Yang W., Wang Z. and Zhong F. 2015; The triplet excited state of Bodipy: formation, modulation and application, *Chem. Soc. Rev*., 44(1): 8904-8939.

Zhu H., Fan J., Wang J., Mu H., Peng X., 2014; An "Enhanced PET"-Based Fluorescent Probe with Ultrasensitivity for Imaging Basal and Elesclomol-Induced HClO in Cancer Cells *J. Am. Chem. Soc*., 136(37): 12820-12823.

Zhou Z., Song J., Nie L., and Chen X., 2016; Reactive oxygen species generating systems meeting challenges of photodynamic cancer therapy, *Chem. Soc. Rev*., 45(1): 6597-6626.

CHAPTER 6

Novel BODIPY photosensitizers and corresponding nano-conjugates as anti-cancer agents

6.1 Introduction

Chapter 6 presents the preliminary cytotoxicity study of BODIPY photosensitizers and corresponding nano-conjugates on UCT Mel-1 cell lines. The results below seek to demonstrate the cytotoxicity effect of the synthesized BODIPY PSs and their resulting platinum nanorods and nanoconjugates. Tables of results are shown and the results are reported as mean ± standard deviation, corresponding figures show the analysis of the results obtained for this study. Furthermore, the statistical data is shown and discussed in this chapter. Additionally, comparisons of the activity of BODIPY PSs to hypericin are made. The significance of the study on UCT Mel-1 cancer cells activity of the test drugs is discussed and concluded.

6.2 Results

6.2.1 Cytotoxic effect of BODIPY 6 PSs and their Pt nanoconjugates

Results of the non-irradiated and irradiated BODIPY 6 PSs and their Pt nanoconjugates are shown in **Table 6.1** and **Table 6.2** respectively. The results showed that there was no significant decrease in cell viability for non-irradiated BODIPY 6 PSs. Moreover, the normal HaCat cells showed a slight sensitivity to BODIPY PSs at concentrations of 3 and 7 μM with a viable difference of negligible 22% and 8% cell mortality respectively (**Figure 6.1 A** and **B**).

However, there was a drop in the cell viability after exposure of cells to irradiation with light (**Table 6.2** and **Figure 6.1**). Cell viability study for BODIPY 6 demonstrated that HaCat cells were more susceptible to photosensitivity after irradiation of the cells with light. The viable cells were reduced by 80% at a concentration at 0.7 μM and a significant drop of 95% of cell viability for HaCat cell lines at 3 μM concentrations compared to the untreated cells respectively.

Mel-1 cells also showed some photosensitivity towards BODIPY 6 PSs with cell viability reduced by 42% at 0.7 μM as shown in **Figure 6.1**. BODIPY PSs loaded Platinum nanorods showed more activity compared to their counterpart BODIPY 6 PSs alone (p-value 0.078). However, comparing the results with hypericin, BODIPY 6 PSs did not show better activity than that of hypericin (p-value 0.40 against BODIPY 6 and p-value 0.37 against

nanoconjugates). For the overall results concerning BODIPY 6 and its nanoconjugates, Mel-1 cells still showed less photoactivity compared to HaCat cells.

Table 6.1 Dark toxicity effects of BODIPY 6 and its nano-conjugates on HaCat and Mel-1 cells.

	BODIPY 6 HaCat						**BODIPY 6 –NR HaCat**						
No Irradiation	**3 μM Hyp**	**0**	**0.7**	**3**	**5**	**7**	**3μM Hyp**	**0**	**0.7**	**3**	**5**	**7**	**Blank**
	0.57	0.54	0.63	0.51	0.56	0.61	0.57	0.54	0.67	0.65	0.85	0.56	0.22
	0.69	0.64	0.67	0.67	0.61	0.63	0.69	0.64	0.63	0.47	0.63	0.58	0.21
	0.60	0.65	0.66	0.55	0.61	0.56	0.60	0.65	0.76	0.58	0.56	0.58	0.22
	0.60	0.61	0.73	0.63	0.69	0.51	0.60	0.60	0.58	0.55	0.56	0.65	0.23
Aver.	0.62	0.61	0.67	0.59	0.62	0.58	0.62	0.61	0.66	0.56	0.65	0.59	0.22
Aver-Blank	0.39	0.39	0.45	0.3	0.39	0.36	0.39	0.39	0.44	0.34	0.42	0.37	
Std. Dev.	0.049	0.050	0.043	0.071	0.052	0.053	0.049	0.049	0.076	0.073	0.13	0.038	
	BODIPY 6 Mel-1						**BODIPY 6-NRs Mel-1**						
	0.74	0.92	0.55	0.61	0.50	0.54	0.74	0.92	0.65	0.57	0.45	0.64	0.72
	0.53	0.64	0.60	0.49	0.50	0.73	0.53	0.64	0.52	0.57	0.50	0.52	0.78
	0.57	0.66	0.58	0.52	0.56	0.59	0.57	0.66	0.53	0.46	0.53	0.60	0.73
	0.52	0.56	0.61	0.53	0.59	0.84	0.52	0.56	0.55	0.50	0.51	0.54	0.78
Aver.	0.59	0.70	0.58	0.54	0.54	0.67	0.59	0.70	0.56	0.52	0.49	0.58	0.75
Aver-blank	0.37	0.47	0.36	0.31	0.31	0.45	0.37	0.47	0.34	0.3	0.27	0.36	
Std. Dev.	0.10	0.15	0.027	0.052	0.042	0.13	0.10	0.15	0.058	0.053	0.033	0.052	

Table 6.2 Phototoxicity effect of BODIPY 6 and its nano-conjugates on HaCat and Mel-1.

Irradiation	**BODIPY 6 - HaCat**						**BODIPY 6-NRs HaCat**						**Blank**
1 J/cm^2	**3µM Hyp**	**0**	**0.7**	**3**	**5**	**7**	**3µM Hyp**	**0**	**0.7**	**3**	**5**	**7**	
	0.29	0.54	0.31	0.28	0.3	0.31	0.28	0.54	0.2	0.26	0.3	0.28	0.22
	0.26	0.64	0.28	0.23	0.26	0.27	0.26	0.64	0.2	0.3	0.31	0.3	0.21
	0.23	0.65	0.3	0.23	0.26	0.22	0.23	0.65	0.29	0.32	0.31	0.2	0.22
	0.29	0.61	0.24	0.21	0.28	0.24	0.29	0.61	0.24	0.33	0.3	0.26	0.23
Aver.	0.27	0.61	0.28	0.23	0.27	0.26	0.26	0.61	0.23	0.30	0.31	0.26	0.22
Aver-blank	0.048	0.39	0.063	0.018	0.055	0.04	0.045	0.39	0.013	0.083	0.085	0.04	
Std. Dev.	0.028	0.049	0.031	0.029	0.019	0.039	0.026	0.049	0.042	0.03	0.0057	0.043	
	BODIPY 6 - Mel-1						**BODIPY 6-NRs Mel-1**						
	0.27	0.92	0.46	0.47	0.44	0.39	0.28	0.92	0.45	0.43	0.45	0.41	0.72
	0.27	0.64	0.53	0.49	0.46	0.39	0.26	0.64	0.51	0.45	0.45	0.40	0.78
	0.29	0.56	0.47	0.47	0.48	0.38	0.23	0.66	0.46	0.47	0.43	0.41	0.73
	0.28	0.56	0.55	0.45	0.44	0.46	0.29	0.56	0.47	0.44	0.45	0.41	0.78
aver.	0.27	0.70	0.51	0.47	0.46	0.41	0.26	0.70	0.47	0.45	0.44	0.41	0.75
aver-blank	0.052	0.47	0.28	0.24	0.23	0.18	0.04	0.47	0.25	0.22	0.22	0.18	
Std. Dev.	0.0073	0.15	0.039	0.012	0.02	0.035	0.026	0.15	0.026	0.014	0.012	0.0055	

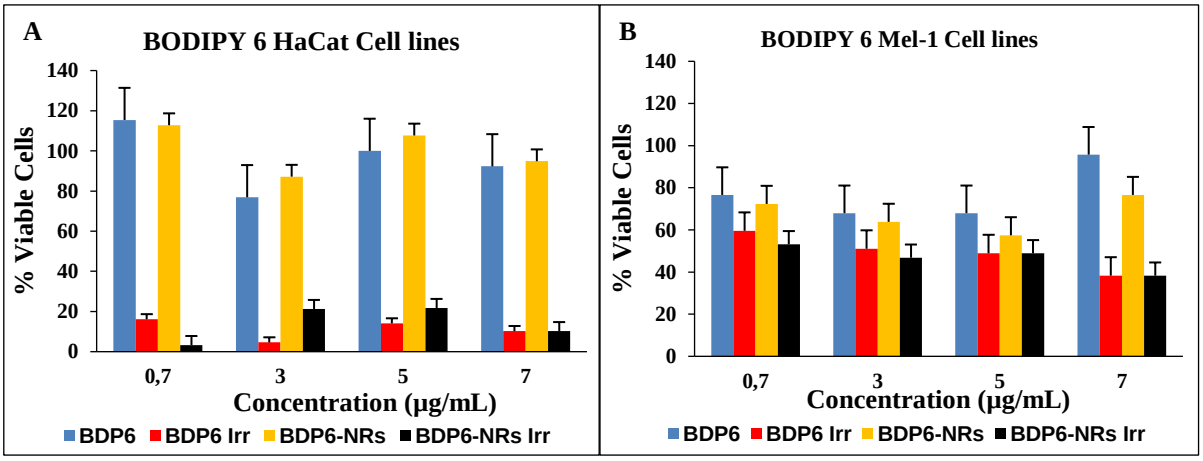

Figure 6.1 The effect of BODIPY 6 on (a) HaCat and (b) Mel-1 cell lines

6.2.2 Cytotoxic effect of BODIPY 6.6.4 PSs and their Pt nanoconjugates

Cytotoxicity of BODIPY 6.6.4 was also measured. **Table 6.3** and **Table 6.4** demonstrates the results of the non-irradiated (dark toxicity) BODIPY 6.6.4 and irradiated BODIPY 6.6.4 respectively. Treatment of HaCat cell lines with non-irradiated BODIPY 6.6.4 did not show significant toxicity (for all concentration) on the cells with cell mortality ranges from 7% to

10% respectively (**Figure 6.2**). Similarly, Mel-1 cell lines also showed low levels of dark toxicity respectively.

As demonstrated in **Table 6.4**, BODIPY 6.6.4 demonstrated very low phototoxicity on UCT Mel-1 cells. A significant cell photomotarlity was induced when BODIPY 6.6.4 PSs were loaded onto Pt nanorods. These observations suggest that there is greater drug availability in cells for nano-conjugates compared to the BODIPY PSs alone. The cell photomortality induced by BODIPY nanoconjugates was recorded at 52 and 31% at 3 µM and 5 µM respectively for BODIPY 6.6.4.

Table 6.3 Dark toxicity effect of BODIPY 6.6.4 and its nanoconjugates on HaCat and Mel-1 cells

	BODIPY 6.6.4 HaCat					**BODIPY 6.6.4-NRs HaCat**					**Blank**
No light	0	3	5	10	30	0	3	5	10	30	
	0.63	0.50	0.61	0.65	0.91	0.63	0.56	0.51	0.95	0.51	0.21
	0.51	0.48	0.79	0.71	0.63	0.51	0.42	0.48	0.89	0.96	0.22
	0.47	0.51	0.52	0.96	0.94	0.47	0.51	0.85	0.84	0.58	0.21
	0.52	0.52	0.54	0.57	0.84	0.52	0.52	0.51	0.92	0.99	0.26
Ave.	0.53	0.51	0.62	0.72	0.83	0.53	0.50	0.59	0.90	0.76	0.23
Aver-blank	0.30	0.28	0.39	0.5	0.60	0.30	0.27	0.36	0.67	0.53	
Std. Dev.	0.070	0.015	0.12	0.16	0.13	0.16	0.061	0.17	0.049	0.24	
	BODIPY 6.6.4 Mel-1					**BODIPY 6.6.4-NRs Mel-1**					
	0.72	0.56	0.55	0.61	0.99	0.72	0.57	0.66	1.12	0.69	
	0.78	0.94	0.44	0.55	0.53	0.78	0.63	0.78	0.82	0.59	
	0.73	0.40	0.69	0.60	0.69	0.73	0.77	0.81	0.78	0.58	
	0.78	0.82	0.57	1.07	0.45	0.78	0.81	0.62	0.66	0.67	
Ave.	0.75	0.68	0.56	0.71	0.67	0.75	0.69	0.72	0.84	0.64	
Aver-blank	0.52	0.45	0.33	0.48	0.44	0.52	0.47	0.49	0.62	0.41	
Std. Dev.	0.030	0.24	0.11	0.24	0.23	0.030	0.11	0.091	0.19	0.053	

Table 6.4 Phototoxic effect of BODIPY 6.6 and its nanoconjugates on HaCat and Mel-1 cells

1 J/cm^2	BODIPY 6.6.4 Mel-1					BODIPY 6.6.4-NRs Mel-1					
	0	**3**	**5**	**10**	**30**	**0**	**3**	**5**	**10**	**30**	**Blank**
	0.72	0.68	0.49	0.62	0.84	0.72	0.45	0.54	0.74	0.84	0.72
	0.78	0.68	0.82	0.75	0.65	0.78	0.55	0.54	0.59	0.79	0.78
	0.73	0.82	0.65	0.74	0.67	0.73	0.41	0.73	0.43	0.71	0.73
	0.78	0.79	0.65	0.54	0.74	0.78	0.51	0.53	0.58	0.56	0.78
Ave.	0.75	0.74	0.65	0.66	0.72	0.75	0.48	0.59	0.59	0.73	0.75
Aver-blank	0.53	0.51	0.42	0.43	0.49	0.53	0.25	036	0.36	0.5	0.52
Std. Dev.	0.030	0.075	0.13	0.10	0.086	0.030	0.065	0.097	0.12	0.12	0.030

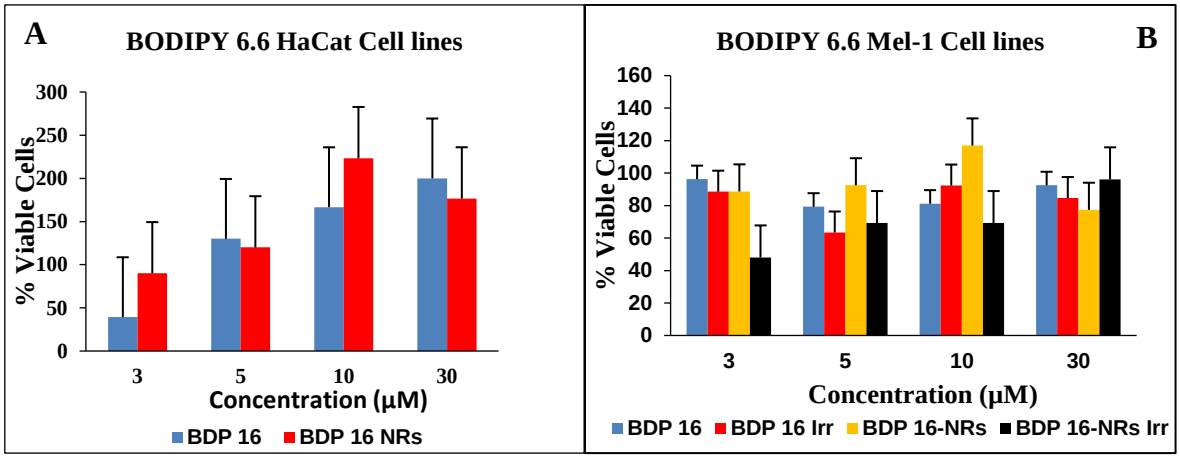

Figure 6.2 The effect of BODIPY 6.6 on (a) HaCat and (b) Mel-1 cell lines

6.2.3 Statistical comparison analysis for BODIPY 6, BODIPY 6.6, and Hypericin

The statistical data results were evaluated as the mean ± standard deviation for four independent experimental data sets. The experimental data for all test compounds were compared using Student's t-test respectively. A p-value <0.05 was considered statistically significant. The statistical analysis was centered at 3 µg/mL for both test compounds for comparison with the positive control (hypericin) respectively.

Figure 6.3 presents the student t-test statistical data for BODIPY 6 and its nanoconjugates before and after light irradiation with 1J/cm^2. The results in **Figure 6.3 A, B,** and **C** for the cytotoxicity study showed no statistical significance for the controls as well as the test compounds (against HaCat and UCT Mel-1 cells) p-value > 0.05 at 3 µg/mL. However, a

comparison of the negative control and irradiated BODIPY 6 and its nanoconjugates showed a statistical significance with the p-values 0.0029 for BODIPY 6 and p-value 0.0033 for nanoconjugates respectively. Moreover, there was no statistical significance when comparing the activity between the test compounds alone p-value of 0.078.

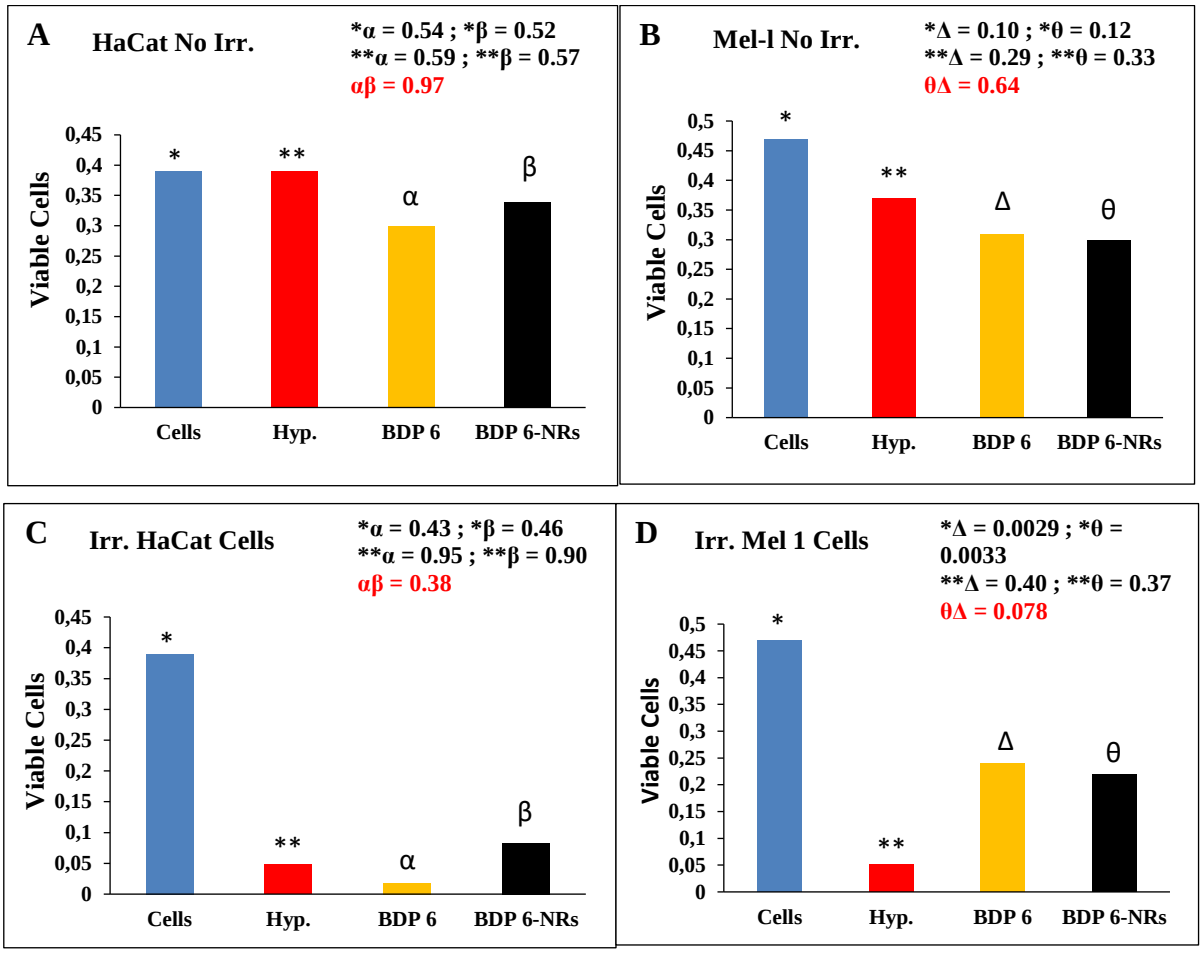

Figure 6.3 shows the independent variable student t-test statistical data analysis for comparison of BODIPY 6 and its nanoconjugates to hypericin, p-value <0.05 was regarded as statistically significant.

Similarly, **Figure 6.4** shows statistical data for BODIPY 6.6.4. Comparison of HaCat, BODIPY 6.6.4 activity, and the negative control showed a statistical significance p-value 0.047 as showed in **Figure 6.4 A**. There was no statistical significance with the positive control which signifies that the BODIPY PSs showed less or equal activity to that of hypericin respectively. Furthermore, there is no statistical significance when comparing the hypericin and BODIPY 6.6.4 at 3 µM concentration p-value 0.19 and 0.87 without irradiation against UCT Mel-1 cells

respectively. However, upon irradiation, the data showed that there is a statistical significance p-value 0.0074 and 0.012 compared with BODIPY PSs against UCT Mel-1 cell lines as shown in **6.4 C**. The data for irradiation of HaCat cells in the presence of BODIPY 6.6.4 was found to be similar to data without irradiation. This data was determined to be inconclusive and thus omitted from further use in statistical analysis.

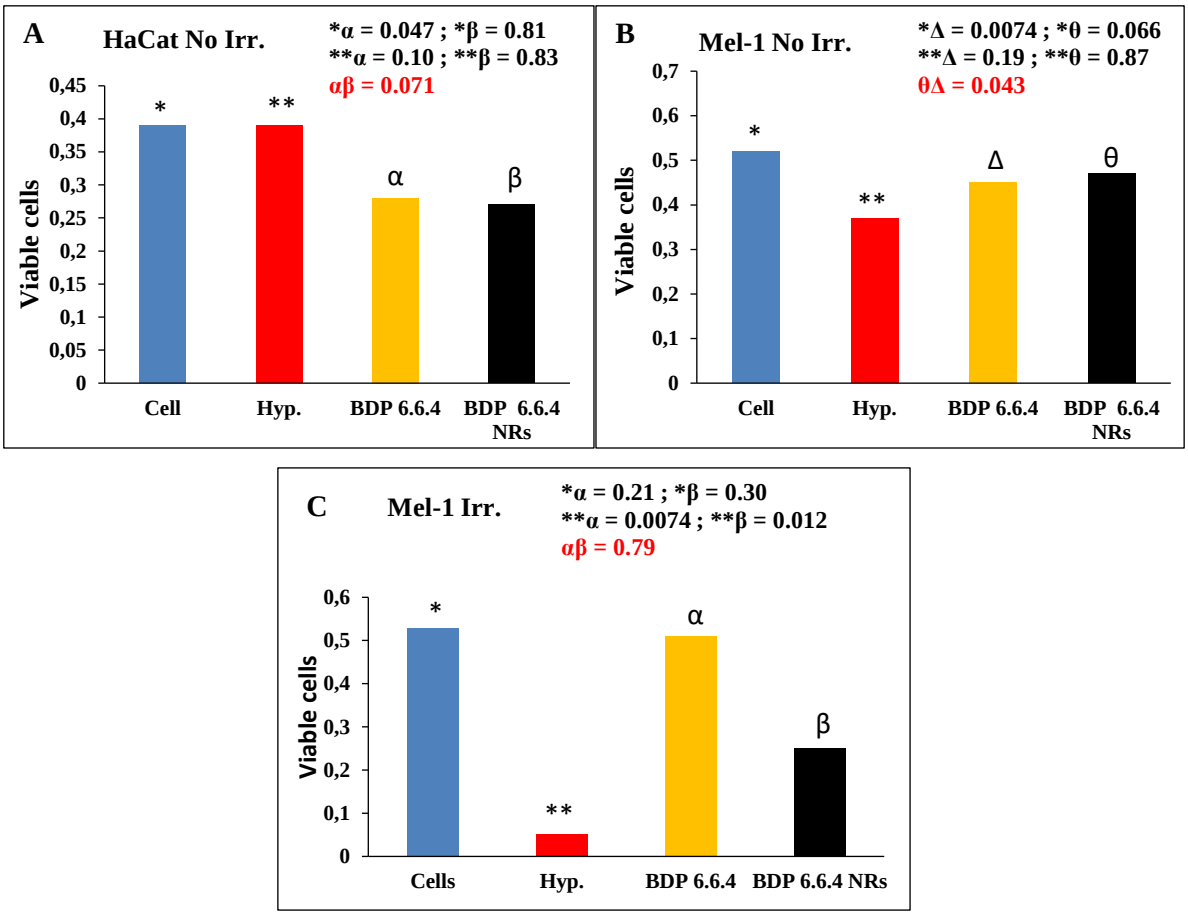

Figure 6.4 shows the independent variable student t-test statistical data analysis for comparison of BODIPY 6.6 and its nanoconjugates to hypericin, p-value <0.05 was regarded as statistically significant.

Table 6.5 demonstrates the half-maximal inhibitory concentration of BODIPY PSs and the nanoconjugates where a "*" was not defined. Both BODIPY 6 and BODIPY 6.6 were shown to induce cell death upon irradiation. BODIPY 6 did not show any considerable cell death in the dark toxicity study, where the IC50 was not defined for both HaCat and Mel-1 cell lines. However, after the irradiation of cells, there was significant cell mortality for HaCat cells, but the IC50 was not defined because the efficacy of PSs to kill cancer cells was significantly high. As a result, the viability of cells was recorded below 20% respectively. The half-maximal

inhibitory concentration (IC50) for Mel-1 was recorded to be at 0.68 for BODIPY 6.6 alone and nanoconjugates were at 0.27 μM respectively. Moreover, BODIPY 6.6 showed some toxicity on HaCat cell lines with the IC50 at 0.52 μM. Furthermore, the nanoconjugates did not demonstrate any dark toxicity on HaCat and Mel-1 cell lines. However, upon irradiation, there was a noticeable photothermal activity on Mel-1 cells with IC50 at 0.47 μM respectively. This study demonstrated that more work needs to be done concerning the use of Pt NRs as drug carriers. The study showed that the novel BODIPY PSs demonstrated the potential to be used for the inhibition of Melanoma cell lines. Moreover, the functionalization of BODIPY PSs through the utilization of the acid chloride and amine (to form amide bond linker) showed a negligible effect on the photosensitization of these compounds. Therefore, a direct heavy atom functionalization should be considered when functionalizing BODIPY PSs.

Table 6.5 IC50 of BODIPY PSs

IC50 no Irradiation				
Compounds				
Cell Type	**BDP 6**	**BDP 6-NR**	**BDP 6.6**	**BDP 6.6-NR**
HaCat	*	*	0.52	*
Mel-1	*	*	*	*
IC50 1J/cm^2 Irradiated cells				
HaCat	*	*	*	*
Mel-1	0.68	0.27	*	0.47

* Not Defined

6.3 Discussion

This study demonstrates the possibility of using BODIPY PSs derivatives as an adjuvant in PDT against pigmented UCT Mel-1 and HaCat cells. The use of BODIPY PSs as agents for melanoma cell inhibition is still a new one; more studies need to be carried out to investigate the potential of BODIPY PSs as candidates for melanoma cell photomortality. A review study by Naidoo *et al*., (2018) tabled a list of therapeutic PSs and their nanoconjugates used in a PDT study of melanoma cell lines and other cancers. This study demonstrated a need to explore further therapeutic agents like BODIPY PSs as potential drugs that can be used for melanoma photo-chemotherapy. The group outlined the therapeutic agents that are clinically approved as well as others that are still investigated for PDT application of melanoma cell lines. Therefore, in this study, I demonstrated a preliminary study to show that BODIPY PSs can be applied for

the photodynamic therapy of metastatic melanoma cell lines. Another study done by Fraix and co-workers (2018) demonstrated photoactivable bimodal chromophoric conjugates. The bimodal framework was a combination of a BODIPY and aniline derivatives as nitric oxide photo donors which showed enhanced phototoxicity on melanoma cancer cell lines (Lazzarato *et al*., 2019). A similar study conducted by Ozdemir and co-workers (2016) also demonstrated that meso-acetyl substituted BODIPY with diiodo groups at 2,6-β positions can readily be embedded in the lipid membrane of Hela cells and it efficiently induced light-dependent apoptotic cell death even at nanomolar concentrations. This study showed the efficiency of BODIPY PSs as potential agents for PDT photomortality of melanoma cell lines even at concentrations less than 3 μM of BODIPY 6. However, there was no statistical significance when compared with Hypericin at the same concentration p-value 0.40 and 0.37. The Pt nanorods (NRs) as drug carriers is a novel one and the nano-vehicles demonstrated efficient drug delivery and enhanced drug phototoxicity of BODIPY PSs on cell lines after irradiation with a very low light dose of 1 J/cm^2 respectively.

BODIPY 6 demonstrated amplified phototoxicity on the HaCat cell line at 0.7 and 3 μM concentrations compared to its counterpart BODIPY 6.6.4 and hypericin. UCT Mel-1 cells at this concentration demonstrated some resistance with cell viability inhibition of 56% which is not far compared to that of hypericin which demonstrated cell viability of 46% cell viability inhibition at 3 μM. Furthermore, it was shown that increasing iodine moieties through benzene iodo-functionalized moiety conjugated through amide bridge did not enhance the phototoxicity of the BODIPY PSs as hypothesized in this study. This may be attributed to the carbonyl effect (the amide linker) which reduces the triplet photosensitization of the BODIPY PSs (Zou et al., 2016, 2017). Also, it was found that extending heavy atoms on the BODIPY PSs leads to self-quenching of ROS production hence reduced phototoxicity (Zou *et al*., 2016, 2017). This reduction may also be explained by the blue auto-fluorescence that was suggested as a possible mechanism (in chapter 4 sections 4.25 during the functionalization of BODIPY 6.6.4). Therefore, the functionalization of BODIPY PSs plays a vital role in the phototoxicity of BODIPY PSs. Similar observations were made on phototoxicity of BODIPY PSs on microorganisms, where fungal strains experienced induced cell death in comparative micromolar concentrations. These results confirm that the synthesized BODIPY PSs have little to no toxicity on cancer cells and normal HaCat cells when they are not activated with light. This is desirable for the PDT application.

6.4 Significance of the results

The data obtained from this study demonstrate that BODIPY PSs can inhibit the growth of melanoma cancer cells. This preliminary study has shown that BODIPY 6 PSs at concentrations as low as 1 μM, can induce cell death upon irradiation. In practical terms, these photosensitizers can be utilized as therapeutic agents for the treatment of Melanoma cancers. However, due to their absorption of light in the visible range of the spectrum, their intravenous use is compromised because they cannot find application in deep-seated tumors due to their short excitation wavelength (Tian *et al*., 2019). Moreover, because these PSs are fairly soluble in aqueous solutions, they may find possible use for PDT applications of skin tumors. These PSs can be used as a rubbing gel that can be applied to tumor cells and allow absorption and adsorption before irradiation (PDT). More studies have to be carried out to identify functionalization methods that will enable shifting the absorption spectrum towards the red region of the visible spectrum.

6.5 Conclusion

BODIPY PSs offer many advantageous characteristics including chemical and optical properties for their application as agents for therapeutic application on cancers. In this study, a novel approach was demonstrated for the successful application of BODIPY derivatives and their Pt-NRs nanoconjugates for photosensitization of the UCT Mel-1 cancer cells and HaCat cell lines. This study demonstrated the role of functional groups in facilitating ISC and triplet state photosensitization of BODIPY PSs that can be enhanced through direct functionalization of heavy atoms to the BODIPY chromophore structure. BODIPY 6 demonstrated that it may be a potential Mel-1 cancer cell photosensitizer for PDT application. Furthermore, both BODIPYs and nanoconjugates did not show any cytotoxicity effects on cells without irradiation (dark toxicity). This suggests that they may be applied for PDT of metastatic melanoma cell lines. In contrast, BODIPY 6 was demonstrated to have comparative efficiency on Mel-1 photomortality to that of hypericin. However, increasing the halogen and π-conjugation through an amide bond on BODIPY 6.6 is inefficient in enhancing the cytotoxicity effects of the cells under this study. This is because the extended π-conjugation tends to result in little to moderate production of ROS (Kue *et al*. 2018). Furthermore, extended iodine moiety on BODIPY PSs results in the heavy-atom competition which leads to less ROS production (Kue *et al*., 2018). Moreover, the study demonstrated that there was more cytotoxicity on HaCat cell lines compared to that of Mel-1 cancer cell lines.

6.6 References

Alderton G.K, 2015; Metastasis: Spreading the seed. *Nat Rev Cancer*, 15(5): 255.

Allen D.C., 2013; Non-melanocytic skin carcinoma. In: Cameron IR, Morton M, Bolesworth J, Schad B, eds. Histopathology reporting. London, England: *Springer*; 2013:197-206.

Amendoeira A., García L.R., Fernandes A.R, and Baptista P.V., 2019; Light irradiation of gold nanoparticles toward advanced cancer therapeutics. *Adv. Therap*., 3(1): 1900153, 1-11.

Banfi S., Caruso E., Zaza S., Mancini M., Gariboldi M.B. and Monti E., 2012; Synthesis and photodynamic activity of a panel of BODIPY dyes. *J. Photochem. Photobiol. B: Biology,* 114(): 52-60.

Bastian B.C., 2014; The Molecular Pathology of Melanoma: An integrated taxonomy of melanocytic neoplasia. *Annu. Rev. Pathol. Mech. Dis*., 9(1): 239-271.

Carlson J.A., Ross J.S., Slominski A., et al., 2005; Molecular diagnostics in melanoma. *J. Am. Acad. Dermatol*., 52(1): 743-75.

Chudnovsky Y., Khavari P.A., Adams A.E., 2005; Melanoma genetics and the development of rational therapeutics, *J. Clin. Invest*., 115(1): 813-24.

Davids L.M. and Kleemann B., 2011; Combating melanoma: The use of photodynamic therapy as a novel, adjuvant therapeutic tool, *Canc. Treatment Rev*., 37(1): 465-475.

Davids L.M., Kleemann B., Cooper S., and Kidson S.H., 2009; Melanomas display increased cytoprotection to Hypericin-Mediated cytotoxicity through the induction of autophagy, *Cell Biol. Int*., 33(10): 1065-1072.

DeSantis C.E, Lin C.C, Mariotto A.B, Siegel R.L., Stein K.D., Kramer J.L., Alteri R., Robbins A.S., and Jemal A., 2014; Cancer treatment and survivorship statistics, 2014, *CA Cancer J Clin*., 64(4): 252-271.

Eggermont A.M.M, Chiarion-Sileni V., Grob J.J., Dummer R., Wolchok J.D., Schmidt H., Hamid O., Robert C., Ascierto P.A., Richards J.M., Lebbé C., Ferraresi V., Smylie M., Weber J.S., Maio M., Konto C., Hoos A., de Pril V., Gurunath R.K., de Schaetzen G., Suciu S., Testori A., 2014; Adjuvant ipilimumab versus placebo after complete resection of high-risk stage III melanoma (EORTC 18071): A randomized, double-blind, phase 3 trial, 16(5):522-530.

Esserman L.J., Thompson I.M., Reid B., Nelson P., Ransohoff D.F., Welch H.G., Hwang S., Berry D.A., Kinzler K.W., Black W.C., Bissell M., Parnes H., Srivastava S., 2014; Addressing overdiagnosis and overtreatment in cancer: A prescription for change, *Lancet Oncol*., 15(6): 234-242.

Fraix A., and Sortino S., 2018; Combination of PDT photosensitizers with NO-photodonors. *Photochem. Photobiol. Sci*., 17(1): 1709-1727.

Garbe C. and Blum A., 2001; Epidemiology of cutaneous melanoma in Germany and worldwide. *Skin Pharmacol. Appl. Skin. Physiol*., 14(5): 280-290.

Gibbs J.H., Robins L/T., Zhou Z., Bobadova-Parvanova P., Cottam M., McCandless G.T., Fronczek F.R., and Vicente M.G.H., 2013; Spectroscopic, computational modeling and cytotoxicity of a series of meso-phenyl and meso-thienyl-BODIPYs. *Bioorg. Med. Chem*., 21(18): 5770-5781.

Guimarães I.S., Daltoé R.D., Herlinger A.L., Madeira K.P., Ladislau T., Valadão I.C., Junior P.C.L.M., Teixeira S.F., Amorim G.M., dos Santos D.Z., Demuth K.R., and Rangel L.B.A., 2013; Conventional cancer treatment. In: Cancer Treatment-Conventional and Innovative Approaches: In Tech. London, England: *InTechOpen Limited*; 2013.

Helmbach H., Rossmann E., Kern M.A., Schadendorf D., 2001; Drug-resistance in human melanoma. *Int. J. Cancer*., 93(5): 617-622.

Jayaraman S.S, Rayhan D.J, Hazany S., Kolodney M.S, 2014; Mutational landscape of basal cell carcinomas by whole-exome sequencing. *J. Invest. Dermatol*., 134(1): 213-220.

Jhappan C., Noonan F.P., and Merlino G., 2003; Ultraviolet radiation and cutaneous malignant melanoma. *Oncogene*, 22(20): 3099-3112.

Kamkaew A., Lim S.H., Lee H.B., Kiew L.V., Chung L.Y., and Burgess K., 2013; BODIPY dyes in photodynamic therapy. *Chem. Soc. Rev*., 42(1): 77-88.

Kleemann B., Loos B., Scriba T.J, Lang D. and Davids L.M., 2014; St John's Wort (Hypericum perforatum L.) photomedicine: Hypericin-photodynamic therapy induces metastatic melanoma cell death, *PloS ONE*, 9(7): e103762.

Kue C.S., NG S.Y., Voon S.H., Kamkaew A., Chung L.Y., Kiew L.V., and Lee H.B., 2018; Recent strategies to improve boron dipyrromethene (BODIPY) for photodynamic cancer therapy: an updated review. *Photochem. Photobiolo. Sci*., 11(1): 1-48.

Kuphal S. and Bosserhoff A., 2009; Recent progress in understanding the pathology of malignant melanoma, *J. Pathol*., 219(4): 400-409.

Lazzarato L., Gazzano E., Blangetti M., Fraix A., Sodano F., Picone G.M., Fruttero R., Gasco A., Riganti C., and Sortino S., 2019; Combination of PDT and NOPDT with a tailored BODIPY derivative. *Antioxidants*, 8(1): 531.

Martin T.A, Ye L., Sanders A.J, Lane J., and Jiang W.G., 2013; Cancer invasion and metastasis: a molecular and cellular perspective. In: Jandial R, ed. *Madame Curie Bioscience Database*. Austin, TX: *Landes Bioscience*; 2013. https://www.ncbi.nlm.nih.gov/books/ NBK164700/.

Moncrieff M.D., Martin R., O'Brien C.J., Shannon K.F., Clark J.R., Gao K., McCarthy W.M., and Thompson J.F., 2008; Adjuvant postoperative radiotherapy to the cervical lymph nodes in cutaneous melanoma: is there any benefit for high-risk patients? *Ann. Surg. Oncol*., 15(11): 3022-3027.

Naidoo C., Kruger C.A, and Abrahamse H., 2018; Photodynamic therapy for metastatic melanoma treatment: A Review, *Technol. Cancer Research and Treatment*, 17(1): 1-15.

Oppermann M., Geilen C.C., Fecker L.F., Gillissen B., Daniel P.T., Eberle J., 2005; independent induction of apoptosis in human melanoma cells by the proapoptotic Bcl-2-related protein Nbk/Bik. *Oncogene*, 24(49): 7369-7380.

Ossio R., Roldán-Marín R., Martínez-Said H., Adams D.J. and Robles-Espinoza C.D., 2017; Melanoma: A global perspective. *Nat. Rev. Cancer*, 17(7): 393-394.

Ozdemir T., Bila J.L., Sozmen F., Yildirim L.T., Akkaya E.U., 2016; Orthogonal BODIPY trimers as photosensitizers for photodynamic action. *Org. Lett*., 18(1): 4821-4823.

Shain A.H. and Bastian B.C., 2016; From Melanocytes to Melanomas. *Nat. Rev. Cancer*, 16(1): 345-358.

Sharma K.V. and Davids L.M., 2012; Depigmentation in melanomas increases the efficacy of hypericin-mediated photodynamic-induced cell death. *Photodiag. Photodyn. Therapy*, 9(2): 156-163.

Siegel R.L, Miller K.D, and Jemal A., 2016; Cancer Statistics, 2016. *CA Cancer J Clin*., 66(1): 7-30.

Slominski A., Tobin D.J., Shibahara S., Wortsman J.., 2004; Melanin pigmentation in mammalian skin and its hormonal regulation. *Physiol. Rev*., 84(1): 1155-1228.

Soengas M.S and Lowe S.W, 2003; Apoptosis and melanoma chemoresistance. *Oncogene*, 22(1): 3138-3151.

Swavey S., and Tran M., 2013; Porphyrin and phthalocyanine photosensitizers as PDT agents: A new modality for the treatment of melanoma, *In Tech*., Recent Advances in the Biology, Therapy and Management of Melanoma, 253-282.

Thompson J.F., Scolyer R.A., Kefford R.F., 2005; Cutaneous Melanoma, *Lancet*, 365(9460): 687-701.

Tian R., Sun W., Li M., Long S., Li M., Fan J., Guo L., and Peng X., 2019; Development of a novel anti-tumor theranostic platform: a near-infrared molecular upconversion sensitizer for deep-seated cancer photodynamic therapy. *Chem. Sci*., 10(1): 10106.

Yin Ng S., Kamkaew A., Fu N., Kue C.S., Chung L.Y., Kiew L.V., Wittayakun J., Burgess K., Lee H.B., 2020; Active targeted ligand Aza-BODIPY conjugation for NIR photodynamic therapy in melanoma. *Int. J. Pharma.*, 119181.

Wilcken N., 2016; The 'enablers': inhibitors of mTOR, PI3K and CDK that prolong endocrine sensitivity. *Cancer Forum*, 40(3): 16-19.

Yamamura H., Ugawa S., Ueda T., Morita A., Shimada S.., 2008; TRPM8 activation suppresses cellular viability in human melanoma. *Am. J. Physiol. Cell Physiol*., 295(2): C296-301.

Zbytek B., Carlson J.A., Granese J., Ross J., Mihm M.C., Slominski J.., 2008; Current concepts of metastasis in melanoma. *Expert Rev Dermatol*., 3(1): 569-585.

Zhou Z., Song J., Nie L., and Chen X., 2016; Reactive oxygen species generating systems meeting challenges of photodynamic cancer therapy. *Chem Soc Rev*., 45(23): 6597-6626.

Zou J., Yin Z., Ding K., Tang Q., Li J., Si W., Shao J., Zhang Q., Huang W., and Dong X., 2017; BODIPY derivatives for photodynamic therapy: influence of configuration versus heavy atom effect. *ACS Appl. Mater. Interfaces*, 9(1): 32475-32481.

CHAPTER 7

Limitations, Conclusion and Recommendations

7.1 Study limitations

The limitations that were encountered during this study are centered on the limited access to resources. The study on the cytotoxicity could have been explored further by running flow cytometry studies and confocal microscopy. Furthermore, it would have been better if the study was centered on the dose-dependent efficiency to understand the most effective concentration concerning cancer cell-killing potential. Also, financial constraints took to play in the limitation to be able to run further studies which hindered further investigation.

7.2 Conclusion

BODIPY PSs were synthesized and characterized and their structural elucidation was successfully carried out (section 4.3.1 to 43.4) of the results chapter 4. The BODIPY PSs with other specified functional groups showed negligible to no phototoxicity towards microbial species. Among all the studied PSs, BODIPY 6 showed high activity towards bacteria and fungi cell killing capacity. These activities can be attributed to the presence of iodine on the BODIPY structure which is known for the promotion of singlet oxygen production and/or other oxygen species that facilitate cell mortality. However, BODIPY 6.6 with extended iodine functional groups did not show the intended activity. The cell mortality was 92% against bacteria and fungi. The excess purification method with a column chromatography reduced the efficacy of these drugs. Preliminary studies carried out on the pigmented UCT Mel-1 and normal HaCat cells showed that BODIPY 6 PSs have limited to no effect on dark toxicity with cell mortality <10%. However, BODIPY 6.6 was shown to have many aggressive effects on normal cells with or without light irradiation. Furthermore, BODIPY 6 showed no significant statistical difference (p-value 0.40) in photodynamic anticancer capacity when compared to hypericin. Upon, irradiation the study observed that the IC50 for BODIPY 6 against Mel-1 cells was < 0.7 µM which showed better activity than hypericin. While on the other hand BODIPY 6.6 showed a significant difference (p-value 0.0075), these results were not anticipated, however, it was reported that extended heavy atom functionalization quenches the cell-killing capacity as discussed in section 6.3.

Platinum (Pt)-based nano-conjugates resulted in increased activity of the PSs. This suggests that there was drug availability, drug bioaccumulation in cells, enhanced reactive oxygen

species production, less toxicity without light, and enhanced solubility from the use of nano-conjugates. All these attributes were highly desired for the success of this study. In conclusion, these BODIPY PSs can find use as anti-microbial as well as anti-cancer agents for photodynamic therapy applications in the future.

7.3 Recommendations and future studies on BODIPY photomortality of Bacterial, Fungal, and UCT Mel-1 cancer cell lines

In the future perspective of the study on the microorganisms, it would be interesting to study the percentage death and the time is taken to kill using a quantitative analysis on BODIPY PSs. These quantities of microorganisms can be determined by counting colony-forming units (cfu).

The mode of action of the BODIPY PSs in the antimicrobial activity can also be studied.

It is also recommended to study the effect of pH on the activity of the BODIPY PSs to understand the photochemical conditions that will enhance photomortality as well as the cell interaction with the drugs.

It is recommended that future studies should focus on investigating the dose-dependent (serial dilution) relationship between the Mel-1 cells and drug concentrations, this will help determine the optimum working concentration of the drugs.

The effective radiation dose can be further studied by looking at increasing the light dose to compare the cell mortality efficacy when increasing the light dose. This study will help optimize the reactive oxygen species generated.

A study on the cell death mechanism using flow cytometry studies should be undertaken. This will enable an understanding of whether the drugs induce apoptotic or necrotic cell death. This can be very helpful in understanding if the drugs internalize and induce nuclease disruptions or if the cells adsorb onto the cell surfaces and induce cell membrane damage. Confocal microscopy studies should also be used as this can give information on drug localization permitting conclusive observations to be drawn on whether cellular nucleases are targeted and to give imaging advantages as well.

It is further recommended to undertake a study on the identification of the photochemical species generated by PSs upon irradiation with a respective light source. This information can help in the quantification of the number of reactive oxygen species generated. To study the photodamage induced by these toxic ROS species.

APPENDICES

Appendix 1A, Mass spectra of BODIPY PSs and their isotopic patterns

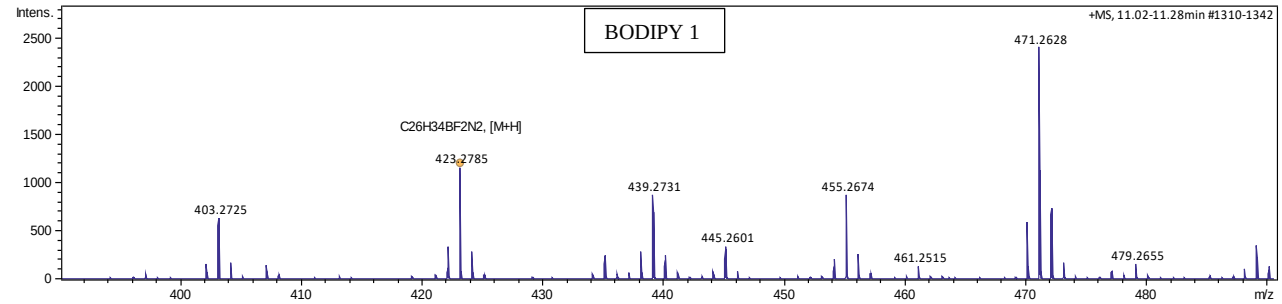

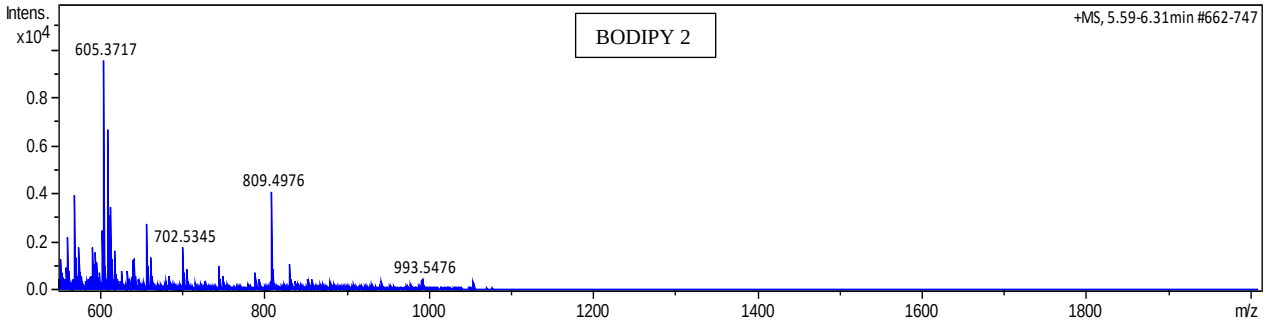

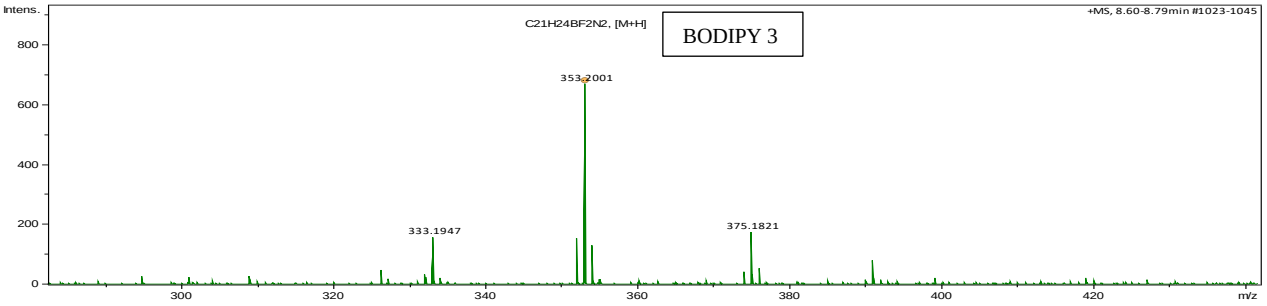

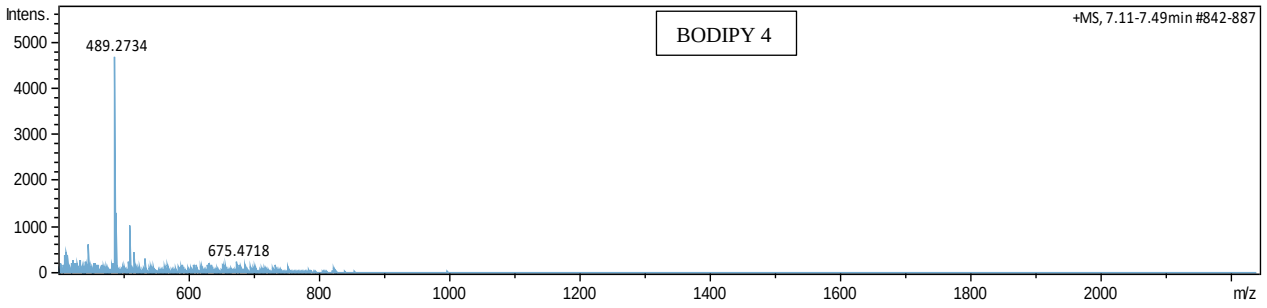

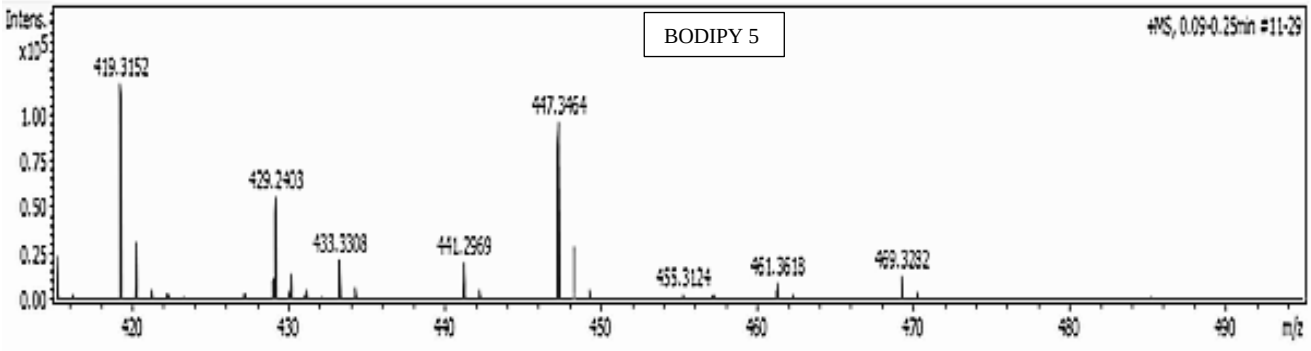

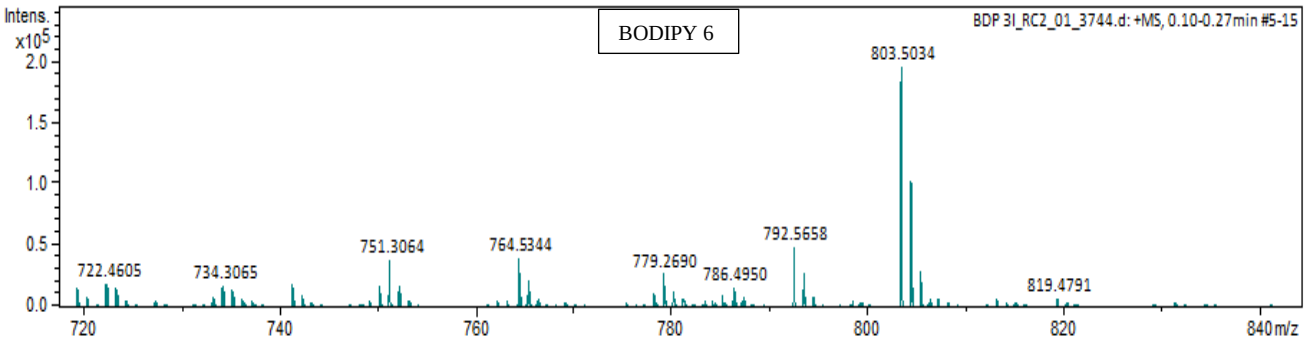
BODIPY 6
BDP 3I_RC2_01_3744.d: +MS, 0.10-0.27min #5-15
Intens.
x10^5
803.5034
792.5658
751.3064
764.5344
779.2690
786.4950
722.4605
734.3065
819.4791
m/z

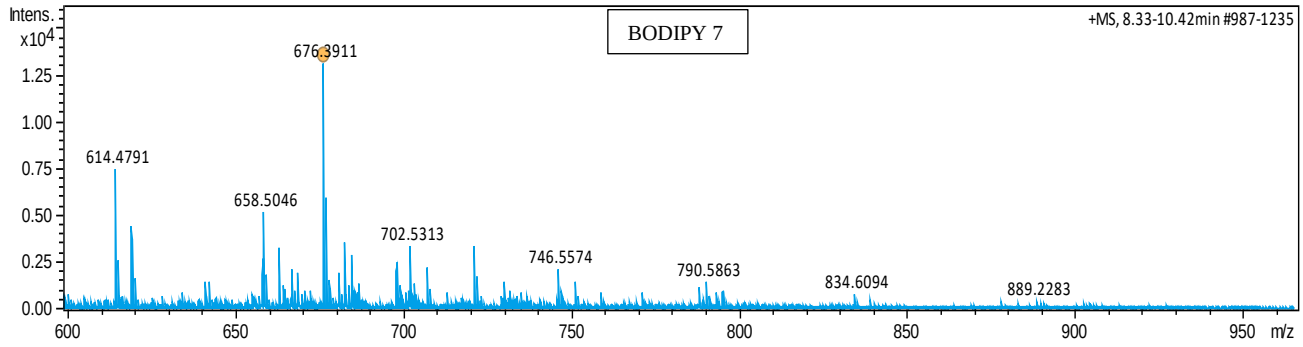
BODIPY 7
+MS, 8.33-10.42min #987-1235
Intens.
x10^4
676.3911
614.4791
658.5046
702.5313
746.5574
790.5863
834.6094
889.2283
m/z

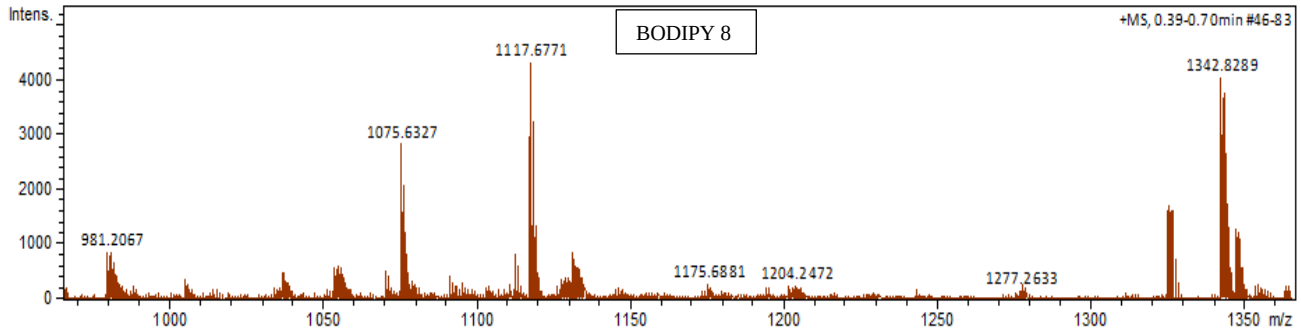
BODIPY 8
+MS, 0.39-0.70min #46-83
Intens.
1117.6771
1342.8289
1075.6327
981.2067
1175.6881
1204.2472
1277.2633
m/z

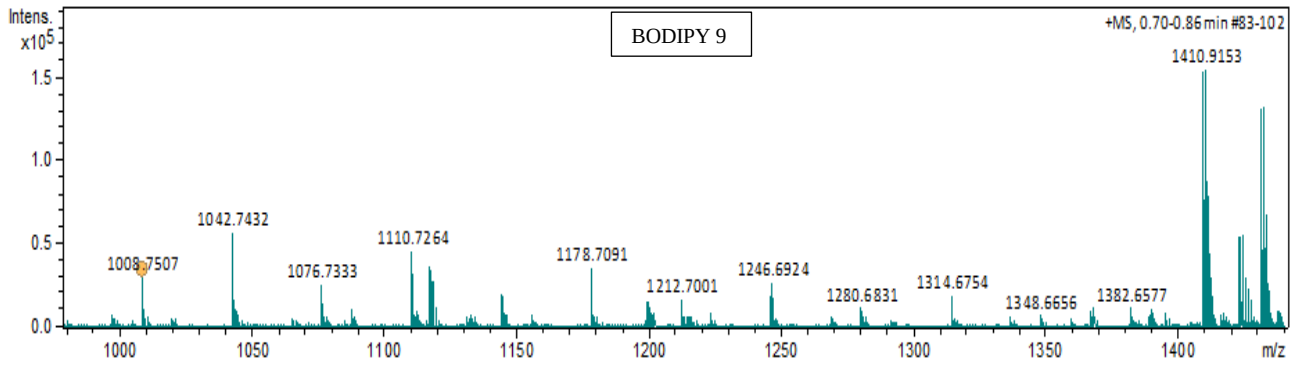
BODIPY 9
+MS, 0.70-0.86min #83-102
Intens.
x10^5
1410.9153
1042.7432
1110.7264
1178.7091
1008.7507
1076.7333
1212.7001
1246.6924
1280.6831
1314.6754
1348.6656
1382.6577
m/z

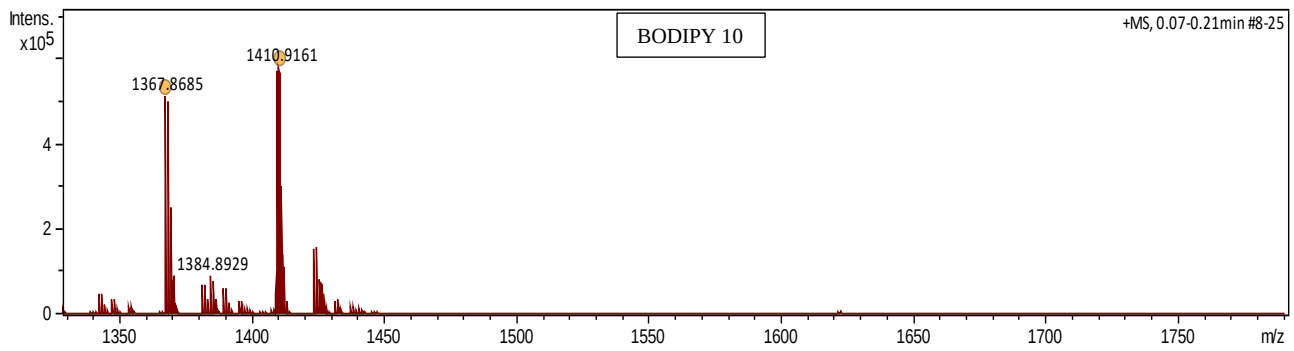
BODIPY 10
+MS, 0.07-0.21min #8-25
Intens.
x10^5
1410.9161
1367.8685
1384.8929
m/z

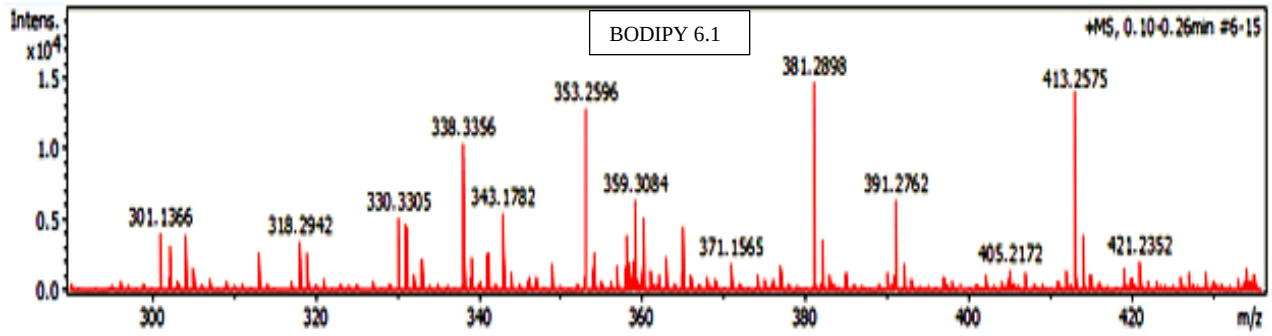
BODIPY 6.1
+MS, 0.10-0.26min #6-15
Intens.
x10^4
1.5
1.0
0.5
0.0
301.1366
318.2942
330.3305
338.3356
343.1782
353.2596
359.3084
371.1565
381.2898
391.2762
405.2172
413.2575
421.2352
300
320
340
360
380
400
420
m/z

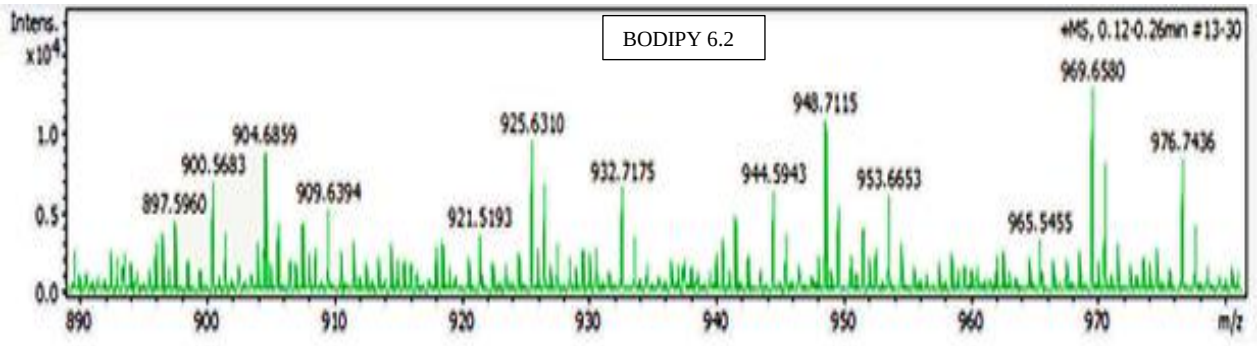
BODIPY 6.2
+MS, 0.12-0.26min #13-30
Intens.
x10^4
1.0
0.5
0.0
897.5960
900.5683
904.6859
909.6394
921.5193
925.6310
932.7175
944.5943
948.7115
953.6653
965.5455
969.6580
976.7436
890
900
910
920
930
940
950
960
970
m/z

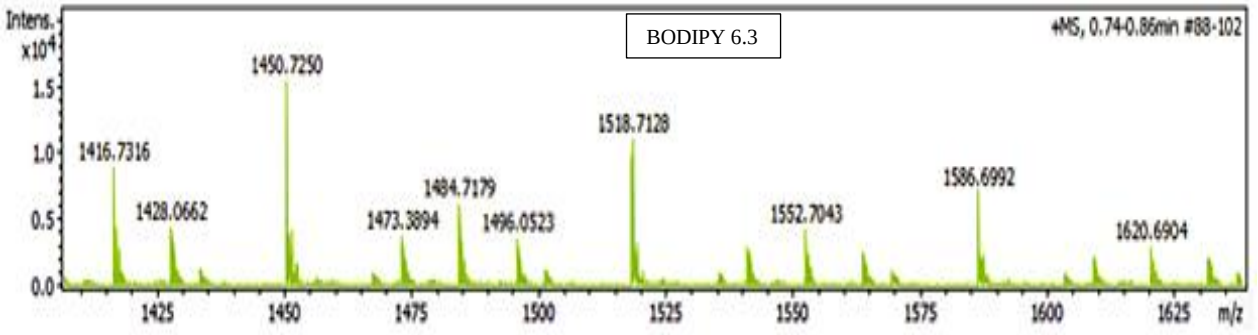
BODIPY 6.3
+MS, 0.74-0.86min #88-102
Intens.
x10^4
1.5
1.0
0.5
0.0
1416.7316
1428.0662
1450.7250
1473.3894
1484.7179
1496.0523
1518.7128
1552.7043
1586.6992
1620.6904
1425
1450
1475
1500
1525
1550
1575
1600
1625
m/z

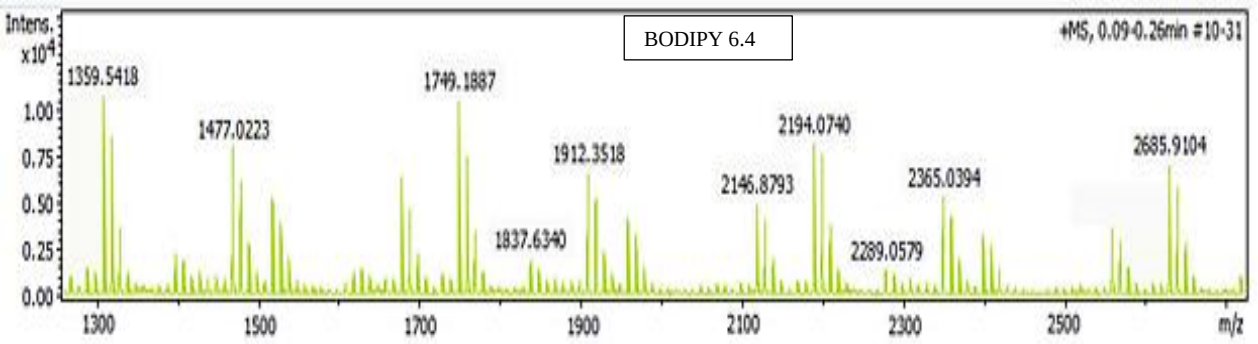
BODIPY 6.4
+MS, 0.09-0.26min #10-31
Intens.
x10^4
1.00
0.75
0.50
0.25
0.00
1359.5418
1477.0223
1749.1887
1837.6340
1912.3518
2146.8793
2194.0740
2289.0579
2365.0394
2685.9104
1300
1500
1700
1900
2100
2300
2500
m/z

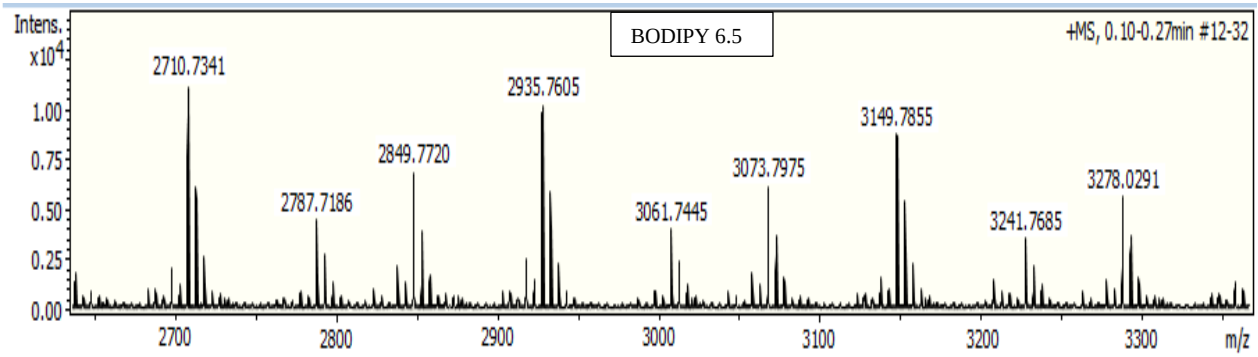
BODIPY 6.5
+MS, 0.10-0.27min #12-32
Intens.
x10^4
1.00
0.75
0.50
0.25
0.00
2710.7341
2787.7186
2849.7720
2935.7605
3061.7445
3073.7975
3149.7855
3241.7685
3278.0291
2700
2800
2900
3000
3100
3200
3300
m/z

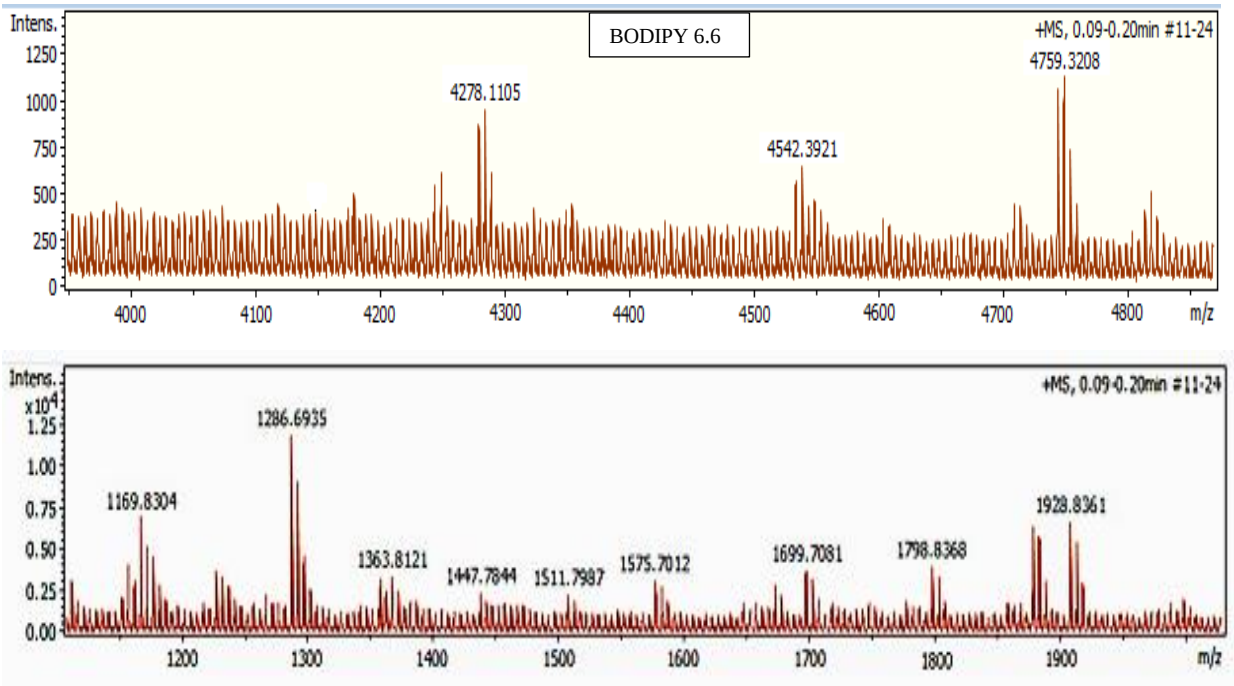

Figure 1 Mass spectra of BODIPY 1 to BODIPY 6.6, acquired in acetonitrile/water solvent mixture (concentration of 10 ppm). A positive ode was used to analyze the samples.

Appendix 1B: Mass spectrometry isotopic patterns

Figure 2 demonstrates the isotopic patterns of the synthesized BODIPY PSs. It shows the abundance of the parent peaks concerning their cleaving and/or protonation patterns. Moreover, BODIPY PSs have more abundance to undergo protonation during ESI during MS analysis. BODIPY 6.2 showed a cleaving of the iodinated phenyl functional group, this may be due to a weaker bond between the functional group and the nitrogen atom of the meso-pyrrole of the BODIPY PS. All other BODIPY PSs demonstrated desired parent peaks for the BODIPY PSs. These results are in agreement with those observed with NMR analysis and elemental analysis as shown in chapter 4 of this thesis. However, there is a need to carry out further studies with fluorine and boron NMR which will help in confirming the structures of the synthesized BODIPY in relation to the mass spectra and elemental composition of the compounds.

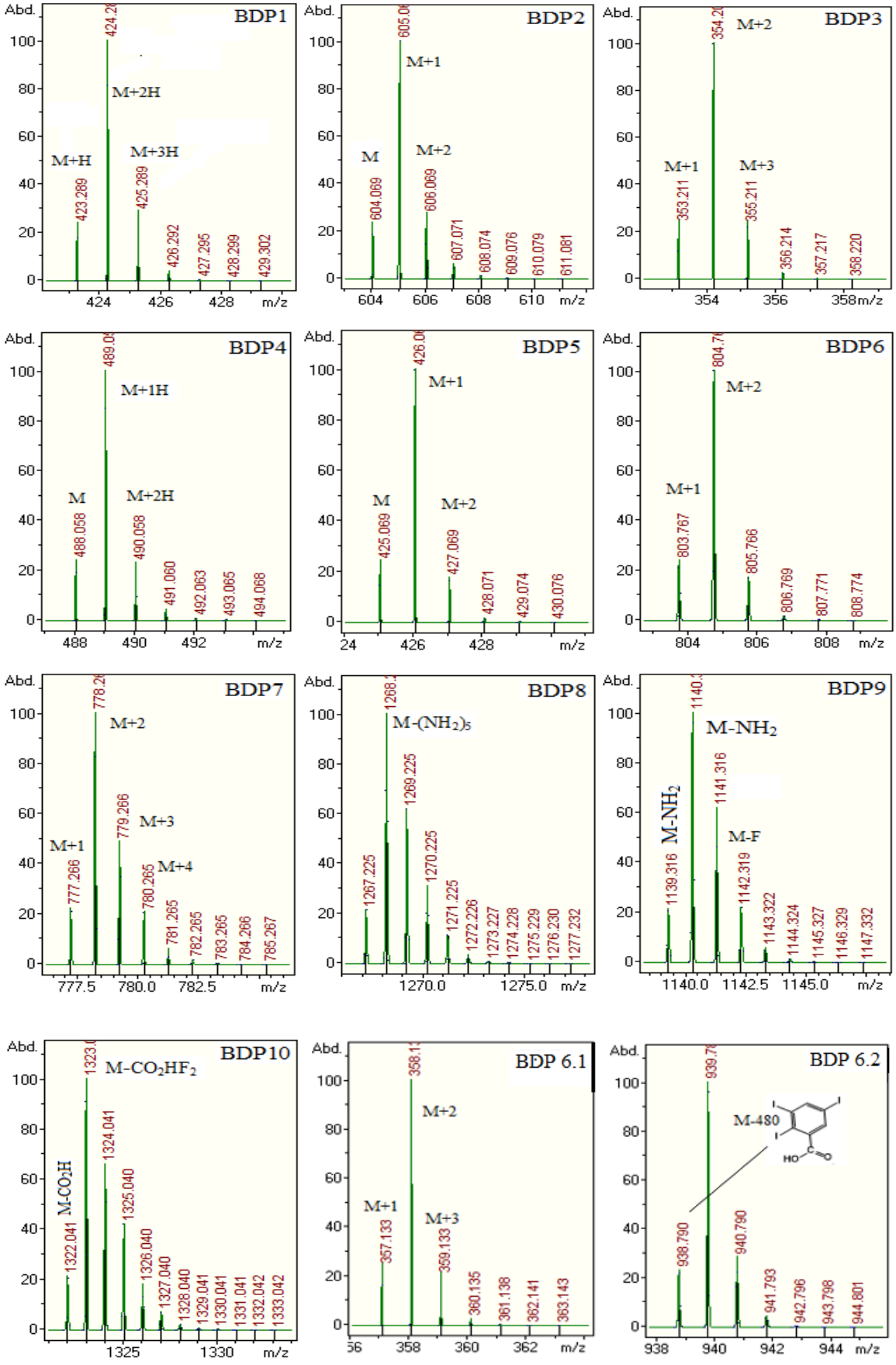
BDP1
M+H
M+2H
M+3H
423.289
424.292
425.289
426.292
427.295
428.299
429.302
BDP2
M
M+1
M+2
604.069
605.069
606.069
607.071
608.074
609.076
610.079
611.081
BDP3
M+1
M+2
M+3
353.211
354.211
355.211
356.214
357.217
358.220
BDP4
M
M+1H
M+2H
488.058
489.061
490.058
491.060
492.063
493.065
494.068
BDP5
M
M+1
M+2
425.069
426.069
427.069
428.071
429.074
430.076
BDP6
M+1
M+2
803.767
804.767
805.766
806.769
807.771
808.774
BDP7
M+1
M+2
M+3
M+4
777.266
778.269
779.266
780.265
781.265
782.265
783.265
784.266
785.267
BDP8
M-(NH2)5
1267.225
1268.228
1269.225
1270.225
1271.225
1272.226
1273.227
1274.228
1275.229
1276.230
1277.232
BDP9
M-NH2
M-NH2
M-F
1139.316
1140.319
1141.316
1142.319
1143.322
1144.324
1145.327
1146.329
1147.332
BDP10
M-CO2HF2
M-CO2H
1322.041
1323.044
1324.041
1325.040
1326.040
1327.040
1328.040
1329.041
1330.041
1331.041
1332.042
1333.042
BDP 6.1
M+1
M+2
M+3
357.133
358.136
359.133
360.135
361.138
362.141
363.143
BDP 6.2
M-480
938.790
939.793
940.790
941.793
942.796
943.798
944.801

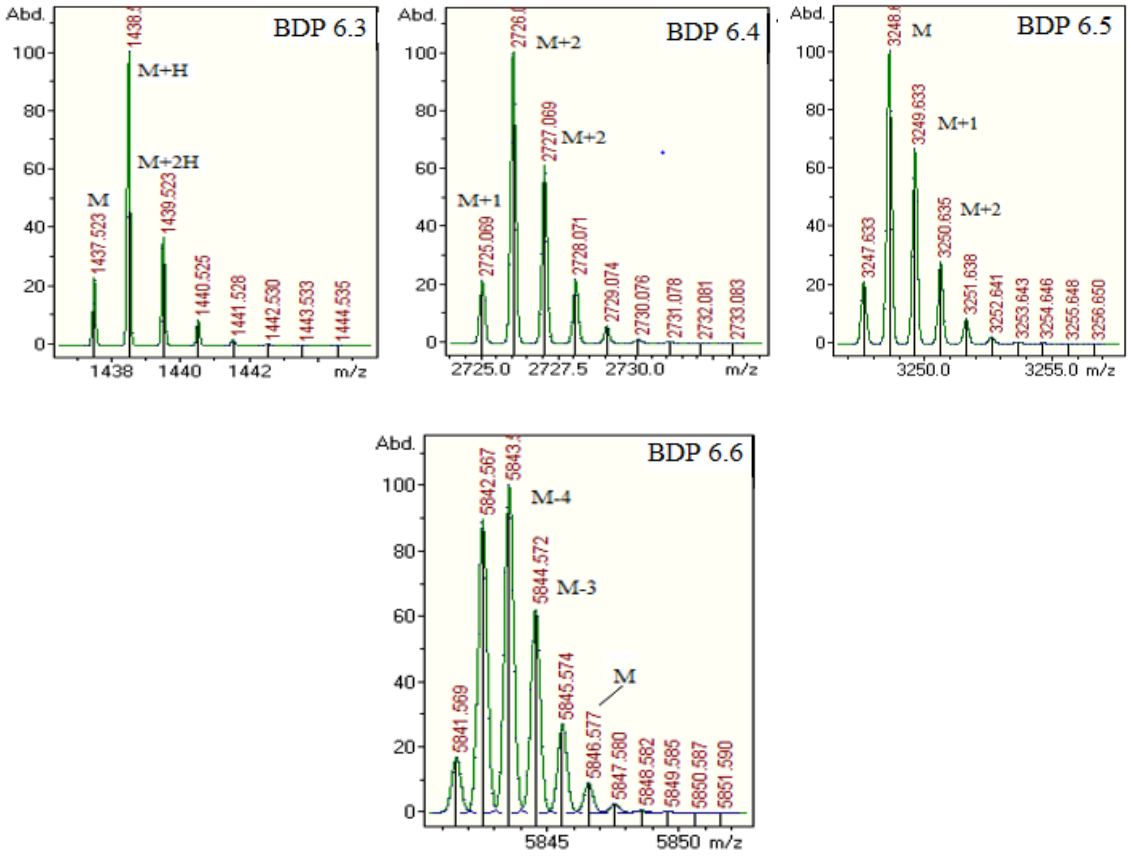

Figure 2 shows isotopic patterns of BODIPY PSs, showing the abundance of the parent peaks of the synthesized BODIPY PSs.

Appendix 2: FTIR spectra of BODIPY 1 to 10, 6.1 to 6.6 showing the vibration wavelengths of the corresponding functional groups.

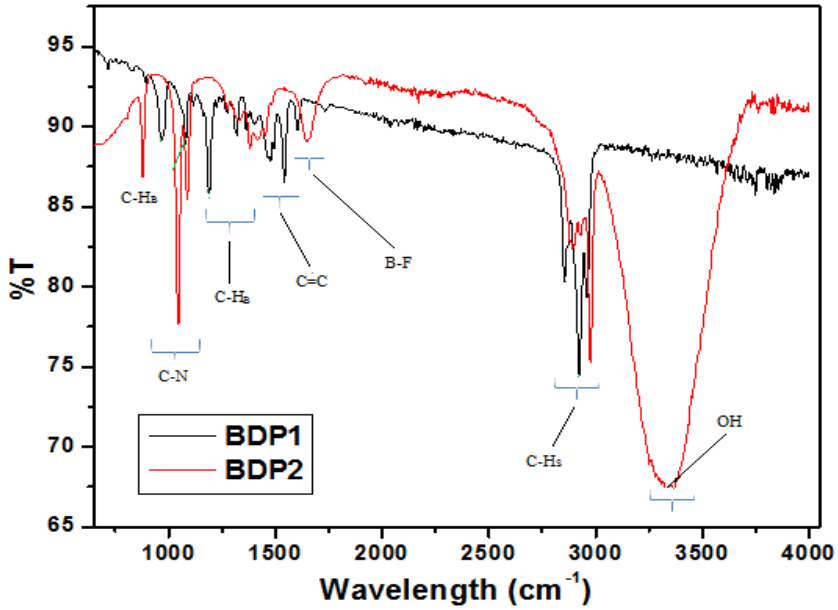

Figure 3 Vibrations of the functional groups for BODIPY 1 and BODIPY 2 acquired in methanol ATR method (concentration 2×10^{-3}M)

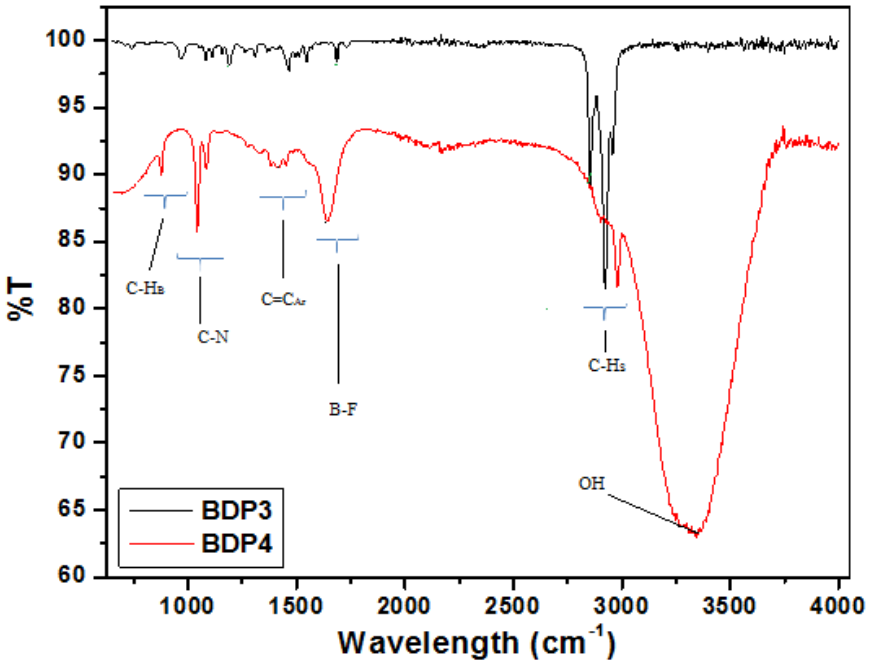

Figure 4 shows the vibrations of the functional groups for BODIPY 3 and BODIPY 4 acquired in the methanol ATR method (concentration 2×10^{-3}M)

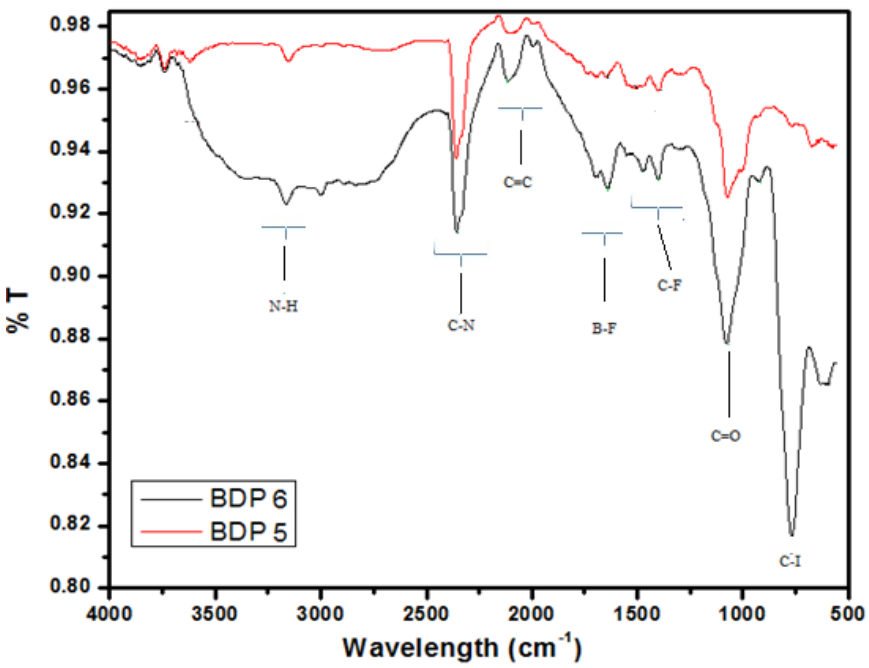

Figure 5 shows the vibrations of the functional groups for BODIPY 5 and BODIPY 6 acquired in the methanol ATR method (concentration 2×10^{-3}M)

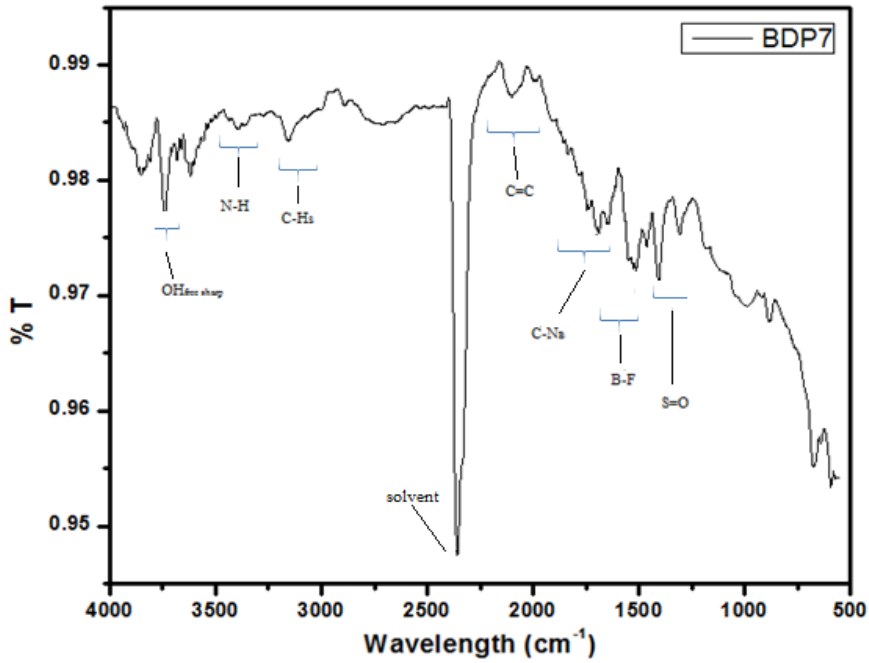

Figure 6 shows the vibrations of the functional groups for BODIPY 7 acquired in the methanol ATR method (concentration 2×10^{-3}M)

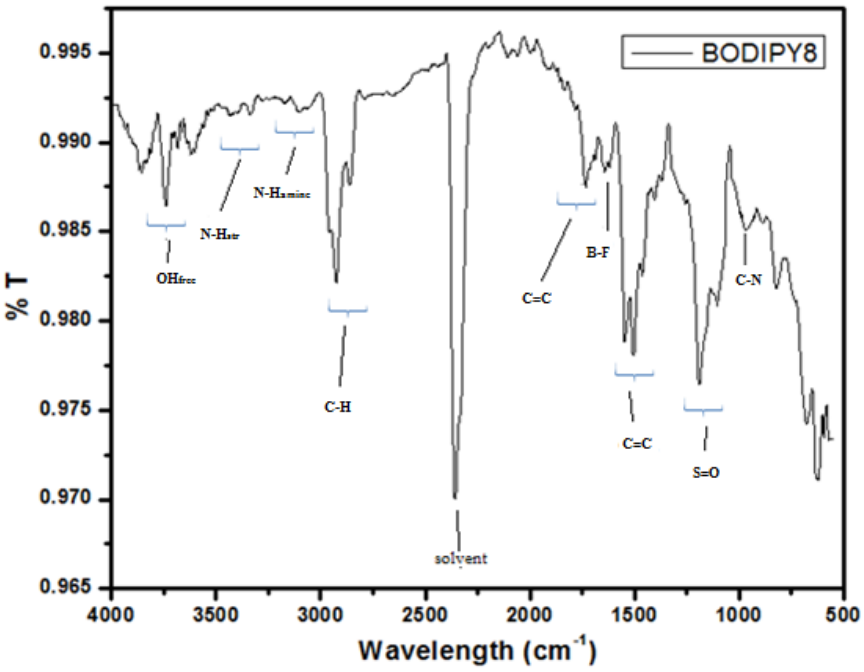

Figure 7 shows the vibrations of the functional groups for BODIPY 8 acquired in the methanol ATR method (concentration 2×10^{-3}M)

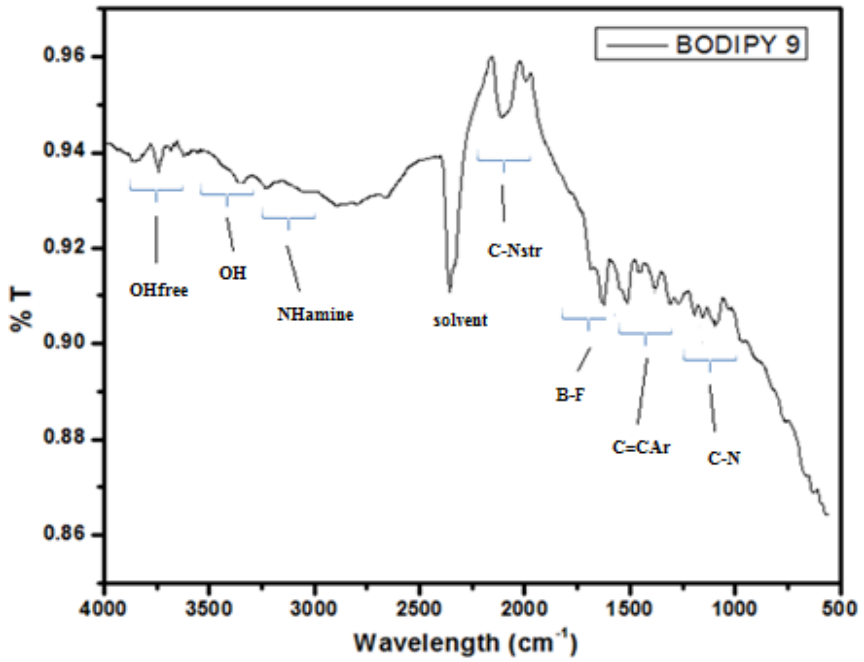

Figure 8 shows the vibrations of the functional groups for BODIPY 9 acquired in the methanol ATR method (concentration 2×10^{-3}M)

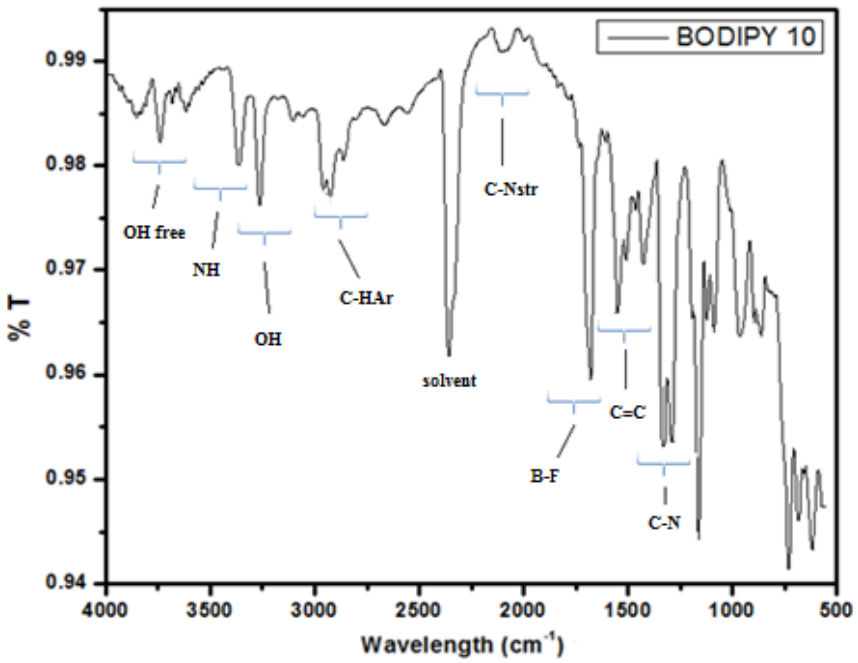

Figure 9 shows the vibrations of the functional groups for BODIPY 10 acquired in the methanol ATR method (concentration 2×10^{-3}M)

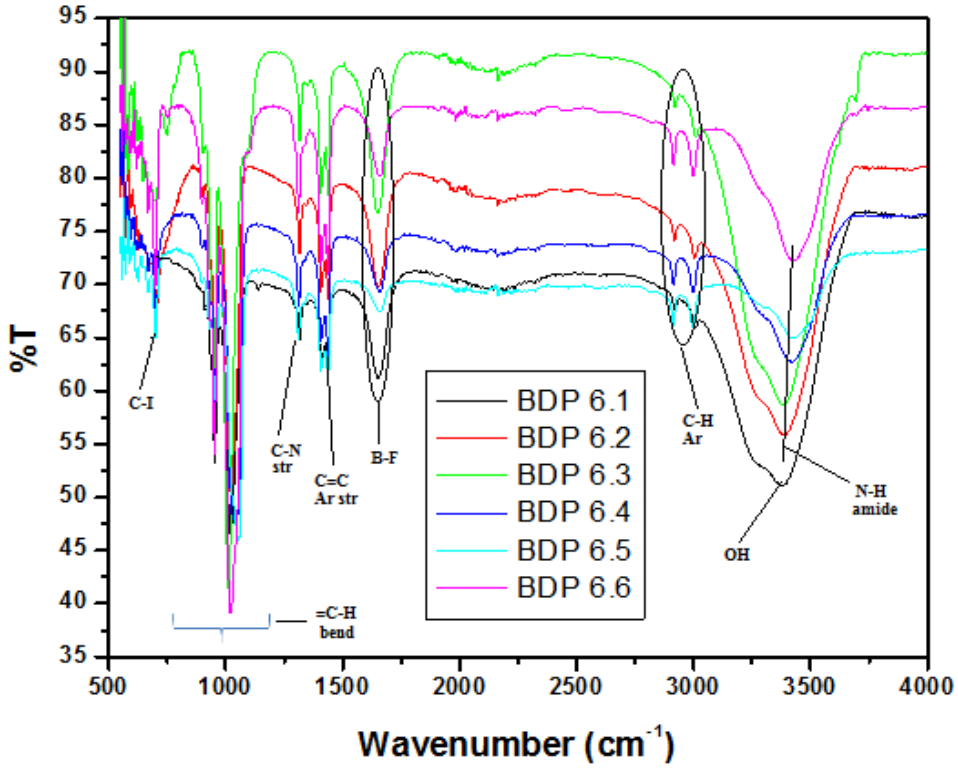

Figure 10 shows the vibrations of the functional groups for BODIPY 6.1 to BODIPY 6.6 acquired in the methanol ATR method (concentration 2×10^{-3}M)

Appendix 3: Nuclear Magnetic Resonance Spectroscopy

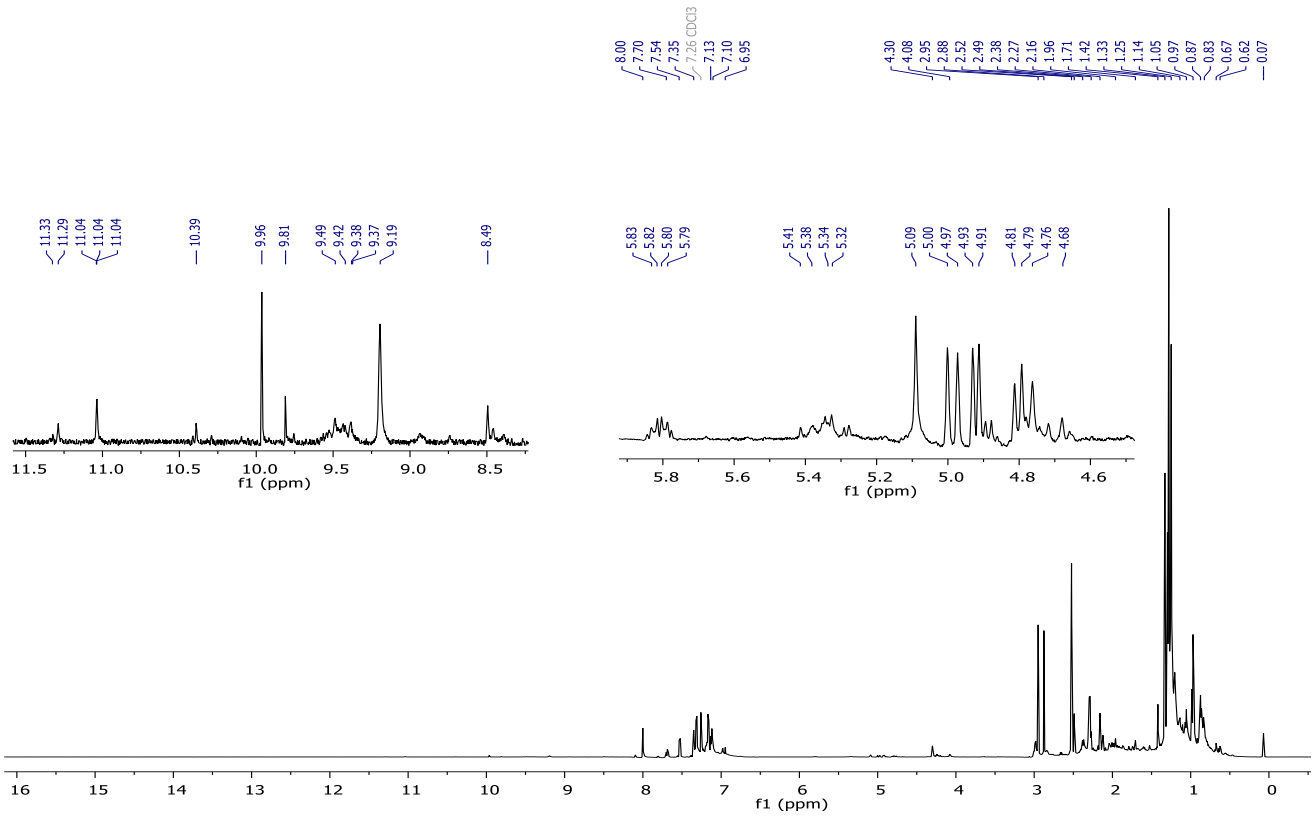

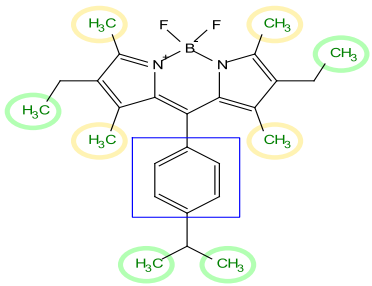

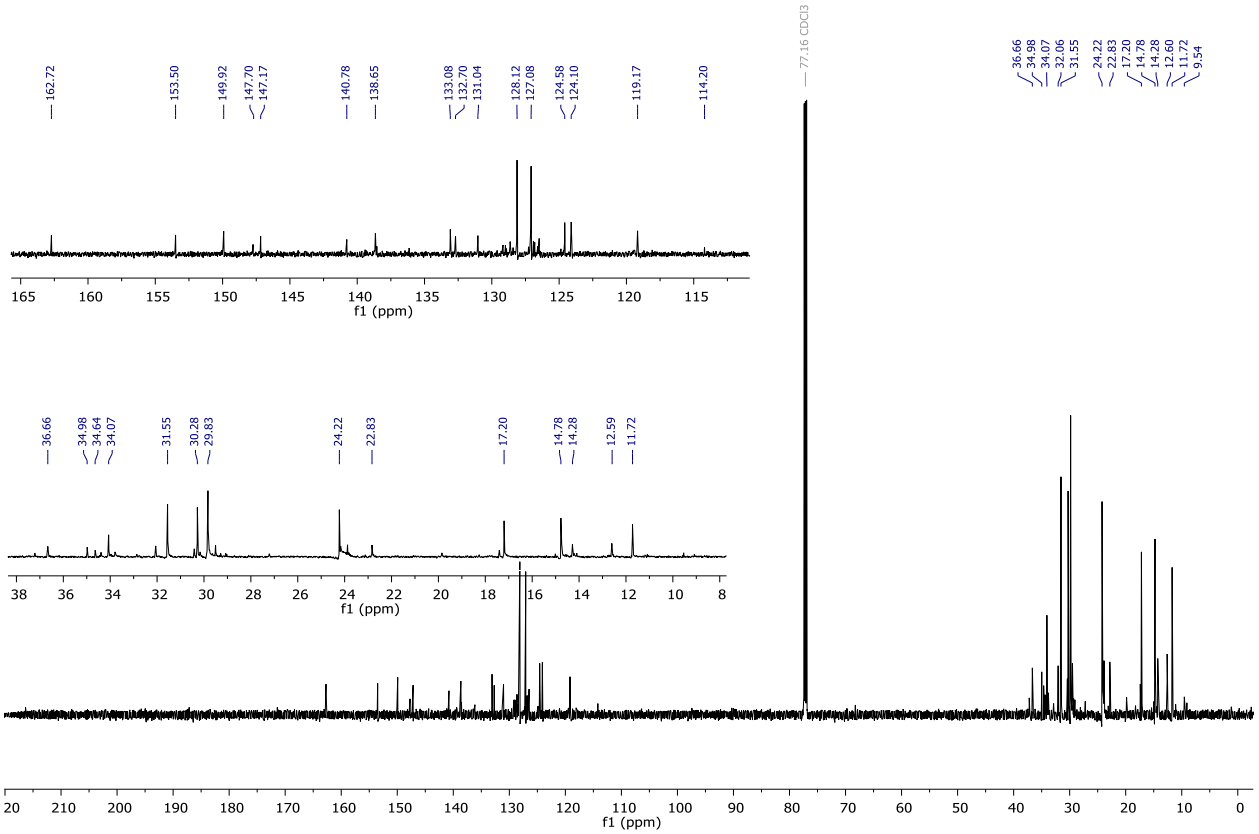

Figure 11 ^{1}H and ^{13}C NMR of BODIPY 1

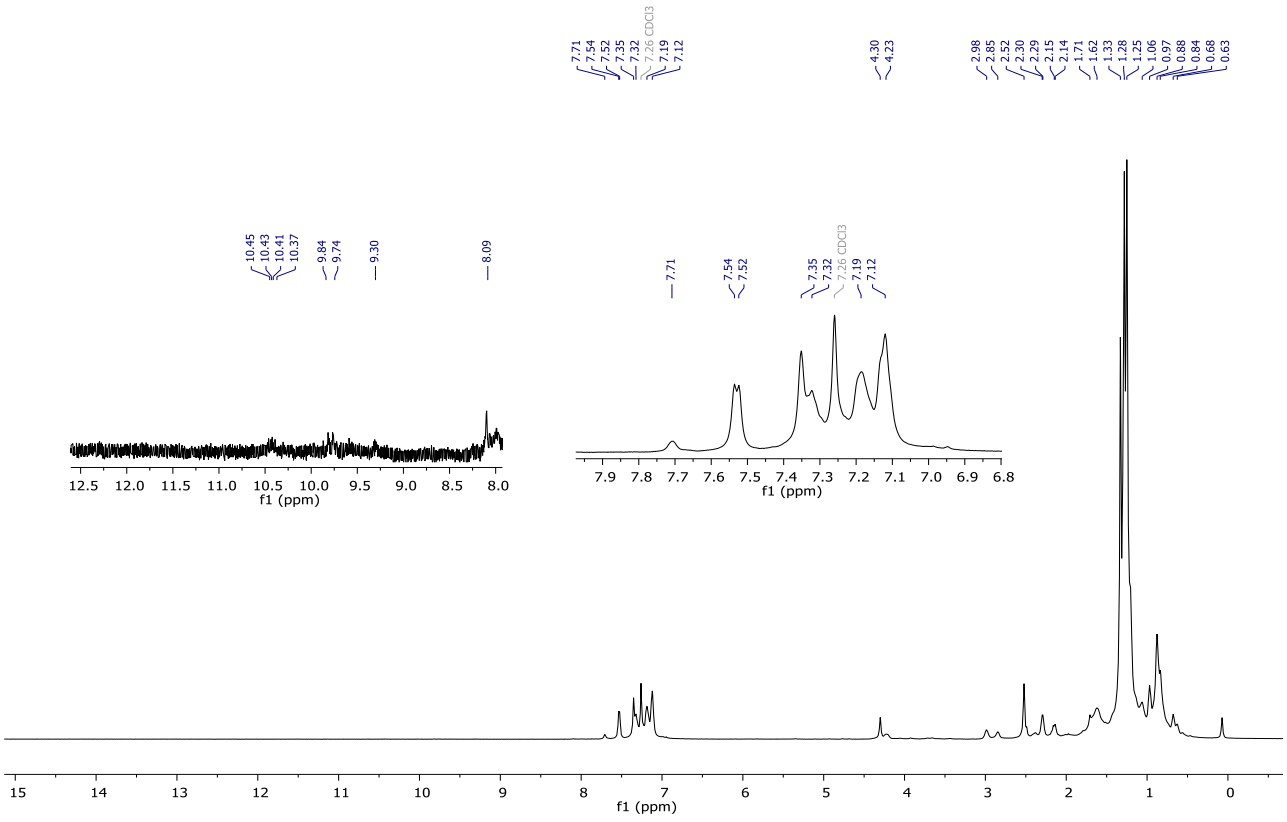

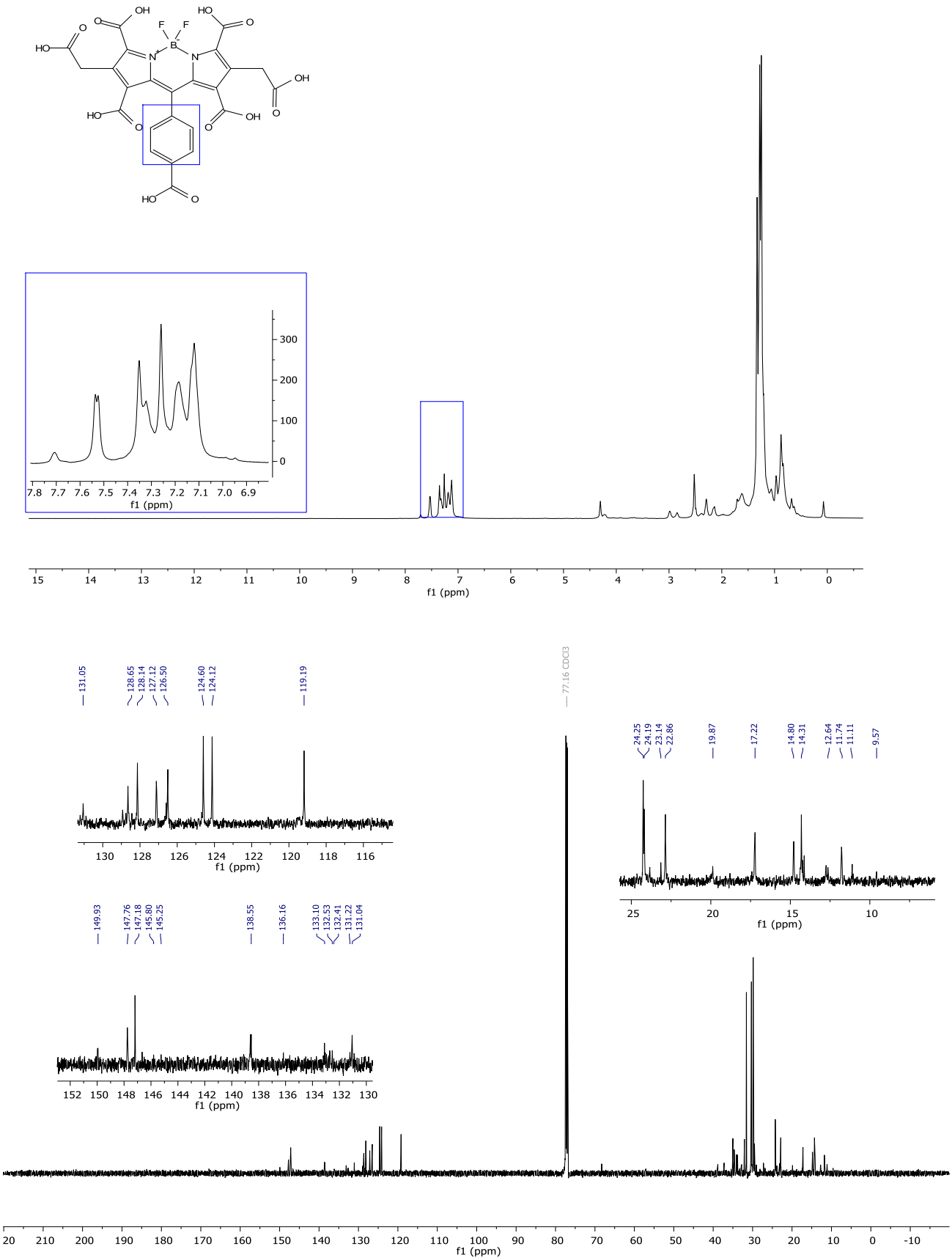

Figure 12 ^{1}H and ^{13}C NMR of BODIPY 2

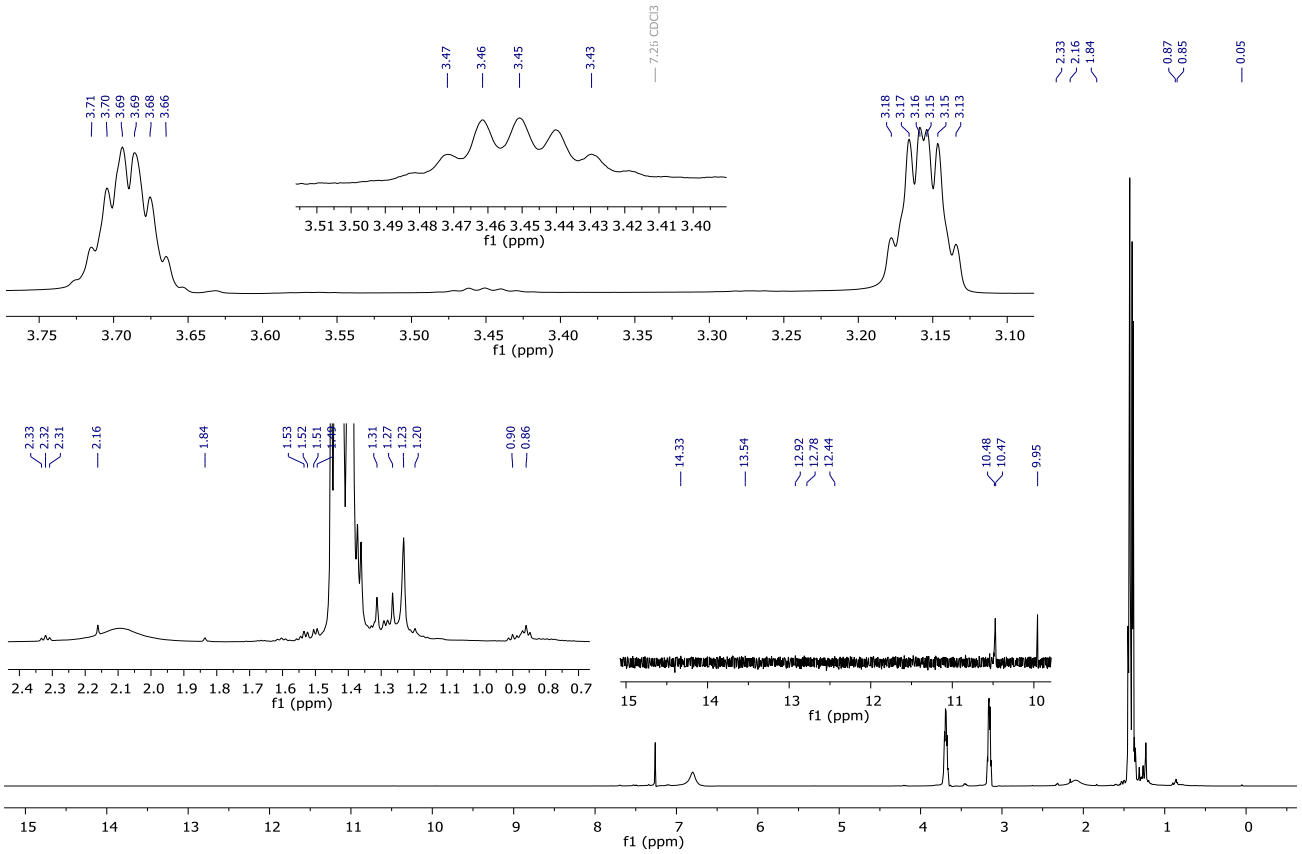
3.71
3.70
3.69
3.69
3.68
3.66
3.47
3.46
3.45
3.43
7.26 CDCl3
3.18
3.17
3.16
3.15
3.15
3.13
2.33
2.16
1.84
0.87
0.85
0.05
f1 (ppm)

2.33
2.32
2.31
2.16
1.84
1.53
1.52
1.51
1.31
1.27
1.23
1.20
0.90
0.86
14.33
13.54
12.92
12.78
12.44
10.48
10.47
9.95
f1 (ppm)

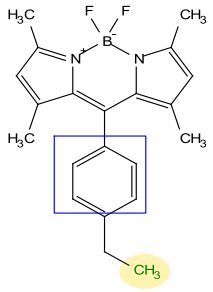
H3C
F
F
CH3
B-
N+
N
H3C
CH3
CH3

300
200
100
0
7.0
6.9
6.8
6.7
6.6
f1 (ppm)

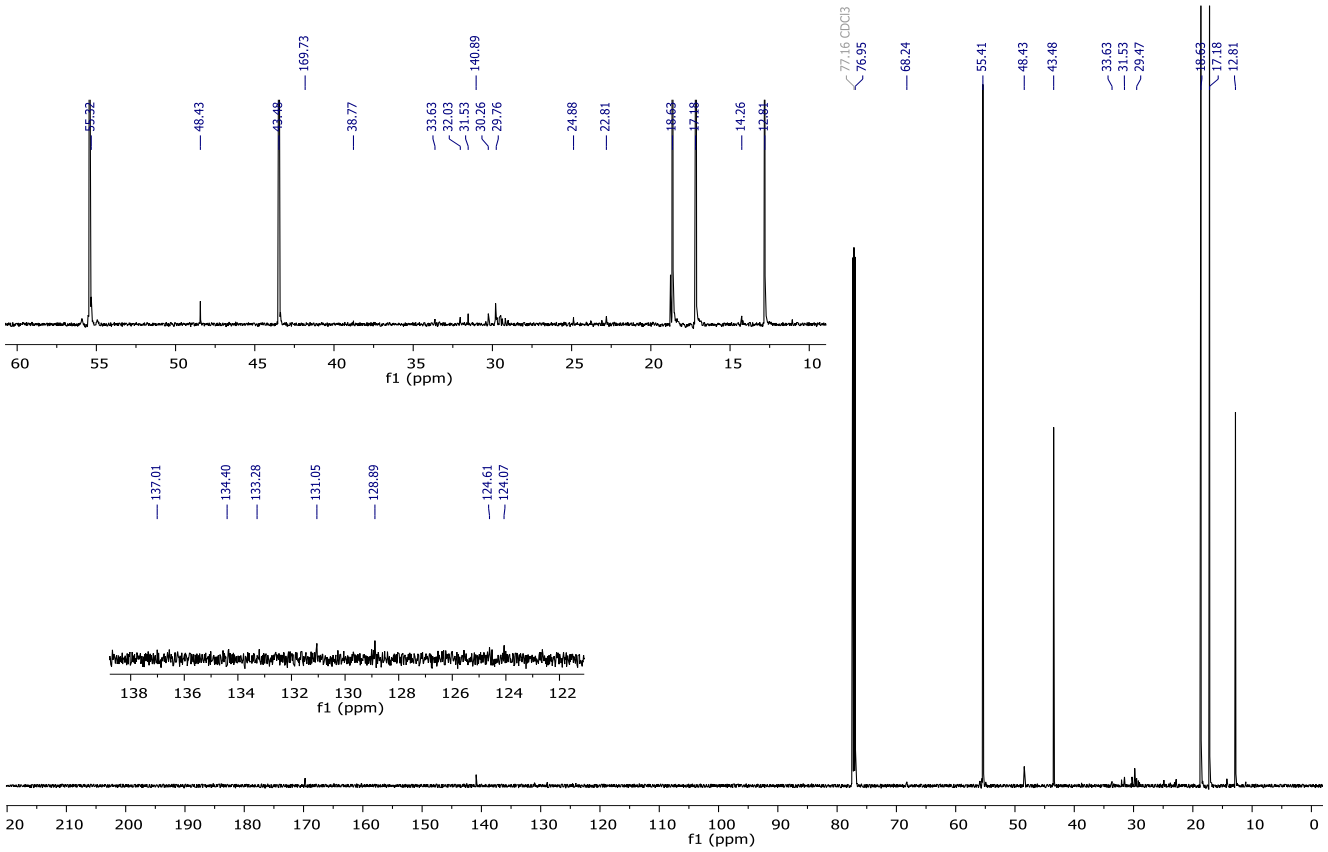

Figure 13 ^{1}H and ^{13}C NMR of BODIPY 3

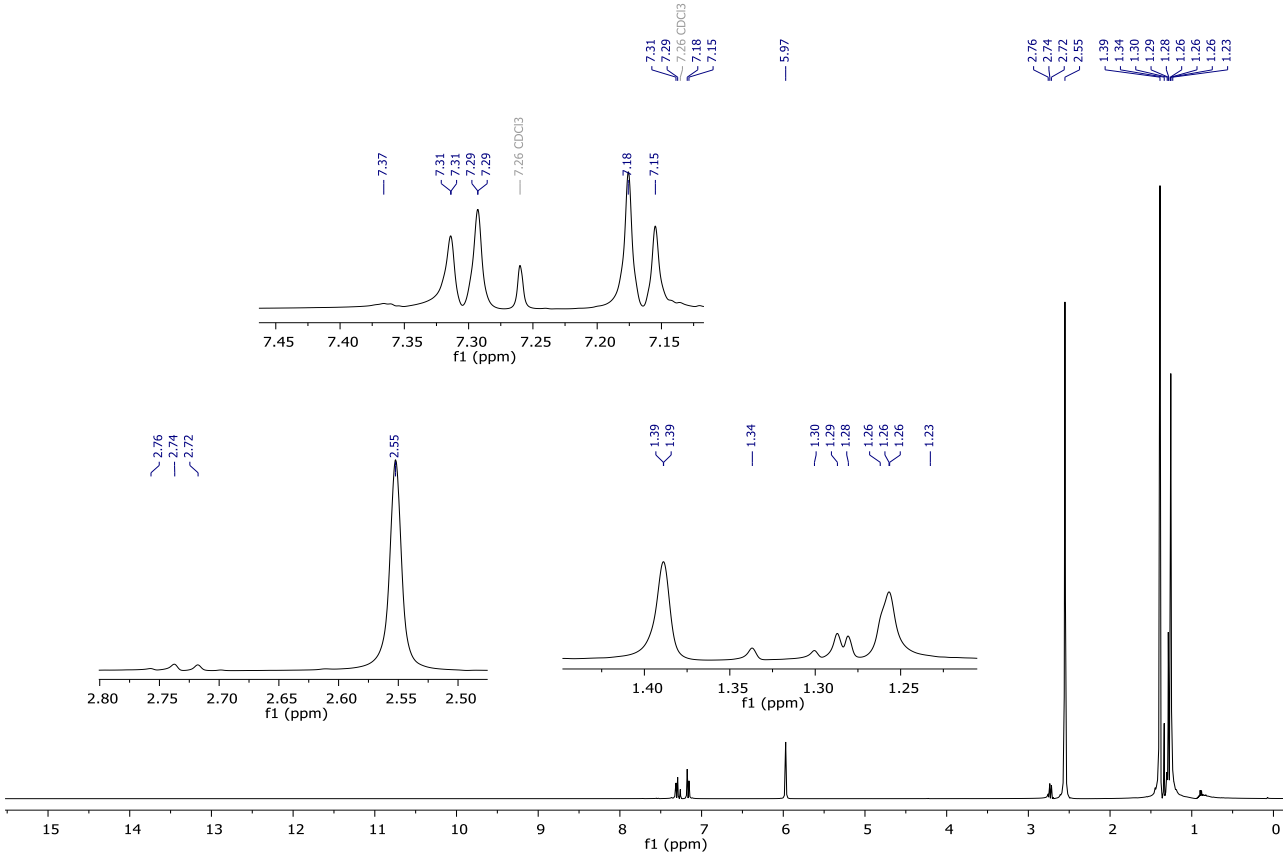

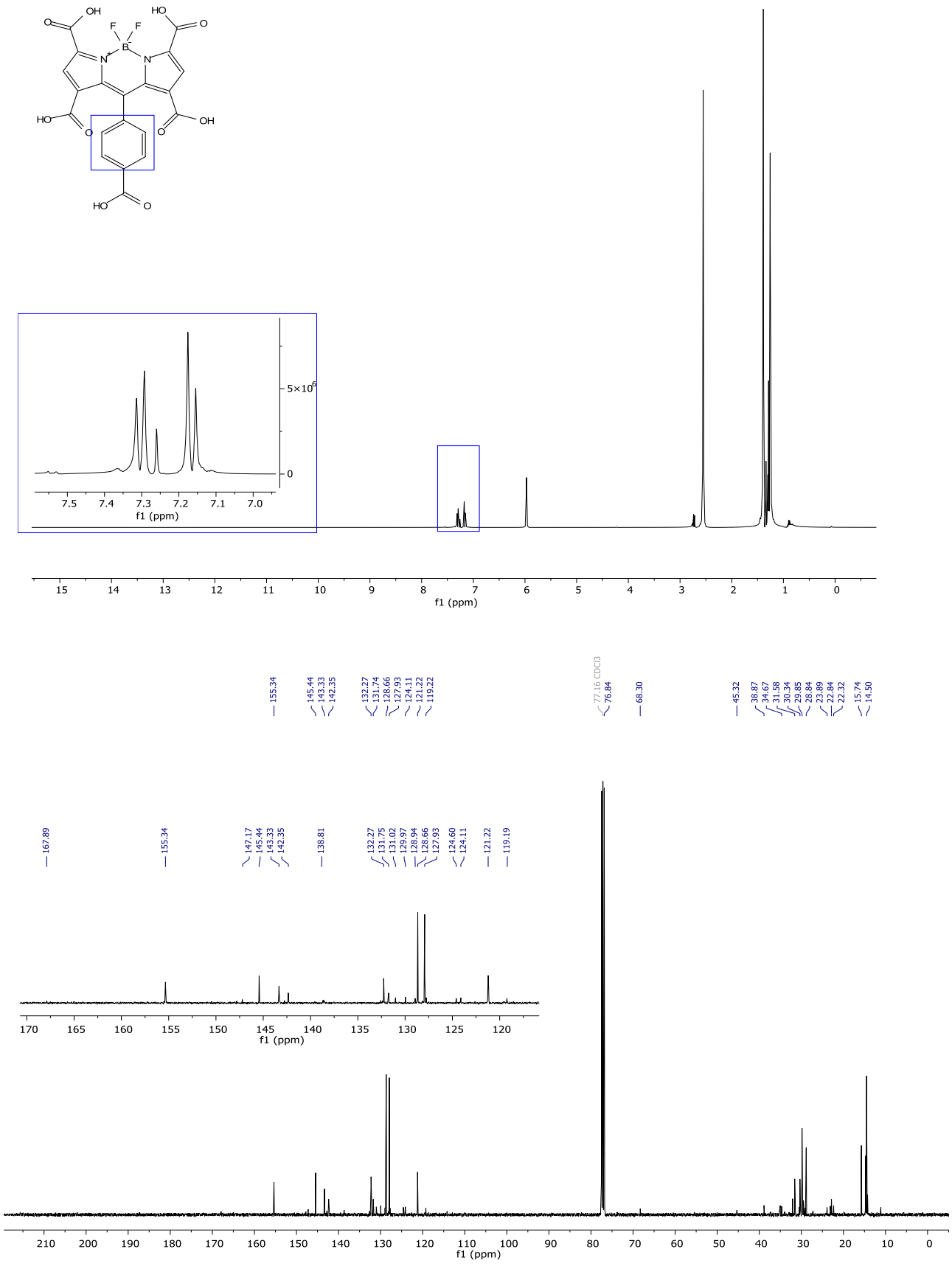

Figure 14 ^{1}H and ^{13}C NMR of BODIPY 4

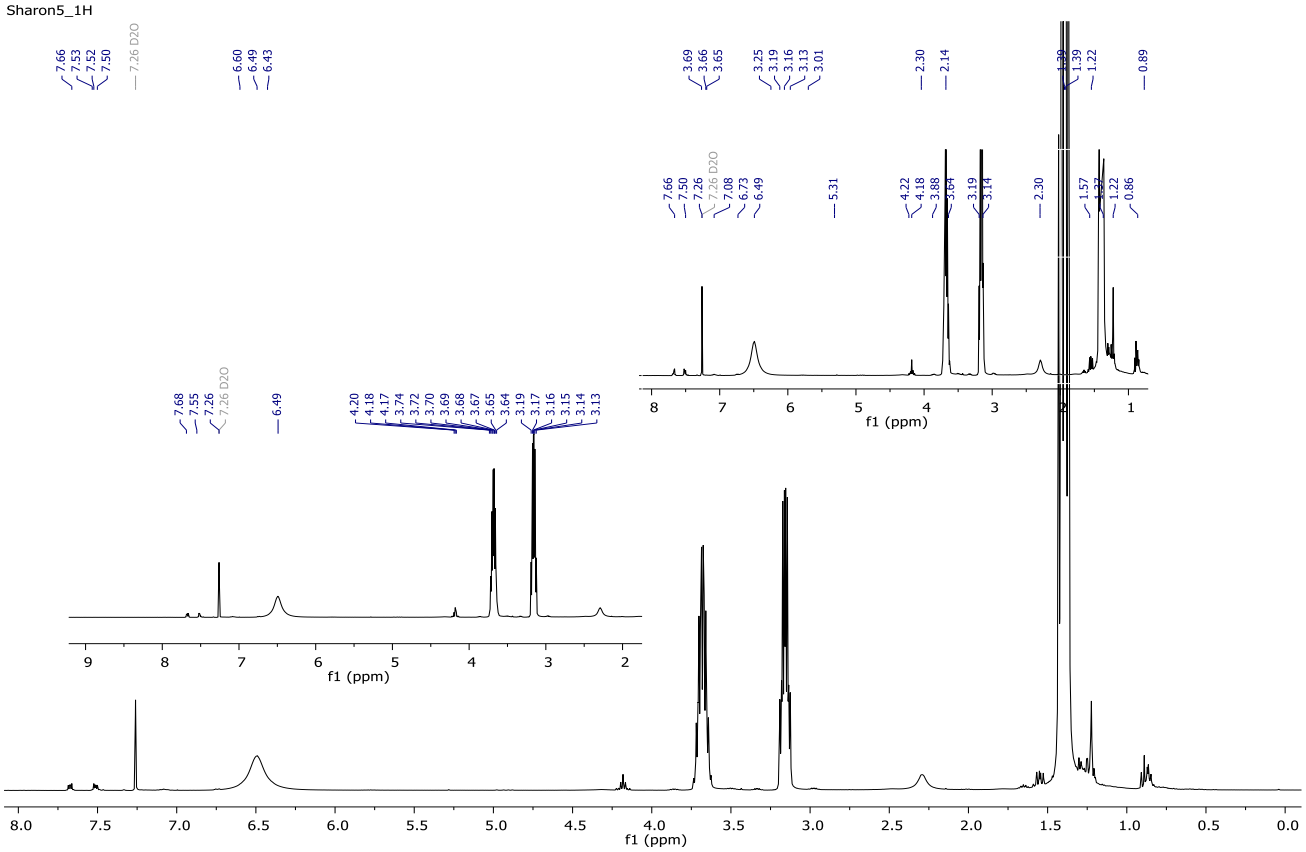
Sharon5_1H
f1 (ppm)

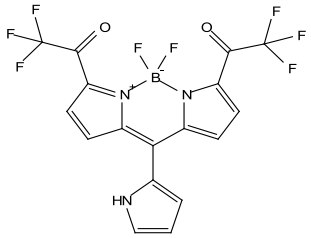
F
F
F
O
F
F
B
N
N
O
F
F
F
HN

f1 (ppm)

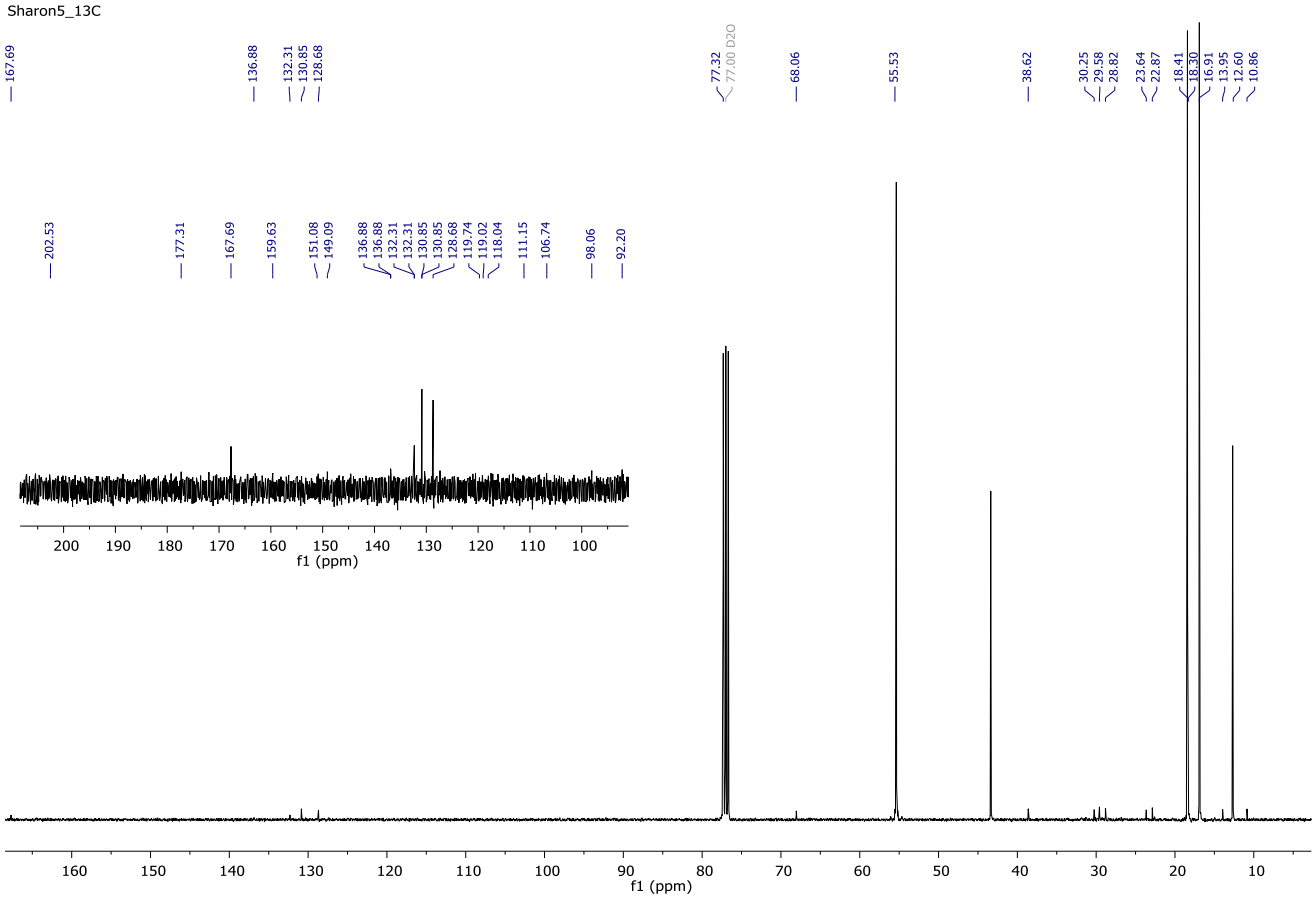

Figure 15 ^{1}H and ^{13}C NMR of BODIPY 5

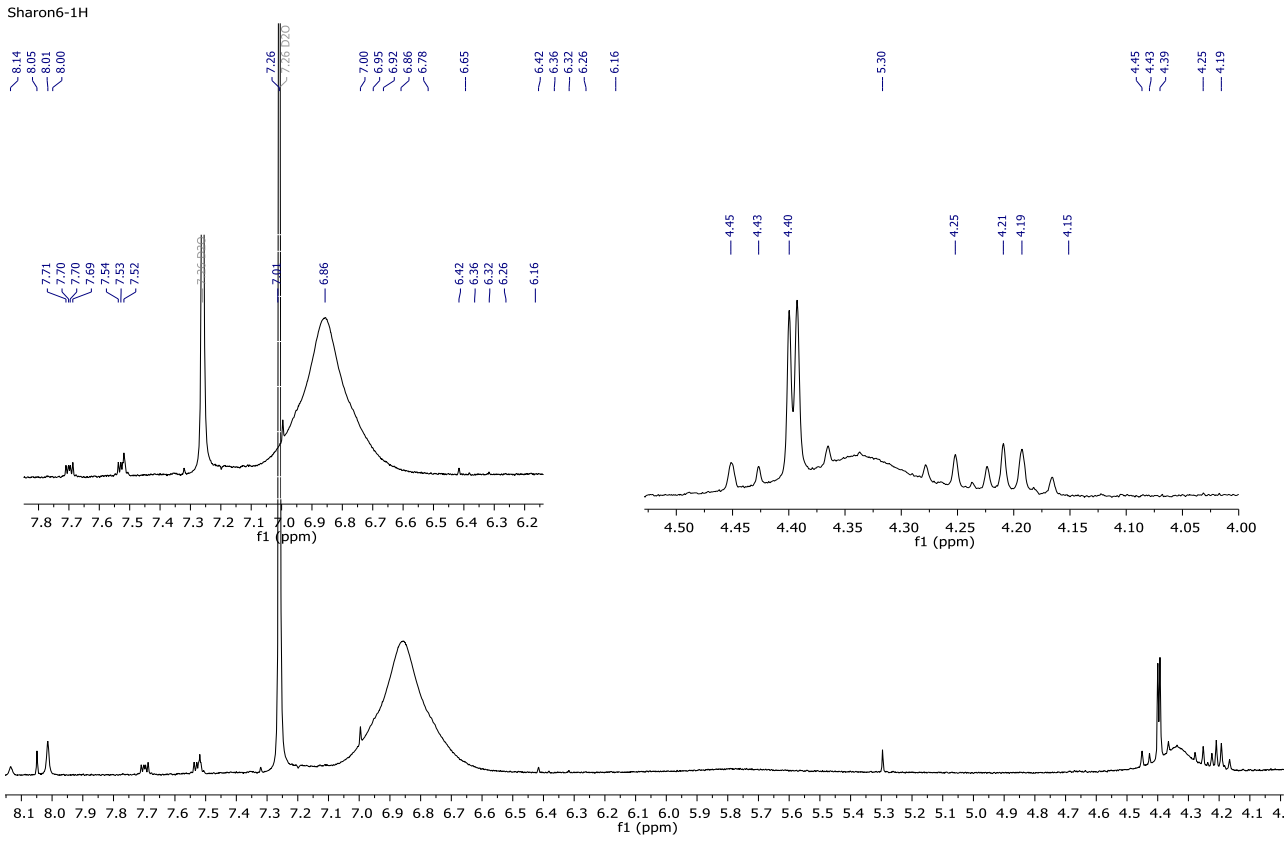

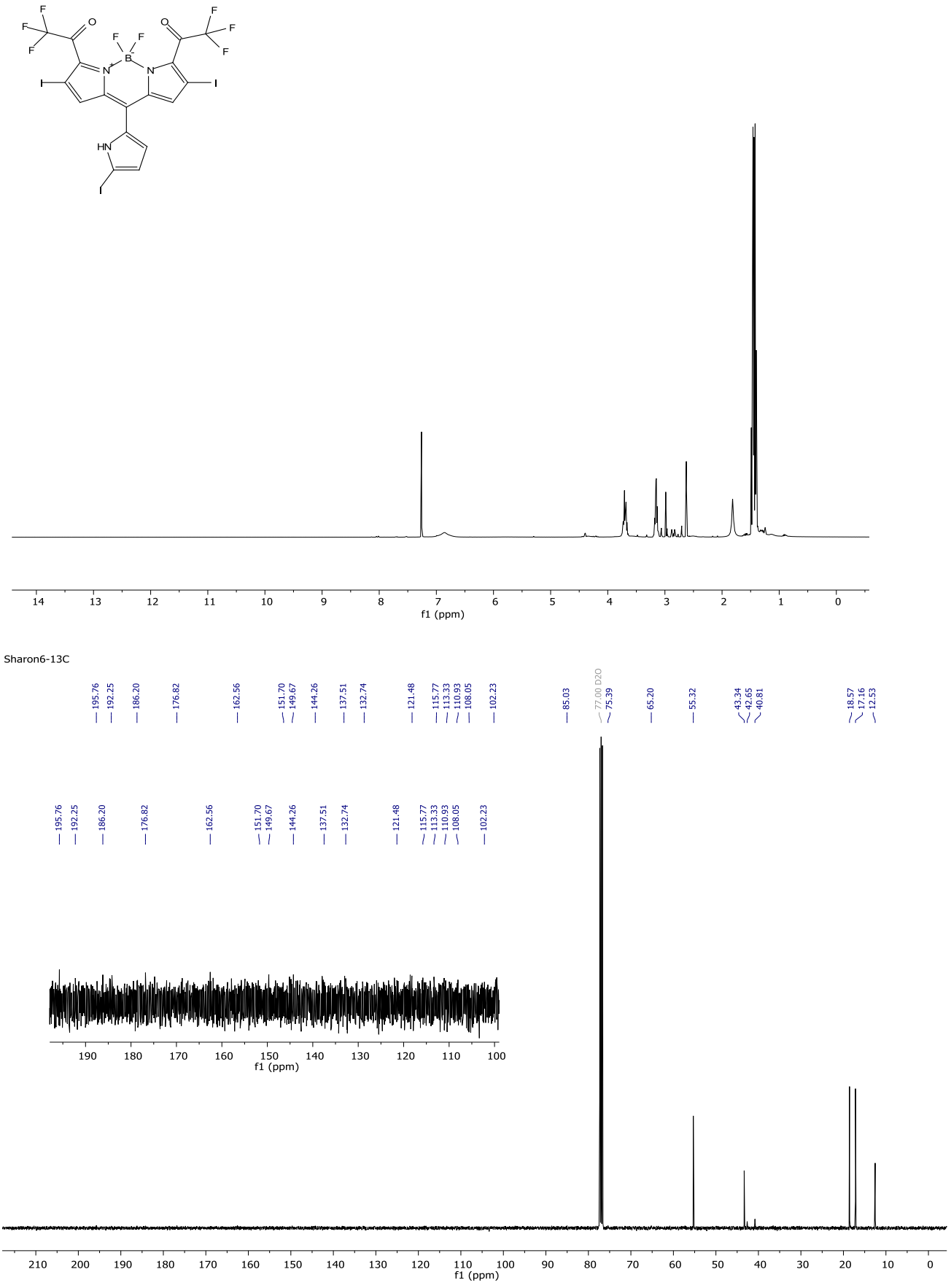

Figure 16 ^{1}H and ^{13}C NMR of BODIPY 6

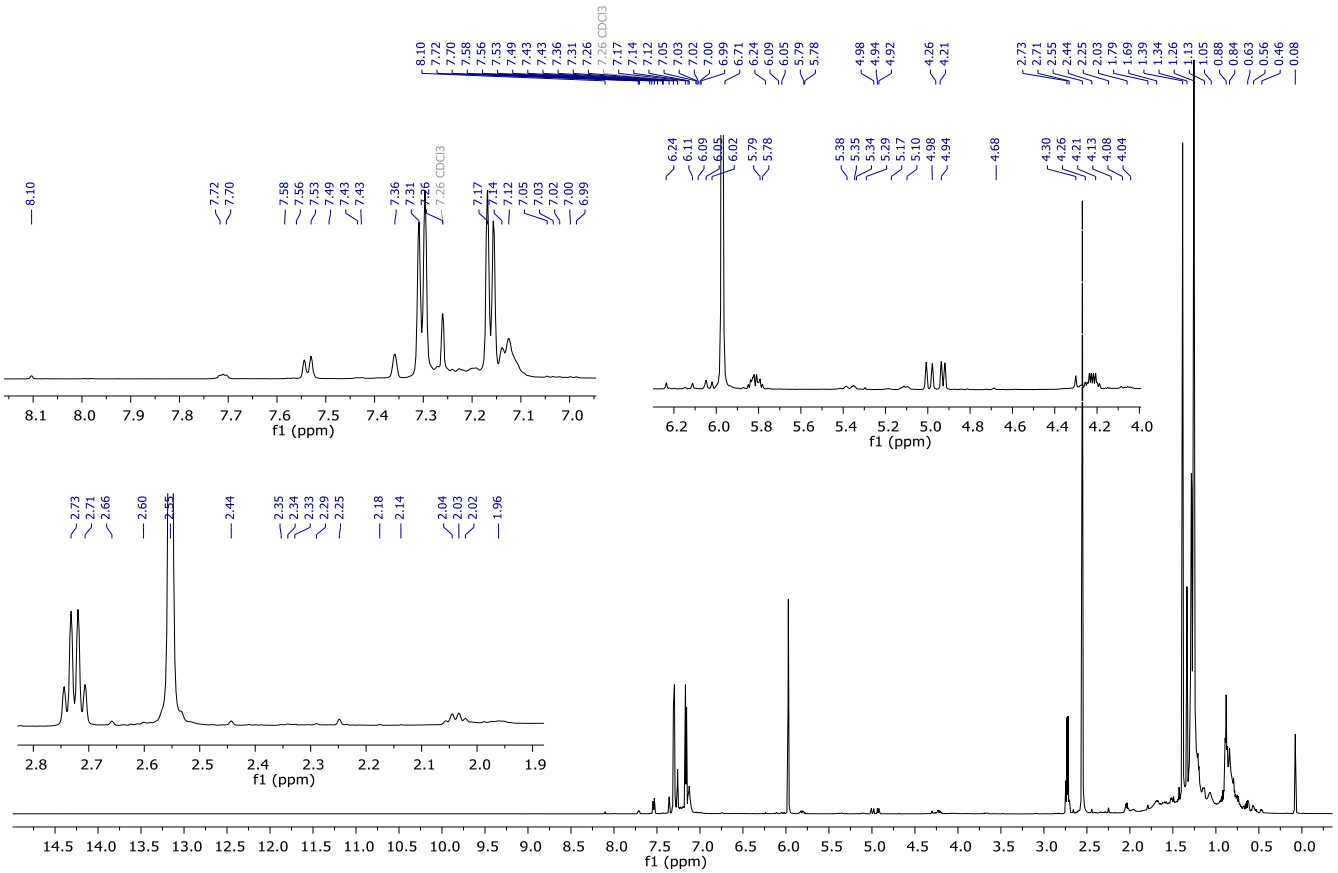
f1 (ppm)

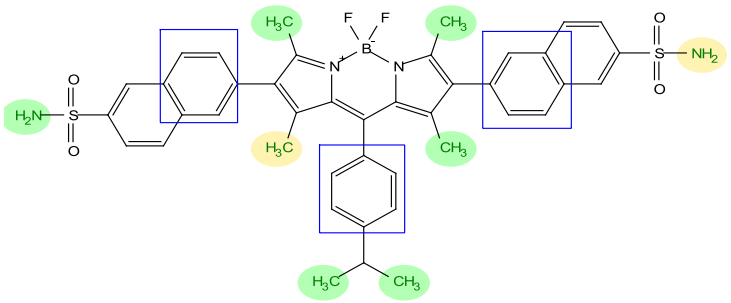
F
F
B
N
N
H3C
CH3
H3C
CH3
H3C
CH3
O
S
O
NH2
H2N

f1 (ppm)

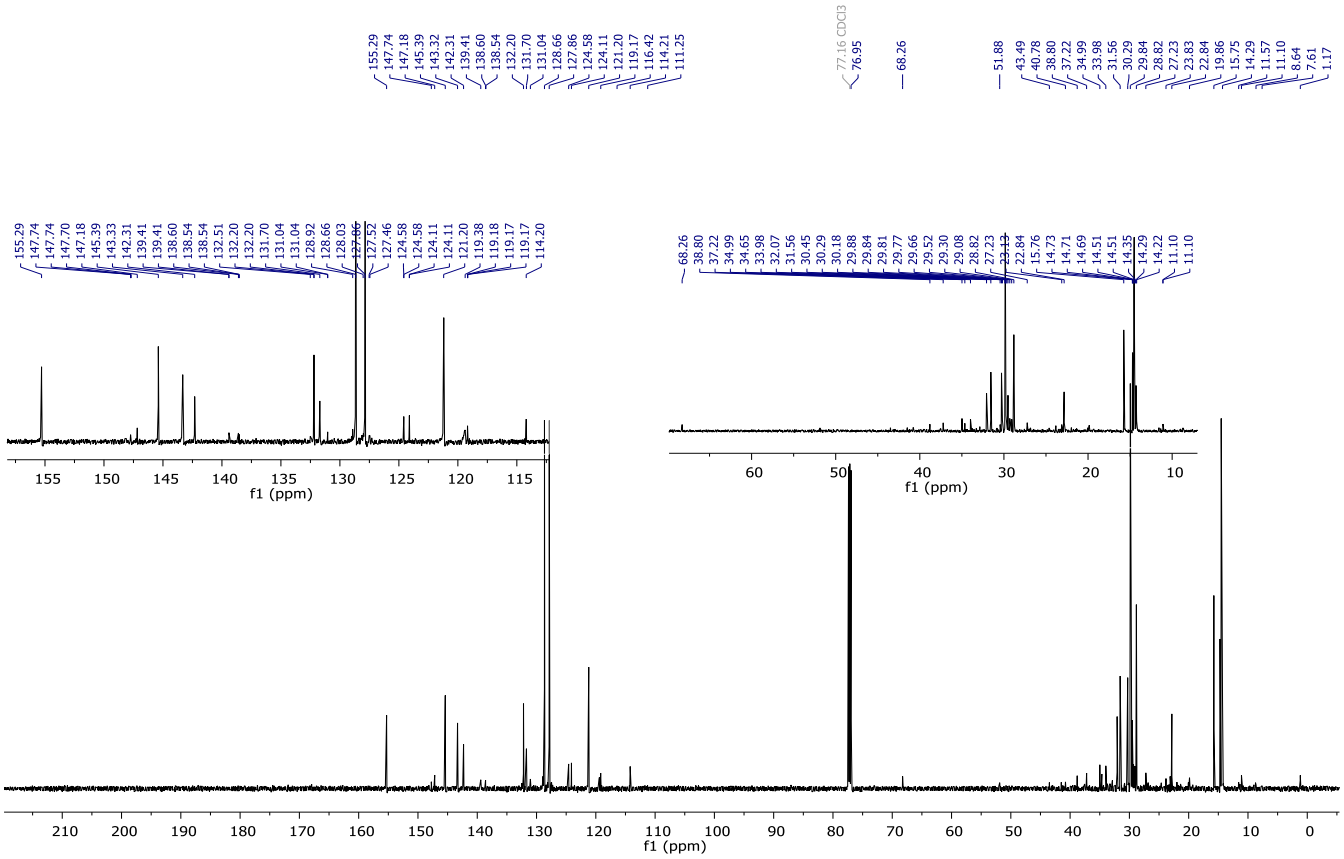

Figure 17 ^{1}H and ^{13}C NMR of BODIPY 7

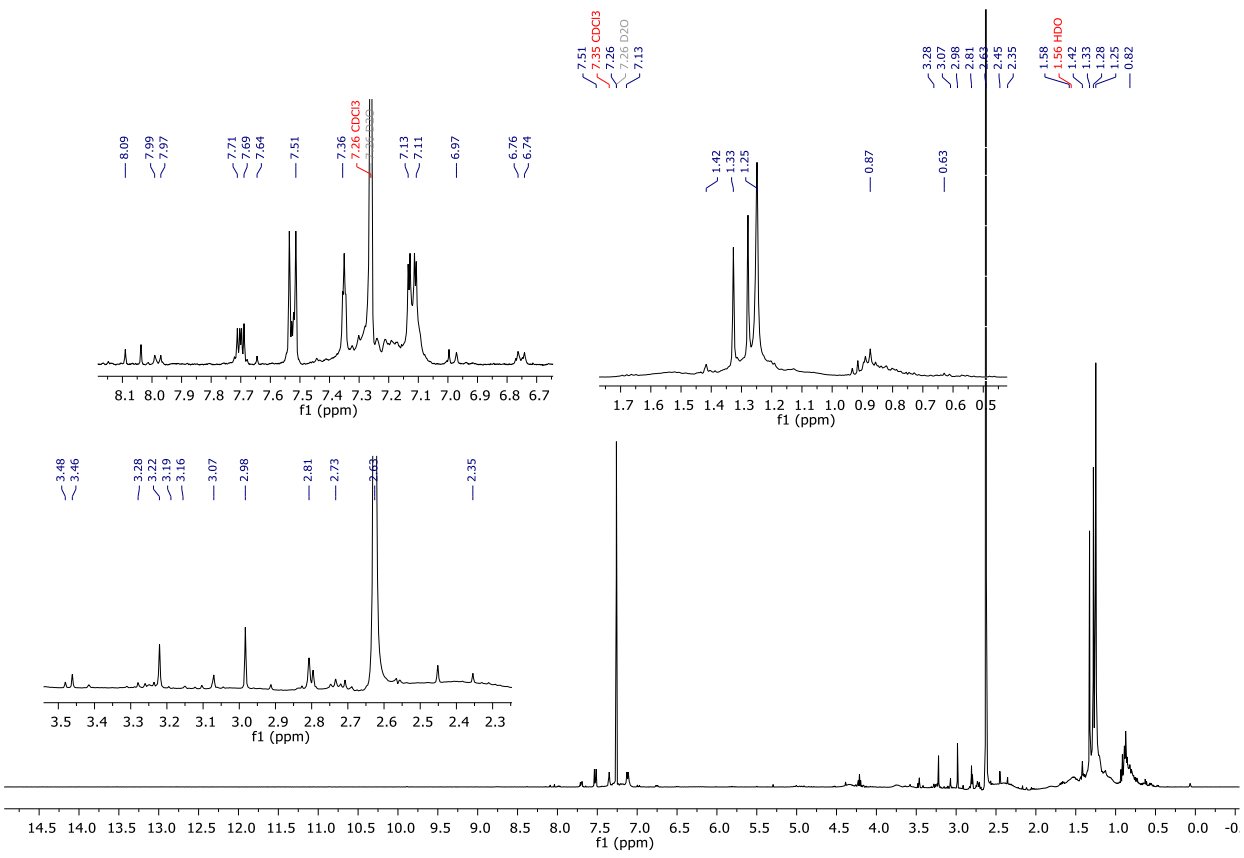

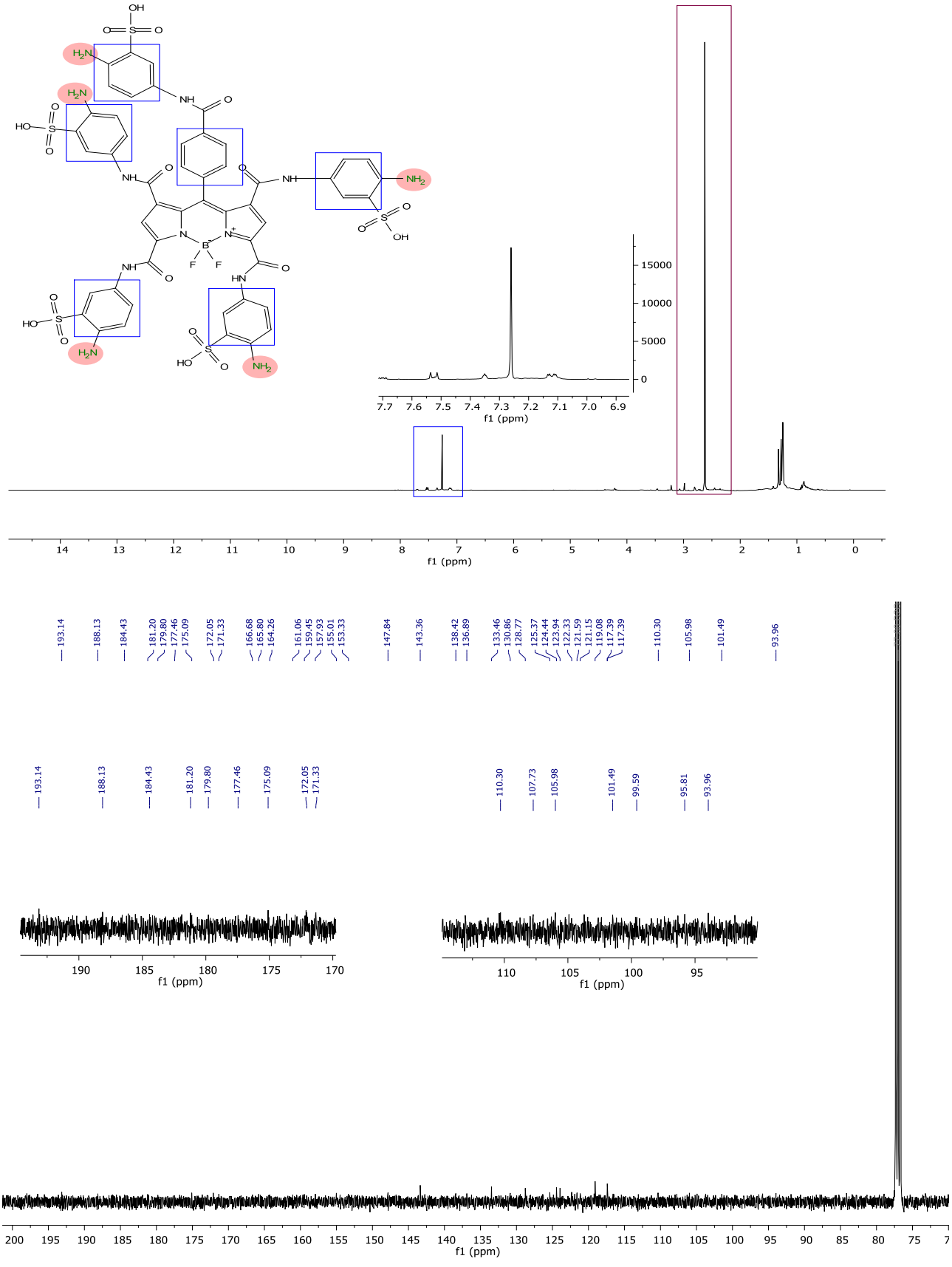

Figure 18 ^{1}H and ^{13}C NMR of BODIPY 8

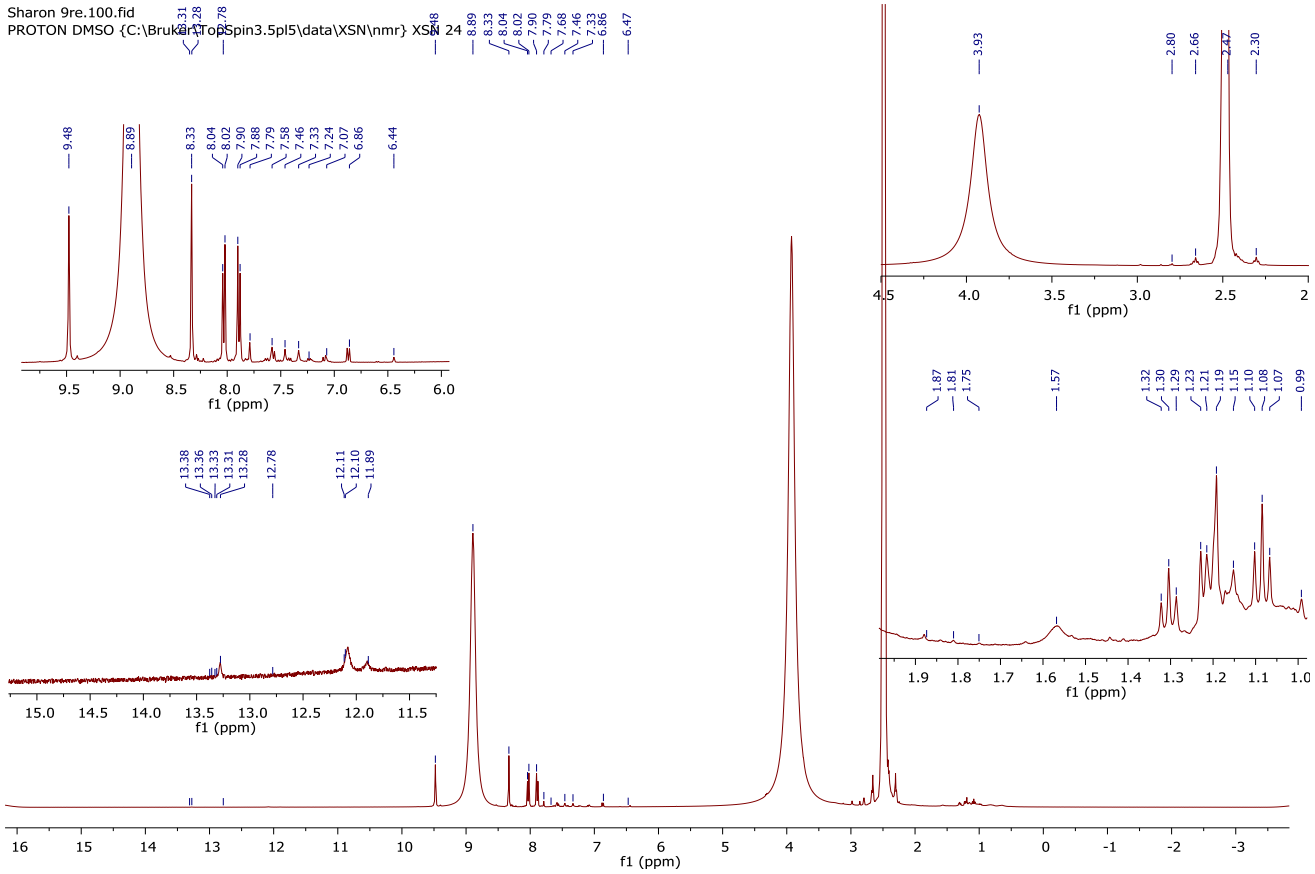
Sharon 9re.100.fid
PROTON DMSO {C:\Bruker\TopSpin3.5pl5\data\XSN\nmr} XSN 24
f1 (ppm)

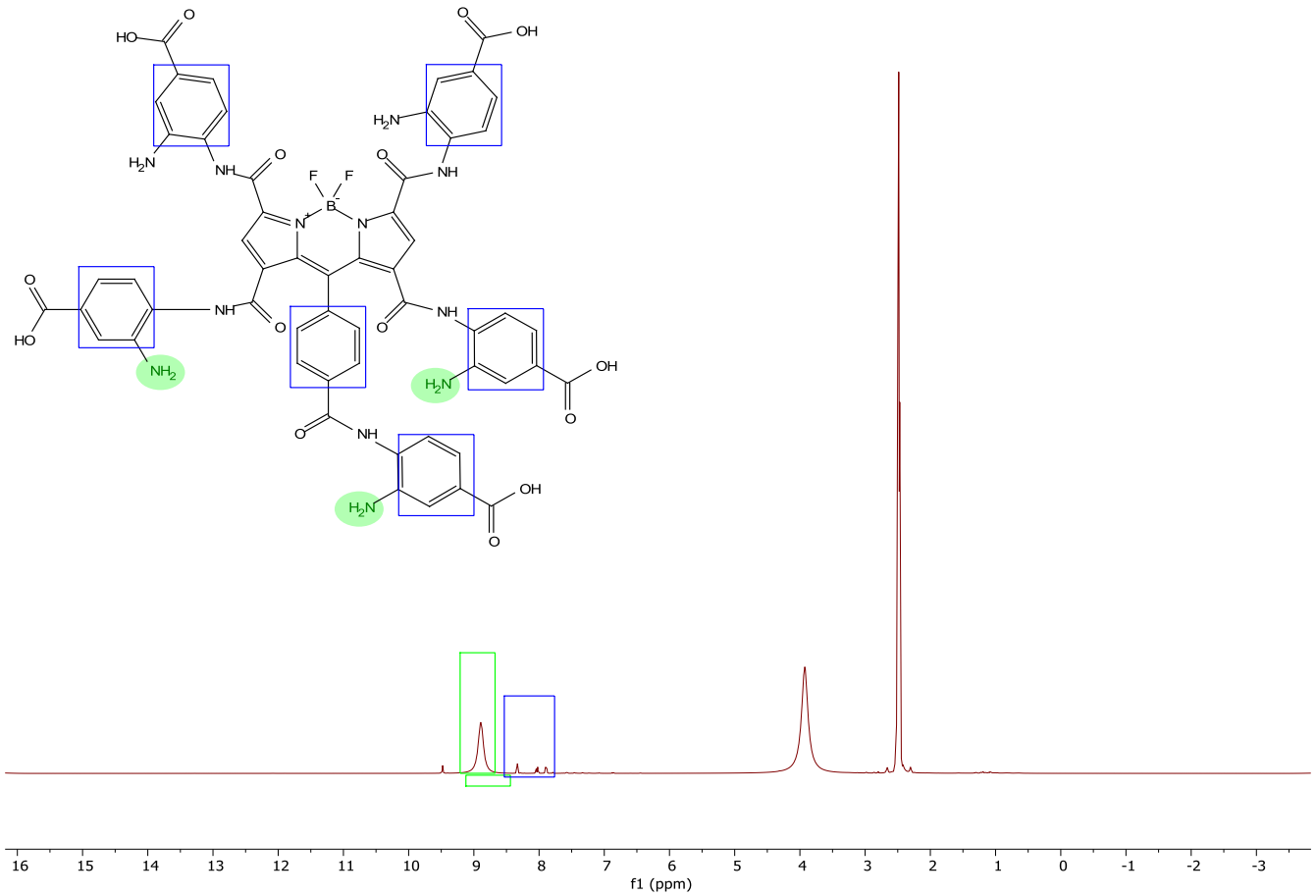
HO
O
NH
H_2N
OH
F
B
N
NH_2
f1 (ppm)

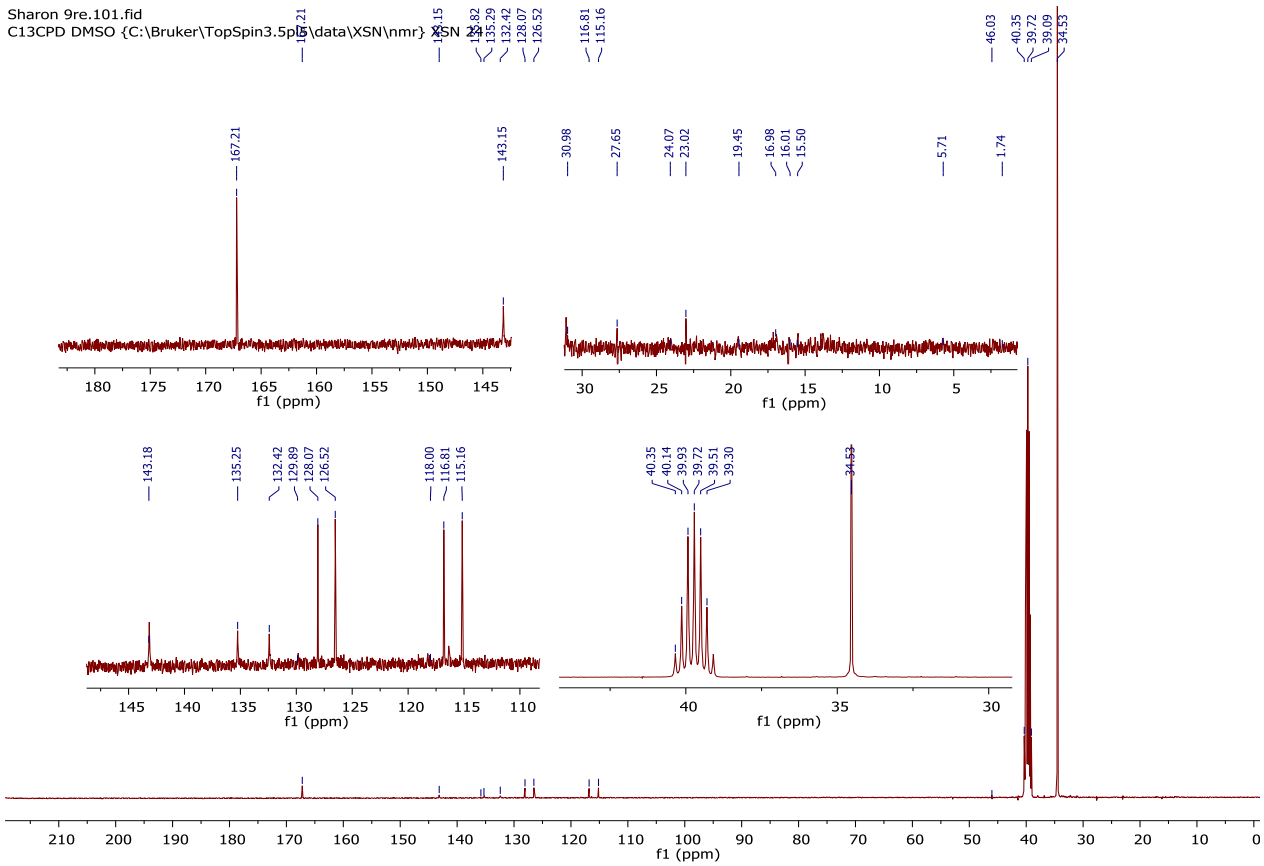

Figure 19 ^{1}H and ^{13}C NMR of BODIPY 9

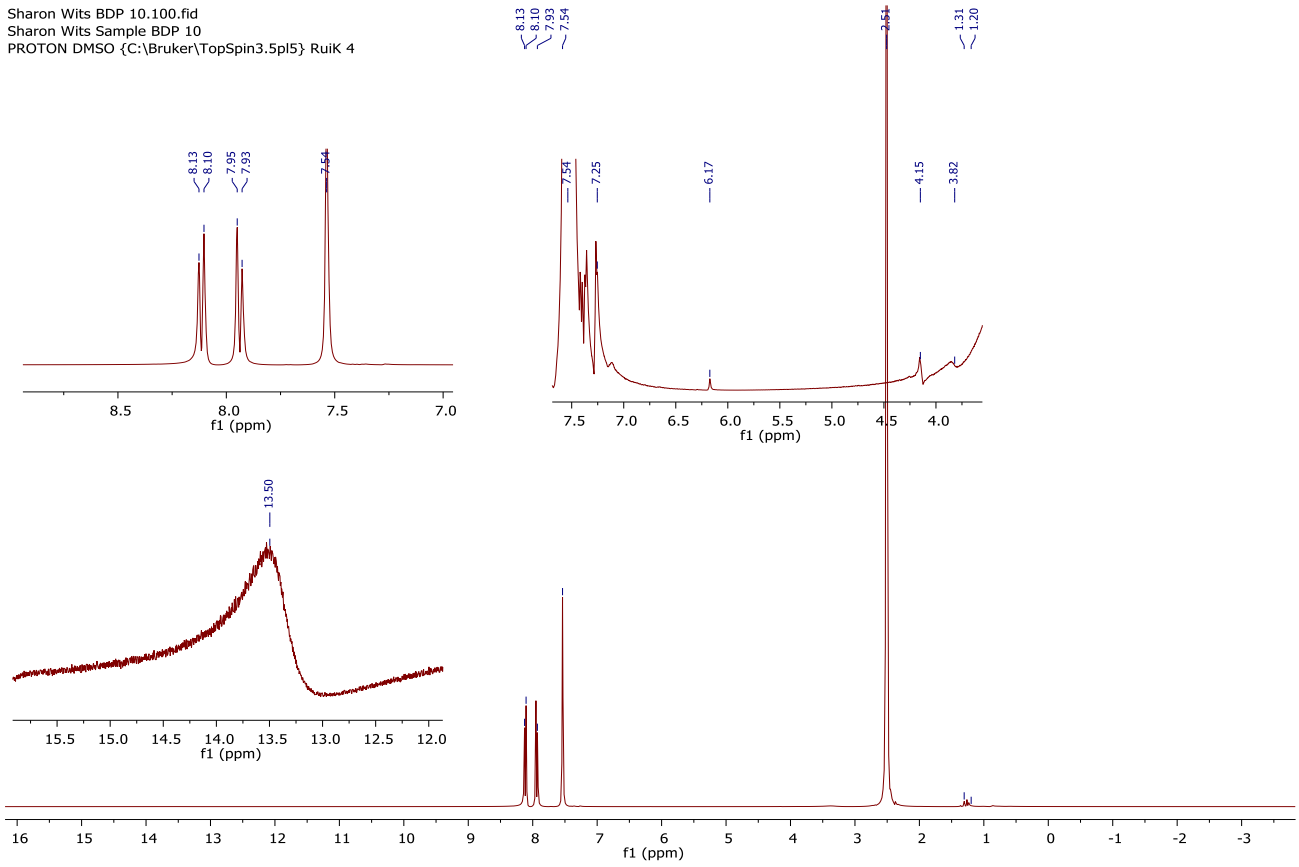

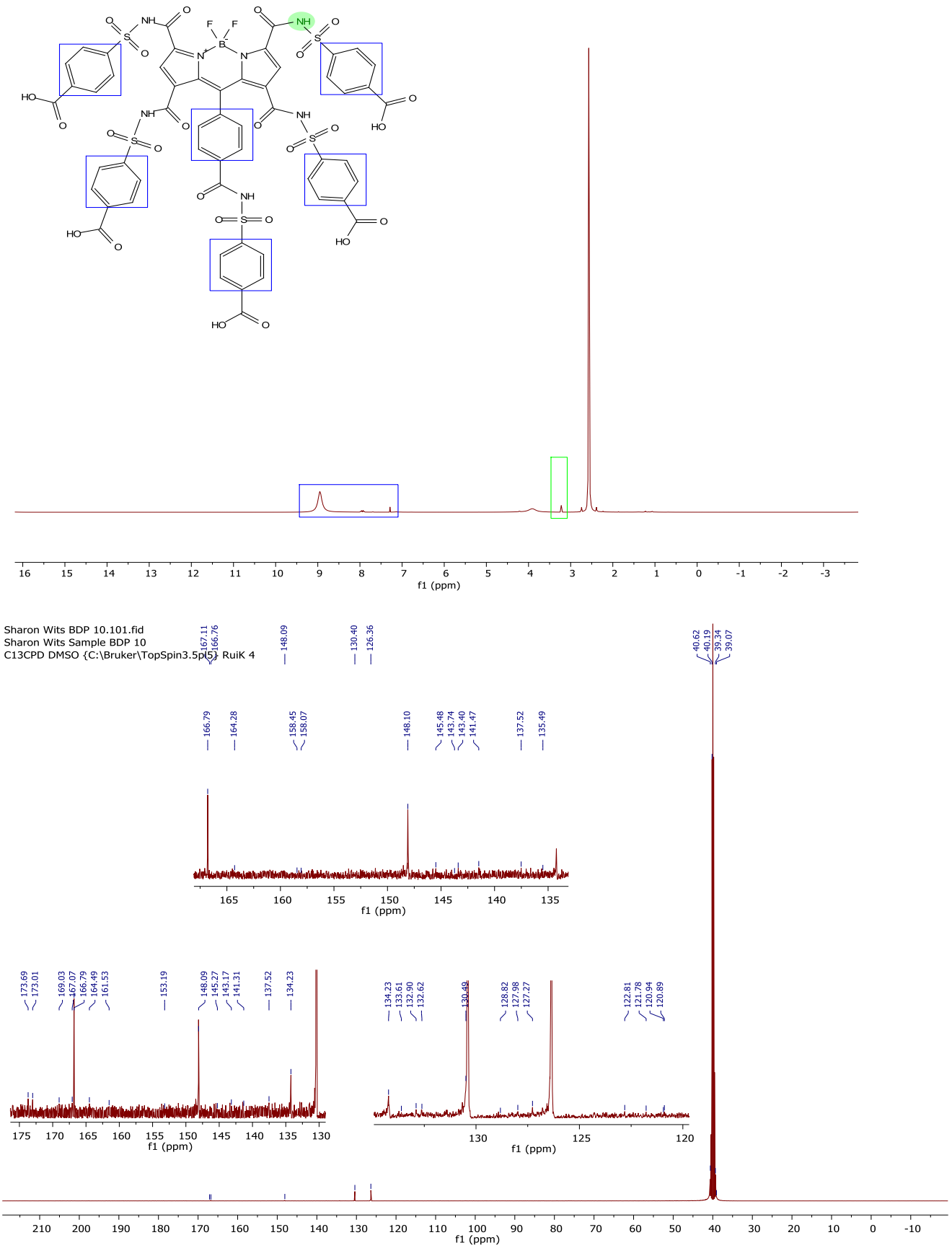

Figure 20 ^{1}H and ^{13}C NMR of BODIPY 10

^{1}H and ^{13}C NMR spectra of BODIPY with extended iodine moieties

BODIPY 6.1 to BODIPY 6.6 showed spectral properties that were insensitive to the NMR analysis. Several reasons may lead to this phenomenon (i.e. the sensitivity of the sample towards the NMR spectroscopy, concerning signal-to-noise ratio (SNR) analysis). Hyberts and co-workers, (2013) suggested that this may be due to spectral acquisition and/or the sampling method used. However, they showed that the signal-to-noise ratio to elucidate structures of larger biomolecular (e.g. protein) samples with high insensitivity to NMR may be enhanced using the non-uniform sampling (NUS) method on the signal-to-noise ratio even though the sensitivity of the methods is not well documented. The group further suggested that, though signal-to-noise ratio and sensitivity are important aspects of NMR experiments, this is of great importance for spectroscopy of biological macromolecular samples with low concentrations. Moreover, they highlighted that the distinction between sensitivity and SNR is not yet clear. Hence the group proposed that while sensitivity is the probability to detect weak peaks, the time-equivalent NUS can considerably increase the detection of weak signals of large insensible biomolecular samples (Hyberts *et al*., 2013). This relates to the BODIPY samples analysis where the instrument picked the solvent peaks compared to the sample peaks. This may be due to the employed method of analysis as well as the time taken to acquire the spectral data, and possibly the sample concentrations leading to poor signal peaks.

BODIPY 6.1 to BODIPY 6.6 ^{1}H and ^{13}C NMR

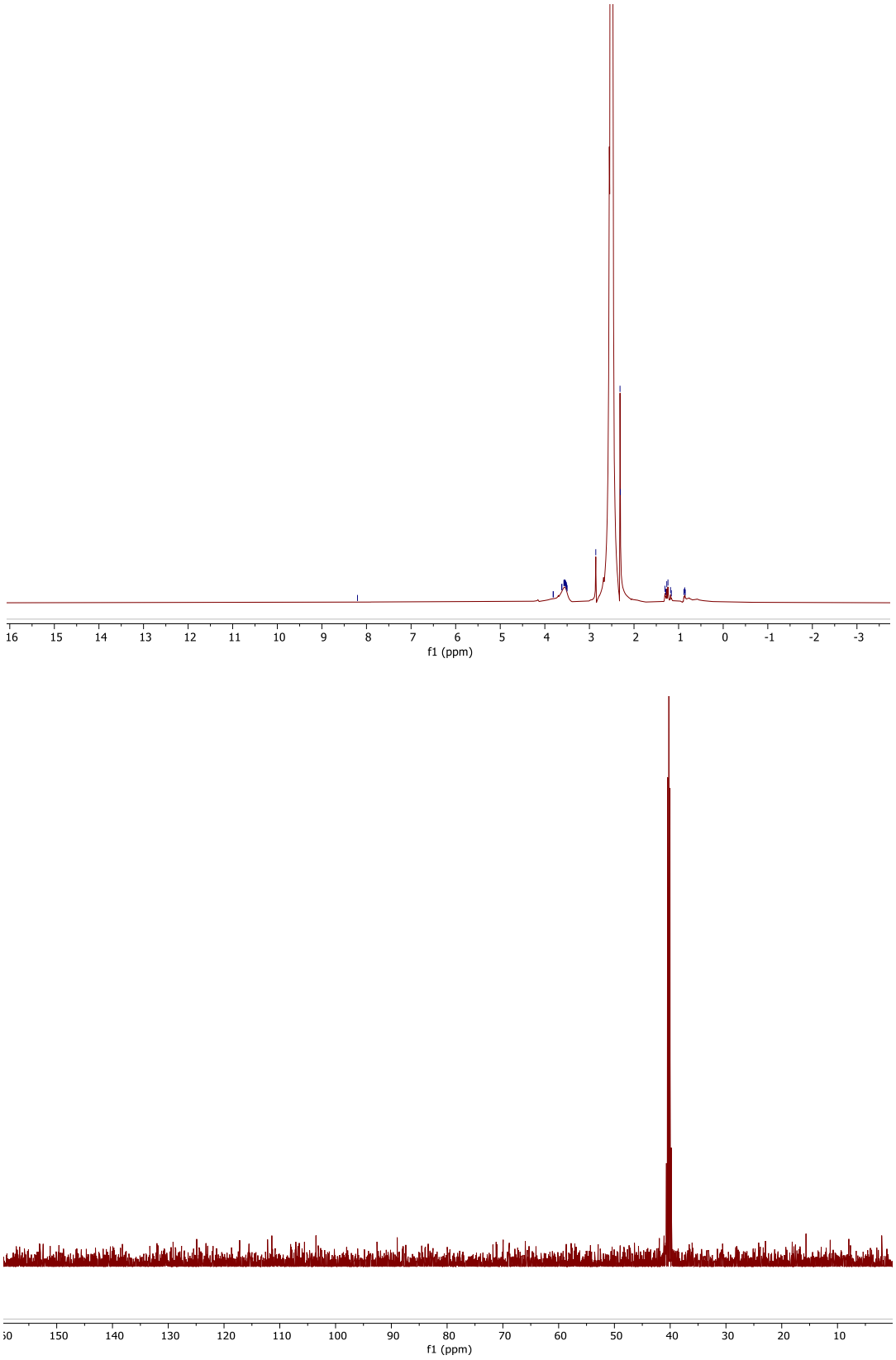

Figure 21 ^{1}H and ^{13}C NMR of BODIPY 6.1

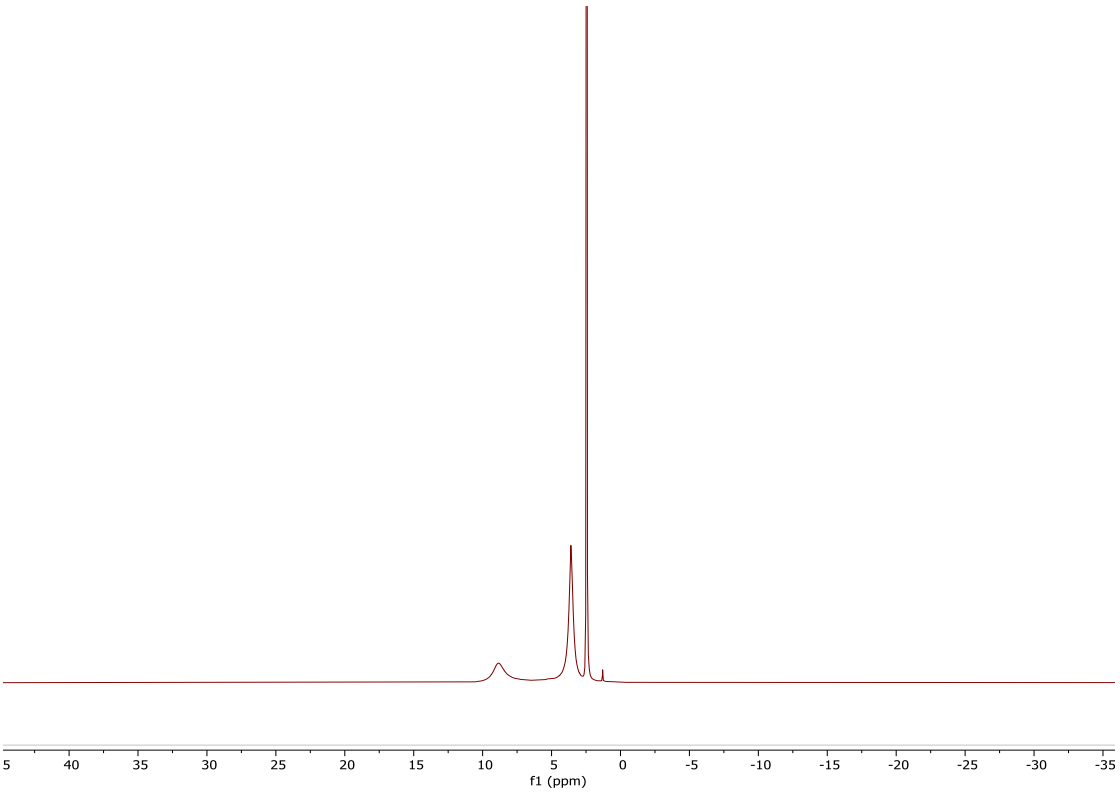

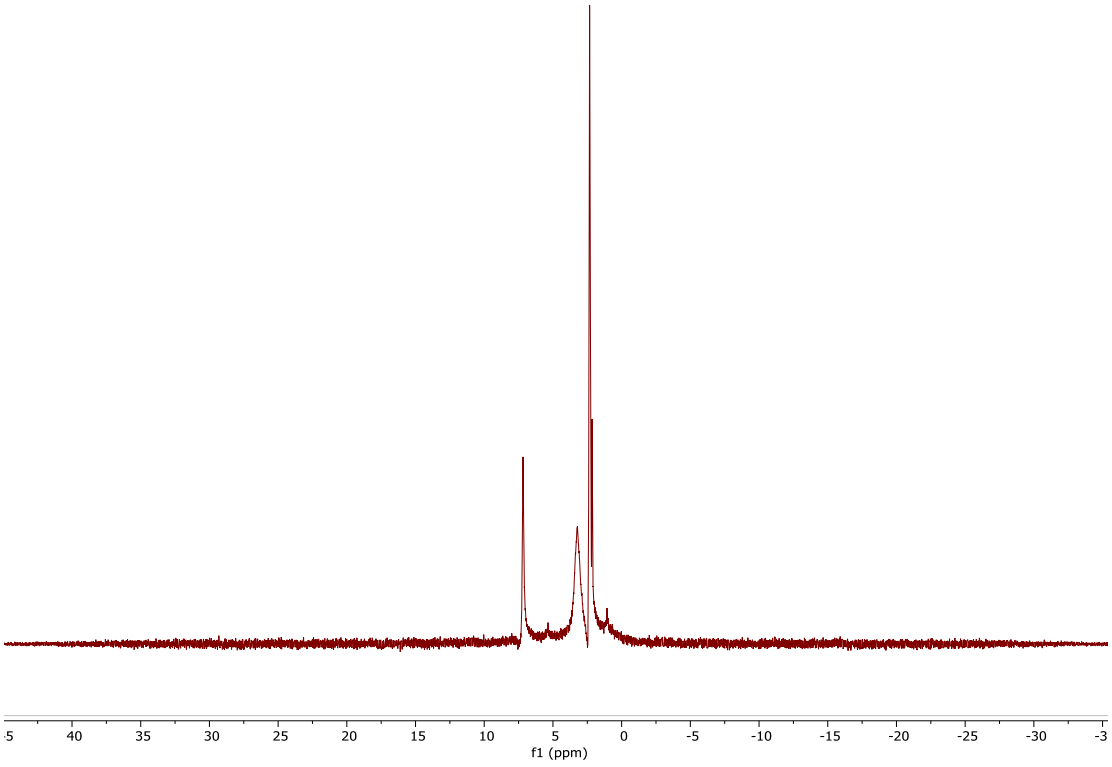

Figure 22 ^{1}H and ^{13}C NMR of BODIPY 6.2

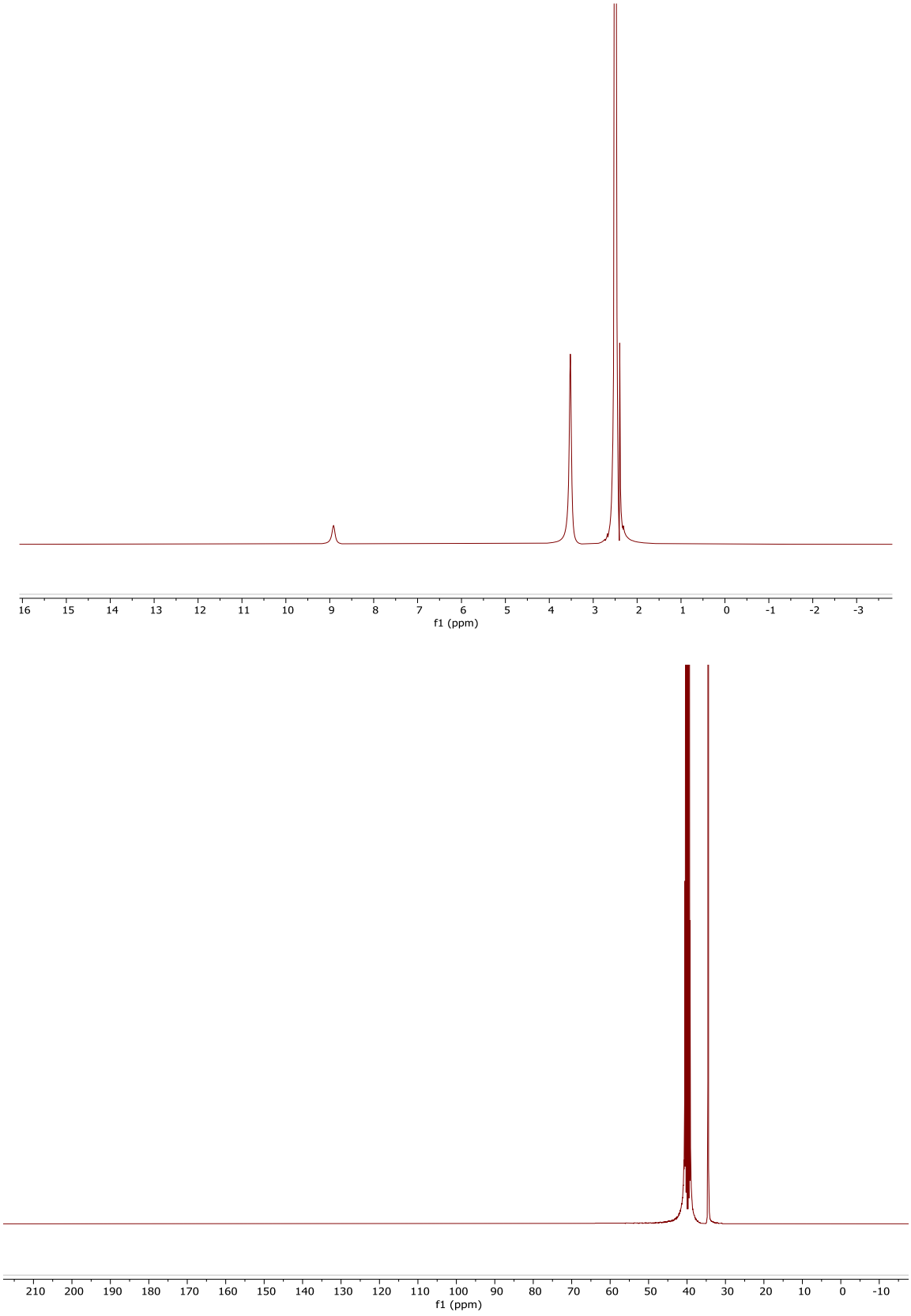

Figure 23 ^{1}H and ^{13}C NMR of BODIPY 6.3

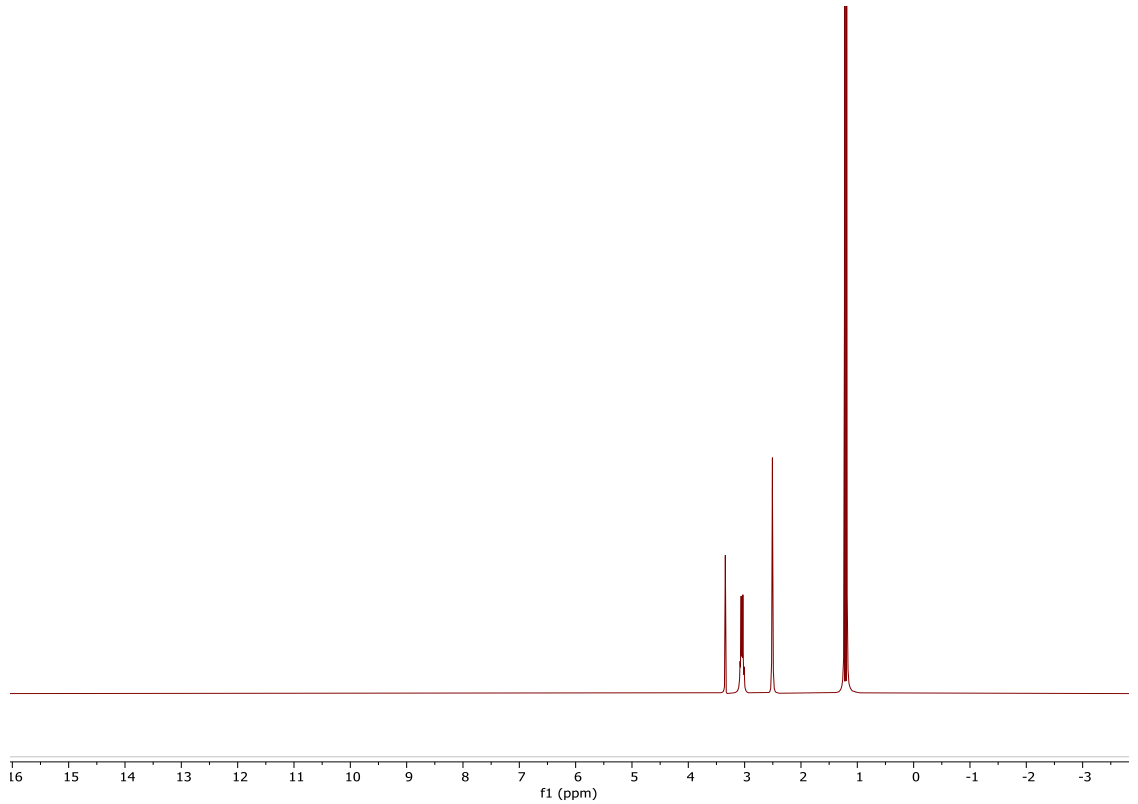

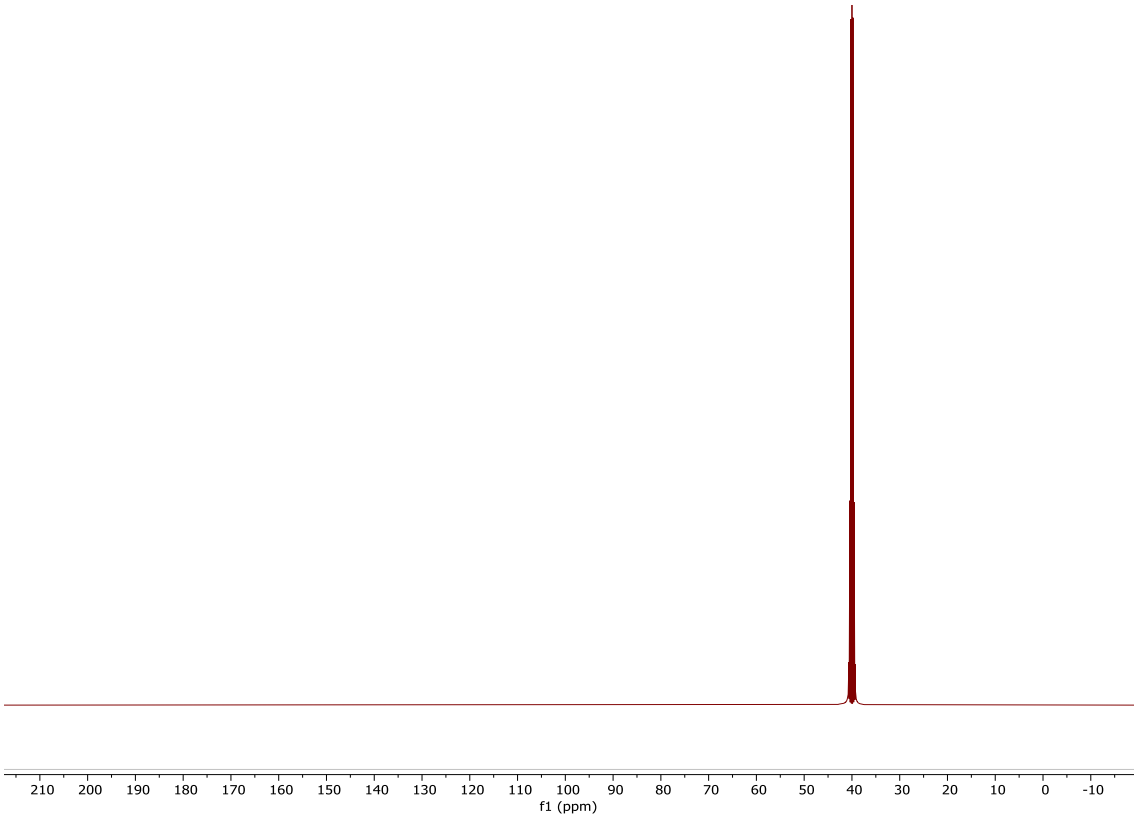

Figure 24 ^{1}H and ^{13}C NMR of BODIPY 6.4

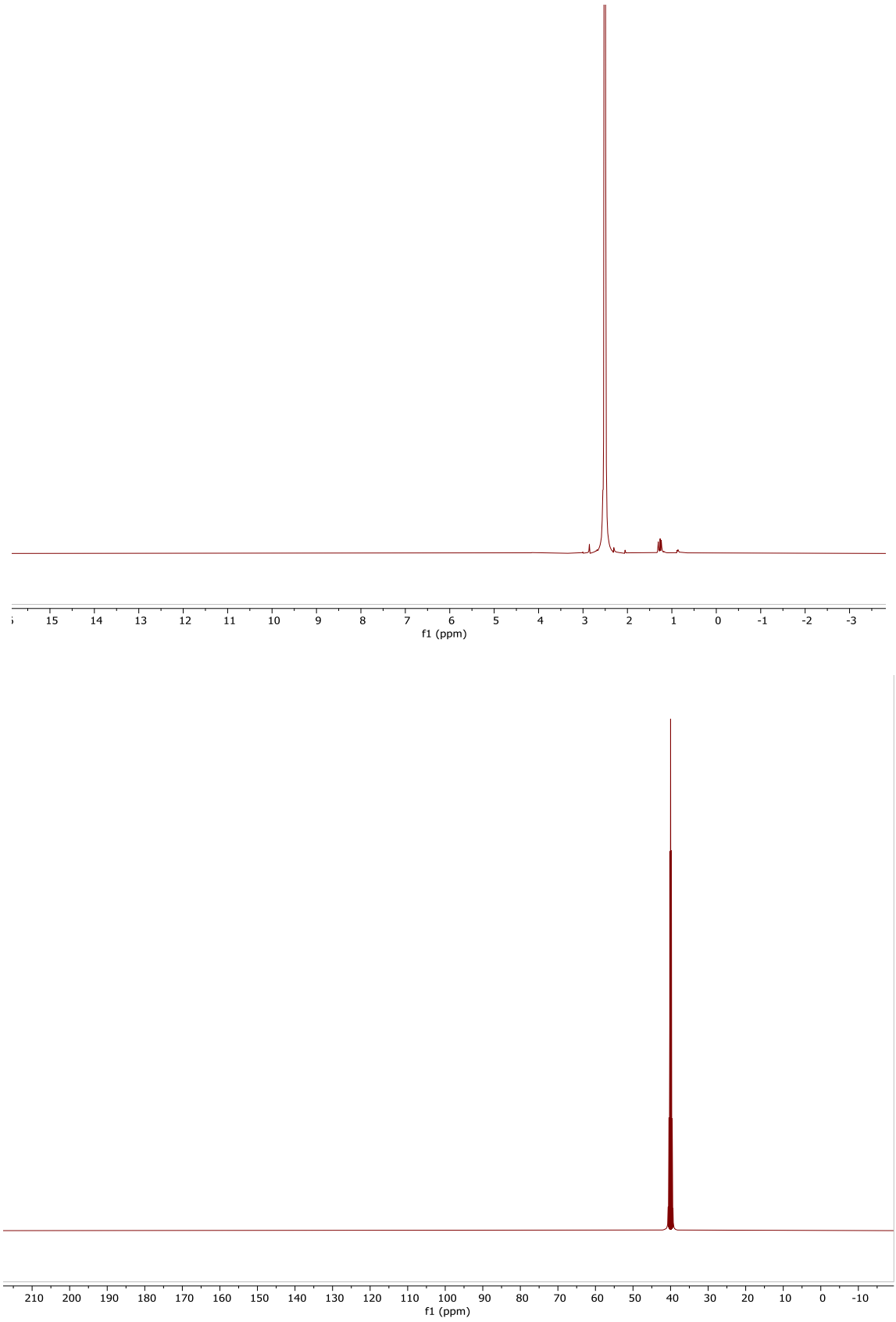

Figure 25 ^{1}H and ^{13}C NMR of BODIPY 6.5

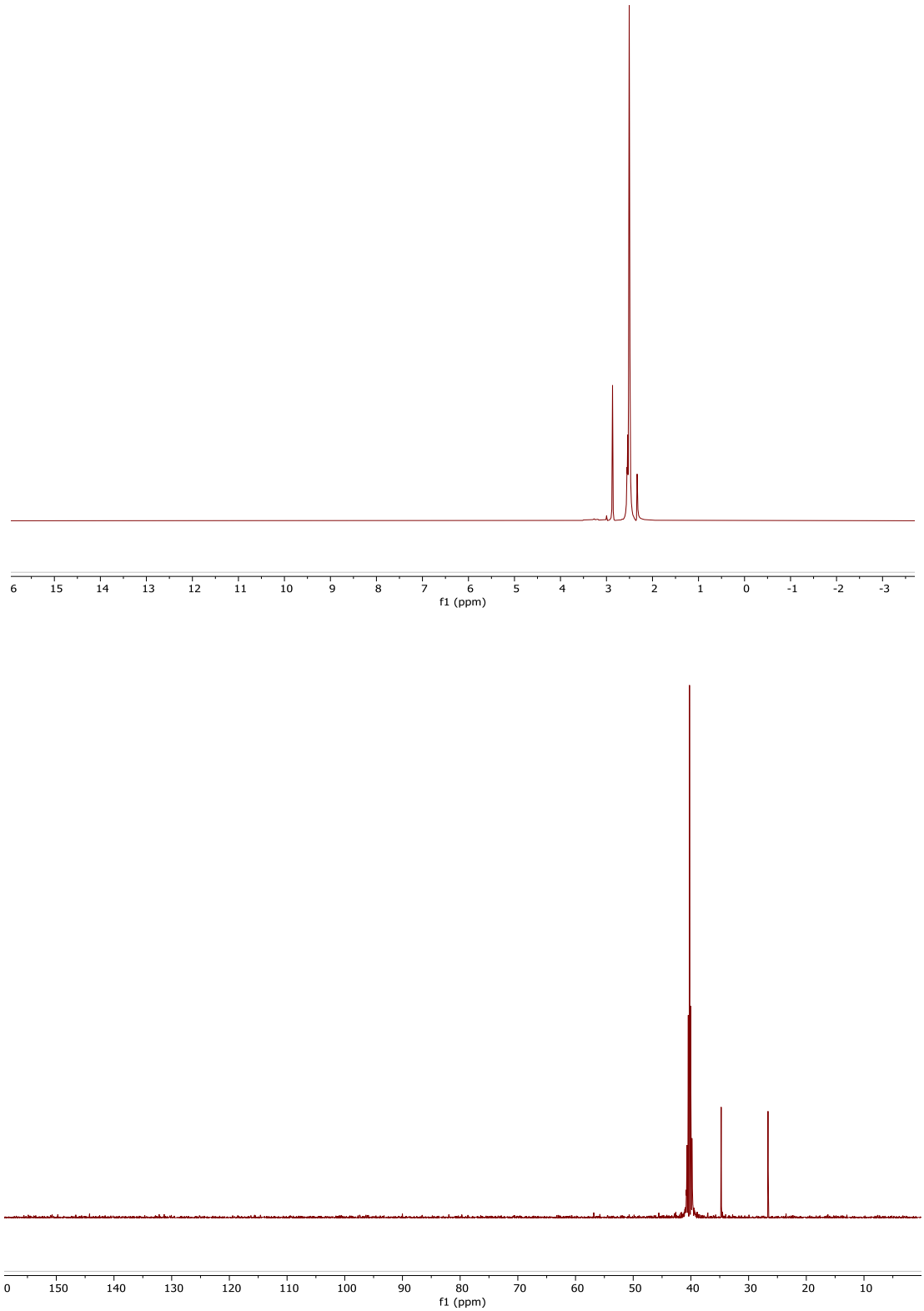

Figure 26 ^{1}H and ^{13}C NMR of BODIPY 6.6

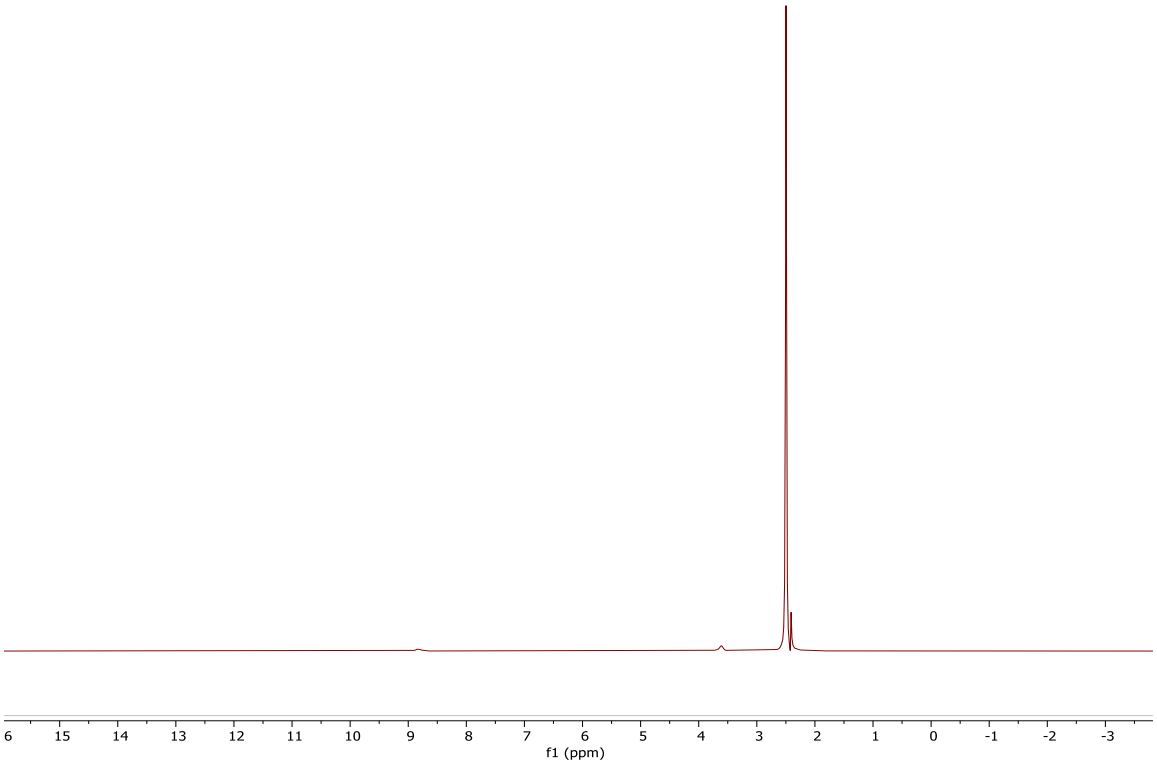

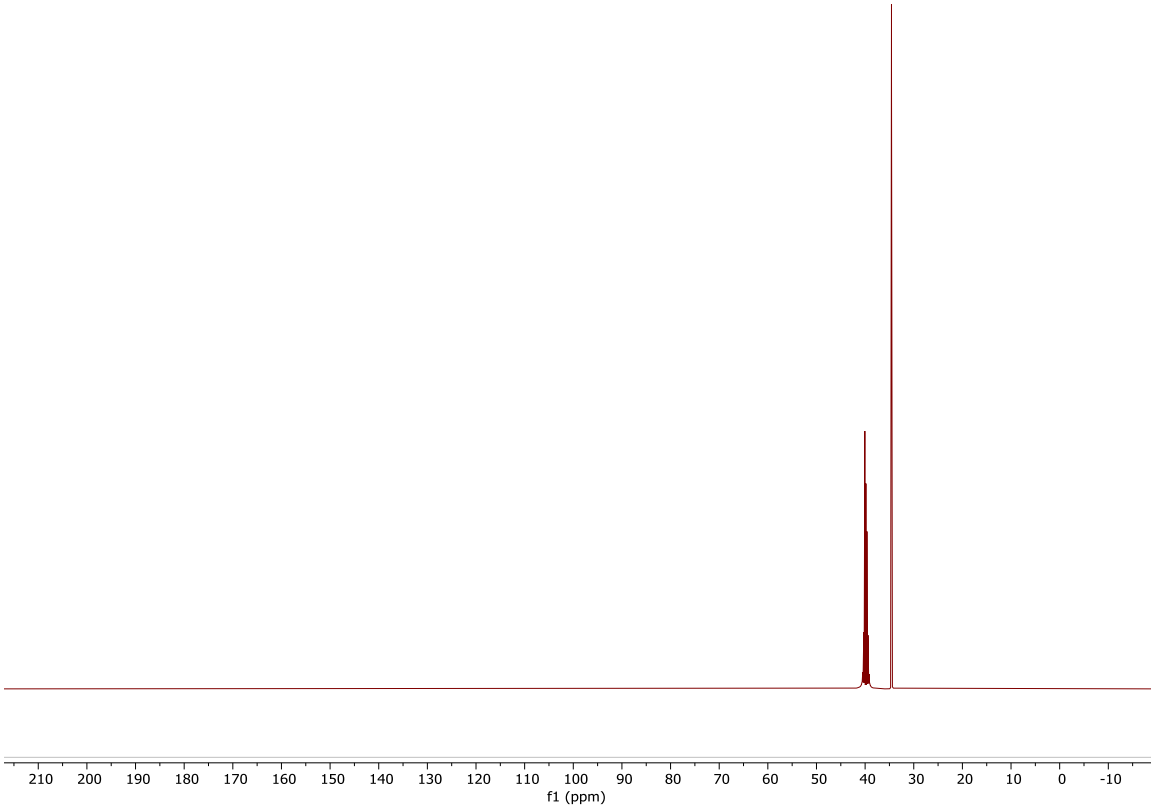

Figure 27 ^{1}H and ^{13}C NMR of BODIPY Mel.

Appendix 4: Antimicrobial study framework

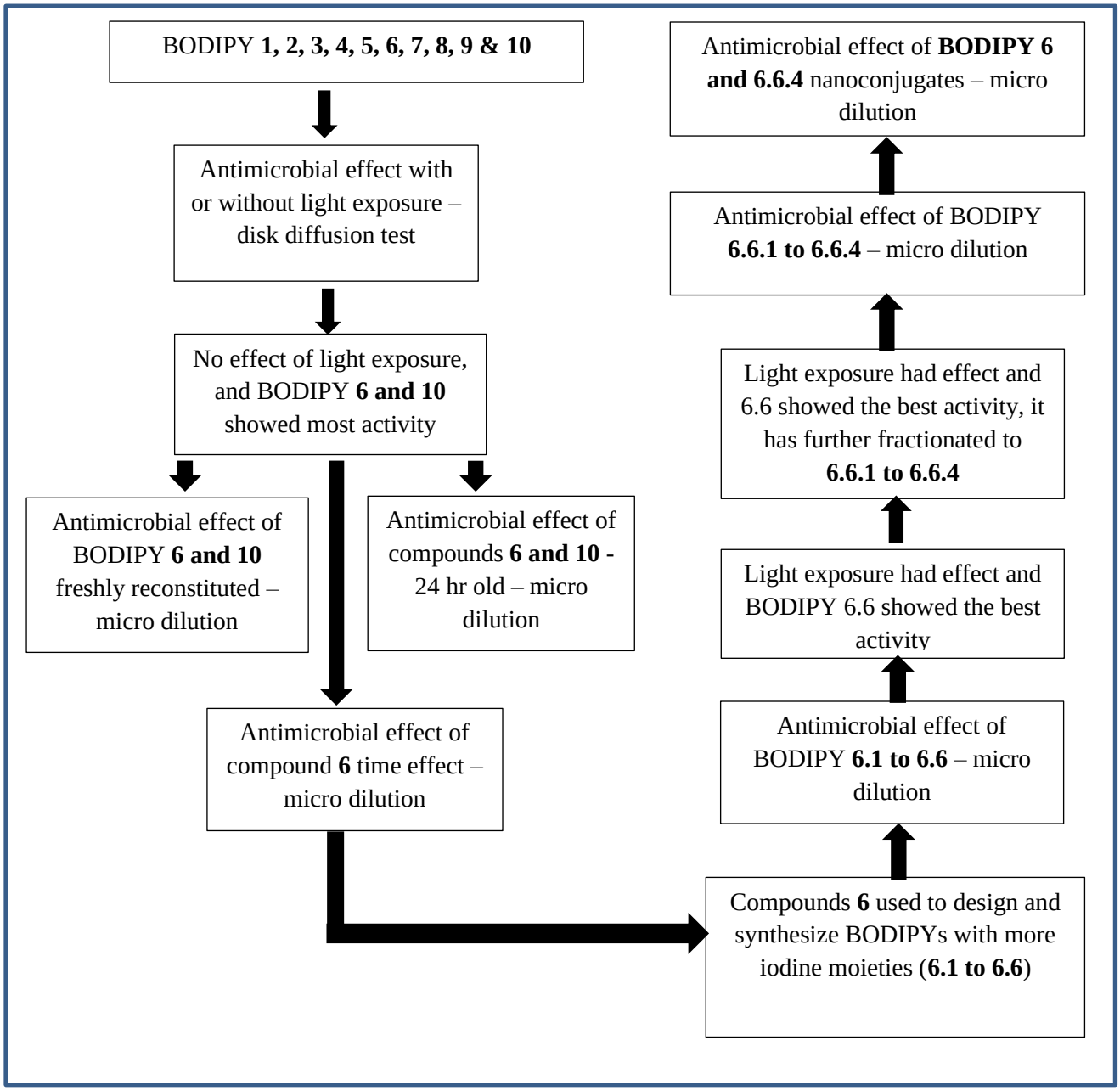

Figure 28 antimicrobial experimental work flow chart

Appendix 5: Cytotoxicity study on HaCat cell lines and UCT Mel-1 cancer cell lines

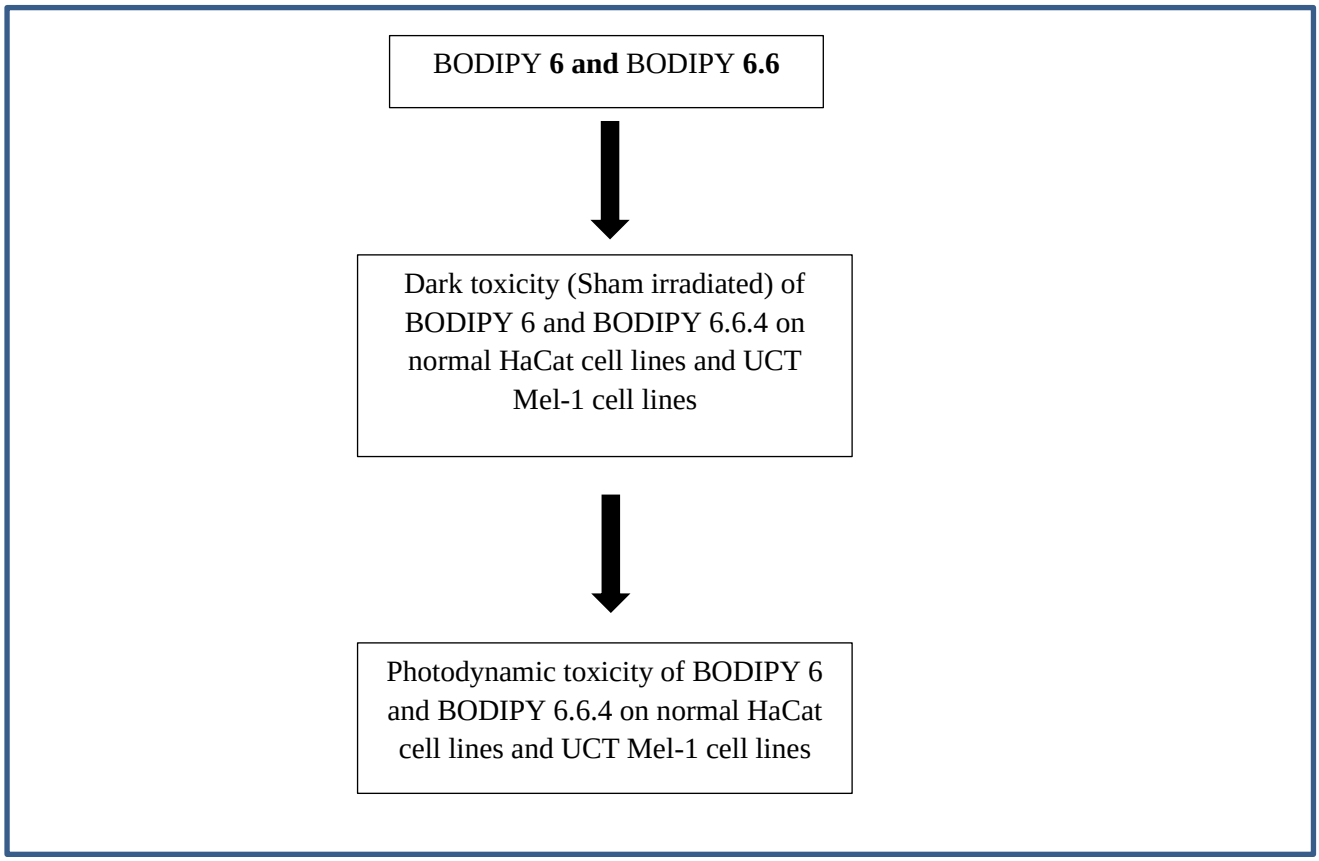

Appendix 6, Ethics clearance

UNIVERSITY OF THE WITWATERSRAND, JOHANNESBURG

HUMAN RESEARCH ETHICS COMMITTEE (MEDICAL)

9 May 2019

Mr M Thatyana
School of Oral Health Sciences
Dept of Oral Biological Sciences
Dental School
University

Sent by e-mail to: thatyanam4@gmail.com

Dear Mr Thatyana

Re: **Protocol Ref No:** W-CJ-170602-2
Protocol Title: *Novel BODIPY photosensitizers and corresponding nano-conjugates in an in vitro antimicrobial and anticancer study*
Principal Investigator: Mr M Thatyana

I refer to recent e-mail correspondence with your supervisor, Dr Moeno.

I confirm that your intention to add two more cell lines to those listed in my letter to you dated 5 June 2018 has been noted and approved. For the record, these are: HaCat (normal keratinocytes) and Mel-1 (melanoma) cells.

Further, we note that your project title has been modified, as now reflected above.

Thank you for keeping us informed and updated.

Yours Sincerely

J. Burns

.....

Mr I Burns
For the Human Research Ethics Committee (Medical)

c.c. Dr S Moeno

Research Office Secretariat:

Physical address: Phillip Tobias Building, 3rd Floor, Office 302, Corner York Road and Princess of Wales Terrace, Parktown, Johannesburg 2193.
Postal address: Private Bag 3, Wits 2050
Tel Nos. +27 (0)11-717-1234/2656/2700/1252
Office E-mail: HREC-Medical.ResearchOffice@wits.ac.za.
Website:http://www.wits.ac.za/research/about-our-research/ethics-and-research-integrity/